Damage Detection in Reinforced Concrete Square Slabs Using Modal Analysis and Artificial Neural Network

Mezgeen Sisen Ahmed

B.Sc. Civil Engineering, **M.Sc.** Structural Engineering and

PGDip Professional Research Practice

A thesis submitted in partial fulfilment of the requirements of

Nottingham Trent University for the degree of

Doctor of Philosophy

Nottingham, UK

March 2016

ii

Dedication

This thesis is dedicated to my parents, wife, brothers and sisters for their sacrifices, constant support and unconditional love. It is also dedicated to my little prince (Seema)

I love you all dearly. That is why this is for you.

Thank you so much.

Acknowledgments

First and foremost, I would like to praise and thank God, Allah SWT, who has granted me a countless blessing, knowledge, and opportunity to accomplish this Ph.D. thesis successfully.

Apart from my efforts, the successful completion of this thesis would not have been possible without the support and encouragement of many people. It is my pride and pleasure to take this golden opportunity to express my profound and sincere gratitude to all those who have been instrumental in the success of this thesis. It would be impossible to list all names here, but several people deserve my special thanks.

At this moment of accomplishment, I would like to express my appreciation and sincere gratitude to the director of study, Dr Fouad Mohammad, who has generously spent precious time in giving the valuable guidance, unending support and experienced advice until this thesis comes to its present form. Special thanks are also expressed to a member of the supervisory committee, Dr. Anton Ianakiev, for his assistance throughout the entire process. I would like to convey my regards to the laboratory technicians, Mr Jez Keeling, Dave Nix, Julian Robinson and Dave Edwards for their help with practical issues throughout some very tough times of the experimental tests.

Far from academic, to all my friends, thank you for your understanding and encouragement in many moments of difficulty. Your true friendship makes my life a wonderful experience. I cannot list all your names here, but you know who you are!. You are always on my mind and in my heart, but I would be remiss without thanking Farsat (Babê Renkoy), Jowad (Xal) and Kamal (Çergu) for their real friendship and every enjoyable moment we shared at St. Ann's Nottingham.

Profound gratitude is also dedicated to the guarantor, businessman Ziyad Askander Uzmani, for guaranteeing me with a severe contract in front of the Kurdistan Regional Government (KRG) sponsor. This unique attitude is unforgettable, and for that I am deeply indebted to him for his help in this matter.

I wish to offer my outstanding appreciation and gratitude to all organisations and individuals who made my graduate studies a great opportunity for my professional and personal growth.

Abstract

Reinforced concrete (RC) structures are usually subjected to various types of loadings, such as permanent, sustained and transient during their lifetime. Reinforced concrete slabs are one of the most fundamental structural elements in buildings and bridges, which might be exposed to unfavourable conditions such as, impaired quality control, lack of maintenance, adverse environmental effects, and inadequate initial design. Therefore, the resistant capacity of the affected elements would dramatically be reduced which most likely leads to the partial or whole collapse of the structure.

Non-destructive testing (NDT) techniques can be used to inspect for defects without further damaging the tested component. Significant research and development have been conducted on the performance of vibration characteristics to identify damage in different types of structures. The vibrations based damage detection methods, particularly modal based methods, are found to be promising in evaluating the health condition of a structure in terms of detection, localisation, classification and quantification of the potential damage in the structure.

Damage in composites and the non-homogeneous material is tricky to assess from a surface inspection alone. Although the development of NDTs, especially experimental modal analysis (EMA), has been pushed forward by the aerospace industry where composites materials are employed in many safety critical applications, EMA is not widely employed to diagnose all types of RC structural members.

Damage detection in reinforced concrete square slabs is the primary aim of this study. This is achieved experimentally using experimental modal analysis (EMA) and numerically using finite element method (FEM). Artificial neural network (ANN) is also used in this study to classify the void sizes.

A whole testing procedure of EMA on freely supported slab was established in this research. It is based on impact hammer technique, as a relevant excitation source for field measurements. After the quality of the measurements had been ensured, the experimental data was collected from four pairs laboratory-scale reinforced concrete slabs modelled with various ranges of parameters. After collecting data, Matlab software was employed to obtain modal parameters, such as natural frequencies, mode shapes and modal damping ratios from two RC square slabs. EMA and FEM

studies were undertaken to assess and improve modelling technique for capturing the aim. FEM was used to model the RC slabs using commercial ANSYS software. To balance model simplicity of RC slabs with the ability to reliably predict their dynamic response, both predicted and measured dynamic results were compared to ensure that the analytical model represents the experimental results with reasonable accuracy. ANSYS software was also employed to numerically extract the natural frequencies of the slab. Then, using Matlab software, the extracted natural frequencies were fed as the input to the ANN to classify the void sizes in the slab. The dynamic properties of the slab were investigated for each of four pairs to evaluate modal parameters (natural frequencies, damping ratio and mode shapes) sensitivity to slab's dimensions, degree of damage owing to incremental loading and induced void.

The performance of EMA based on impact hammer technique was credibly tested and verified on measurements, which were collected from eight slabs with various parameters. EMA efficiency was conclusively proved on data from modal parameters sensitivity to slab's dimensions, incremental loading and induced void. The results indicated that using a bigger reinforced concrete slabs (1200 x 1200 mm^2) could potentially have further reduced the discrepancy between theoretical (analytical and numerical) and experimental natural frequencies than smaller slabs (600 x 600 mm^2).

 In general, for the specimens tested slabs, natural frequencies were more sensitive to the damage introduced than the damping ratio because the damping did not consistently increase or decrease as damage increased. The changes in mode shapes tended to increase with increasing damage level. Even small damage induced poised changes to the mode shapes, but it may not be obvious visually. Utilising sophisticated methods for damage identification, which are vital steps in higher level of damage detection in structures, is one of the major contributions to the knowledge. The proposed Modal Assurance Criterion (MAC) and Coordinate Modal Assurance Criterion (COMAC) techniques as advanced statistical classification model were employed in this study. From the vibration mode shapes induced void location can be identified via MAC and COMAC techniques when both intact and damaged data were compared. MAC provided a clear change in the mode shape while the COMAC provided the change in specific a location whereby

the location of damage was identified. The outcomes of this two techniques can show the realistic location of the void.

Beside the aforementioned contributions in this research, the feasibility of a Feed-Forward Back Propagation Neural Network (FFBPNN) was investigated using ten natural frequencies as input and the void sizes as output. Excellent results were obtained for damage identification of four void sizes, showing that the proposed method was successfully developed for damage detection of slabs.

The results proved that the precision of the models was reduced when dealing with small size void. The large size void was detected more accurately than small size void as expected. This is because the natural frequencies of the small void of different location attributed together. Therefore, natural frequencies alone were not considerably good enough to make good identifications for small size void. Moreover, the natural frequencies set of three untrained void specifications were used as FFBPNN inputs to test the performance of the neural networks. The obtained results show that the proposed network can predict the void specifications of the unseen data with high accuracy.

Overall, the methodology followed in this work for damage detection in reinforced concrete square slabs is novel when compared to the breadth and depth of all other previous works carried out in the field of reinforced concrete structures.

Publications

The following papers have been published as a direct outcome of this thesis:

Refereed Journal Papers

Ahmed, M. ; Mohammad, F. (2015), 'Experimental Modal Analysis of Reinforced Concrete Square Slabs', World Academy of Science, Engineering and Technology, International Science Index 99, International Journal of Mechanical, Aerospace, Industrial and Mechatronics Engineering, 9 (3), 326 – 330.

Ahmed, M. ; Mohammad, F. (2014), 'Theoretical Modal Analysis of Freely and Simply Supported RC Slabs', World Academy of Science, Engineering and Technology, International Science Index 96, International Journal of Mechanical, Aerospace, Industrial and Mechatronics Engineering, 8(12), 1936 - 1940.

Mohammad F. A., Ahmed M. S. and Ianakiev A. (2015). Modal analysis of reinforced concrete square slabs. Submitted to Civil engineering ICE Journal.

Mohammad F. A., Ahmed M. S. and Ianakiev A. (2015). Natural frequencies reduction of reinforced concrete slabs subjected to incremental concentrated load. Submitted to Engineering Structures Elsevier journal.

Refereed Conference Papers

Mezgeen S. Ahmed (2013). Effect Of Main Factors On The Strengthening Of Reinforced Concrete Beams By Using Carbon FRP, *Proceedings of the 5*th Annual Conference, Research Practice Course, Nottingham Trent University17th May 2013, UK

Mezgeen S. Ahmed (2014). Comparison between theoretical and experimental natural frequencies of RC slabs. Proceedings of the Inaugural College of Art, Design and Built Environment Doctoral Conference 9th and 10th June 2014, Nottingham, UK.

List of Contents

List of Figures

List of Tables

Nomenclature

This section represents list of symbols as well as matrix and vector that are common in the chapters of this thesis.

List of Symbols

A^r	Modal constant / residue of rth mode of vibration
b	shorter side length of the plate
b_i	Bias in neural network
D	Bending rigidity of the plate
d(n)	Corresponding target output
E	Modulus of Elasticity of the material making the beam
E_c	Modulus of elasticity of concrete expressed in MPa
E_d	Dynamic (tangent) elastic modulus expressed in MPa
F	Transfer function
f	Natural frequency, measured in Hz
f_{cu}	Concrete compressive strength based on cube test at 28- days, expressed in MPa
f'_c	Concrete compressive strength based on cylinder test at 28-days, expressed in MPa
$G_{ff}(\omega)$	Single-sided auto-spectrum of the input signal
$G_{fx}(\omega)$	Single-sided cross-spectrum between input and output signals
$G_{xx}(\omega)$	Single-sided auto-spectrum of the output signal
h	Plate thickness
$H(\omega)$	Frequency response function
$H_{jk}(\omega)$	Individual FRF element between coordinates j and k (response at j due to excitation at k)
i	Imaginary unit ($\sqrt{-1}$)
I	Moment of inertia
j	Notation refers to the output degree of freedom (physical location and orientation)
k	Notation refers to the input degree of freedom (physical location and orientation)
L	Total number of paired modal vectors included in comparison
ℓ	Longer side dimension of the plate

M	Bending moment
m	Number of neurons in the output layer
M_r	Modal mass for r^{th} mode
m_{ANA}	Number of analytically investigated modes
m_{EXP}	Number of experimentally investigated modes
N	Total number of degrees of freedom
n	Number of observations (rows in a data matrix)
net_j	Weighted sum of the jth neuron for the received input from the preceding layer with n neurons
P	Response DOF
q	Force excitation DOF
Q_r	Scaling factor in relation to r^{th} mode of vibration
O_p	Predicted outputs
O_t	Target outputs
Out_j	Actual output of the neural network value for i^{th} input
r	Mode number
$S_{ff}(\omega)$	Dual-sided auto-spectrum of the input signal
$S_{fx}(\omega)$	Dual-sided cross-spectrum between input and output signals
$S_{xx}(\omega)$	Dual-sided auto-spectrum of the output signal
t	time variable represent in second
T	Repeat period / data acquisition period
T_i	Target output of the neural network value for i^{th} output
x(n)	Input to the network
X_i	Output of the ith neuron in the proceeding layer
Xi (k)	Input value in discrete time k where I ranges from zero to n
x (t)	Time-varying displacement degrees of freedom
y	Element transverse deflection
y (k)	Output value in discrete time k
y"	Second derivative of displacement (curvature)
ε	Strain
ρ	Radius of curvature
κ	Curvature

$\bar{x}$	Mean of feature vector in original data
$\gamma^2(\omega)$	Coherence function
$\Delta\mathrm{x}$	Length of the element in x-driection
ζ_r	Viscous damping ratio of rth mode of vibration
η_r	Structural damping loss factor of rth mode of vibration
φ_{jr}	j^{th} element of the rth mode of vibration
ω	Natural circular frequency expressed rad/sec
ω_{exp}	Natural frequency obtained experimentally expressed in Hz
ωij	Weight between the jth neuron and the ith neuron in the proceeding layer
ω_{theo}	Theoretical natural frequency obtained analytically and numerically
ω_r	Natural frequency of rth mode of vibration measured in Hz
$\omega_n(x,y)$	Spectral components of $\omega(x,y,t)$
Φ_{ANA}	Mode shape expressed in matrix from (Eigen mode matrices) of (n x mANA)
Φ_{EXP}	Mode shape expressed in matrix from (Eigen mode matrices) of (n x m_{EXP})
σ_r	Damping factor
∇^2	Laplace operator
∇^4	Biharmonic operator
ρ	Density of the plate material
υ	Poisson's ratio of the plate material
μ	Mass density per unit area of plate (ρh)
λ	Dimensionless natural frequency factor
γ_m	Partial safety factor, which is 1.5
η	Damping loss factor

List of matrix and vector notation

[ ]	Matrix
$[\ ]^{-1}$	Inverse of a matrix
$[A]^r$	Driving point residue matrix
$[\ ]^T$	Transpose of a matrix
[I]	Identity matrix
$[\backslash\omega^2\backslash]$	Diagonal natural frequencies matrix
$[\backslash\lambda\backslash]$	Diagonal eigenvalue matrix
[C]	Viscous damping matrix of the structural system
$[H(\omega)]$	Frequency response function matrix
[K]	System stiffness matrix
[M]	System mass matrix
{ }	Vector
$\{\ \}^T$	Transpose of a vector
$\{\dot{x}(t)\}$	Nodal velocities vector
$\{\ddot{x}(t)\}$	Nodal accelerations vector
{f(t)}	Nodal forces vector
{x(t)}	Nodal displacements vector
$\{\varphi\}^r$	r^{th} mode shape vector
|H|	Maximum amplitude of a receptance FRF

List of Abbreviations

ADALINE	Adaptive Linear Neuron
ANN	Artificial Neural Network
ANNs	Artificial Neural Networks
ART	Adaptive Resonance Theory
BP	Back Propagation
BPNN	Back Propagation Neural Network
CFC	Coherence Function Check
CFRP	Carbon Fibre Reinforced Polymer
CFS	Carbon Fiber Sheets
DA	Data Acquisition
DLAC	Damage Location Assurance Criteria
COMAC	Coordinate Modal Assurance Criterion
DOF	Degree of Freedom
DTA	Dynamic Testing Agency (UK)
ELSA	European Laboratory For Structural Assessment
EMA	Experimental Modal Analysis (also known as Modal Testing)
FE	Finite Element
FEA	Finite Element Analysis
FEM	Finite Element Method
FFBP	Feed-Forward Back Propagation
FFBPNN	Feed-Forward Back Propagation Neural Network
FFT	Fast Fourier Transform
FFTDNN	Feed-Forward Time Delay Neural Network
FRC	Frequency Response Component
FRF	Frequency Response Function
FRFs	Frequency Response Functions
GFRP	Glass Fiber Reinforced Plastics
HIPs	High Impact Polystyrene
IEEE	Institute of Electrical and Electronic
IMOs	Intrinsic Modal Oscillators
IRC	Immediate Repeatability Check
IRFs	Impulse Response Functions
LVDT	Linear Variable Displacement Transducer

LMS	Least Mean Square
MA	Modal Analysis
MAC	Modal Assurance Criterion
MDOF	Multiple Degree of Freedom
MLP	Multi-Layer Perceptorn
MSE	Mean Squared Error
NDE	Non-Destructive Damage
NDT	Non-Destructive Test
NMM	Normal Mode Method
NN	Neural Network
NSI	Nonlinear System Identification
QA	Quality Assurance
PCA	Principal Component Analysis
RBF	Radial Basis Function
RC	Reinforced Concrete
SDOF	Single Degree of Freedom
SHM	Structural Health Monitoring
SOM	Self-Organized Map
SSE	Sum Square Errors
TFM	Transfer Function Method
VBDD	Vibration-Based Damage Detection
VBDIT	Vibration Based Damage Identification Technique
XFEM	Extended Finite Element Method

1. Introduction

1.1   Overview

Reinforced concrete (RC) is one of the widely used building materials, which was introduced in the late nineteenth century, after the invention of Portland cement. Afterwards, reinforced concrete structures were taken up quickly and nowadays they are widely used in the world. Even though reinforced concrete structures such as building and bridges are relatively durable and robust, they can be severely weakened when they are frequently exposed to unfavourable conditions. The resistant capacity of the structural members can seriously weakened by inadequate initial design, impaired quality control, poor or lack maintenance, and a very harsh environment. In addition, reinforced concrete (RC) structures are usually subjected to various types of loadings, such as permanent, sustained and transient during their lifetime. These loads may have affected the structure either individually or in combination with one another (Nair et al., 2008). A significant number of reinforced concrete structures are might be old, subject to increasing traffic loads and intensity, and some with functional deficiency. The unexpected collapse of structures has a notorious symbolic impact on the economy as well as the stability of the country. Therefore, extra attention is considerably important to be paid to providing awareness about the behaviour of the structures under different situations. When the process of describing the natural characteristics of the structures is continuously known, the adverse consequences such as discomfort, malfunctioning, destruction and sudden collapse will be minimised if they are not completely controlled (Nagarajaiah et al., 2008).

During the years following World War II, the building industry boomed worldwide. As a consequence, numerous civil engineering structures are now, or will soon be, approaching the end of their design lives. As it is economically not permissible to replace all of the aged structures, health monitoring and integrity assessment are important to ensure the reliability of the structures and the safety of the public (Dackermann, 2010). The proper inspection of existing structural components can help to identify deficiencies and reveal generalised dangers. Then, the decision will be made whether the tested structures are required to improve their integrity and robustness in order to ensure resistance, durability and safety or they are needed to

be replaced. The most important factors such as estimated budget, time consumption, level of risk and the importance of the intended elements should be taken into account to decrease the allocated budget to return buildings to service. The primary target to decrease the allocated budget is that concentrating on the strengthening and rehabilitation of the existing structures, rather than demolition and reconstruction. That is why the priority solution to refurbish and increase number of ageing of the elements in the structure in order to keep in service for a longer time, is repairing otherwise the demolition is the superior solution.

In civil engineering realm, current non-destructive damage detection methods in the field are based, for example, on visual inspection, ultrasonic or acoustic method, magnetic field method, radiography method, thermal field method and eddy current method. However, most of these methods have two main limitations. Firstly, the vicinity of damage must be known a priori. Secondly, the portion of the structures that is being inspected is readily accessible (Farrar and Doebling, 1997). Thus, these methods are very time-consuming, costly or may be not applicable when utilized to large structures. Subjected to the aforementioned limitations, the only type of damages that are near or exactly on the surface of the structures can be detected through these experimental methods. However, in most fields of engineering such as civil, aerospace and mechanical engineering communities, previous knowledge about area of damage or information related to damage is usually unknown before damage identification.

Consequently, there is a need to have more powerful techniques to overcome the deficiency of the aforementioned experimental methods. Vibration-Based damage identification techniques are global methods that can assess the condition of the entire structure at once. These methods are based on the belief that defect alters both the physical properties of a structure (for instance mass and stiffness) as well as its dynamic characteristics (for example frequency response functions (FRFs), natural frequencies, damping ratios and mode shapes). Accordingly, by analysing a structure's dynamic properties from structural vibration or more specifically from vibration-Based damage identification techniques, any defect including its location and severity can be identified. Furthermore, these types of methods provide better understanding of vibration characteristics of the structures, and examine changes in these characteristics and solving structural problems in existing designs (Maia and Silva, 1997).

It should be noted that, notwithstanding the fact that considerable research work has been published on damage detection methods, not much research work has been reported on methods applicable to reinforced concrete structures (Wang, 2010). The tardy development of damage detection methodology for reinforced concrete structures is since reinforced concrete, unlike metals, is a non-homogeneous material with varying composition, raw materials and complex binding behaviours between different materials of the specimen. Hence, many damage detection methods that appear to work well on other structures might perform poorly when being applied to reinforced concrete structures.

It is truly known that almost all reinforced concrete structures are inevitably witnessed to deterioration and assemblage damage during its service life due to adverse conditions. The critical phase is to reliably and robustly locate and quantify damage in an impaired structure at the earliest possible stage. It is preferable to detect damages as early as possible so that to prevent or minimise the occurrence any collapse or catastrophe. To rehabilitate or strengthen damaged reinforced concrete structures, identification of both nature and extent of damage, careful analysis of the remaining capacity of the structure are essential. Then, the selection of the most efficient solution for treatment of the injured structure are imperative. Different strengthening techniques have been developed to satisfy the demand of the defective structures to increase the durability, design or construction errors and to change the function in order to fulfil certain serviceability. Different techniques for strengthening RC slabs have been used, for instance, section enlargement, steel plate bonding, and adding supplementary support. Each of which having both advantages and disadvantages depending on the applied circumstances (Emmones, 1993; Radomski, 2002).

Over the last few decades, an extensive research has been conducted to develop a strengthening technique using Carbon Fibre Reinforced Polymer (CFRP) sheets. The uses of CFRP sheets are becoming very popular in structural retrofitting realm because of their superior physical and mechanical properties. Compared to conventional construction materials, comprehensive experimental investigations have shown that CFRP sheets offer engineers some unique advantages such as light weight, ease of installation, immunity to corrosion, excellent tensile strength and stiffness. In addition to its availability in convenient forms, these materials are easy to handle during construction (Alsayed et al., 2000). Due to these unique

advantages, CFRP composites have been pushed in various fields such as aerospace, automotive, military and civil engineering applications. This strengthening technique is widely used because the advantages previously mentioned. In recent years, considerable experimental and theoretical researches were performed to investigate the performance of concrete structures with externally bonded CFRP sheets. However, most of the previous research was mainly focused on the column and beam elements and little attention was paid on slab. Moreover, CFRP has become commercially available at relatively affordable prices.

1.2   Problem Definition of the Study

Over the past decades, an excessive number of technical articles were published on structural health monitoring (SHM), which has attracted considerable attention in both research and development. The available technical articles highlighted that there are two main damage identification techniques such as local and global methods (Zapico and Gonzalez, 2006; Gunes and Gunes, 2012). In the former method, the assessment of the state of a structure is performed either by direct visual inspection or using experimental techniques, for instance ultrasonic, radiography, eddy current and magnetic particle inspection. A bad feature of all these methods is that their applications require a prior localisation of the damaged zones. Therefore, the limitations of the local methodologies can be overcome by using vibration-based methods, which give a global damage assessment. The available technical articles in the literature highlighted that there are a number of vibration-based methodologies that are used to detect, locate and quantify the damage in structures.

The most common vibration damage detection techniques seem to be based on modal parameters. It is accepted that have not yet been an appropriate method to be utilised for identifying, locating and estimating the severity of damage in structures by exploiting the vibration data. Furthermore, no algorithm has yet been suggested to apply globally to detect any defect in any structure (Wenzel, 2009). The development of powerful damage detection and location algorithms based on response monitoring data of an in-use structure is still a challenge. Therefore, the availability of such detection techniques will open the door to more accurate estimation of the remaining life of a structure (Friswell, 2007).

The amount of literature covering non-destructive vibration methods for damage scenarios on beam structures is relatively extensive. On the other hand, limited literature is available for damage scenarios on slab. Most existing methods are based on specific materials such as metal rather than reinforced concrete, and most authors demonstrate these methods mainly on automotive structure and their systems and components (Huang et al, 1997; and Storck et al, 2001).

This research treats the problem of damage evaluation in reinforced concrete slab in order to understand the behaviour of reinforced concrete slabs and ensure their integrity and safety. There is thus a need for a comprehensive and reliable modal analysis implementation for behaviour assessment of reinforced concrete slab, which is the aim of the proposed research. The proposed work suggests a novel methodology to solve some problems available in academic research. After comprehensive reviews, the common problems in modal analysis, as well as reinforced concrete structural system, can be summarised as:

Firstly, it is noted that changes in natural frequencies alone may not provide enough information for integrity monitoring (Farrar and Cone 1995). Secondly, in the process of performing the proposed damage detection method, some researchers preferred natural frequencies as the most indicator to identify and estimate the severity of damage to the structures. However, others preferred the modal damping ratio is a good damage indicator. Damage detection and condition assessment of civil engineering structures is considerably important especially when the building is old or it is subjected to overloading. A wide range of civil engineering structures is of unknown history. This is another problematic obstacle confronts the use of the vibration-based monitoring systems in civil engineering structures. Therefore, data from a real-life as-built model of the structure is commonly unavailable. As a consequence, a prediction of a numerical model using commercial software for the original intact condition will serve as a basic guide to which the deviation of obtained measurements are finally compared with.

Finally, in this study, the numerical results can be used as input to the artificial neural network (ANN) for training to identify damage presence, location and severity. The proposed damage identification and condition assessment procedure, therefore, fills the gap of knowledge and it enhances the reliability and usefulness of ANN based structure diagnosis systems.

1.3   Aim and Objectives of the Study

The primary aim of this study is to investigate the application of experimental modal analysis on RC slab specimens and also to identify damage presence and location in the slabs. Moreover, the feasibility of using modal analysis for the structural behaviour of reinforced concrete slab is examined during the tests. Artificial neural network, on the other hand, is used to identify the severity of void in the slab. In order to achieve the aim, the following objectives were required to be done.

1- Extracting modal parameters (natural frequencies, damping ratios and mode shapes) to evaluate the behaviour of reinforced concrete slabs.

2- Considering the effect of reinforced concrete slab's dimensions on modal parameters and finding the difference between theoretical prediction and experimental measurements of natural frequencies of the two different slab's dimensions.

3- Studying the effect of flexural rigidity of reinforced concrete slabs on the dynamic characteristics by changing the thickness.

4- Investigating the influence of different degrees of cracks and strengthening on the modal parameters, by introducing different degrees of cracks to reinforced concrete slabs as well strengthening using CFRP sheets. Using MAC and COMAC to identify the effect of different degree of cracks on mode shapes.

5- Validating the reliability of the location of the inflicted single damage scenario in reinforced concrete slab using experimental modal analysis and MAC and COMAC techniques.

6- Employing the artificial neural network (ANN) in the final stage to evaluate the severity of voids in the slabs in order to validate the accuracy of using such technique for detecting different levels of void severity.

1.4   Outline of the Thesis

The present work consists of nine chapters. The outline of the following chapters and their content is listed as follows:

The thesis began with an introduction to the structural behaviour together with a brief summary of the main damage detection methods and discussion their ability

for detecting defects in a structure. In addition to an introduction to the main parts of the thesis, for instance, problem definition, research aims and objectives and the outline of the thesis are presented in this chapter.

The chapter two presents a literature review regarding the existing method in damage detection; focusing on the application of modal parameters and ANN. Subsequent to the damage detection techniques, the main developments of global non-destructive vibration-based damage detection methods over the past three decades are extensively reviewed. In addition, this chapter addresses a brief description of the research problems. Accordingly, the knowledge gap is specified in this chapter.

Chapter three embarks on the introduction of modal analysis followed by the theoretical relationships among the three models of the dynamics of structures. A brief theoretical background to the analytical and experimental modal analysis is also provided in this chapter followed by degree of freedom of a structure. Besides, derivations for the formulae related to the calculation of modal data for instance FRF and its components and coherence function are presented. The chapter is ended up with provides the EMA procedures that can be entirely achieved in four specific phases. Four phases of a typical modal test are discussed to check the reliability of the instrument (quality assurance checks).

Chapter four explains the main stages of the research methodology followed in this research. This chapter also describes the experimental modal analysis of reinforced concrete slabs. The characteristics of each individual piece of the equipment associated with the procedure used to perform the experimental modal analysis work are clearly explained in this chapter. Discussion of different reliability and quality checks for experimental modal analysis are also discussed in this chapter. Moreover, the laboratory reinforced concrete slab specimens are classified into four main groups. The specifications of each group of RC test slab were described.

Chapter five starts how to estimate modal parameters from FRF measurements in the post test analysis and presenting them in the meaningful manner. In this context, modal parameters which is included as resonant frequencies, damping ratios, and mode shapes. The theoretical estimation is also explained. It is also important to mention that dynamic modulus of elasticity and Poisson's ratio are clarified and used for estimating the theoretical results. In the final section of this chapter, experimental

results of control group (A) are compared with theoretical results to ascertain the validity and reliability of the results.

Chapter six deals with the parametric studies of four pairs of RC slabs using modal parameters estimation. After obtaining the data of each slab from the experiment, the Fast Fourier Transform (FFT) was used to transfer the time domain to frequency domain. As a result, the modal parameters of different status condition are determined, analysed and explained. Then, the experimental results (natural frequencies and mode shapes) are compared with the theoretical results. In addition, the experimental results of the control slab are also compared with experimental results under different status conditions to find the parametric studies on modal parameters.

Chapter seven presents the correlation between the mode shapes of two models. It introduces MAC and COMAC values of the two groups, for instance intact vs defected slabs, with their state conditions. The characteristics of each individual conditions of the MAC and COMAC values associated with the degree of damage or the location of damage which are clearly explained in this chapter. Using the values of both MAC and COMAC, the location of void is precisely identified.

Chapter eight gives an introduction to the neural network, neural network model, classification and architecture. Subsequently, five elements that comprise the neural network's architecture are well explained. Moreover, the chapter describes mathematical functions and type of neural networks. In addition, this chapter proposes an algorithm to detect different void severities, which is based on neural network. More specifically, explanation of the feature extraction input-output of the network is presented. This chapter also covers the main stages of the used Feed-Forward Back Propagation Neural Network (FFBPNN) for identifying void severity in reinforced concrete slabs.

Chapter nine summarises the overall findings of this thesis and provides a set of conclusions. In this chapter, pertinent subjects for further future research are also recommended.

At the end of the document (thesis), four appendices are included. Appendix A, describes preparation of experimental work. Appendix B, shows Matlab code for transforming data, averaging and drawing the FRF. Appendix C, focuses on RC

Slab analysis according to EC2, BS8110 and ACI 318 codes. Finally Appendix D presents Matlab code for determining MAC and COMAC values of mode shapes whereby damage severity and the location in the slab is identified respectively.

2. Literature Review and Research Problem

2.1   Structural Health Monitoring

Civil infrastructure, including bridges, buildings and other type of structures have direct effects on our daily lives. Civil infrastructure is the artery of social and economic activities and an essential element of human wellbeing. In spite of ageing and the associated accumulation of defects in infrastructure in some country especially in the developing countries, most of the existing infrastructure are still being in service. Hence, evaluation of the condition of these types of structures is critical particularly after natural hazards (e.g. earthquakes) or manmade hazards (e.g. blast or fire). Monitoring of the status of these structures followed by an immediate repair should they need to, is considerably important to society in order to prevent or at least to minimise the impact of the disaster and to facilitate the recovery. This is because tragic disasters on the civil structures, for instance, the collapse of bridges, buildings, dams and stadiums often result in an enormous number of casualties as well as social and economic problems (Sundaram et al, 2013).

Structural health monitoring (SHM) is emerging as a technology that allows to detect, measure, and record the change that affects the performance of a structure to improve its safety and maintainability. SHM techniques are widely employed to detect the symptoms of incidents, anomalies, deteriorations, and defects through the response that may impact structure's serviceability and safety. For instance, the response of a structure needs to be one or a combination of any of the accelerations, strains, deformations, environment effects (humidity, temperatures, pressure), and other attributes of a structure (Dong et al, 2010). Based on the knowledge of the structural condition, certain precautions measures can be taken into account to prolong the structural service life and prevent catastrophic failure in an unpredictable fashion. Anomalies, deteriorations, and faults detection strategies can eventually reduce life-cycle cost. Therefore, most of the industrialised countries are on the verge of increasing their budget for SHM of their major civil infrastructure. The integrity and robustness of structural components are required to be improved before series damages accumulate so as not to require more expensive repairs (Gassman and Tawhed, 2004).

After decades of carelessness to the sector of maintenance in Iraq, rehabilitation or reconstruction costs of the ruined and neglected infrastructure require billions of dollars (Iraqi Planning Minister, 2009). As a result, SHM is required to be taken into account for Iraq and most probably other similar third world country in order to minimise the budget spent on infrastructure repairs and maintenance. This means that SHM system usually offers an opportunity to reduce the budget for the maintenance, repair and retrofit throughout the life of the structure. A reliable inspection and condition assessment system has the potential to extend the periodic maintenance scheme for the existing structures. Inspection is typically conducted to decide if the tested structure is in demand of repair or demolition, estimate the amount of needed repair or whether further testing is required.

It is important to mention that some cases can also be introduced as damages to the structure. For example, changes in materials, connections and boundary conditions can be defined as damage because these factors cause deteriorated performance of the structure (Gao and Spencer, 2008). Furthermore, building structure can be damaged due to ageing, corrosion and daily activities, whereas wave loading, spalling and corrosion due to sea water cause damage to offshore structures. In addition to building structure, bridges suffer from traffic, wind loads, and some other environmental effects. Moreover, excessive loads produced by earthquakes, hurricanes and cyclones can potentially cause disturbance as well as moderate to severe damage to structures (Sundaram et al, 2013).

SHM may involve the use of various devices, techniques and systems that are designated as non-destructive damage identification methods. Such methods can be classified as either non-destructive evaluation (NDE) or local damage identification and non-destructive testing (NDT) or global damage identification (Doebling et al. 1998). The authors reported that damage diagnosis and integrity evaluation for a structure are conducted through a wide range of local damage identification techniques such as visual inspection, ultrasonic method and X-ray method and so forth. These type of techniques usually need that the vicinity of a defect is known a priori, and it is readily accessible for testing, which cannot be guaranteed for most cases in civil engineering. As a consequence, the global damage identification technique, such as vibration-based damage identification method, has been developed to overcome these difficulties.

Although there is no formal delineation between each previous approach, there is a difference between NDT/NDE and SHM. The primary difference between NDE/NDT and SHM. NDE/NDT refers to a one-time assessment of the condition of materials at a single or multiple points on the structures. The effect or extent of the deterioration in the structure using required equipment external to the structure can be evaluated. However, SHM normally refers to activities focused on assessing the condition of the whole structure or its key elements based on response to different types of loads. It involves on-going or repeated assessment of such response. It is interesting to note that, in SHM, some sensor systems may need to be embedded in or attached to the structure for the complete monitoring period (Dong et al, 2010).

Thus a SHM system will typically consist of the following common components: sensors and data acquisition networks; communication of data; data processing; storage of processed data; diagnostic and prognostic analysis (i.e. damage detection and modeling algorithms, event identification and interpretation); and retrieval of information. Figure 2.1 shows a schematic diagram of a typical SHM system (Büyüköztürk and Yu, 2003; Bisby, 2006).
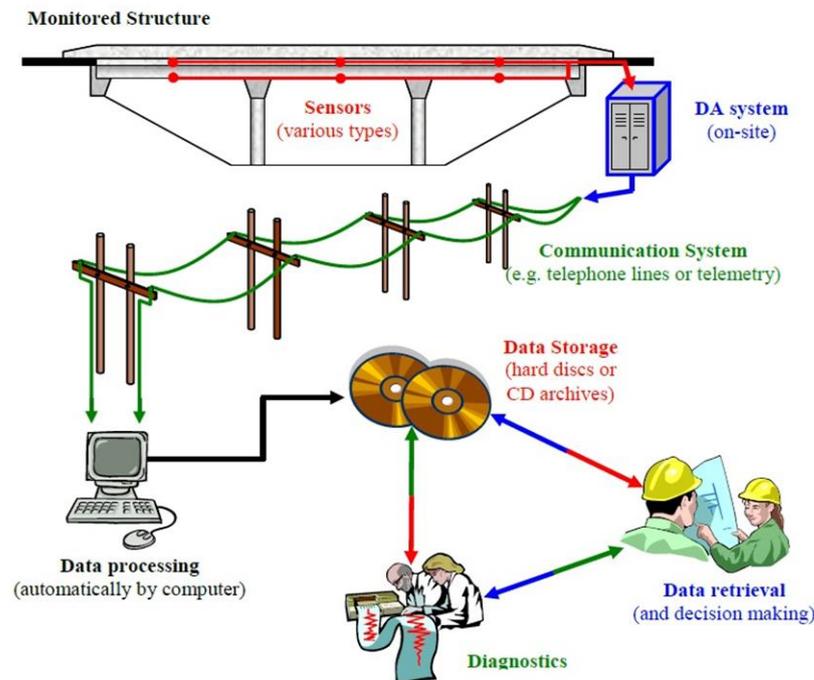
Figure 2.1: Visual schematic of a typical SHM system (after Bisby, 2006).

Bisby (2006) classified SHM into at least two categories in terms of the type of field testing such as continuous and periodic monitoring. SHM is offering the potential

for continuous and periodic assessments of the safety and integrity of a structure. Periodic monitoring is carried out to examine the structural response or any detrimental change that might happen in a structure at specified time or time intervals (such as weeks, months, or years apart). Data analysis of this type of monitoring may indicate deterioration. For instance, monitoring crack growth, monitoring a structure after a repairing; and continuous monitoring through moving traffic, all these can be achieved periodically. In such type of monitoring, sensors may be permanently mounted on the structure or temporarily installed at the time of testing. As it is implied from the name that continuous monitoring refers to monitoring of a structure without causing interruption for an extended period (such as weeks, months, or years). Logged data at the structure are either collected or stored on site for analysis, and interpretation at a later time. Due to the higher costs and complexity of SHM system, this type of monitoring has only been used in full-scale field applications.

Customarily, the latter is implemented to those structures that are in the following cases. Firstly, the structure is either exceedingly important or if there is doubt about the integrity of a structure. Secondly, it might be the case if the structure is likely to be exposed to extreme natural hazards, such as hurricanes and severe earthquakes. Finally, if the structural design includes an innovative concept that does not have a history of performance to sustain its long-term safety.

SHM presents a number of key benefits for structures. Some of the most commonly cited benefits of these methods include (Bisby 2006; and Dong et al, 2010)): early damage detection; improved understanding of in-situ structural behaviour; assurances of a structure's strength and serviceability; improved maintenance and management strategies for better allocation of resources; reduction in downtime.

SHM is a multidisciplinary system integration approach, which involves some components, for instance, sensing technology, power technology, communications technology, storage technology, signal processing, and health evaluation algorithm. The system should be competent in providing information on demand about the status of a structure. Detailed information is required to be provided on each particular component of the system due to their effects. Here, more information is given on sensors component since sensors are essential to a successful SHM system, which is the first part of condition evaluation.

The Data acquisition DAQ system, which is also called data-logger, is the onsite system where signal demodulation and storage of measured data are conducted before being transferred to an offsite location for analysis. The specific types of sensors should be selected for a project depending on sensor ability to measure the desired response, such as strain gauges, accelerometers and anemometers. Mechanical quantities, thermal quantities and electromagnetic/optical quantities are examples of some measurable quantities (Büyüköztürk and Yu, 2003). Mechanical quantities are for instance, displacement, velocity, acceleration, pressure, force/torque, twisting, strain, rotation, distortion and flow. Thermal quantities are for example, temperature and heat. Whereas, electromagnetic/optical quantities are for instance, voltage, current, frequency phase, visual/images and light. It is worthwhile to mention that the sensors communicate with the DAQ system by either wired or wireless connection. Sensor gains its popularity after its emergence mainly owing to its relatively low cost as well as higher reliability compared to the traditional inspection methods. Wired sensor technique is often useful for the structures that are small and in which the structure is physically in touch with the sensors. While in wireless sensor technique, the sensors are not in physically in touch with the structure (Dhakal et al., 2013).

Wired sensors are commonly used to monitor the dynamic responses of many buildings, including the Chicago Full-Scale Monitoring Program (Smart wireless sensor networks, 2015). In this type of technique, sensors are placed throughout the structure and then wired to a central data acquisition device (data logger). Figure 2.2a shows schematically the layout for wired sensors technique. The wired system has been applied to a wide range of structures, and it has proved to be exceptionally reliable and practical technique. However, it suffers from two serious problems associated with its cables. Firstly, instrument cables are very costly as well as difficult to deploy and maintain in certain circumstances. Secondly, lengthy cables serve as antennas, allowing noise to infiltrate the system (Kijewski-Correa et al., 2006; Kwon et al., 2011). With a large number of sensors employed in the system, the amount of cable involved will increase accordingly.

As a consequence of wired sensor system shortcomings, contemporary developments invest in the wireless sensing field. Wireless sensors connection is required for some high-rise building structures where long lead cables are impractical, or lead cable transmitted excessive noise might corrupt sensor signals. Figure 2.2b exhibits the architectural design for a wireless sensor network system. A key aspect of wireless sensor network is its capacity to accommodate dense sensing mesh because the system is independent of multiple cables. Hence, multiple cables are limited by the number of channels existing in a data acquisition system (Wenzel, 2009).
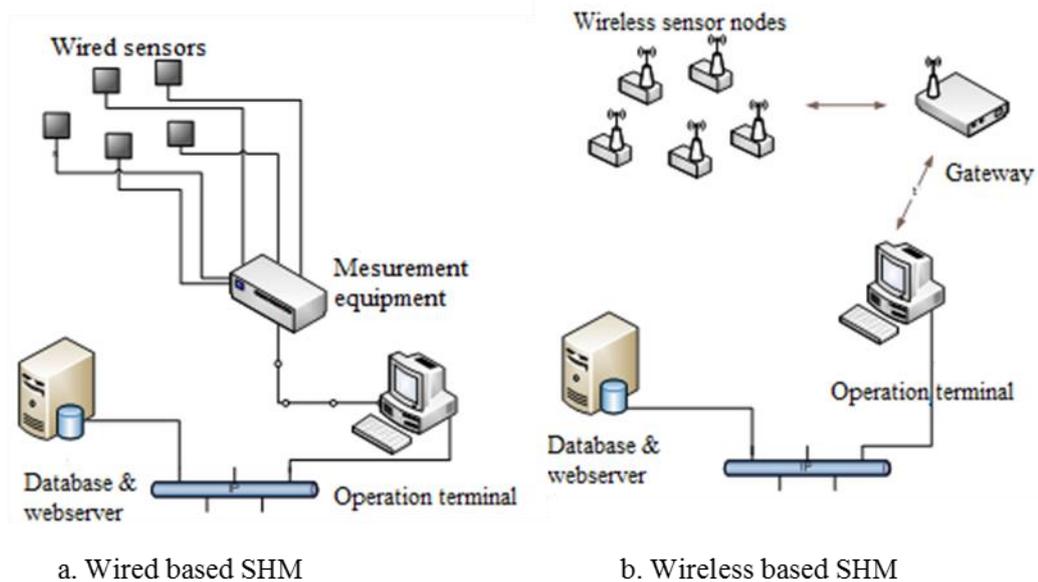
Figure 2.2: Typical configuration of wired and wireless based SHM system (after Smart wireless sensor networks, 2015).

In addition to aforementioned explanation on wired and wireless sensors, wired sensors can be employed for different materials. For instance, if sensors are used for detecting a flaw in concrete structure it can also be utilised in the steel structure. Conversely, in wireless sensor technique, a sensor is restricted to one type of material. For example, if one smart sensor are manufactured to detect a fault in concrete structure it cannot be used for steel structure (Dhakal et al., 2013).

2.2   Damage Detection

Damage detection of structures is commonly defined as one of the essential parts of SHM. Damage is defined as a change in a structure which affects structural

characteristics because of weakness. Occurring changes within a structural system negatively influence on the current and then the future performance of that system. Damage is not really meaningful without comparison between two different states of the same system, one of which is intact (undamaged) and other one is the damaged state (Sohn et al., 2004). Therefore, by comparison between these two states, the reduction which is caused due to damage or any other weakness will be revealed. For instance, cracks that form in structure produce changes in its stiffness. The dynamic behaviour of the system is altered because of stiffness reduction. Gaining wide acceptance based on the idea that deficiency modifies both the physical properties (mass, stiffness and damping) as well as its modal properties (natural frequencies, damping ratios and mode shapes) of a structure. The reduction in stiffness not only depends on the size of the deficiency, but also on the location of the deficiency. As a consequence, damage detection in structural systems requires the identification of the location and also quantification of the degree of damage. The process of damage detection in structures at the early stage plays a crucial role to prevent sudden failure of structural components (Sinou, 2009). This is why special attention has been paid to detect the damages in recent years using different non-destructive techniques.

Rytter (1993) defines that there are four classification levels of damage identification in any inspection process.

- Level 1: Determination of the present of damage in the structure (Damage detection).

- Level 2: Level 1 plus determination of the geometric location of the damage (Damage localisation).

- Level 3: Level 2 plus quantification of the severity of the damage (Damage quantification).

- Level 4: Level 3 plus prediction of the remaining service life of the structure (Prediction and health assessment).

By diagnosing dynamic characteristics of a structure from EMA or similar other technique, targets problems such as level 1, level 2 or level 3 can be identified. However, level 4, which is related to the prediction of remaining service life the decision, is required to be taken to evaluate the need of the structure for repair and/or replacement. This level is typically based on fatigue life analysis and fracture

mechanics measurement; and also may require more accurate sensors and further mathematical tools leading to the life estimation of the structures (Kiremidjian et al, 1997).

2.3   Damage Simulation Techniques

Damage simulation techniques are widely used in the field of Vibration Based Damage Identification Techniques (VBDIT). Comprehensive review of damage/crack simulation techniques have been given by Dimarogonas (1996) and Ostachowicz and Krawczuk (2001). Some broad categories of damage simulation techniques have been defined which frequently employed by researchers.

Friswell (2007) defined three different damage simulation techniques such as: local stiffness reduction; discrete spring elements; and complex models in two or three dimensions. Local stiffness reduction approach can be achieved in different ways. It is therefore the simplest among all three different simulation techniques. Local stiffness reduction can be achieved either by creating a notch type damage or reducing second moment of area (I) or the Young's Modulus (E).

Owolabi et al. (2003) used notch type damage simulation technique by thin saw cuts. During their experimental study, the authors aimed to detect cracks in aluminium beams using frequencies and amplitudes. Similar technique has been used by Dackermann et al. (2011) in multi-story buildings. Frequency response functions were used as the input parameter to artificial neural networks to identify damage locations and severities. Theoretically, numerical modelling of a complex two storey frame structure inflicted with notch type damage of different locations and severities was created using ANSYS software and analysed under ambient vibration. The results show that the suggested algorithm is capable of precisely and reliably identifying damage in complex multi-storey structures.

Shih et al. (2009) used the finite element software SAP2000 to model both steel beams and plates. Undamaged and damaged simply supported 1-span, 2-spans and 3-spans steel beams with the same span length of 2.8 m were set up. Single and multiple flaws with two different size of 10mm x 5mm and 20mm x 5mm (length x depth) on the previously tested beam were simulated, where the selected damaged elements were removed from the bottom of the beams in the FE models. The damage simulated technique in their work was adopted from the paper published by

Cornwell et al. (1999), where the loss of the stiffness was simulated by reduction the flexural rigidity (EI) of the structure. The plate-like structures were divided into elements in both directions. In the first and second cases studied, the stiffness of four elements was reduced by 25% and 10% respectively. The results revealed that the algorithm was able to locate the areas with stiffness reductions as low as 10% using relatively few modes.

Zhou (2006) conducted the experimental study of vibration-based damage detection (VBDD) techniques in structural health monitoring (SHM) of bridge. Small-Scale damage was induced on the top surface of the deck of a simple span bridge. The form of damage induced in the physical bridge system was small square cubes of concrete, 100x100x25 mm, which were physically removed from the top surface of the deck. Damage on the surface of the deck was induced incrementally at nine different locations. The experimental work consisted of estimating the dynamic properties of the intact system, and then incrementally inducing a new state of damage and determining the properties associated with each state. Results of the study demonstrated that the five non-model vibration-based damage detection techniques (e.g. change in mode shape, the mode shape curvature, the change in flexibility, the change in uniform flexibility curvature methods, the damage index were adequate for detecting and locating damage on a simply supported bridge deck or bridge girder.

Regarding the crack damage, two type of damage, namely saw-cut, and honeycomb damage, were adopted in the experimental work conducted by Wang (2010). Three levels of damage severity in reinforced concrete beam, namely light, medium and severe damage, were created by a saw-cut. The light damage was of 5mm long and 50mm deep. The cuts were 5 mm $\times$ 100 mm and 5 mm $\times$ 150 mm for medium and severe damage respectively. In this cases, the cracks were located at 1/4, 3/8, and 1/2 span of the beam. Regarding the honeycomb damage scenario, the damage was created by replacing concrete with a polystyrene hexahedron block of size 89 mm (length) $\times$ 75 mm (width) $\times$ 100 mm (height) during the casting process. The honeycomb damage is located at 3/4 span of the reinforced concrete beam. The aim of the work was to localise the damage and estimate its severity based on a combination of mode shape and mode shape curvature. The proposed method was able to identify the location of damage and quantify its severity with high reliability.

There are some forms of damage induced in the physical system. As it is mentioned, a small square cube of concrete can be physically removed from the top surface of the model. In other cases, damages might be created by a saw-cut or it is created by replacing concrete with a polystyrene hexahedron block. When concrete is physically removed from the model, this may cause some extra damage to other parts of the specimens. Therefore replacing concrete with a polystyrene hexahedron block during the casting process is an appropriate way for damage induced. This type of damage does not cause any hurt to the specimens. As a consequence, replacing concrete with a polystyrene hexahedron block during the casting process was used in this study.

2.4   Non-destructive Damage Detection Techniques

Structural damage identification technique has gained increasing attention from the scientific and engineering communities because the unexpected structural collapse may cause both catastrophic economic and human life loss. A reliable and effectual non-destructive damage identification technique is essential to sustain safety and integrity of structures. Non-destructive damage identification techniques can be classified as either local or global damage identification methods (Doebling et al. 1998).   As previously mentioned that, example of local damage identification techniques are ultrasonic methods and X-ray methods. Whereas vibration-based damage identification method is an example of global damage identification technique.

Great attention and development has been paid to global damage identification method due to limitations of local damage detection methods. This is due to the fact that, for local damage detection methods, the vicinity of the damage should be known before damage detection and the location of damage being inspected should be easily accessible. However, the information regarding damage is not always available before damage detection and damage location may be inaccessible. Therefore, global detection methods is not only developed to detect unknown and inaccessible damage, but also to facilitate analysis of such damage in complex structures.

After reviewing non-destructive damage detection methods, several challenges can be found to provide Level 1 and Level 2 damage identification (Lee et al., 2004).

However, there are just a few articles addressing Level-3 damage identification, including damage location and severity estimates. When vibration-based methods are coupled with a structural model, Level 3 damage identification can be obtained in some cases (Li et al., 2007).

Owing to advantages of vibration-based damage detection methods, especially simplicity for implementation, they have attracted most attention during the last decades. These methods are generally relies on the fact that the dynamic characteristics, such as the modal frequencies, mode shapes, and modal damping have direct relation to the stiffness of the structure (Ručevskis et al., 2009). Thus, occurring change in dynamic characteristics implies a loss of the stiffness.

Vibration-based damage identification methods could be mainly divided into two categories, namely model based and non-model-based (Farrar and Doebling 1997; Huang et al., 2012). On the other hand, Lee et al., (2004) classified vibration-based damage identification methods into four main categories which differ from each other in the features used in the damage detection process. These methods are presented in Table 2.1. Another broad classification has been presented by Bakhary (2008), who classified damaged identification methods into three categories: namely, direct methods, model updating methods, and Artificial Neural Network (ANN) methods. In a separate study, Wang (2010) classifies such techniques into three broad categories, such as methods based on vibration, methods based on artificial Intelligence and methods based on wavelet analysis.

Table 2.1: Damage detection categories and methods as proposed by Lee, et al., 2004).

Category		Methodology
Modal Parameters	Natural Frequencies	Frequency changes
		Residual force optimisation
	Mode shapes	Mode shape changes
		Modal strain energy
		Mode shape derivatives
Matrix Methods	Stiffness-based	Optimisation technique
		Model updating
	Flexibility-based	Dynamically measured flexibility
Machine learning	Genetic Algorithm	Stiffness parameter optimisation
		Minimisation of the objective function
	Artificial Neural Network	Back propagation network training
		Time delay neural network
		Neural network systems identification with neural network damage detection
Other techniques		Time history analysis
		Evaluation of FRFs

The author of this study decided to present the literature review in the following subcategories, which is relevant to the focus of the research or future development of the work. The subcategories are listed as follows.

1- Method based on Modal Parameters

- Natural frequency changes based method

- Mode shape changes based method

    1- Direct mode shapes
    2- Mode shapes curvature

- Damping changes

2- Method based on Artificial Neural Networks ANNs

2.4.1   Modal Parameters Based Method

Modal parameters such as natural frequency and its corresponding mode shapes and modal damping are the essence of global assessment to identify the dynamic behaviour of the selected structures. Modal parameters play key roles in classifying the structures according to their properties because the values and changes in these parameters signify altering the physical properties (mass, damping and stiffness) and boundary conditions of structures (Farrar et al., 2001; Owen and Pearson, 2004). Chen et al., (1995) indicated that changes in the stiffness of a structure, among physical properties, dominate the conditions of adequacy and safety of structures. In studying vibrations, the most popular modal parameters which are used in the damage identification are modal frequencies and mode shapes (Hearn and Tesa, 1991).

2.4.1.1   Natural Frequency Based Method

Picking the natural frequency to evaluate the existence of deficiencies in a structure is the earliest and most popular approach. Use of this technique has received wide acceptance due to some reasons: Firstly, a single sensor is sufficient for many applications whereby natural frequencies are determined or even they can be conveniently estimated from just one accessible point on the structure. Therefore, using natural frequencies as damage or deficiencies detection method are relatively low cost and ease of implementation. Secondly, natural frequencies are usually less contaminated by experimental noise. The existence of damage, deterioration, delamination and de-bonding in a structure poses obvious alterations in the natural frequencies of that structure (Salawu, 1997). For damaged /undamaged structure of given dimensions, the natural frequency is mainly related to the stiffness of the system. For a given length and moment of inertia of a structure, the equivalent modulus of elasticity of a structure can be estimated. In other words, the basic feature for detecting damages in a structure is changing the natural frequency.

Most of the early works related to natural frequencies shifts were based on very simple structures and structural elements (Adams et al., 1978). One of the pioneered papers on the use of natural frequencies shift in damage detection, which was most commonly quoted, is published by Cawley and Adams (1979). They mentioned that a single point in a structure can be used to detect and quantify damage using changes in frequencies. Since then, a considerable amount of research has been

carried out to detect damage using changes in frequencies. A large amount of literature on this subject was discussed by Salawu (1997) and Doebling et al. (1998).

Ndambi et al. (2002) performed an experimental test in order to evaluate the correlation between the progressive cracking processes in reinforced concrete beams. For this purpose, two types of tests were combined on two RC beams of 6 m long. In the first experiment, static loading test was performed to gradually introduce the cracks in the RC beams as shown in Figure 2.3. The two loading configurations were different and allow to introduce a symmetrical or an asymmetrical (case a or b) test, with the beams simply supported. Each loading step was followed by unloading and removed of the beams supports. Then, the second experiments were performed, which was the dynamic tests, on the same suspended beam with a simulated free-free boundary condition. It was concluded that Eigen frequencies were affected by accumulation of cracks in the RC beams. However, their evolutions were not influenced by the crack damage locations. It was also concluded that if the Eigen frequencies decrease monotonically during the cracking process, the severity of the damage was allowed to be followed.
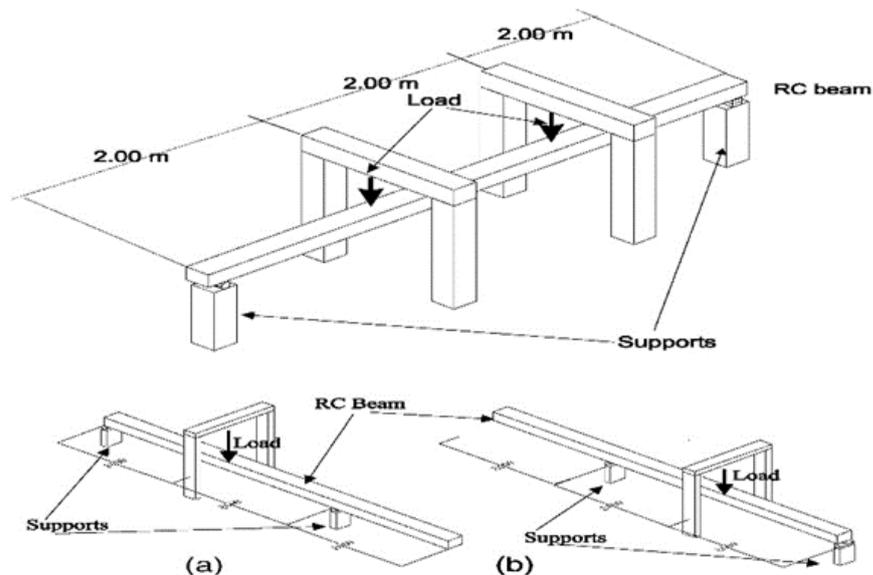
Figure 2.3: Static loading test, symmetrical and asymmetrical loading configurations (after Ndambi et al., 2002).

It is worthwhile to highlight that the natural frequency parameter is practically more accurate to be collected than the incomplete measured mode shapes (Shi et al., 2000). In addition to detect damages, natural frequencies changes have been used to detect delamination (Gadelrab, 1996; Sultan et al., 2012), de-bonding (Paolozzi and Peroni, 1990; Kim and Hwang, 2002) and determination of elastic constants (Deobald and Gibson 1988; Bledzki et al., 1999).

Wahab and De Roeck (1997) studied the effect of temperature on the modal parameters of a prestressed concrete highway bridge, which was excited under a drop weight and ambient vibration. The dynamic response of the bridge was recorded at two different times: the first reading was in the spring (May 1997) when temperature around 15ºC and in the winter (January 1997) when temperature around 0ºC. After analysing and interpreting the change in natural frequency of the bridge, the results showed that a decrease was about 4-5% due to the increase in temperature. The authors concluded that the effect of fluctuating temperatures should be taken into account for damage detection in a structure using natural frequencies.

However, the feasibility of damage identification using natural frequencies is occasionally limited for some reasons. The first drawback of methods is that very precise measurements are required for damage which association with low frequencies (Doebling et al., 1998). The second drawback is that natural frequencies are affected by fluctuating environmental changes such as temperature or humidity. Hence, very small changes in natural frequencies could be undetected due to measurement errors. Depending on natural frequencies alone to detect damage may lead to unrealistic predictions (Maeck and De Roeck, 2002). Accordingly, besides natural frequencies changes, it is better to employ further methods such as mode shapes and damping to enhance damage detection ability.

In order to obtain clear evidence of damage, recent development has been employed to couple the measurement of natural frequencies with other modal parameters. For example, Garesci et al. (2006) presented a methodology for identifying the presence of damage and its location. In utilised method, combined Experimental Modal Analysis (EMA) and Finite elements method (FEM) data were employed to localise the damage on mechanical components. Their method assumed a linear behaviour of the materials and compare Eigen values and eigenvectors obtained from FE

modelling with experimental Eigen values on damaged specimens. The method was firstly applied on regular shape, such as rectangular steel plates which had a milled slot in different positions, to check its reliability for discovering damages in homogeneous and isotropic material. Afterwards the method was applied to irregular shape, such piston rod. The results of the tests show that the developed method was able to accurately identify the damaged zone. However, an appropriate choice of scale for the graphic output was required to obtain clear evidence of damage detection.

Mohan et al. (2014) proposed correlation in cantilever steel beam model based on natural frequency change. Numerical models of an intact cantilever beam with four different damage locations have been modelled using finite element method. After meshing the model, the model has been divided into 50 elements. The damaged were created at element 4, 20, 33 and 49 starting from the fixed end as shown in Figure 2.4. Reduced mass was considered to incorporate as damage in the study. Damage Location Assurance Criteria (DLAC) was adopted Mohan's study for damage assessment. It was concluded that four damage scenarios chosen for damage location were exactly matched using the DLAC correlation. However, it was shown that support had an effect on the results when the damage was closer to the support.
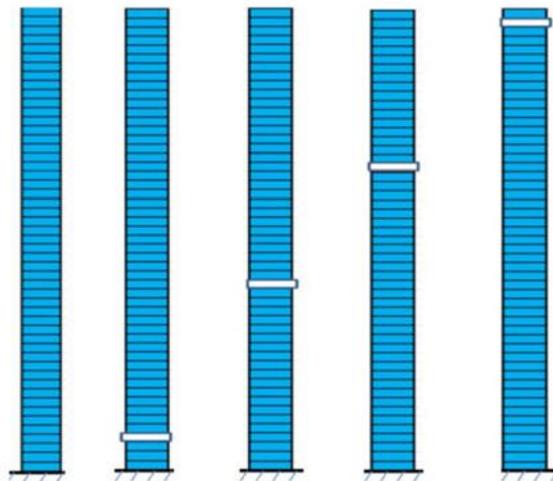
Figure 2.4: Undamaged and damaged cantilever models (after Mohan et al., 2014).

2.4.1.2   Mode Shape Based Method

As mentioned before, depending on the natural frequency changes alone for identifying damage location in structural may not be sufficient because frequencies are more global in nature, and the existence of cracks at two different locations with similar lengths may cause the same amount of frequency change. In contrast, mode shapes have obvious advantage for a unique identification of the damage. In addition, damage detection is local phenomenon and natural frequency is global property of the structure and therefore it is less sensitive to local change in a structure. Employing the mode shapes which is known local property of a structure and they are more powerful for damage detection than natural frequency (Farrar and Doebling, 1997) and they are less sensitive to the environmental effects, such as temperature, than natural frequencies changes (Farrar and James, 1997; Ko et al., 2003). Moreover, mode shapes are not only more sensitive to local damages than natural frequencies, but also have direct capability of multiple damage detection due to containing local information. However, using mode shapes for determining the damage location are not easy to be utilized because large number of measurement are required to precisely characterise mode shape vectors. It is noteworthy to mention that various number of damage identification methods have been existed and developed based on direct mode shapes or other properties such as curvature or modal strain energy as reviewed in the following sections.

a.   *Direct Comparison of Mode Shape*

Two commonly used methods are available for direct comparison between two sets of mode shapes, for example, the Modal Assurance Criterion (MAC) (Allemang and Brown 1983) and the Coordinate Modal Assurance Criterion (COMAC) (Lieven and Ewins1988). The value of MAC can be measured as the similarity of two mode shapes and takes a value 0 and 1. MAC value of 0 is dissimilar match and a value of 1 means the two mode shapes are completely similar. While, the COMAC is a pointwise measure of the difference between two sets of mode shapes, which compares them at each degree-of-freedom or node. It gives an indication of the contribution of each degree of freedom to the MAC for a given mode pair. That is why consistency of modes needs to be established a priori using MAC or even similar criterion. The value of COMAC takes a value between 0 and 1, and a low

COMAC value would indicate defect at a point. Therefore mode shape is a promising indicator for damage location.

Two-lane reinforced concrete Highway Bridge of 104 m six-spans was tested before and after repairing by Salawu and Williams (1995) in order to investigated any correlation which may exist between the repair works and changes in dynamic properties of the bridge. The results showed that the substantial changes of MAC values leading the authors to conclude that among modal parameters, comparison of mode shapes can provide much more information and thus is more encouraging method for damage detection.

The examples of studies and applications focus primarily on MAC and COMAC values to identify damage are provided by Salawu (1995), Yoo et al., (1999) and Foti (2013). It is important to mention that extensive publications review dealing with the detection of damage in structures and their components through MAC are presented by Allemang (2003), and through MAC and COMAC together are provided by Jassim et al., (2013).

Iliopoulos et al. (2015) found that prediction of dynamic responses on a monopile Offshore Wind Turbine (OWT) was mandatory because the turbines are becoming structurally more flexible. Three numerical mode shapes using ANSYS software as shown in Figure 2.5 with three experimental mode shapes using modal decomposition and expansion approach were extracted. Three mode shapes of the wind turbine on a monopole foundation in the Belgian North Sea were evaluated using a limited number of vibration sensors. To check the accuracy of the numerically with experimentally obtained mode shapes, the MAC was utilised to compare these two types of obtained mode shapes. The results indicated that there is good agreement between the modes obtained from the measurements and the modes computed from the FEM analysis using ANSYS software.
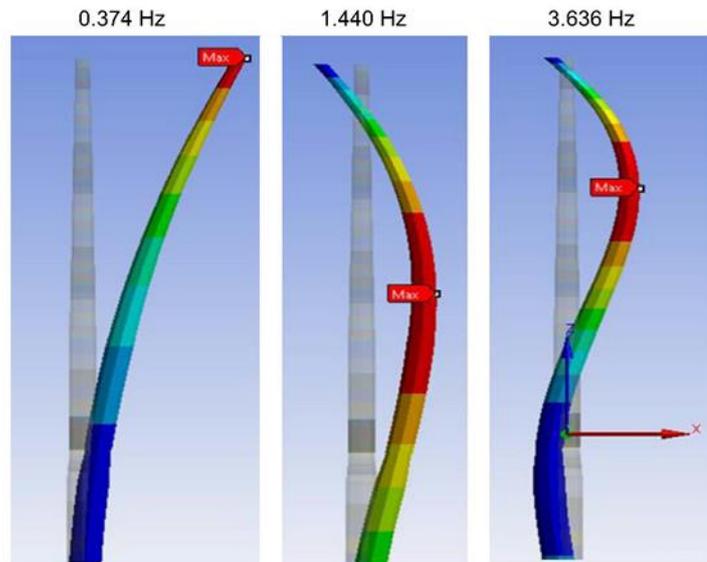
Figure 2.5: Wind turbine modes with their corresponding frequencies obtained through
modal analysis in ANSYS (after Iliopoulos et al., 2001).

Chen et al. (2014) performed dynamic analysis of cantilever beam. At ten evenly
spaced positions along a cantilever beam, the acceleration signals were
experimentally measured. The authors examined how Vibro-impacts influence the
low and high frequency modes in global and local senses. The statistical measures
such as the MAC and COMAC were calculated. MAC and COMAC were
calculated by obtaining information about the mode shape. MAC values are more
affected by induced defects. Therefore, MAC can provide a global aspect of damage
occurrence in the model. Whereas, the COMAC values can narrow down the
locations of damages.

b. Mode Shape Curvature Based Methods

Using mode shape derivatives, such as curvature is an alternative way to obtain
spatial information about sources of vibration changes. There is direct relationship
between curvature and bending strain for beams, which are mathematically
represented as (Carrera et al., 2011):

$$\varepsilon = \frac{y}{\rho} = \kappa y \qquad (2.1)$$

where:

ε is strain

28

y   is transverse displacement of structural element

ρ   is radius of curvature

κ   is curvature.

Additionally, using the finite difference method is a common way to find derivatives of a continuous function at discrete points. The accuracy of the derivative depends on the number of surrounding points and even depends on used type of difference method. The central difference approximation, as defined as Equation (2.2), is commonly used to successfully compute the curvature of continuous deflection mode shape, whereby the location of damage is detected.

$$y'' = \frac{y_{i+1} - 2y_i + y_{i-1}}{(\Delta x)^2}$$

(2.2)

where:

Δx   is the length of the element.

y'' is second derivation of displacement (curvature)

Since difference between intact and damaged mode shapes of a structure occasionally could not give clear damage location as demonstrated by Ismail et al., (1990), it is necessary to employ mode shape curvature based method to localize the damage. This method relies on the fact that the maximum difference in a mode shapes occur within the vicinity of the region where damage presence (Zhang and Aktan, 1995). It is possible to cause change in more than a region. It is therefore, only mode shape curvature can provide an indication of multiple damage locations (Salawu and Williams, 1994). For these reasons, the second derivative of displacement is considered a feasible way and considerably more sensitive to find small crack location than natural frequencies and even mode shape itself (Farrar et al., 2001; Jassim et al., 2013; Foti, 2013).

Pandey et al. (1991) proved the correlation between the changes in mode shape curvature and the local loss of the stiffness with an assumption that damages in structure are typically related to cause changes in the stiffness and not to the mass matrix. The authors initiated this concept using change in mode shape curvature as an index of reduction in the flexural rigidity (EI) value of the beam cross-sections.

The given expression is the curvature at any point of a beam element can be expressed mathematically (Carrera et al., 2011).

$$y'' = \frac{M}{EI}$$

(2.3)

Where:

M   is bending moment

E   is modulus of elasticity of the material making the beam

I   is moment of inertia of the beam cross section

Modal curvature and modal flexibility differences for identifying and localising damage in reinforced concrete beam were employed by Dawari and Vesmawala (2013). Finite element analysis using ANSYS was used to model the undamaged reinforced concrete beam model. The dimensions of the beam were 3660 mm in length, 300 mm in depth and 150 mm in width. Honeycomb damage was considered as a reduction in reinforced concrete beam at specific location. Honeycomb damage was then identified by comparing the typical dynamic properties of the intact and damaged beams. After applying modal curvature and flexibility difference methods, it was concluded that these methods effectively detected the existence of damage. Moreover, they can locate the position of single and multiple damage scenarios for reinforced concrete beam. Also, results exhibited that mode shape curvatures differences were observed to be effectively localised to the region of damage. The highest curvature difference for each of the damaged cases happened in damaged zone. The difference increased with increase reduction in stiffness (damage intensity) of the damaged region. More sensitivity to damage was observed in the higher modes.

It is concluded from theses paragraphs that the absolute changes in the curvature mode shapes are not only used for damage detection, but also for damage localisation. The changes in the mode shape curvature increase with increasing size of damage. This information implies that in addition to the pervious feature of mode shape curvature, it can be used to estimate the severity of damage in the structure.

2.4.1.3   Damping Based Method

In addition to natural frequencies and mode shapes, damping has been proposed as another sensitive indicator for existence of deficiencies (Montalvao et al., 2008). Pandey and Biswas (1994) pointed out that damping in the structures was increased owing to occurrence of cracks or localised damage. Zhang and Hartwig, (2004) recommended that damping in the evaluation of damage process which seemed more sensitive than the natural frequencies that associated with stiffness. Similarly, Saravanos and Hopkins (1995) experimentally showed that delamination had a profound effect on modal damping of composite beams. Although, many authors recognize that modal damping parameter can be used as damage index, this is not widely used like other measurements in localisation problems.

Razak and Choi (2001) performed modal tests on three full-scale reinforced concrete beams. One of them was used as undamaged, control while the other two were subjected to the different state of reinforcement corrosion, which used as damaged. The states of damage in the beams were assessed through measurement of both crack width and spalling. Corrosion damage and structural capacity details are presented in Table 2.2. Changes in the modal damping ratio for the Transfer Function Method (TFM) and the Normal Mode Method (NMM) were also observed as displayed in Figure 2.6. It was concluded that modal damping of the second and third modes implied a consistent indication with the severity of the corrosion damage in the beams.

Table 2.2: Corrosion damage and structural capacity (after Razak and Choi, 2001).

Beam	Crack width [a]	Degree of concrete [b] cracking/spalling	Loss of Area [c] %	Failure load kN
D1	5.0	Very slight spalling	7.77	28.59
D3	1.0	Moderate cracking	7.65	41.85
Control	-	-	-	66.64

where:

[a]   is average major crack width due to corrosion

[b]   is evaluation of degree of concrete cracking/spalling

^c   is a percentage of material loss by direct measurement
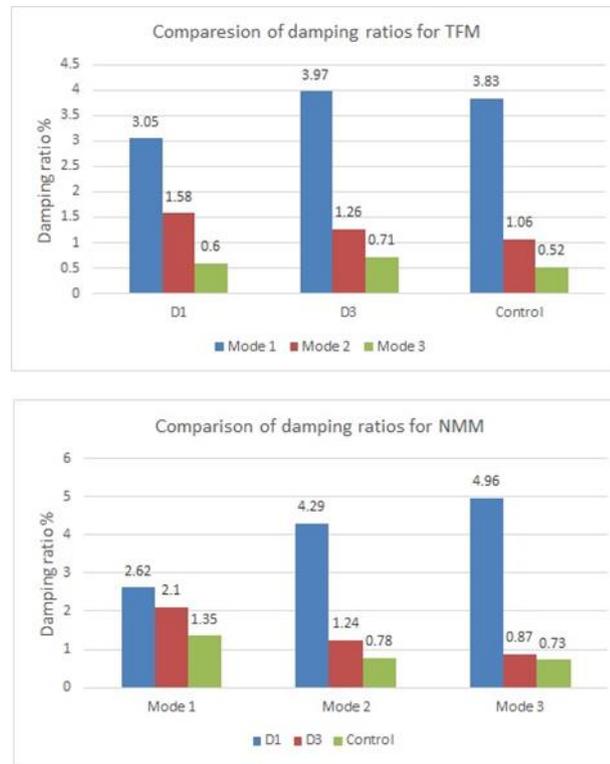
Figure 2.6: Comparison of damping ratio for three modes using TFM and NMM (after
Razak and Choi, 2001).

Another successful application of damping identification was reported. In some
cases, evidence suggests that damping is quite sensitive to damage in structural
elements. It is even more sensitive than natural frequencies. For example, Modena
et al. (1999) concluded that visually undetectable cracks cause slight or negligible
changes in natural frequencies and they require higher mode shape to be detected.
However, the same cracks cause considerable changes in damping that can be
conveniently employed to localise the cracks in reinforced concrete elements. The
authors justified that the use of damping changes in the building may directly be
sensitive to a local loss of stiffness.

Gomaa et al. (2014) conducted both theoretical and experimental modal analysis of
steel beam. Experimental modal analysis (modal testing) consists mainly of impact
hammer, accelerometers, and analyser with its consultant software installed on a
laptop. The three cases were employed including free-free vibration, simply
supported boundary condition and simply supported boundary condition with the

concentrated static load. A cut in lower beam flange at mid-span of the steel beam was created as artificial crack. The effect of natural frequency, damping factor and mode shape to change of steel member condition was studied. The theoretical modal analysis was performed using the finite element analysis software ANSYS. The obtained results such as natural frequencies and mode shapes were compared with experimental ones. The numerical damping ratios were computed from improved FE. The variation of damping ratios according to mode number in case of undamaged and damaged beam is illustrated in Figure 2.7. The results showed that modal parameters may be used to identify structural damage with saving time. It was concluded that the damping ratio is more sensitive than natural frequency. Therefore, damping is considered as a good damage indicator.
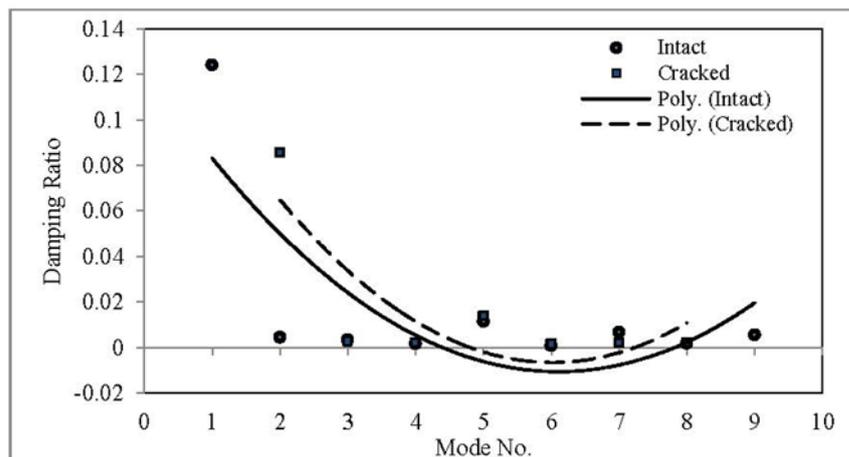
Figure 2.7: Variation of damping ratios according to mode number in case of intact and cracked beam (after Gomaa et al., 2014).

Another successful application highlighted damping as a promising damage indicator which was presented by Curadelli et al. (2008). The main purpose of their research was to detect structural damage by means of the damping coefficient identification employing a wavelet transform. Two methods namely numerical simulations as well as laboratory tests were used in the study. The results showed that structural damage alters obvious changes in damping coefficient and therefore it can be conveniently employed for damage detection.

Havaldar and Chate (2015) investigated the damping properties of pure materials such as Cork Material, Polyurethane foam, Aluminium, and of laminated sandwich composites such as Glass fibre reinforced plastics (GFRP) materials. The modal damping ratios for the fundamental mode of the sandwich panel's structure from both analytical and experimental technique were determined. The damping ratio for the sandwich panels were predicted by using a mathematical expression, which depends on the physical and geometric dimensions of the samples. The modal test was conducted on the materials specimens with free-free vibration conditions. All the sandwich specimens were subjected to impulses through a hard tipped hammer while the response was measured through the accelerometer. The sample was subjected to impulses at 25 different locations. The obtained results were then validated with experimental modal testing results and found to be in good agreement. The comparison between theoretical and modal testing results gave impetus towards understanding damping mechanisms in composite systems.

Even though consistency in changes of damping values have been noted previously and many researchers believe that damping is a reliable indicator for damage detection, some others draw a different conclusions. For instance, Slastan and Pietrzko (1993) explained that values of modal damping were not sensitive to give sufficient information about damage in concrete beams. Moreover, Salawu and Williams (1995) tested two reinforced concrete highway bridges before and after repairing. The results showed that identifiable pattern was not caused the changes in damping values by the repairs. Furthermore, it was concluded through other study that, in modal parameters estimation procedures, the damping values usually have the utmost degree of suspicion. Therefore, depending on damping values alone is incapable and may not provide a reliable denotation of damage detection (Williams and Salawu 1997).

Soltis et al. 2002 utilised vibration testing techniques for inspecting timber structures. Component systems such as floor systems were evaluated rather than individual members. The behaviour of three floors was assessed. Two floors were constructed with new joists, and one was with salvaged (recovered from a demolished) joists having some deterioration, checks, and splits. The practical considerations required in the inspection of three timber floor systems could be extracted through natural frequency and damping ratio. It was concluded that both

frequency and damping ratio were good indicators of decay. However, the natural frequency could be estimated more precisely than the damping ratio. The effects of deterioration in the recovered floor system were identified by a decreasing the frequency and increasing damping ratio compared to that of a new floor.

It seems quite clear that the use of damping coefficient towards damage detection has achieved much research interest by some researchers. There are couple of successful applications of damping as reported by a group of researchers. However, other group of researchers have indicated that the damping coefficient is not sensitive to detect the damage in the structures. As a result, damping coefficient is a controversial factor in the damage detection of the systems. Since this topic is still controversial, it is taken into account in this research to further explore the characteristics of such method.

Notwithstanding of advances in vibration-based damage detection methods of some laboratory experimental implementations and numerical simulations, limited progress has been published in the field of reinforced concrete structures. Very limited progress is due to the main obstacles in field applications. There are some obstacles associated with the uncertainties, for example, measurement noise; error due to limited measurement points and the complexity of civil structures or their materials. This is manifest by the fact that less research and development has been published for reinforced concrete structures in terms of damage detection method. It is, therefore, essential to investigate effects of some important parameters on the behaviour of the reinforced concrete slab and develop a novel robust and reliable technique to detect, locate and quantify the damage.

2.4.2   Artificial Neural Network

Artificial neural networks (ANNs), or Neural networks (NNs) are computational models which comprise of simple possessing units. These units communicate with each other over a large number of weighted connections by sending signals. ANNs were originally developed from the human brain's conception (Kumar, 2014 and Sharma et al., 2012). One of the distinct characteristics of these networks is their qualification to learn from experience and examples and then to adapt with nature, changing situation to solve the problems (Rafig et al., 2001). By the derivation of back propagation in 1986, the modern era of ANNs was ushered. Since then,

extensive amount of literature on the topic of neural networks has been written. In this study, a brief history of ANNs is presented to highlight their starting and evolution. In addition, a detailed review on neural network application in civil engineering problems is discussed.

2.4.2.1   Brief History of Neural Networks

The first step toward artificial neural networks can be traced back to the work of trying to model the neurons. The first model of a neuron was by a neurophysiologist and a young mathematician, McCulloch and Pitts (1943). They wrote a paper on how the McClloch-Pitts Neurons work. The created model had two inputs and a single output. The bad feature of this model was that the weights for each input were fixed and therefore the model was not able to learn from the examples, which is the important feature of the ANNs technique (Kumar, 2014). This concept of neurons was reinforced by Hebb (1949) when he proposed a learning scheme for adjusting a connection weight as explained in the book entitled "Organization of Behaviour". It is important to note that Hebb's law is one of fundamental learning rules in neural network realm. Rochester from IBM research laboratories led the first effort and worked on simulation of neural network with particular emphasis on using computers (McCarty et al., 1955). Rosenblatt (1958) proposed the perception model which is the first model for learning with a teacher, for instance supervised learning. The perception model had weight adjustable by the perception learning law. Widrow and Hoff (1960) proposed a model was called ADALINE (ADAptive LInear NEuron) network for computing elements. In addition to the model, they proposed learning algorithm was called LMS (Least Mean Square) to adjust the weights of the model. Both Perception and ADALINE models had the same basic structure, except that the transfer function of ADALINE was linear, instead of hard limiting. Hopfield (1982) not only created a simple model but also create useful devices. With mathematical analysis, the operation of a certain class of recurrent ANNs (Hopfield networks) was explained. Besides showing how such networks work, what these networks did was also known. As a consequence, several events were more responsible for the re-birth of ANNs in that moment. Rumelhart et al. (1986) announced the discovery of method that allowed adjusting the weight of a multilayer feed forward neural network in a systematic way in order to learn the

implicit mapping in a set of input and output patterns pairs. The learning law method was called, backward propagation of errors, a generalization of the LMS rule. The Institute of Electrical and Electronic Engineers (IEEE) held the first international conference on neural networks on 21-24, 1987, in San Diego, California. The first journal article was published on neural network application in civil engineering in Computer-Aided Civil and Infrastructure Engineering journal by Adeli and Yeh (1989). Since then, a considerable amount of neural networks research have been published on civil engineering applications. The neural network is not only developed in civil engineering realm but also in different field of sciences and becomes the hot topic everywhere.

2.4.2.2   Artificial Neural Network Based Methods

One of the important aspects of structural characteristics to be defined is the presence of defects and their severity whereby the life expectancy of structures may be known. This generally requires knowledge of the structural model in great detail which is not always possible. Artificial Neural Networks (ANN) derived from studying the physiology of groups of neurons or nerve cells which emerged as one of the effective computational model in pattern recognition, classification and identifying the faults in structural systems (Pandey and Barai 1994).

In addition to self-organisation and learning capabilities, ANNs can provide several advantages on structural damages detection application which are (Bakhary, 2008).

- Different vibration parameters can be employed as an input data for ANNs. This implies that with certain flexibility both inputs and outputs can be chosen without making any complexity of the training algorithms.
- ANN can exhibit considerable tolerance of noisy, which is particularly useful when the data are expected to be uncertain and noise corrupted.
- ANN has capability to detect damage even though the trained data are predictable to be incomplete.
- ANN calculation is comparatively fast and no need to be constructed after proper mathematical modelling and training.

It is important to mention that the two main steps in ANN model are training and testing stages. In training stage, a network is crucial to be trained by data of different damage cases using a proper training algorithm to recognize the changes of

the structural characteristics. Through a training process, ANN is capable to estimate the relationship between inputs and outputs and then keep within the connection strengths (Wu et al. 1992). However, in the testing stage, the set of data that required for knowing their situation are needed to be tested. In order to test the data, the trained ANN is fed with input data which has not been used in the training process. Therefore, the basic strategy in applying ANN for damage detection and classification is needed to test the network with intact cases to check the capability of the network to the known outputs (Fang, et al., 2005).

The multilayer perceptron (MLP), trained with the back-propagation technique and its rival radial basis function (RBF) are the most common neural network architecture (Bishop, 1995). A much more discussion and details on the algorithms and properties of ANNs can be followed in reference (Bishop, 2006). Adeli (2001) conducted extensive research and summarised comprehensive review of ANN in civil engineering application.

In a research carried out by Kudva et al. (1991), MLP neural networks was used to identify damage on a plate, by applying a static uniaxial load to the structure. The gained readings from a strain gauge were used as input to the neural network, while the location and size of a hole used as outputs. Damage was modelled by cutting holes of varied diameters. Although difficulty was experienced in predicting the size of a hole, the results show that the neural network was able to predict the error location prior to failure. The neural network successfully identified the size of a hole. This is due to the reason that strain values is unable to provide unique representation of damage location and severities.

Wu et al. (1992) published the first journal article to detect damage from dynamic parameters by employing MLP neural network to identify damage in a model of a three-story building. Damage was modelled by reducing the stiffness of the member from 50% to 75%. The Frequency Response Function (FRF), between 0 and 20Hz, of acceleration data used as the input vector, while binary number,1 and 0, were used as the output to represent the level of damage in each member, damaged and undamaged conditions, in a simulated three-story building. The network was able to diagnose damage within 25% accuracy.

Worden et al. (1993) applied MLP neural network to classify damaged and undamaged of an experimental framework structure. Twenty-member structures in

term of a binary number are identified. The strain of twelve members was used as input to the neural network. It is important to say the network was trained by using data from the finite element FE model. It was suggested that ANN should be trained using noise-corrupted data to produce better classification results if experimental data were employed.

Masri et al. (1996) carried out a study for the detection of changes in the characteristics of unknown system of structure based on a back propagation ANN. The model was trained to detect the abnormality in a linear and nonlinear single degree of freedom. This is also regarding the effect of different lengths of vibration to check the performance of the network. In order to monitor the health of the structure, the network was trained and fed from comparable vibration measurements under different condition of the same structure. The relative velocity and displacement were used as the input to the network, whereas the output was the restoring force. It was shown that even when the vibration measurements were noise-polluted; this approach was still capable to identify changes in the characteristics of the structure. In addition, the results showed that when longer vibration signature was utilised as the input, better training network and prediction performances were obtained. This means that more information given to the network during the training can provide better prediction results for the tested data. However, there was not specific guideline to identify the proper length of the vibration signature for the training and testing. The application of this method was experimentally applied by Masri et al. (2000) on nonlinear multi-degree of freedom system.

Two popular networks, the multilayer perceptron (MLP) with the back-propagation and the radial basis function (RBF) were applied by Rytter and Kirkegaard (1997) to discerning damage of full-scale four-story RC building. Both of the networks consisted of one input, hidden and output layers. It is important to note that the test of the building was conducted at the European Laboratory for Structural Assessment (ELSA) under earthquake, which was generated by a pseudo-dynamic testing method. A finite element model of the building was utilised to simulate random damage, reduction in the stiffness of the members at each floor, to generate data sets for training the neural network. The relative changes in the frequencies and the mode shapes of the frame element, the beams and columns, were used as inputs, and

the relative bending stiffness were used as outputs. It was concluded that the MLP neural network demonstrated the ability to detect damage and therefore it was recommended to be used as a damage identification tool. The authors stated, however, that the RBF network was not completely successful in this aspect.

Important progress has followed by many researchers, thereby moving forwards the practice of RBF neural networks technique in structural health monitoring SHM. For example, Levin and Lieven (1998) applied a RBF neural network and modal properties to identify errors in the FE model of a cantilevered beam. It was concluded that this technique was advantageously able to identify the faults not only with limited number of experimentally measured degrees of freedom and modes but also with the presence of noise in the data.

Kondru and Rao (2103) numerically modelled cantilever beam using ANSYS Software to evaluate first three natural frequencies for different crack parameters and used as input to the neural network. Back propagation neural network was attempted to identify depth and location of crack, see Figure 2.8, as the outputs which were main parameters for the vibration analysis. The ANN was trained with different nine groups. The Back propagation neural network could identify damage depth and length at which damage occurred within 73.3% and 73.2% accuracy respectively. If the network was further trained more accurate results could be achieved in detecting crack efficiency.
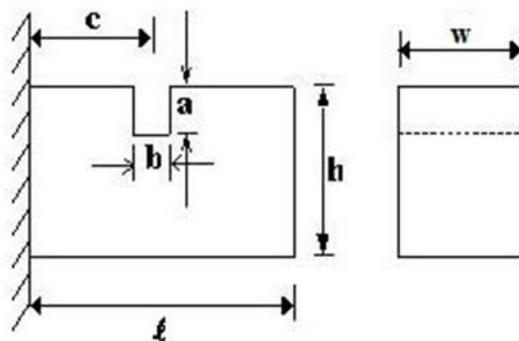
Figure 2.8: Cantilever beam with crack specifications (after Kondru and Rao, 2013).

where:

a   is crack depth

b   is crack width

c   is crack location

ℓ   is beam length

w   is beam width

In 2014, Razaviet et al. investigated the load-deflection analysis of the RC slab strengthened with Carbon Fiber Reinforced Polymer (CFRP). Their method was based on Feed-Forward Time Delay Neural Network (FFTDNN). A model was developed to predict the mid-span deflection of the slabs. Six reinforced concrete slabs of dimension 1.8×0.4×0.12 m with a similar steel bar were used. These slabs strengthened with different length (700, 1100 and 1500mm) and width (50 and 80mm) of CFRP. The strengthened slabs were tested and then compared with similar samples without CFRP, control. Using MATLAB software, the load-deflection results were uploaded, normalised, and converted to a time sequence parameter. Time, loading and the effect of the different CFRP strip lengths on the slab moment of inertia were utilised as the input to the network; and mid-Span deflection was used as the output. From 122 load-deflection data, 111 of which employed for training while the rest 11 data employed for testing. The results of the proposed model ascertain that the generated FFTDNN was able to predict the load-deflection analysis of the slabs with a correlation of 0.98. The ratio between predicted deflection of the slabs by using the feed-forward neural network and the experimental result was in the range of 0.92 to 1.23. A sample of the obtained and predicted load-deflection of the slab can be found in Figure 2.9.
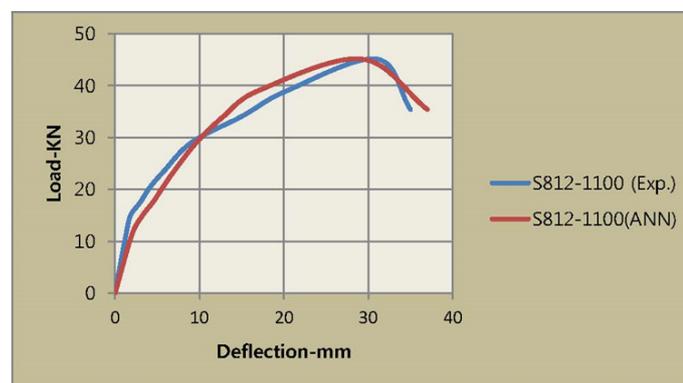
Figure 2.9: Comparison between target and predicted load-deflection of beam had length (1100mm) and width (80mm) (after Razavi et al., 2014).

Another strategy to detect damage under varying temperature influence using artificial neural networks was proposed by Kostic and Gül (2015). The Purpose of their work was to detect damage of numerical footbridge model under temperature effects. A numerical model of a typical footbridge based on two typical damage cases was analysed. The artificial neural network was employed, where temperature measurements were used as the input to the neural network. The outputs of the neural network were used for determining damage features. It was concluded that the model with variable temperature load gives satisfactory results for detection, localization, and estimation of the structural damage.

Although Zang and Imregun (2001a) proposed different techniques to reduce the size of data as input variables, they exploited a Principal Component analysis (PCA) to reduce the size of Frequency Response Function (FRF) as the input variables to ANNs instead of using full-size. The output of the ANN model was a prediction for the actual state of the railway wheels, whether it was healthy or damaged. The original FRF data was having 4096 spectral lines. The FRF were grouped in x, y and z direction and a compression ratio was achieved for each direction of around 400. Three different ANN models, each corresponding to coordinate direction, were trained with 80 FRFs samples, while 20 compressed FRFs cases were used for testing. The results show that it was possible to correctly classify all the damage cases between healthy and damaged. In 2001b, Zang and Imregun published a paper in which they described the application of FRF to detect damage severities and location.

Nguyen et al. (2015) identified damage in a concrete arch beam replica section of the Sydney Harbour Bridge. Comprehensive laboratory testing and numerical modelling were undertaken to validate the method. Acceleration measurements were recorded from impact testing technique for damage cases and then derived to obtain residual frequency response function. Then, these were compressed into dimensionally smaller data size using PCA. The local damage was inflicted to the specimen with four different damage cut lengths (damage severities). The commercial ANSYS software was utilised to carry out the numerical analysis. A numerical model was performed to simulate the experimental setup as well as to introduce more damage cases to the model. A limited number of damage cases were utilized to train the ANNs, and the residual damage cases were employed to test the

models. The compressed data of both intact and damaged cases beams were used as input to the ANN. The ANN outputs were designed to render the length of damage cut (damage severity). The results of the experimental showed that the testing cases were successfully capable for interpolating among the trained cases applying the compressed FRF data of the Sydney Harbour Bridge. Moreover, a numerical model was created to generate additional damage cases to be trained in the ANN model. It was concluded that training the ANN models with extra damage cases enabled the model to capture better relationship between the input and output of the network which improved the interpolation capabilities of the ANN models.

2.5   Research Problem

Over the past decades, an excessive number of technical articles were published on structural health monitoring (SHM), which has attracted considerable attention in both research and development. The available technical articles highlighted that there are two main damage identification techniques such as local and global methods (Zapico and Gonzalez, 2006). In the former method, the assessment of the state of a structure is performed either by direct visual inspection or using experimental techniques, for instance ultrasonic, radiography, eddy current and magnetic particle inspection. The main drawback feature of all these methods is that their applications require a prior localisation of the damaged zones. Therefore, the limitations of the local methods can be overcome by using vibration-based methods, which give a global damage assessment. The available technical articles highlighted that there are a number of vibration-based methodologies have been found in the recent literature that are used to detect, locate and quantify the damage in various types of structures.

The most common vibration damage detection techniques seem to be based on experimental modal parameters. Among theoretical vibration-based techniques, numerical model updating and neural network based methods have recently gained popularity. It is accepted that there is no yet an appropriate perfect method to be utilised for identifying, locating and estimating the severity of damage in structures by exploiting the vibration data. Furthermore, no algorithm has yet been suggested to apply globally to detect any defect in any structure (Wenzel, 2009). The development of powerful damage detection and location algorithms based on

response monitoring data of an in-use structure is still a challenge. Therefore, the availability of powerful damage detection technique will open the door to more accurate estimation of the remaining life of a structure (Friswell, 2007).

The amount of literature covers non-destructive vibration methods treating damage scenarios in beam structure is extensive. However, limited literature has been found for damage scenarios of plates and slabs. Most existing methods are based on materials rather than concrete, such as metal and composite mercury. Moreover, most researchers demonstrate these methods mainly on automotive structures and their systems and components (Huang et al., 1997; Storck et al., 2001).

From the literature review, it is manifest that there is limited published research papers on using modal analysis to detect damage in reinforced concrete structures, particularly reinforced concrete slabs member. Hence, the existing technical papers do not provide adequate information on behaviour of reinforced concrete slab with defected and subjects to gradually concentrated loads. Therefore, this research treats the problem of damage evaluation in reinforced concrete square slab in order to understand the behaviour of reinforced concrete slabs and ensure their integrity and safety. In addition to investigation, the effects of some important parameters on the behaviour of the reinforced concrete slab member, it is essential to develop a new robust and reliable artificial intelligence technique to detect void in RC slabs. There is, thus, a need for a comprehensive and reliable modal analysis implementation and artificial neural network for behaviour assessment of reinforced concrete slabs, which is the primary aim of the current proposed research.

The present investigation provides a novel methodology to deal with the current problems of damage detection in RC slabs. From the initial research in the literature review, the common limitations of modal analysis technique on reinforced concrete structural system, can be summarised as:

1- It is noted that changes in natural frequencies alone may not provide enough information for integrity monitoring (Farrar and Cone 1995). That is why three modal parameters of reinforced concrete slabs have been extracted.

2- In the process of performing damage detection method, some researchers prefer natural frequencies as the most indicator to identify and estimate the severity of damage to the structures. While, others prefer the modal damping ratio. Therefore, both frequencies and modal damping ratio based damage

44

detection method are applied to reinforced concrete slab in this research. This is to emphasise which idea that mentioned above is more powerful for detecting damage in RC slab.

3- It is found that one of the most common vibration-based damage detection techniques focusses on changing of mode shapes. Therefore, the mode shapes change method is chosen for damage localisation in this thesis as their corresponding algorithms can be equally applied to different structural members, for example, beams, plates, trusses and their coupled structures.

4- Damage detection and condition assessment of civil engineering structures is considerably important, during their life, especially when the building is old or is suspected to have been subjected to overloads. A wide range of civil engineering structures is of unknown history. This is another problematic obstacle confronts the use of the vibration-based monitoring systems in civil engineering structures (Wenzel, 2009). Therefore, data from a real-life as-built model of the structure is commonly unavailable. As a consequence, a prediction of a numerical model using commercial software for the original intact condition will serve as a basic guide to which the deviation of present measurements is finally compared with it. Therefore, theoretical methods using closed form expression and numerical using ANSYS software in this study are performed alongside each other to ascertain validity and reliability of the experimental modal parameters.

5- Small damage induced poised changes to the mode shapes, but it may not be obvious visually. Therefore, two sophisticated statistical methods for damage identification, which are vital steps in higher level of damage detection in structures can be utilised namely MAC and COMAC techniques. They are used to identify the degree of damage in one group of the slabs, while to indicate the location of damage in other group.

6- Since there is not available artificial neural network (ANN) for void size classification of RC slab in the literature, it will be used in this study. The numerical results using ANSYS software can be used as input to the ANN for training to identify damage presence. The proposed damage identification and condition assessment procedure fills the gap of knowledge and it enhances the reliability and usefulness of ANN based slab diagnosis systems. The accuracy of void size identification in slab using ANN is then checked.

2.6   Summary

This chapter started with a brief introduction on Structural Health Monitoring (SHM), followed by the basics of damage detection and damage simulation technique, specific to structural members. A brief description of previous reviews and surveys of non-destructive damage detection methods, particularly, vibration-based damage detection was introduced. Furthermore, the method based on modal parameter were briefed, including the important explanation of the three parameters of damage detection, such as, natural frequency, damping ratio and mode shape. Then, global non-destructive vibration based damage detection methods was extensively reviewed. In addition to experimental work, some relevant work using the finite element to model the structures was highlighted.

It is clear from the literature review that despite promising research has been performed on non-destructive vibration based damage detection in the engineering field including reinforced concrete structures, there are still many challenges before making the models practical. Besides, non-destructive modal based damage detection method which is sensitive to the presence of damage in aerospace and reinforced concrete structures. There are limited research on its sensitivity to the presence of damage in reinforced concrete slabs. Therefore, non-destructive vibration based damage detection needs to be extended and extensively used in reinforced concrete slabs. The final section of this chapter embarks on the research problem by discussing the investigations of model-based damage identification methods. This section presents a brief description of investigation in the field of reinforced concrete structures, particularly reinforced concrete slabs member and knowledge gaps.

3. Theory of Modal Analysis

3.1 Introduction

Modal analysis (MA) is a method used to estimate the structure's dynamic characteristics such as natural frequencies, damping values and mode shapes. It generally consists of experimental (using Impact or mechanical shaker) and theoretical (using Finite Element Method) modal analysis. It is either used as complementary or stand-alone technique, depending on some important aspects, including time, cost, and nature of the structure and availability of the analysis tools. Experimental Modal Analysis (EMA), which is also called Modal Testing (MT), is the only method that can provide an understanding of the dynamic characterisation of structures under real mechanical conditions, under a known excitation (Maia and Silva, 1997). On the other hand, theoretical (analytical) modal analysis is mainly implemented to describe how the physical system relates to a mathematical representation that used to estimate the model parameters (Prader, 2012).

It is important to highlight that when depending on one method such as experimental analysis only, insufficient or probably wrong information might be obtained. The obtained data from the experiments are required to be analysed by comparing with different approaches. This is because it is difficult to understand, explain and even judge the outcome without comparing with the results of different approaches (Reynolds, 2000; Ewins, 2000). Conversely, the model in analytical analysis without experiments poses difficulties of the validation and verification results. Therefore, embarking on the problem through both experimental and analytical models is extremely important due to two reasons. Firstly, experiment results can be subsequently used to correct and update the analytical model. Secondly, a preliminary analytical model would help to carry out reliable measurements (Al-Ghalib, 2013).

As already mentioned, the modal analysis is the process comprising of experimental and theoretical analysis in order to estimate the dynamic behaviour of a structure in term of modal parameters such as the following. Firstly, natural frequencies indicate how much a structure oscillates, after ceasing the forces. It is a direct and inverse function of stiffness and mass respectively. Secondly, mode shapes are the

associated patterns of a structural deformations, each mode is related to its natural frequency. Finally, damping factors is known as an internal property of dissipating energy, and it plays a key role to gradually reduce the amplitude of oscillations.

Thus, modal analysis is really a crucial method and its key to better understanding is the ability to understand the relationships between both experimental and analytical models. Nowadays, the applications of this method is extended to a wide range of vibration field applications, including estimations of vibration behaviours; detection and identification of structural damage; assessment of the robustness of structures; correlations and updating of analytical models; modifications and corrections for design models; development of experimentally based models and development of specifications for the design and test practice (Maia and Silva, 1997).

3.2   Structural Dynamic Characteristics

Generally, the dynamic characteristics of a structure can be defined in three related presentations. Ewins, (2000) termed these related categories into three models, such as the spatial model, modal model and response model. The first phase in vibration analysis is referred as the spatial model which represents the physical properties of the structures, as determined by the mass, damping and stiffness properties. The second phase is referred as the modal model; this model always describes the various ways in which a structure will naturally oscillate without any external excitation. This description is provided in the form of modal parameters that included Eigen frequencies (natural frequencies), with corresponding Eigen vectors (mode shapes), and modal damping factors. Moreover, the response model in vibration analysis, which is the last phase, is a description of the manner in which the response of structure under the influence of an external excitation is analysed. This means that the latter vibration depends not only on the structure's inherent properties but also on the nature and magnitude of the induced force (Ewins, 2000).

The three models are related to each other, but they are different in presentations. The interrelations of the spatial model, modal model and response model are depicted in Figures 3.1, 3.2 and 3.3 respectively. The spatial model is determined by the physical properties of the structures, the mass [M], damping [C] and stiffness [K] matrices, each matrix of a dimension N x N. From the spatial model, Modal

model can be obtained by solving the Eigenvalue problem. The modal model comprises a set of modal parameters of N natural frequencies (ω_r) with associated N modal damping ratios (ζ_r) and N vibration mode shape vectors $\{\varphi_r\}$. The last phase, which is the Response model, is that where gives the response in the forms of Frequency Response Functions (FRF) or Impulse Response Function (IRF) , which is the resulting time response.
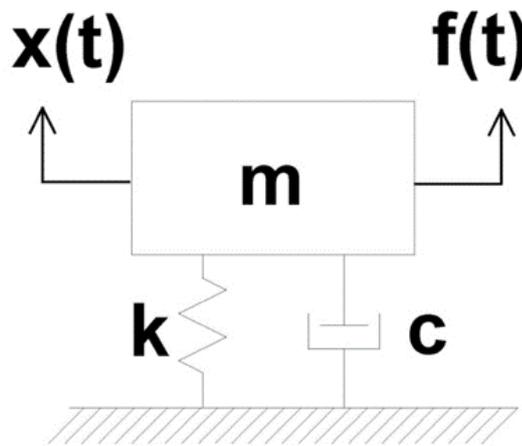
Figure 3.1: Spatial Model of a structural system (Avitable, 2012).

where:

    [M]   is mass matrix

    [K]   is stiffness matrix

    [C]   is viscous damping or structural (hysteretic) damping matrix

Matrices have NxN dimensions; N is number of degrees of freedom and is equal to number of equations of motion.
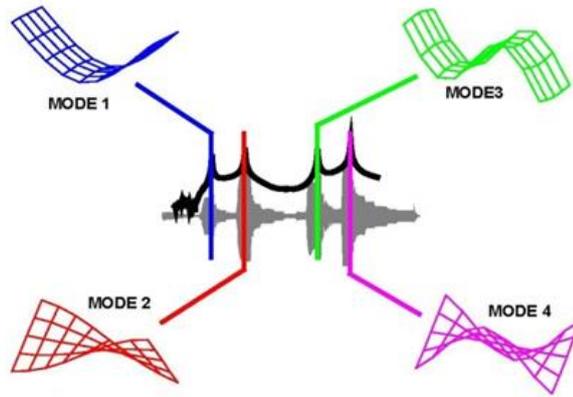
Figure 3.2: Modal Model of a structural system (Avitable, 2012).

where:

      (ωr) is natural frequency

      (ζ_r) is modal damping ratios

      $\{\varphi r\}$ is vibration mode shape vectors
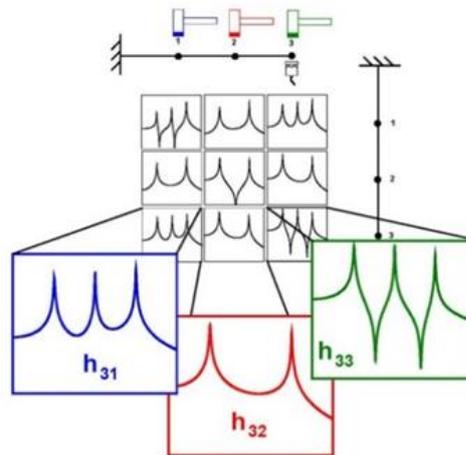
Figure 3.3: Response Model of a structural system (Avitable, 2012).

where:

$[H(\omega)]$ is matrix of frequency response functions (FRF)s, in terms of Receptance, mobility and accelerance. Or it is impulse response functions (IRFs)

50

3.3   Theoretical and Experimental Routes

In the common theoretical route as shown in Figure 3.4 it is possible to launch the description of the structure's physical properties, by introducing its stiffness [K], damping [C] and mass matrix [M], which is referred as the Spatial Model (structural model). Subsequently, the theoretical modal analysis, calculating the so-called Modal Model can be made from the spatial model, by using Eigen value problem. The last phase, which will give the Response Model, can be deduced from the modal model by employing transfer function.
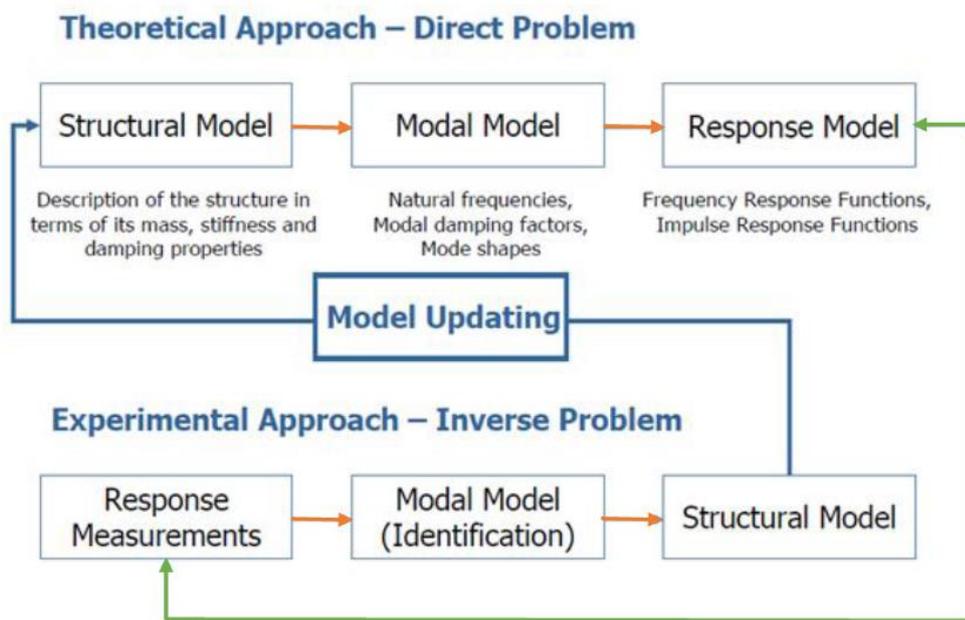
Figure 3.4: Interrelation between the various types of models in theoretical and experimental routes (after Golinval, 2009).

On the contrary, the experimental route is also called modal testing, as shown in the same Figure 3.4, starts by conducting a structure on a laboratory. Response model can be deduced from measuring response to a known excitation of the structure, the acquired data is analysed by using specific software. This model approach contains most of the interesting information about the response of a system which is represented in the form of FRF. Owing to complexity of FRF, it cannot be fully displayed on a single two dimensional plot. However, it can be presented in several formats, and each of which has its own uses. Then, the modal model can be calculated from the experimental data using the modal parameters estimation techniques. By using coordinate transformation, it is also possible to recovering the

spatial model from the modal model, modal parameters. This process can be done by proving the relations between the structural matrices and the modal parameters, which are expressed in Equation (3.1) (Ewin 2000).

$$[K] = \sum_{r=1}^{N} \{\phi\}_r^{-T} [\omega_r^2] \{\phi\}_r^{-1} \qquad (3.1)$$

where:

$\{\phi\}_r$ is mode shape vector

ω is natural circular frequency

3.4   Multiple Degrees of Freedom System

The mathematical formulation becomes much more complicated when more masses, spring, and damper are considered. Since most structural engineering systems are continuous and have an infinite number of degrees of freedom, they are more complicated than the Single Degree of Freedom (SDOF) system (single mass, spring, and damper system). Therefore, the general case for a Multiple Degrees of Freedom (MDOF) system will be utilised in order to explain how the frequency response functions of a structure are related to the modal vectors of the intended structure. Figure 3.5 shows a three story, single bay framed structure and has an infinite number of degrees of freedom.

(a)   (b)
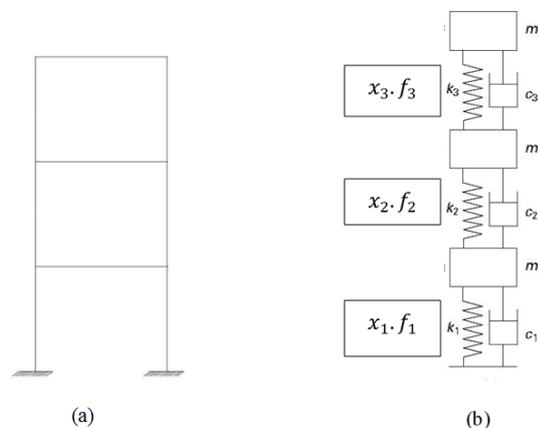
Figure 3.5: Three story building system (a) reinforced concrete building (b) modelled 3 degree of freedom.

One common method of a continuous system, as a MDOF system, involve considering the geometry of the system by a large number of elements. By considering a simple solution within each element, the principle of both compatibility and equilibrium are employed to find the approximate solution to the original system, as many as necessary to ensure enough accuracy. Therefore, such analysis always entails an approximation which characterises the behaviour of the structure through the use of a finite number of degrees of freedom.

Another method of a continuous system is when replacing the distributed mass or inertia of the system by a finite number of rigid bodies or lumped masses. The masses are assumed to be connected with another one. The motion of the lumped masses is described by using linear or angular coordinates. These types of models are called, lumped mass, lumped parameter or discrete mass systems. Generalized degrees of freedom are the minimum number of coordinates necessary to describe the deformed shape of the System. Figure 3.5a indicates a three degree lumped mass model which represents the three story building as shown in Figure 3.5b. To study the dynamic behaviour of a multi-storey frame in the x direction, the generalized coordinates x_1, x_2, x_3 can be considered. The general equation of motion of the assumed free body diagram of the three masses is expressed in matrix form by Equation (3.2), (Ewins, 2000).

$$[M]\{\ddot{x}(t)\} + [C]\{\dot{x}(t)\} + [K]\{x(t)\} = \{f(t)\} \tag{3.2}$$

where:

$\{\ddot{x}(t)\}$ is the acceleration vector

$\{\dot{x}(t)\}$ is the velocity vector

$\{x(t)\}$ is the displacement vector

3.5   Frequency Response Functions

The frequency response function (FRF) is the most commonly used measurement to identify the inherent dynamic characteristics of a mechanical structure. For this reason, the estimation of the FRF is substantial processing of experimental modal

analysis. Modal parameters such as frequency and its associated mode shape and damping are extracted from FRFs measurements. FRF are normally used to describe the input-output (force-response) relationship between two points of any system as a function of frequency. Both excitation and motion have direction associated with them since they are vectors quantity. This type of function is an indication of how much acceleration, velocity or displacement response has at an output DOF per unit of excitation force at an input DOF. On this basis, the FRF contains all the essential information that the unknown modal parameters to be obtained to characterise a system.

$$FRF = [H(W)] = \frac{Response}{Excitation}$$

Generally, experimental modal analysis as shown in Figure 3.6 involves exciting and measuring the response of the structure. Excitation forces (by means of impact hammers) and the response (by means of accelerometers) associated to these forces over the structure are known. For a linear system in time history, the input-output (force-response) model of a system can be expressed mathematically, $\{f(t)\}$ as the input force, and $\{x(t)\}$ as the output response. McConnell and Varoto, (2008) describe the relationship between both the known input forces and output responses in the time domain, which is called Duhamel integral and it is expressed by Equation (3.3).
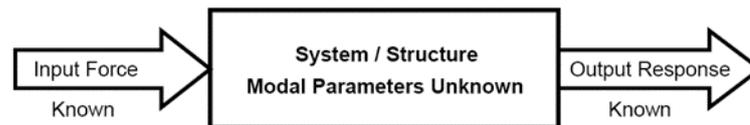
Figure 3.6: Experimental modal analysis, basic of both the known input forces and output responses.

$$x(t) = \int_{-\infty}^{t} f(\tau)h(t-\tau)d\tau \qquad (3.3)$$

The time domain recorded input-output signals ($f(\tau)$ and $x(t)$) are then transformed into the frequency domain, using Fast Fourier Transformation, which is much better to be understood than time domain (Avitable, 2012). In this work a special purpose subroutine was set using Matlab to carry out Fast Fourier Transformed process. Transferring time domain to frequency domain is explained in these three Equations (3.4), (3.5) and (3.6).

$$F(\omega) = \mathcal{F}[f(t)] \tag{3.4}$$

$$X(\omega) = \mathcal{F}[x(t)] \tag{3.5}$$

$$H(\omega) = \mathcal{F}[h(t)] \tag{3.6}$$

where:

$\mathcal{F}$ is used to represent the Fourier transform of the corresponding time signal.

The relationship between input-output and FRF for a linear structure in terms of frequency domain are subsequently expressed by (McConnell and Varoto, 2008).

$$X(\omega) = H(\omega)\, F(\omega) \tag{3.7}$$

Then, the frequency domain signals, referred as $F(\omega)$ and $X(\omega)$, are utilised to calculate both auto and cross power spectrum. This is achieved by multiplying the Equations (3.4) and (3.5) by the conjugate of the input frequency spectrum, $F^*(\omega)$. The computed auto spectrum of the input is referred $S_{ff}(\omega)$, while the computed cross power spectrum of the input and output is referred $S_{fx}(\omega)$. Auto and cross power spectrum are formulated by Equations (3.8) and (3.9) respectively.

$$S_{ff}(\omega) = F^*(\omega)F(\omega) \tag{3.8}$$

$$S_{fx}(\omega) = F^*(\omega)\, X(\omega) \tag{3.9}$$

It is worthwhile to mention that the computed auto and cross spectrums are employed to estimate the corresponding FRF, as defined by in Equation (3.10) and (3.11).

$$F^*(\omega)\, X(\omega) = H(\omega)F^*(\omega)F(\omega) \tag{3.10}$$

$$H(\omega) = H_1(\omega) = \frac{S_{fx}(\omega)}{S_{ff}(\omega)} \tag{3.11}$$

where:

$S_{fx}(\omega)$ is the dual-sided cross-spectrum between input and output

$S_{ff}(\omega)$ is the dual-sided auto-spectrum of the input excitation signal

$H(\omega)$ is the frequency response function

It is important to mention that cross and auto spectrum are computed by multiplying Equations (3.4) and (3.5) by the conjugate of the output response spectrum, $X^*(\omega)$, Thus, $H_2(\omega)$ can be expressed as:

$$H(\omega) = H_2(\omega) = \frac{S_{xx}(\omega)}{S_{xf}(\omega)} \tag{3.12}$$

$H_2(\omega)$ is the second estimate of $H(\omega)$ which is obtained by dividing auto-spectrum of the output response by the cross-spectrum between output and input.

where:

$S_{xf}(\omega)$ is the dual-sided cross-spectrum between output and input

$S_{xx}(\omega)$ is the dual-sided auto-spectrum of the output response signal

The coherence function $\gamma^2(\omega)$ is a verification check which shows the linearity between the output signal and the input signal for each frequency. Using such function, the degree of correlation between the two types of $H(\omega)$ can be specified through the following equations.

$$\gamma^2(\omega) = \frac{H_1(\omega)}{H_2(\omega)} \tag{3.13}$$

$$\gamma^2(\omega) = \frac{|S_{fx}(\omega)|^2}{S_{ff}(\omega).S_{xx}(\omega)} \tag{3.14}$$

The FRF contains both magnitude and phase information. The former is typically shown on a logarithmic Y axis in dB scale, while the latter is often shown on a 0 to 360 degree scale.

3.5.1   Frequency Response Components

Consider a single-degree-of-freedom system subjected to a force excitation, which can mathematically be expressed by equation (3.15).

$$m\ddot{x} + c\dot{x} + kx = F \tag{3.15}$$

By dividing both sides of Equation (3.15) by the mass.

$$\ddot{x} + \frac{c}{m}\dot{x} + \frac{k}{m}x = \frac{F}{m} \tag{3.16}$$

Knowing that:

$$\left(\frac{c}{m}\right) = 2\xi\omega_n \tag{3.17}$$

$$\left(\frac{k}{m}\right) = \omega_n{}^2 \tag{3.18}$$

Equation (3.16) can be re-defined as:

$$\ddot{x} + 2\xi\omega_n\dot{x} + \omega_n{}^2 x = \frac{\omega_n{}^2}{k}F \tag{3.19}$$

where:

ω_n is natural circular frequency in (rad/sec)

ξ is damping ratio

The Fourier transform for each side of the Equation (3.19) may be taken to derive the steady-state transfer function for the absolute response displacement. After doing some mathematical manipulations, the resulting transfer function is formulated by Equation (3.20).

$$\frac{X(\omega)}{F(\omega)} = \left[\frac{1}{k}\right]\left[\frac{\omega_n{}^2}{\omega_n{}^2 - \omega^2 + j(2\xi\omega\omega_n)}\right] \tag{3.20}$$

This transfer function represents output response to input force, which is sometimes called the receptance function. FRF can be presented in polar coordinates (amplitude, magnitude, vs. Frequency; and phase vs. frequency). These two sets of the transfer function can be mathematically represented by Equations (3.21) and (3.22) and graphically in Figure 3.7.

$$\frac{X(\omega)}{F(\omega)} = \left[\frac{1}{m}\right]\left[\frac{1}{\sqrt{(\omega_n{}^2 - \omega^2)^2 + (2\xi\omega\omega_n)^2}}\right] \tag{3.21}$$

$$\phi = arctan\left[\frac{2\xi\omega\omega_n}{\omega_n{}^2 - \omega^2}\right] \tag{3.22}$$
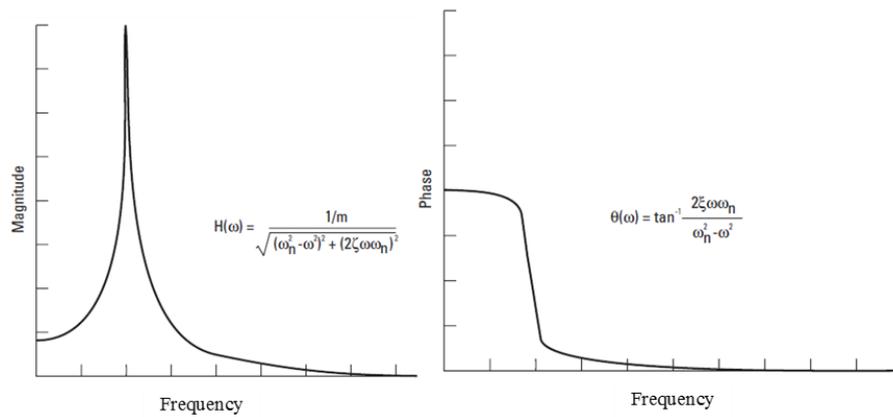
Figure 3.7: Frequency response - polar coordinates (Agilent Technologies, 2000).

Alternatively, FRF can be presented in rectangular coordinates (real part vs. frequency, and imaginary part vs. frequency), which are depicted in Figure 3.8.
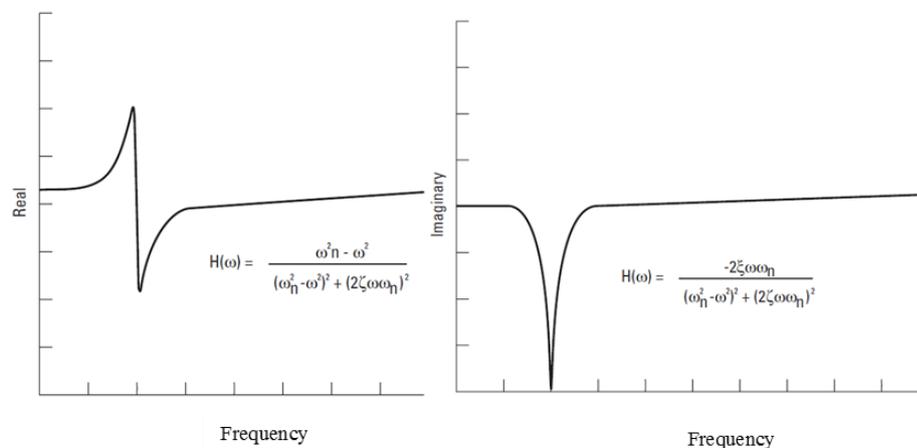
Figure 3.8: Frequency response - rectangular coordinates (Agilent Technologies, 2000).

It is important to note that in the polar coordinates presentation, as shown in Figure 3.7, the magnitude of the FRF reaches a maximum value at resonance, whereas the phase lag approaches 90^0. In the rectangular system as shown in Figure 3.8, the real part of the FRF is zero, while the imaginary part reaches its maximum value.

3.5.2   Formulation of the Frequency Response Function

It is worthwhile to note that the essential stage of the response model representation starts by solving a system of the forced vibration motion equations of the spatial form. It equates the mass, stiffness, and damping of the system to the applied external forces.

In the case of harmonic excitation, a steady-state solution is sought and the force excitation vector $\{f(t)\}$ and the corresponding response $\{x(t)\}$ can be expressed as follows:

$$\{f(t)\} = \{F\}e^{i\omega t} \tag{3.23}$$

$$\{x(t)\} = \{X\}e^{i\omega t} \tag{3.24}$$

where:

{X}   is the complex amplitude of the response; i.e. $\{X\} = \{x_o e^{i\varphi}\}$

{F}   is the complex amplitude of the force, i.e. $\{F\} = \{f_o e^{i\varphi}\}$

Both {X} and {F} are independent of time containing information on the Magnitude and Phase respectively.

The solution of the system of motion equations given in Equation (3.2) in the frequency domain constitutes the following formula:

$$[[K] - \omega^2[M] + i\omega[C]]\{X\}e^{i\omega t} = \{F\}e^{i\omega t} \tag{3.25}$$

In such form, the whole system motion equations can be represented by a single matrix. This matrix is specified as FRF matrix [H(ω)] and it is encompassed all system dynamic characteristics. The elements of this matrix are complex numbers

which contain both magnitude and phase. Each element in this matrix, $H_{ij}(\omega)$, represents the ratio of a response Xi, caused by a harmonic force Fj, as given below:

$$\{X\} = [H(\omega)]\{F\} \tag{3.26}$$

where:

$$[H(\omega)] = \left[[K] - \omega^2[M] + i\omega[C]\right]^{-1} \tag{3.27}$$

For the undamped system, [C] becomes null matrix. As a result, the solution of the system of motion equations given in Equation (3.27) in the frequency domain is specified as:

$$[H(\omega)] = \left[[K] - \omega^2[M]\right]^{-1} \tag{3.28}$$

Note that the three common formulations listed in Table 3.1 can all be considered the definitions of the frequency response functions and its inverse because each of these formulations can be numerically manipulated (differentiation and integration), which are easily obtainable from each other.

Table 3.1: Definition of common FRFs terms (after, McConnell and Varoto, 2008).

Response	Definition of FRF	Name	Inverse FRF
Displacement	$H(\omega) = \alpha(\omega) = \dfrac{displacement}{force}$	Receptance	Dynamic stiffness
Velocity	$Y(\omega) = \dfrac{velocity}{force} = i\omega H(\omega)$	Mobility	Mechanical Impendence
Acceleration	$A(\omega) = \dfrac{acceleration}{force}$ $= -\omega^2 H(\omega)$	Accelerance	Apparent Mass

3.5.3   Measuring FRF Matrix Rows or Columns

It is customary in modal testing to measure at least one row or column of the FRF matrix in order to develop the mathematical model. It is crucially required to represent the dynamic behaviour of a structure. Since the modal frequency and its associated damping are known as the global properties of a structure, they can be evaluated from any or all of the FRFs measurement in a row or column of the FRF matrix. On the contrary, mode shape is contained in every a row or column of the residue matrix. This means that assembling together FRF numerator terms (called residues) from at least one row or column of the FRF matrix are required to be measured in order to obtain the mode shapes. It is important to mention that nodal points or nodes are those nodes, DOFs, where a mode shape vector equals to zero. In practice, this phenomenon means that if the structure is excited or its response is measured at such points of the modes of interest, no FRF measurements from the row or column will contain a resonance peak (Schwarz and Richardson, 2003). To minimise the risk of missing mode shapes, the number of excitation points can be increased or the location of nodal points should be known. Once the positions of nodal points are known, excitation forces and the response measurements should not be positioned on such points for the previous reason.

Measuring a column of the [H] matrix as shown in red colour in Equation (3.29) is accomplished by using a single, fixed, input (exciter system) with a roving response (accelerometer). While measuring a row in such matrix is accomplished by using roving input (hammer) and a single fixed response.

$$
\begin{Bmatrix} X_1 \\ X_2 \\ X_3 \\ X_4 \\ \vdots \\ X_n \end{Bmatrix} = \begin{bmatrix} H_{11} & H_{12} & H_{13} & H_{14} & . & H_{1n} \\ H_{21} & H_{22} & H_{23} & H_{24} & . & H_{2n} \\ H_{31} & H_{32} & H_{33} & H_{34} & . & H_{3n} \\ H_{41} & H_{42} & H_{43} & H_{44} & . & H_{4n} \\ . & . & . & . & . & . \\ H_{n1} & H_{n2} & H_{n3} & H_{n4} & . & H_{nn} \end{bmatrix} \tag{3.29}
$$

3.5.4   Improving Measurement Accuracy

Several techniques can be employed to acquire the improved data quality. To attenuate the statistical variance of a measurement with a random excitation function

(such as random noise) and also to diminish the effects of nonlinearities, it is considerably essential to utilise an averaging process. By averaging the records repetition, statistical reliability can be significantly enhanced and random noise associated with nonlinearities can be obviously minimised. For each test and at each singular point, the dynamic testing should be repeated several times and the average of both excitation and response are then taken. The corresponding averaged FRFs are obtained, from the iteration of loadings, and then plotted. Plotting averaged FRFs is indicated to extract obvious modal parameters. As a consequence, more accurate representation of dynamic behaviour of the specimen under vibration is achieved.

The characteristics that used to select or reject certain frequencies of an input signal are called filtering, and a circuit inside an electronic device which does this is called a filter. It is a high-pass filter when gives easy passage to high frequencies and difficult passage to low frequencies. Conversely, it is a low-pass filter when gives easy passage to low frequencies and difficult passage to high ones.

In addition to averaging and filtering, obtaining more frequency resolution is another measurement capability that is often needed for increasing measurement resolution.

3.5.5   Modal Frequency Response Analysis

Modal frequency response analysis is known as an alternative method for computing the frequency response of a structure. This modal form uses the mode shapes of the structure. This is not only to minimise the size or uncouple the equations of motion, when modal or no damping is used, but also it makes the numerical solution more efficient than its alternative, which is a direct frequency response analysis. Therefore, it is considerably faster to be solved than the direct method. Once the modal responses are individually calculated, physical responses are then recovered as the summation of the modal responses.

Based on the modal frequency response, FRFs which is defined by Equation (3.30) can be written in different ways. To uncouple the equations, pre-multiply and post-multiply sides of the equation (3.27) by $[\Phi]^T$ and $[\Phi]$ to obtain Equation (3.30).

$$[\Phi]^T\big[[H(\omega)]\big]^{-1}[\Phi] = [\Phi]^T\big[[K] - \omega^2[M] + i\omega[C]\big][\Phi] \qquad (3.30)$$

where:

$[\Phi]^{\mathrm{T}}[\mathrm{M}][\Phi]$ is modal (generalised) mass matrix

$[\Phi]^{\mathrm{T}}[\mathrm{K}][\Phi]$ is modal (generalised) stiffness matrix

$[\Phi]^{\mathrm{T}}[\mathrm{C}][\Phi]$ is modal (generalised) damping matrix

Using the orthogonality property of the mode shape to formulate new form of equation of motion in terms of the generalised mass, stiffness and damping matrices as defined in Equation (3.31). If a damping $[\mathrm{C}]$ matrix exists, the orthogonality property of the modes does not diagonalise generalised damping and stiffness matrices, i.e.

$[\Phi]^{T}[K][\Phi] \neq diagonal$

$[\Phi]^{T}[C][\Phi] \neq diagonal$

$$[\Phi]^{T}\big[[H(\omega)]\big]^{-1}[\Phi] = [\omega_r^2 - \omega^2 + 2i\zeta\omega_r^2] \tag{3.31}$$

where:

$$[K] = \sum_{r=1}^{N}\{\phi\}_r^{-T}\,[\omega_r^2]\{\phi\}_r^{-1} \tag{3.32}$$

$$[M] = \sum_{r=1}^{N}\{\phi\}_r^{-T}\,[I]\{\phi\}_r^{-1} \tag{3.33}$$

$$[C] = \sum_{r=1}^{N}\{\phi\}_r^{-T}\,[2\zeta_r\omega_r]\{\phi\}_r^{-1} \tag{3.34}$$

Conversely, the modal flexibility matrix can be determined from a system stiffness matrix [K] as:

$$[F] = [K]^{-1} = \sum_{r=1}^{N}\frac{\{\phi\}_r\{\phi\}_r^{-1}}{\omega_r^2} \tag{3.35}$$

After doing some mathematical manipulations with equation (3.27), the system receptance matrix $[H(\omega)]$ can be expressed as:

$$[H] = \sum_{r=1}^{N} \frac{\{\phi\}_r \{\phi\}_r^{-1}}{\omega_r^2 - \omega^2 + 2i\zeta_r \omega_r^2} \tag{3.36}$$

In this representation, $H_{j,k}$ is the FRF in term of modal properties measured by exciting the system at DOF (k) and measuring the response at DOF (j). The notations $_{jk}$ refer to the ratio of the dynamic response at DOF (j) to the dynamic excitation at DOF (k). Similarly $H_{k,j}$ is the FRF in term of modal properties measured by exciting the system at DOF (j) and measuring the response at DOF (k). Likewise, H_{jk} and $H_{,kk}$ can be calculated by exciting the system at DOF (k) and measuring the dynamic responses at both DOF (j) DOF (k) respectively. The FRF for the damped system in term of modal properties can be defined in equation (3.37). However, the frequency functions for undamped system as specified in equation (3.38).

$$H_{jk}(\omega) = \sum_{r=1}^{N} \frac{\phi_{jr} \phi_{kr}^T}{\omega_r^2 - \omega^2 + 2i\zeta_r \omega_r^2} \tag{3.37}$$

$$H_{jk}(\omega) = \sum_{r=1}^{N} \frac{\phi_{jr} \phi_{kr}^T}{\omega_r^2 - \omega^2} \tag{3.38}$$

where:

    j   is this notation refers to the output degree of freedom (physical location and orientation).

    k   is this notation refers to the input degree of freedom (physical location and orientation).

Table 3.2: Relationship between the three models of an undamped dynamic system (after, Maia and Silva, 1997).

Derived from	To obtain		
	Spatial model	Modal model	Response model
Spatial model	-----------	$[[K] - \omega^2[M]]\{\phi\} = \{0\}$	$[H(\omega)] = \big[[K] - \omega^2[M]\big]^{-1}$
Modal model	$[M] = \big([\phi][\phi]^T\big)^{-1}$ $[K] = \big[[M][\phi][\omega_r^2][\phi]^T[M]\big]$	-----------	$H_{ij}(\omega) = \sum\limits_{r=1}^{N} \dfrac{\phi_{ir}\, \phi_{jr}}{\omega_r^2 - \omega^2}$ $[H(\omega)] = [\phi][\omega_r^2 - \omega^2]^{-1}[\phi]^T$
Response model	$[K]^{-1} = [H(\omega)]_{\omega=0|}$ $[M] = \dfrac{[H(\omega_1)]^{-1} - [H(\omega_2)]^{-1}}{\omega_2^2 - \omega_1^2}$	$H_{ij}(\omega) = \sum\limits_{r=1}^{N} \dfrac{\phi_{ir}\, \phi_{jr}}{\omega_r^2 - \omega^2}$	-----------

3.5.6   Modal Parameters Estimation

The modal parameters estimation of a structural system from measured data may require an intricate knowledge of structural dynamics as well as signal processing theory. In general, modal parameters are extracted from measured data and specifically FRFs or IRFs. After the data have been processing to a suitable form such as FRFs, the next step is to determine the modal properties for each mode of vibration that consist of resonant frequencies, damping ratios and mode shapes. These parameters can be obtained by applying a curve fitting to the acquiring FRFs. Although several methods and algorithms exist in which curve fitting can be categorised, single-mode methods and multiple-mode methods can be commonly used to achieve the purpose. In addition to an axiomatic reasoning for single- and multiple-mode approximations, there are some other practical reasons for this classification. The difference in the level of damping among curve fitters is between a single-mode and a multiple- mode method. The former can be reasonably

performed for lightly damped structures and well separated modes. However, the latter can be employed for heavily damped structures and closely spaced modes. Furthermore, the single-mode methods are based on the Single Degree Of Freedom (SDOF) assumption, and their states are that the FRF is generally dominated by the contribution of a particular mode of vibration and neglecting all the others. As a result, such methods can be simply applied to acquire the modal parameters for a single mode (Agilent Technologies, 2000). On the other hand, the effect of all the modes can be simultaneously considered by multiple-mode methods (He and Fu, 2001).

The clarification of modal parameters identification of a SDOF structural system is presented in this section, which is the final and important step of experimental modal analysis. The two main stages procedure are generally required to be followed to estimate modal parameters from a system. Once the FRF is plotted, the modal frequencies and damping ratios are estimated after some steps. However, further steps are required to estimate the modal vectors and scaled mode shapes.

Estimation of natural frequency of a structure is very important and is simply calculated from FRF. Natural frequency (ω) is well known as the highest amplitude in the magnitude of the FRF set of the specific mode of vibration. In addition to natural frequency, the damping ratio is derived from the width of resonance frequency. It is identified through the simple, quick and common method which is called half-power band width. Damping coefficient can be expresses as (He and Fu, 2001).

Mode shapes of a structural system are obtained through a simplistic approach which is commonly referred as Quadrature Picking, or Peak Picking. This technique is applicable for structure that its modes of vibration are lightly coupled, sufficiently separated; otherwise it is not valid (Agilent Technologies, 2000). Therefore, other SDOF method such as Circle Fit can be used instead when modes of a structure are heavy coupled modes. Extracting modal parameters will be clearly explained in chapter five.

The results will be more reliable when they are obtained theoretically and experimentally. Uncertainties in numerical modelling of the vibration phenomenon in a structure require the validation of analytical formulas to obtain confident results. This is not only important to predict the behaviour of the structure during both

analysis and design stages. It is of paramount importance to know that numerical model can save both cost and time as compared to full-scale structures or any physical model (Salawu and Williams, 1997). However, it is inevitable to be confident from the theoretical analysis to predict the true behaviour of the structure. This cannot be achieved without validating the theoretical models with experimental data. In particular, reinforced concrete element with steel bars exhibits a heterogeneous internal structure and thus, the study of its behaviour become complex. Therefore, validation of theoretical models against their experimental counterparts of reinforced concrete structure is a main purpose of engineering disciplines to obtain reliable results (Yu et al., 2008). As a result, experimental and theoretical will be taken into account in this study.

3.6   The Phases of a Typical Modal Test

According to the UK Dynamic Testing Agency (DTA), the EMA procedures can be entirely achieved in four specific phases as follows (Reynolds, 2000; Reynolds and Pavic 2000):

Phase I: The preparatory phase

Phase II: The exploratory phase

Phase III: The measurement phase

Phase IV: The post-test analysis and modal parameter estimation phase

In order to acquire high quality measurements and to satisfy the predetermined requirements, EMA during this project should be completely followed these four phases. In addition to the theoretical description of these four phases in this section, the experimental results of preparatory phase and related checks will be explained in chapter four.

3.6.1   Phase I: The Preparatory Phase

The first step of the preparatory phase launches with the definition of the test objectives. On this basis, appropriate resources can be efficiently allocated to the test. The second recommended step in this phase is to estimate the likely dynamic properties of the structure by performing the numerical modelling. This information will be significantly helpful in the selection of data acquisition analyser, exciter and

transducer (Frangigan and Hunt, 1993 and Reynold, 2000). Based on estimating the numerical dynamic behaviour of the structure in term of frequencies and their associated mode shapes, an appropriate data acquisition analyser, depending on sampling rate is chosen. Besides data acquisition analyser, a suitable measuring kit and accelerometer are properly selected depending on frequencies range and the acceleration respectively. Numerical modelling may also be applied to check the test grid during that the reference accelerometer locations are selected. As a consequence, the adequacy of the test grid check is performed prior to testing to avoid any spatial aliasing between different mode shapes (Reynold and Pavic, 2000; Al-Ghalib, 2013).

The next recommended step in this phase prior to performing EMA comprises of two minor stages such as preparation of the structure and equipment set-up (Reynold, 2000). During the preparation of the structure, the specimen and space for testing are needed to be ready for the test. Moreover, preparation of the recommended boundary condition that used in the test should be taken into account. During the equipment set-up, pre-prepared form of set-up is required to be known to precisely identify which items will be used and therefore they are required to be ready. Such a systematic plan ensures that the process of the test will be achieved properly and accurately.

3.6.2   Phase II: The Exploratory Phase

In the exploratory phase, the suitability of the structure, data acquisition and the consistency of the measured data for modal testing is preliminary determined by conducting a number of measurement checks. These checks are performed to confirm that the whole process of the test in the EMA is systematic and thorough. Therefore, such measurements play a key role in the quality assurance (QA) system applicable to EMA fields (Reynolds and Pavic, 2000). They include a number of successive checks which are described in the remainder of this section.

A. Excitation/Response Check

The aim of excitation/response check is to applying an input excitation to a structure, and capturing both the excitation signal and the corresponding response of the structure with a proper sampling rate. When an appropriate sampling rate is selected depending on hammer excitation and shaker excitation, both the time domain signals and its counterpart frequency spectra are visually examined due to some remarkable

purposes. Firstly, the shape, clarity, and strength of each measured signal, and simultaneously other main characteristics, such as the duration of the impact signal, should have looked satisfied. Secondly, impact time histories have a half-sine shape function when the excitation force is applied using the soft hammer tip on the concrete surface (Reynolds, 2000). When harder tip is employed for an excitation force, sharper peak with shorter duration of a delta shape function can be predictable. In the context of frequency domain, the shape of the time signal results in a flat spectrum over the excited range of frequency where a good idea about the frequency bandwidth can be drawn. Next, in term of response time signals, the response should launch almost instantly, whilst there is   commonly a small delay for remote transfer function owing to the speed of wave transmission through the portions of the structure (Reynolds, 2000). Then, using impact hammer, it is potential the accelerometer is jumped following the blow of hammer. Any potential jump of the accelerometer would spoil the FRFs measurements and would be revealed through the visual examination of time domain input/output signals. If this phenomenon is occurred, it is necessitated to decrease the hammer blow strength to a level which prohibits the accelerometer to jump. Finally, in addition to notice any jump occurred to accelerometer through time domain plots, indications of loose connection of transducer cables may be identified, especially when aggravated by the movement of the hammer or the tested object (Reynold, 2000; Reynolds and Pavic, 2000; Al-Ghalib, 2013).

B. Immediate Repeatability Check

For each test and using exactly the same instrumentation set-up, two nominally identical driving point FRF measurements one immediately followed by another are acquired, using the averaging of number of readings for each measurement. These two FRF measurements are plotted and then compared. In theory, these two plots of FRF measurements are seen to be almost identical, while in practice, some differences can be predictable between such plots owing to extraneous unmeasured noise (Reynolds and Pavic, 2000; Reynolds, 2000). Therefore, this discrepancy is inevitably present and is tolerable in the field tests and laboratory conditions. The immediate repeatability check is considered to be significantly essential in EMA. This is because it is the first time to be seen that the FRF calculations are performed for a particular structure. It is therefore an extremely convenient stage to investigate

the good quality of FRF data in term of shape, duration, and frequency content (Al-Ghalib, 2013). As a result, the measured FRFs can be utilised to extract the global properties of the structure, such as natural frequency and damping ratio, by performing single degree of freedom curve fitting or peak amplitude analysis. Once the global parameters of the structure are extracted, the reliability of the measurements compared with the preliminary analytical results can be reconnoitred and explored.

C. Homogeneity Check

The homogeneity test is one of the two tests endeavoured to check the degree of linearity of the structural characteristics, which is the fundamental assumption of the EMA (Ewins, 2000; Reynolds and Pavic, 2000). This check consists of measuring various consecutive FRFs measurements to conduct the reliability of the structure for performing the EMA. For this reason, different hammer tips are employed to induce different levels of excitation. Al-Ghalib, (2013) highlighted that this check is somewhat different from the previous check , which is repeatability check, due to using various excitation signals, to the original signal. Once low level and relatively high level of excitations give any significant inconsistency between the FRF measurements, this means that the structure is not behaving as a linear structure. However, due to the experience of Reynolds (2000), some related objects may occasionally introduce nonlinearity into the structures. For example, furniture or non-structural elements can cause non-linearity into floor of structure. Therefore, in the laboratory condition, it is possible some associated aspects, which have direct contribution with specimen, such as hanging; testing may cause non-linearity into the tested structure.

D. Reciprocity Check

This is the second of the two tests that is carried out to check the degree of linearity, the quality of the measured data, of the structure which is obeyed Maxwell's Reciprocity Theorem (Reynold, 2002; Al-Ghalib, 2013). The states of this theorem is that, for a linear structure, the measured FRF for an exciter at location i and the response at location j should be identical to the measured FRF for an exciter at location j and the response at location i. In other words, the reciprocity check is performed by measuring two FRF measurements, swapping the location of both the

excitation force and the accelerometer between the two measurements. Then, the two different transfer measurements are compared and they should have a good correlation, the same as those displayed for the first linearity check, the homogeneity check.

E. FRF Shape Check

It is known that the dynamic characteristics of a structure, which dictates its behaviour under external excitation, can be described by resonances and anti-resonances. The occurrence of relatively clear anti-resonances troughs between adjacent resonances on the FRF plot using logarithmic scale is a major goal of the check. However, for transfer point FRF; it is generally possible to expect a valley between two adjacent resonances rather than trough (Al-Ghalib, 2013). From transfer function, other observation can be noted that a negative phase shift through resonances and a positive phase shift through anti resonances, and the value of phase can always be viewed between 0° and 180° (Maia and Silva, 1997; Avitable, 2003). During this check, other beneficial observation can be found from the region of the FRF at lower frequencies. This observation is that the first mode of vibration should almost represent the static stiffness behaviour of testing prototype civil engineering structure (Reynold, 2000).

F. Coherence Function Check

Coherence check is generally conducted for the accuracy of measurements. Coherence function γ^2, as defined by equation 3.14, is employed as a data quality assessment tool. This function identifies how much the degree of linearity of the output signal is related to the linearity of the input signal. The values of the coherence function are located between 0 and 1. It is important to ensure that the value of coherence function is close to unity in the regions of modes of vibration of the examined structure. Reynolds (2000) reported that although the UK Dynamic Testing Agency (DTA, 1993) prefers a minimum value of coherence function of 0.9 for civil engineering structures, roughly a value of 0.8 is considered to be adequate owing to the noisy nature measurements. It is worth to say that the acquired signals are a particular concern in coherence measurements. Due to this reason, averaging several individual time measurements can eliminate contamination come from the random instrumentation noise on the force, response or both channels (Ewins, 2000).

Therefore, almost statistical authentic measurements can be obtained. In addition to contaminating the value of coherence function when noise is randomly entered, there could be another factors that cause the coherence values lower than 0.9 at all resonances in the points of modes of vibration. For example, Maia et al. (1997) and Reynold, (2000) highlighted that the value of coherence function can be dropped less than 0.9 and indicate poor coherence not only through leakage errors in the estimation of the spectra, but also through non-linearity of the structures or unmeasured extraneous excitation.

3.6.3   Phase III: The Measurements Phase

The measurement phase is performed as the major experimental data acquisition step of the modal testing process. By this phase, any abnormalities in equipment or structure should have been revealed because all necessary measurements should have been selected in the previous phase, which is the exploratory phase. Supposing that no abnormality is observed, the reference accelerometers should place into position on the structure and the impact force is hit to the first point, and the data is acquired. Then, the accelerometers are moved to the next test points and the procedure will be continuing until all marked points have been recorded. Theoretically, single row or column of the FRF matrix should provide enough information, as given in equations 3.29, to estimate natural frequencies, corresponding mode shapes and modal damping ratios (Ewins, 1995; Reynold, 2000 and Al-Ghalib, 2013). Every single point of FRF gives sufficient information on natural frequencies and mode shapes, while every single row or column contains enough information to describe the mode shape. Experimentally, it is strong possibility to select response measurement location which is close or maybe on a node of some modes of vibration of the structure. For such a situation, it is likely that those modes of vibration are poorly identified or even they are completely failed. Therefore, several successive measurements of FRF matrix is more practicable to overcome the previously mentioned difficulties from happening.

3.6.4   Phase IV: The Post-Test Analysis Phase

The post-test analysis phase is generally launched when two important steps are achieved. First, all necessarily field measurement, in the exploratory phase, is

performed and satisfied. Second, sufficient measurements, in the measurement phase, to describe all modal parameters are acquired and assured. It is worth to mention that FRF measurements are started to be analysed in this phase to calculate modal parameters of the structure and presenting them in the meaningful manner. For this purpose, different methods are implemented to perform a convenient analysis and extract the modal parameters.

It is found that suitable algorithm to the measurements of this research is peak picking or peak amplitude to estimate all parameters properties. It is recommended that peak picking or peak amplitude is the most successful method for a structure when their FRFs show well-defined separated modes at resonance frequencies (Ewins, 2000 and Al-Ghalib, 2013).

3.7   Summary

This chapter is mainly divided into several subsections. The first section of the chapter embarks on the introduction of modal analysis followed by the theoretical relationships among the three models of the dynamics of structures, specifically: the spatial, modal and response models. Furthermore, the criteria and their related derivations needed to define each model are made. A brief theoretical background to the analytical and experimental modal analysis is also provided in the third section of this chapter followed by degree of freedom of a structure. Besides, derivations for the formulae related to the calculation of modal data for instance FRF and its components and coherence function are presented. The knowledge gained from the mathematical formulations is used to compare theoretical and experimental modal measurements. The first part is ended up with provides the EMA procedures that can be entirely achieved in four specific phases. Four phases of a typical modal test are discussed to check the reliability of the instrument.

4. Research Methodology and Experimental Work

4.1   Introduction

As concluded from the literature review covered in Chapter two, the research problem was underlined in the field of research. The investigation of the study is formulated following a comprehensive review of published research in the area of vibration analysis and artificial neural network. This chapter provides an explanation of the research methodology adopted in this study.

Experimental work consists of quality assurance checks followed by classification of slabs into groups. Moreover, the modal testing instrument used to collect the data, including methods implemented to maintain validity and reliability of the instrument, are described. For this purpose, this chapter describes the main stages of experimental work and the checks associated to signal data used in this study. Once the quality assurance checks were assured, the experimental work programme that achieved in this study is explained. Four laboratory groups of scaled RC slabs were constructed and then tested. Each group consists of two RC slabs, which were had similar concrete strength and steel reinforcement type and spacing. After passing the quality assurance checks, modal parameters was extracted for each slab of all groups to study the effect of various parameters.

4.2   Research Methodology

The main aspect of the proposed methodology is to extend the modal analysis application on reinforced concrete slab realm. Furthermore, the proposed methodology is adopted to develop a new robust and reliable technique to detect void severity in the slab. Experimental and its theoretical counterpart analysis was carried out on freely suspended RC slabs to ascertain the validity and reliability of the results.

The theoretical work was mainly analytical and numerical of the RC slabs. In theoretical part, the detailed equations were derived to provide the natural frequencies for RC slabs. The natural frequency equation for the slabs is given in general form of freely supported boundary conditions. Analytical solutions only exist for limited number of idealised structures in term of geometry, loading and

boundary conditions. Therefore, numerical methods have to be referred to solve wider range of practical cases. In this study, finite element modelling using ANSYS software was utilised to extract natural frequencies and mode shapes of square RC slabs.

The experimental work involved experimental modal analysis on four pairs RC square slab specimens of various dimensions. The samples were excited by an impact hammer to induce vibration while accelerometers and Pico Scope were used to acquire the data from the experiments and MATLAB software was employed to process and plot the required results. Then, the modal parameters were extracted from the plot of Frequency Response Function (FRF).

A further numerical simulation was also essential to perform the dynamic behaviour of voided slab. The natural frequencies of the numerical model were utilised as input to Feed-Forward Back Propagation Neural Network (FFBPNN) to identify void severity in RC slab. FFBPNN was performed by using mathematical software, MATLAB. This is to address the parameters associated with the dynamic load and slab geometry that might not be carried out by ANSYS or any other commercially available software.

These research activities are taken together in order to build up the existing gap in previous research and develop the activities that no one did it before in such depth and width to the best of author's knowledge. Figures 4.1- 4.3 provide the summaries of research methodology adopted in this study.

In addition to the novel methodology, one of the major contributions to the knowledge of this research is to establish the sophisticated statistical methods for damage identification in RC square slabs, namely MAC and COMAC techniques. Firstly, they are used to identify the effect of partially concentrated load in three increments as well as strengthening on the slabs. Secondly, they are employed to determine the location of the void in RC square slabs. Beside the above-mentioned contributions in this research, Feed-Forward Back Propagation Neural Network (FFBPNN) is adopted to classify void sizes in reinforced concrete slabs.
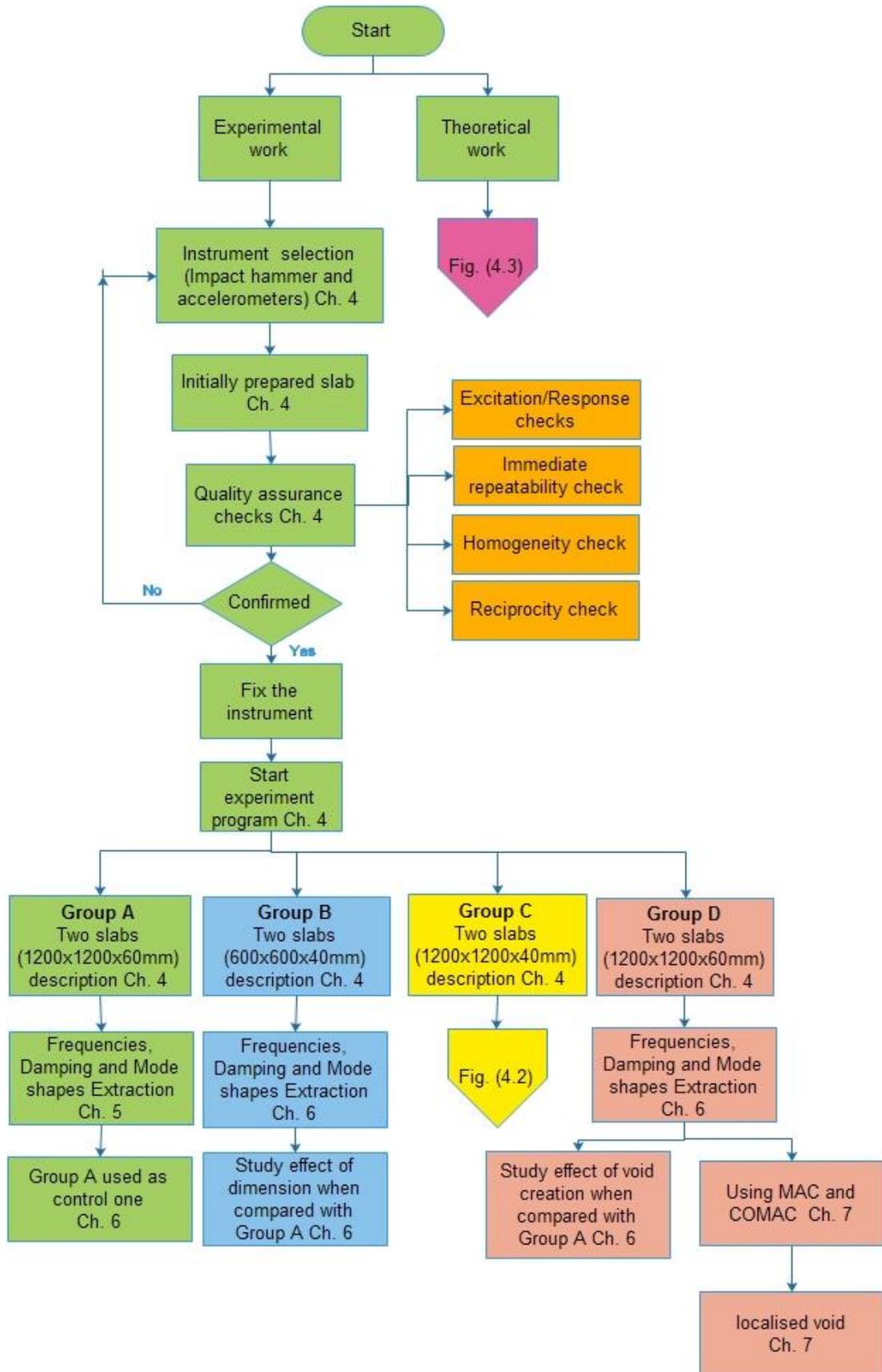
Figure 4.1: Flowchart of research methodology adopted in this study.
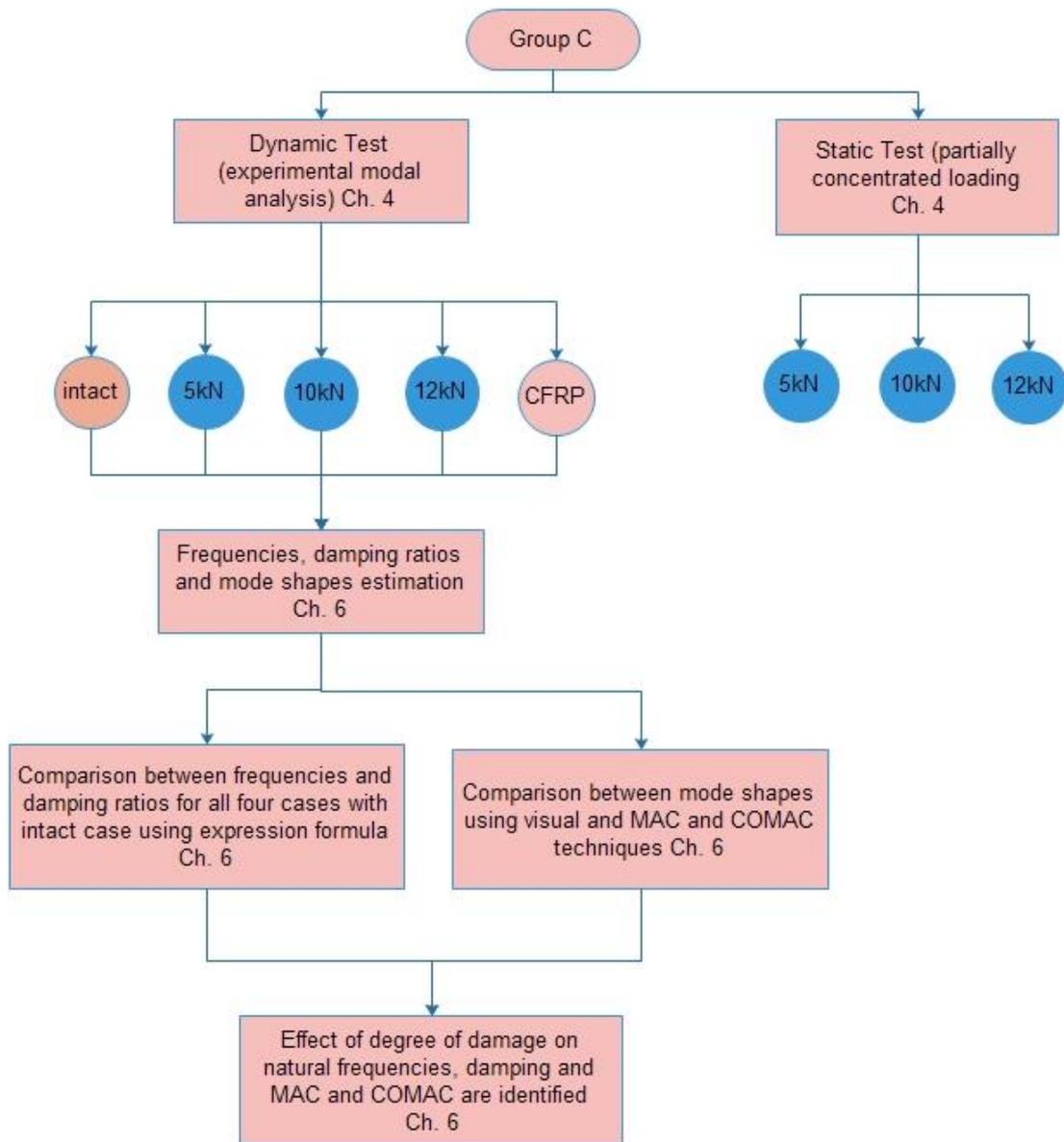
Figure 4.2: Flowchart procedure for testing Group C slabs.
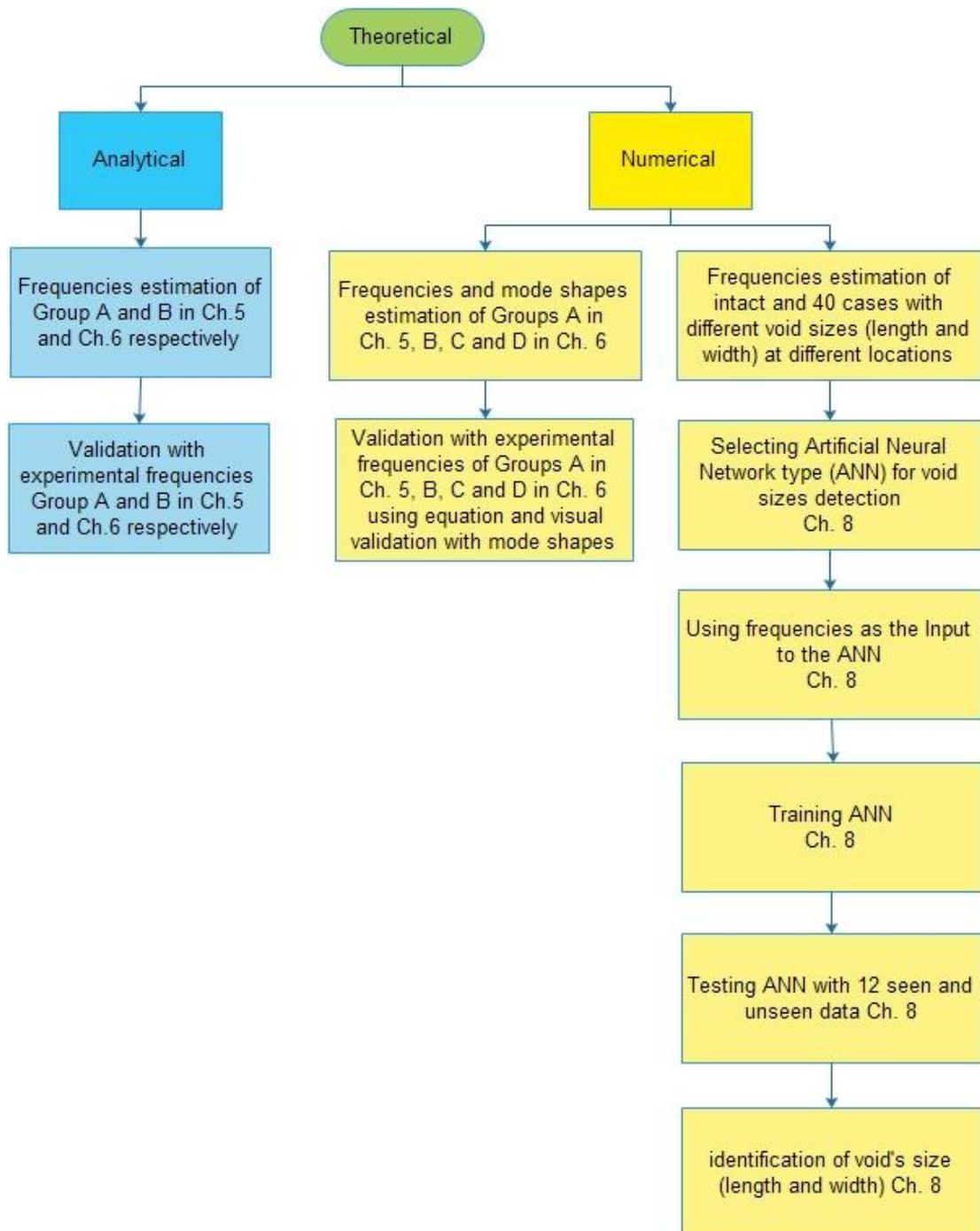
Figure 4.3: Flowchart of research methodology of theoretical part.

4.3   Experimental Work

This section discusses the experimental modal analysis of reinforced concrete slabs. It is important to mention that how to implement experimental modal analysis are given in the first part of this section. While, the rest of the chapter highlights experimental modal analysis of freely suspended RC slabs and validates quality assurance checks. Carrying static tests on RC elements becomes a standard procedure and straight forward approach to follow. However, dynamic testing of RC elements needs a careful consideration and detailed attention to all the steps required from the beginning till the end. The first and most important task to take into account is to choose the right equipment as well as the right size of the slab specimen. For this reason, the preliminary natural frequencies of the specimens were required to be known. The equation (4.1) offers interesting information for finding out approximate natural frequencies of laboratory slab specimens before doing any of the experimental work specimens. By knowing the preliminary natural frequencies, appropriate equipment such as impact hammer and accelerometers were chosen for exciting the specimens as well as acquiring the responses of such specimens. On this basis, the suitable dimensions of the specimens was selected otherwise the available equipment was not capable to clearly acquire the signals which are related to the behaviour of the specimens. Equation (4.1) played a key role to select slabs dimensions, its derivative is presented in the next chapter.

$$f = \frac{\lambda^2}{2\pi \cdot l \cdot b}\sqrt{\frac{D}{\mu}} \qquad\qquad (4.1)$$

$$D = \frac{Eh^3}{12(1 - v^2)} \qquad\qquad (4.2)$$

where:

f is natural frequency, measured in Hz

l is length of the longer side of the plate

b is length of the shorter side of the plate

h is plate thickness

μ is mass density per unit area of plate (ρh)

λ is a dimensionless natural frequency factor

D   is flexural, bending, rigidity of the plate

E is modulus of elasticity

υ is the Poisson's ratio of the plate material

4.3.1   Properties of RC slab Specimen

Two square RC slabs of dimensions 1200 x 1200 x 60 mm as shown in Figure 4.4 were initially prepared in this study. The RC slabs were cast using a 10 mm maximum aggregate size with grade of concrete f_{cu}30. Six mm diameter, single layer of reinforcement with 60mm spacing was arranged for reinforcing the slab. The effective depth of the slab is about 45mm. Further details of RC slab specimen's preparations can be found in Appendix A.
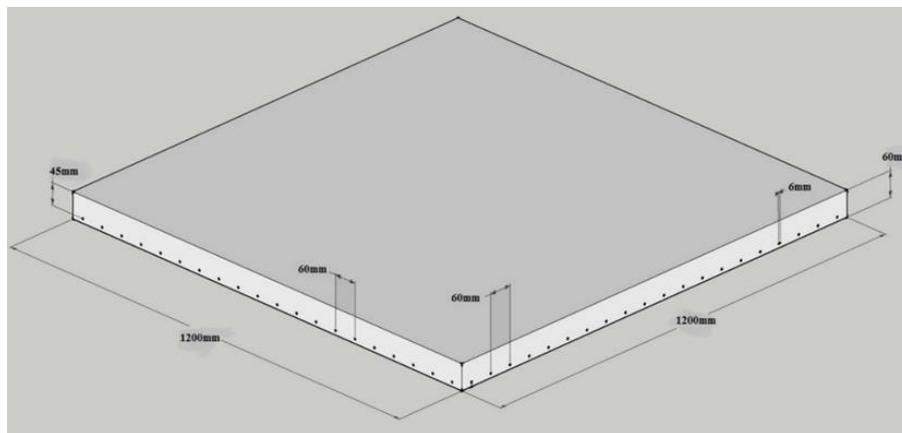
Figure 4.4: Dimensions of RC models (Specimens).

4.3.2   Dynamic Testing

As previously stated, the main aim of this study is to identify the behaviour of the slabs using dynamic testing, in a process known as experimental modal analysis (EMA). It consists of three essential stages, such as modal testing, data processing and modal parameters estimation. The experimental modal analysis of the freely supported slabs were conducted. Then, the tests would be carried out to realise how

the dynamic properties of the slabs changes as RC slabs was progressively damaged. In the final part of the programme, artificially introduced damage in the RC slabs would be localised using experimental modal analysis technique.

The tests were planned to conduct on simply supported RC slabs in order to introduce more realistic case. However, it was not achieved on simply supported conditions because of insufficient time availability and budget.

4.3.2.1   Modal Testing Instrument

Modal testing consists of three main components as the basic required for test setup, which are excitation source, response source and data acquisition system.

A. *Excitation Source*

It is known that to study the dynamic behaviour of structures, they have to be excited in order to measure their response signal. Controlled excitation and ambient excitation are the two common methods for modal testing. The former method is a method that input excitation forces are usually utilised in a controlled manner and can be measured accordingly. However, for the latter method, the input excitation forces to a system cannot be measured. In a standard modal analysis, a high quality frequency response function (FRF) for the subsequent modal estimation can be obtained by using the controlled excitation methods. On other hand, in the output-only, operational, modal analysis, the quality of the estimated modal parameters from the ambient vibration is compromised (Yousaf, 2007). Therefore, the controlled excitation method is widely used in research on vibration based damage detection, including the current study.

Generally, there are two categories of controlled excitation methods, non-destructive methods, namely instrumented impact hammer and electromagnetic vibration shaker. Due to the availability, cheaper cost and accuracy of results, the use of impact hammer may be preferable. Moreover, impact hammer merely requires one person to perform the excitation with more easily transported at different points of measurements. In addition to these merits that this instrument has, impact hammer is quicker to use on site compared to shaker. As a consequence, Impact hammer which is one of the controlled excitation methods is adopted in this study to excite the reinforced concrete slab specimens, as shown in Figure 4.5. In addition to Delta

Tron® Impact hammer version 8208, force transducer, this figure shows a set of four interchangeable impact tips, with black (hard), red (tough), green (medium) and orange-red (soft) colour, that are used to control the frequency content and the impulse. The frequency content that is controlled by varying the stiffness of the hammer tip is considerably important, since it is not feasible to change the stiffness of the tested specimens. The harder the tip, the shorter the pulse duration and thus the higher the frequency content, as illustrated in Figure 4.6.

Figure 4.5: Delta Tron version 8208 instrumented impact hammer with four tips.

In general, small low-mass objects have higher response frequencies and thus require higher frequencies of excitation at lower force levels. However, heavier structures with lower fundamental frequencies require lower frequency excitation at higher input force levels (Labonnote, 2012).
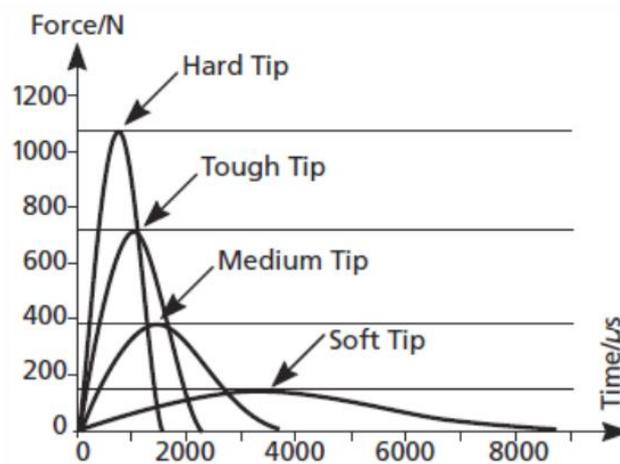
Figure 4.6: Impulse shapes of the modal hammer as a function of used impact tip (after, Brüel and Kjær, 2012).

B. Response Source

In this study, acceleration response time histories are the vibrational response signal of the test structure. The data acquisition is one of the important phases of experimental modal analysis (EMA). For this purpose, a piezoelectric transducer was adopted to acquire the acceleration data. Accelerometers are the most widely used transducers for measurement of acceleration response of the intended structure. In this experimental work, three piezoelectric accelerometers were used to measure the response signals (acceleration) of the RC slabs.

The type of accelerometers that was used in this research is depicted in Figure 4.7 (Delta Tron® model 4514). The frequency range of these types of accelerometers is between 1Hz-10kHz with a sensitivity of $1.005mV/ms^{-2}$ (9.86mV/g). When the acceleration response of the RC slabs was intended to be measured, steel studs were firstly glued, by using super glue, on the RC slabs' surface. Prior to glue the steel stud on the RC slabs, the mating surfaces were properly cleaned. Then, the accelerometers were ready to be attached to the glued studs. The screwed accelerometers were attached to the glued studs, and then accelerometers were subsequently available for acquiring data.

Figure 4.7: Delta Tron® model 4514 accelerometer.

C. Data Acquisition System

Data acquisition system is a process, in modal testing, which employs to collect information to analyse the phenomenon, such as behaviour of the specimen under dynamic loading. As technology has recently progressed, such process has been simplified widely and made more versatile, accurate, and reliable through non-big

electronic equipment. In modal testing, this process requires a system consists of three main components, namely, signal amplification unit; Data acquisition unit; and personal computer.

Figure 4.8 shows the signal amplification unit, it is also called Amplifier, which was used in this study, and it acts as a power source for the connected devices. It comprises of eight channels, four input and four output. It is important to mention that the Impact hammer is attached to one of the input channel of the Amplifier, while the accelerometers are distributed among the rest of the input channels.

Figure 4.8: Signal amplification unit.

It is also important to mention that amplifier is linked with the Data acquisition unit, which is depicted in Figure 4.9, through the four channels, and Data acquisition unit is attached to the computer, which is shown in the Figure 4.10, through data acquisition card. In Data acquisition unit, the data is filtered in order to remove high frequency components, and also to increase signal to noise ratio of the lower frequency components of the signals. The signal is also converted from analogue-to digital.
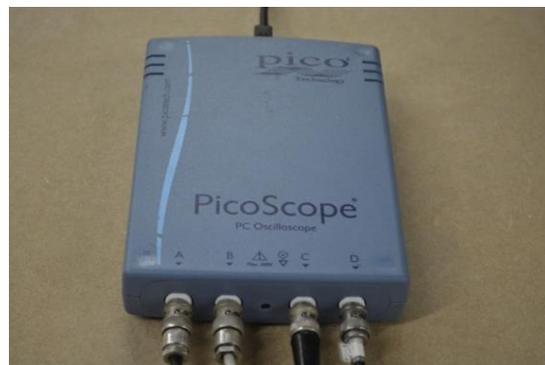
Figure 4.9: Data acquisition unit.

On the computer, the acquired digital signal is viewed and synchronised using the installed Pico-scope software.
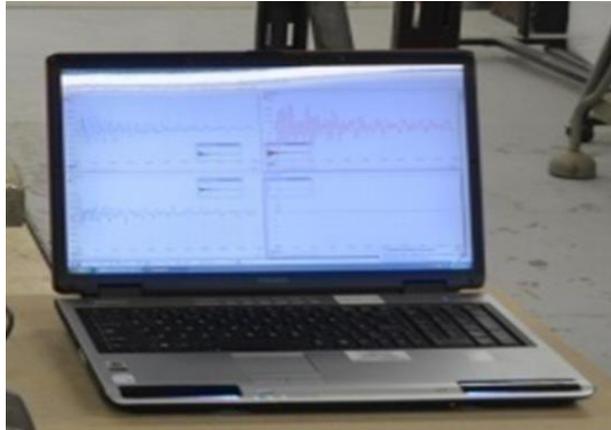
Figure 4.10: Personal computer.

In general, Impact hammer was employed to excite the specimen to produce the input signal and the accelerometer was attached to the specimen to gain the output signals. Then, the signals were acquired and amplified. Then, by using the installed Pico scope software the analogue and digital signals could be viewed and they were available for further process such as copy and paste in different extensions.

4.3.2.2   Data Processing

Practical software implementation is MATLAB, which was employed in this study to run the specific code for signal processing. Firstly, spectral analysis involving Fourier transformation was performed to convert the time domain data into the frequency domain. Then, auto and cross spectrum were calculated. The final stage of signal processing was to calculate and plot coherence functions and the FRF with its components. The components of FRF consist of magnitude, phase, real and imaginary parts. Once FRF set was obtained and drawn, the final stage of EMA, which is modal parameter estimation, was going to start.

4.3.2.3   Modal Parameter Estimation

Although, numerous modal parameter estimation technique have been developed, the peak picking method is employed to extract the modal properties (damping ratios, frequencies and mode shapes). From the experimental time history data of a test structure, the FRF and its components were plotted. Modal parameters can be extracted from the obvious peaks of FRF. For example, the natural frequencies are

obtained from these obvious peaks, while modal damping ratios can be obtained from their width. Using these information as well as FRF components, the mode shapes are plotted. Extracting modal parameters will be explained in details in chapter 5. When modal properties of the slab are determined, slab's dynamic behaviour can be described and explained.

4.3.3   Support Condition

There are normally various options of how to support a structure during the measurement. Free-free support condition was specifically used in this study. Freely suspended support (free-free conditions) is one of the most popular ways that is most frequently employed in experimental modal analysis. It is theoretically such a style of support where the test model is completely isolated from the ground. In other words, the tested structure is freely suspended in the space to avoid the influence of boundary conditions. Without the involvement of support rigidity, the structure is then exhibited rigid body modes which are completely extracted by its mass and inertia properties.

In the laboratory testing, free support is usually achieved either by suspending (floating) the structure in the space or positioning the structure on a very soft pad. The most difficult aspect in dynamic testing is how to create the ideal boundary condition especially for relatively small structures. This is because Eigenvalues and eigenvectors are significantly influenced by the rigidity of the support. For this reason, it is quite important to eliminate any spurious contribution which comes from the supporting elements.

It is, thus, the free support condition will be the superior choice of supporting type as no extraordinary attention requires excluding the effect of support's rigidity. However, in cases where a structure is relatively large or in case of real-life structures, the free support condition is almost impossible to be achieved. For such situations, it is generally feasible to provide the test article with a simply supported system that closely approximates the real-life structures. Achieving both support condition types, the interference of simply supported condition is then to be known. When measuring dynamic characteristics of a structure, McConnell and Varoto (2008) preferred one type of boundary condition (free-free, pinned and fixed respectively) over another, based merely on the rigidity of boundary condition.

4.3.4   Vibration Measurement Points

After the RC slabs specimen were prepared and properly cured for not less than 28 days, the responses were acquired with a grid of 25 driving points. Thus, the slab's surface was marked with a grid of 25 equally spaced locations, 29.5cm spacing any two consecutive points as seen in Figure 4.11. This would help measure a frequency response at each point of the grid. A single drop of wax super glue was applied at each point. Then, steel studs were placed on the RC slab surface at the marked points by applying pressure for about 1 minute wait for the glue to be hardened. Afterwards, accelerometers were mounted on the studs, and they were ready to acquire the responses.

The dividing point is a vibration measurement locations that remained fixed throughout the data collection process of modal testing. Such points were used as the reference points to calculate and plot the Frequency Response Function (FRF) over all 25 points of the slabs. These points are also known as the Degrees of Freedom, DOF. Every response locations sampled on the slab in order to identify the magnitude and direction of the measurement points of mode shapes.

 It is important to mention that if a coarse pattern is employed with relatively few sample points, the response of the specimens may not sufficiently capture the various modes of vibration and it may be difficult to properly analysis the case. However, fine pattern with significant number of points were employed in order to accurately portray the change of the mode shapes. Therefore, using the proper mesh density and choosing reliable vibration measurement points requires experience and an understanding of vibration of the specimens.
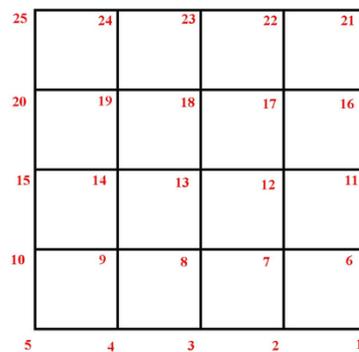
Figure 4.11: Vibration grid measurement points.

4.3.5   Testing Setup

Figure 4.12 shows the experimental set-up used in this study in order to conduct the measurement of the frequencies response function FRF of the specimens. The hanging method was applied to the dynamic analysis of a square RC slab in the laboratory to simulate free-free boundary conditions. All the four corners of the RC slab were hanged using two flat webbing slings. The connections of the devices, for examples, laptop, analyser, accelerometers, impact hammer, and their cables to the system were done as per the guidance of experimental modal analysis. Then, the accelerometers were attached to the RC slabs to pick up the dynamic signals, acceleration response, at all selecting points of the plate. After mounting the accelerometers, input excitation was applied through an impact hammer to provide stationary impact excitation at one of the selected points of the free-hanging plate. When impact hammer was hit the slab, the responses with a grid of 25 accelerometers equally spaced were acquired and analysed.

For each tested slab and at each singular points, the dynamic testing was repeated five times by striking hammer and the responses were acquired simultaneously. The average of five trials of each excitation and response were utilised for analysis. Averaging the repetition attenuates the effect of measurement noise and excitation characteristics. The corresponding averaged FRFs were obtained, from the iteration of loadings, and then plotted. Plotting averaged FRFs was indication to extract obvious modal parameters. As a consequence, more accurate representation of dynamic behaviour of the RC specimen under vibration was achieved.
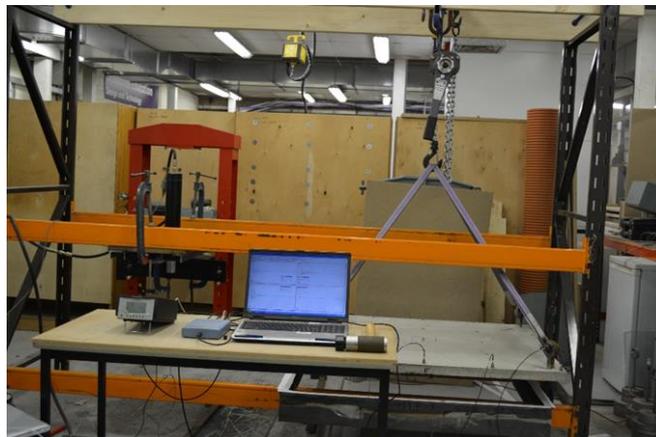
Figure 4.12: Experimental test set-up.

4.3.6   Quality Assurance Checks

The test slab and equipment had been prepared and ready for the first experimental modal analysis. Thus, as Quality Assurance (QA) checks stated by the UK DTA procedure and outlined in section 3.6.2 were performed.

Firstly, Excitation/Response checks which is satisfied when applying the impact hammer and the accelerometer at test point (1) on the initially prepared slab and simultaneously captured their signals. The Excitation/Response check result of slab in both time history and frequency spectrum are shown in Figures 4.13-4.16. Some important observations might be drawn from these Figures.

It is important to mention that the impact excitation resembled a regular half-sine shaped signal, which is shown in Figure 4.13. Figure 4.14 shows the corresponding response which is introduced due to impact excitation. Figures 4.15 and 4.16 show the frequency spectra for the excitation and response signals respectively. These signals look like what was expected without observing any strange behaviour. It is seemed that, in Figure 4.16, the shape and frequency content up to 800Hz is compatible to be used in this study. To know the maximum frequency range, the meaningful numbers of mode shape could be decided to be extracted, which were required to be captured clearly and far from noisy area. On this basis, enough number of modes can be obtained which were in smooth zone, as shown in Figure 4.16. As a result, the selected accelerometers and impacted hammer were confirmed to be used in this study.
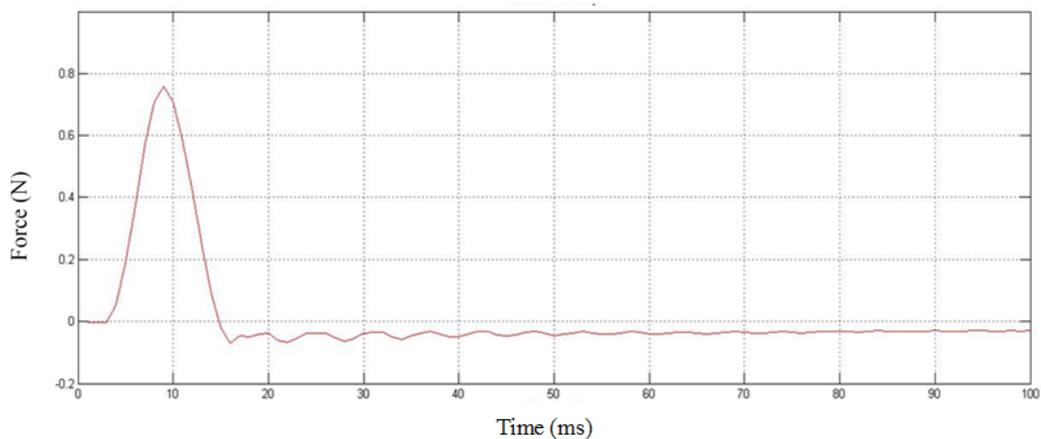
Figure 4.13: Excitation check (time domain).
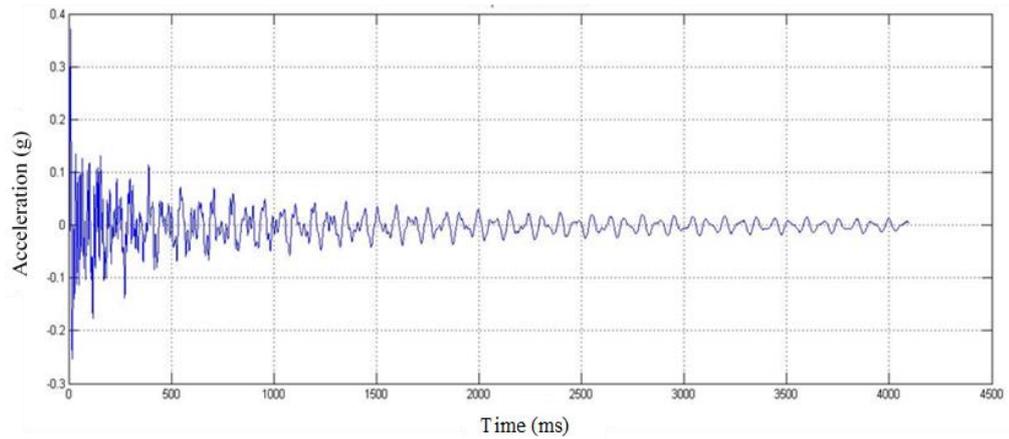
Figure 4.14: Response check (time domain).
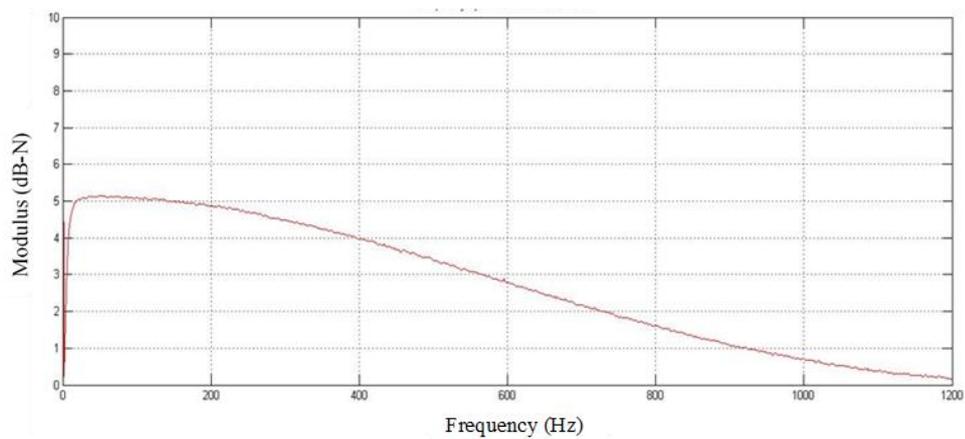
Figure 4.15: Excitation check (frequency domain).
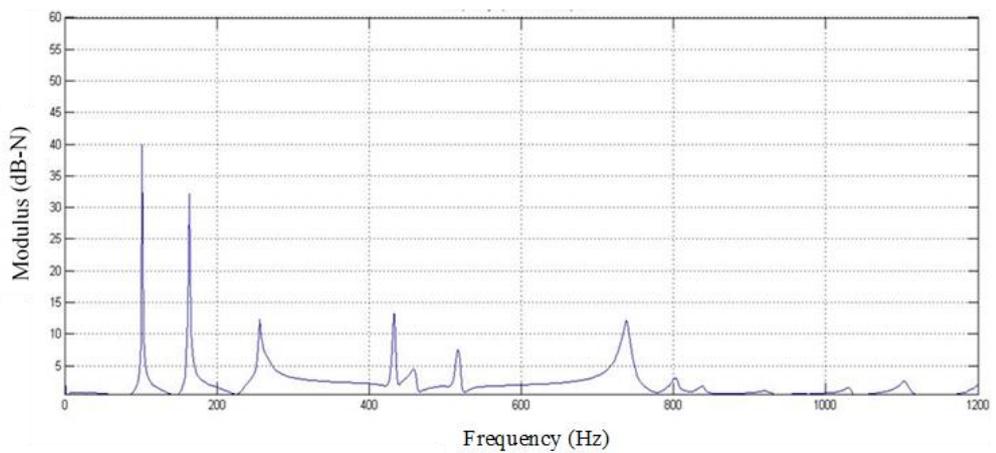
Figure 4.16: Response check (frequency domain).

Secondly, immediate repeatability check was conducted to ensure the repeatability of particular measurement, as shown in Figure 4.17. This check is the first attempt to display the data in term of FRF measurement. The figure shows the results of FRF from the immediate repeatability conducted at test point (1). From the visual inspection, It is evident the two plots overlaid reasonably well up to the frequency below 630 Hz. From 630-800 Hz they overlaid and kept away in some regions, while they become nosier and kept away beyond 800 Hz and thus the vibration modes beyond this range did not well response to the excitation.
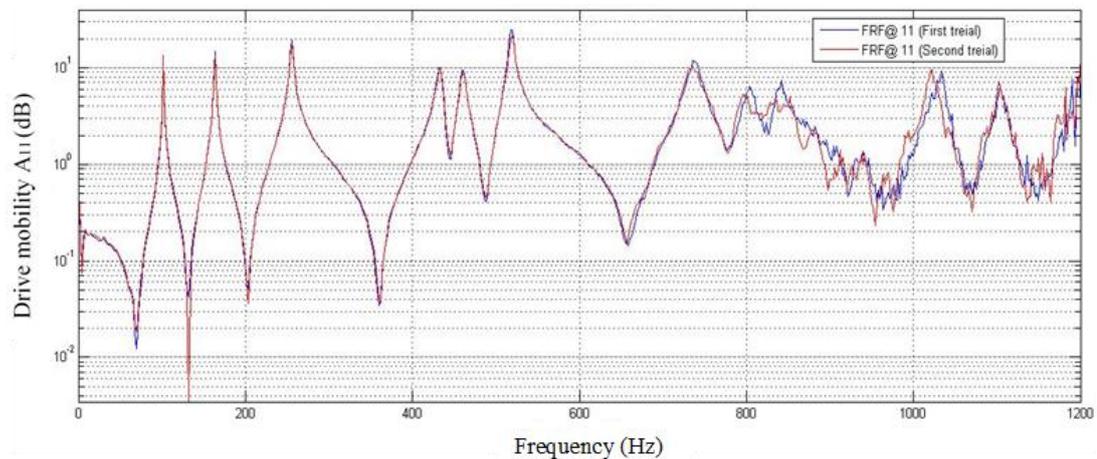
Figure 4.17: Immediate repeatability check for drive mobility at point 1.

Then, homogeneity check concerned with the linearity of the tested slab when different excitation were applied using four different hammer tips. Figure 4.18 shows the homogeneity check when only using the hard and tough hammer tips. It is clearly shown that the measurement made using the low level (tough tip) excitation was little bit noisier than the high level measurement made using the high level (hard tip) excitation, which is vividly shown beyond the 800 Hz. Whilst, Figure 4.19 shows the same check using four hammer tips. It is also clear that the results are more desired and less noisy by increasing the level of hammer tips, from soft to hard level.
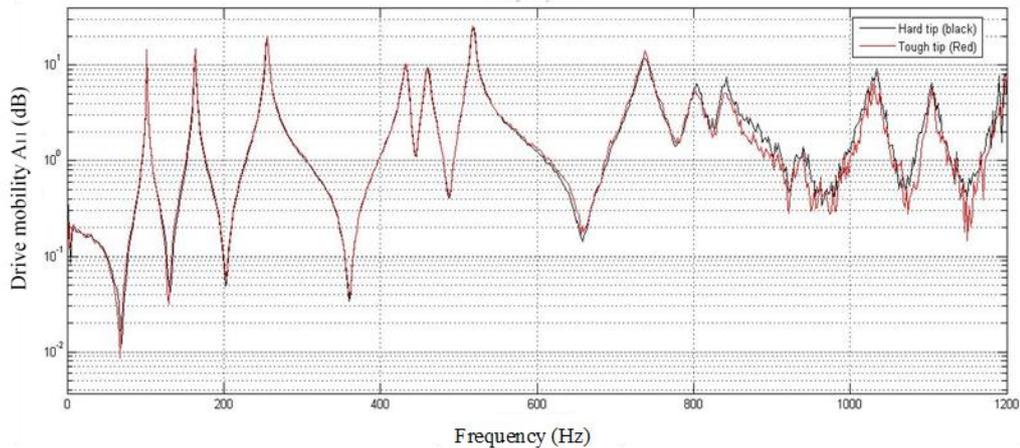
Figure 4.18: Homogeneity check using two different level excitations.
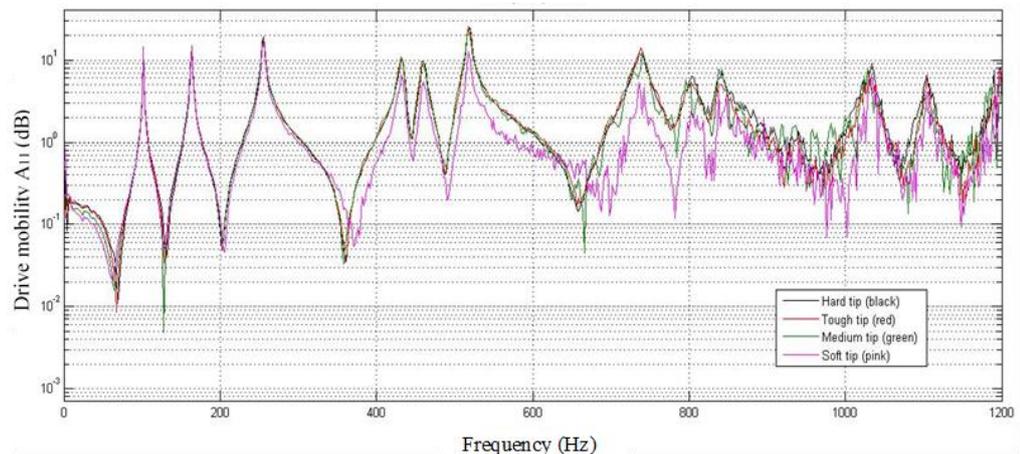
Figure 4.19: Homogeneity check using Four different level excitations (four hammer tips).

Next, the reciprocity check was performed twice between points 1 and 2 and points 2 and 25, as shown in Figures 4.20 and 4.21 respectively. For first check, excitation and response were swapped between two locations (points 1 and 2), while in the second one it was swapped between other two locations (points 2 and 25). In both cases, good agreement and identical amplitudes were provided except beyond range 500 Hz. In addition, it is shown in both figures that one measurement looks noisier than the other. In first case, the excitation at point 1 is nosier than when at 2. While, in the second case, the excitation at point 25 is nosier than when at 2. It is concluded from these two cases that a bit noise was found in the frequency beyond 800 Hz when the slab was excited at the corners.
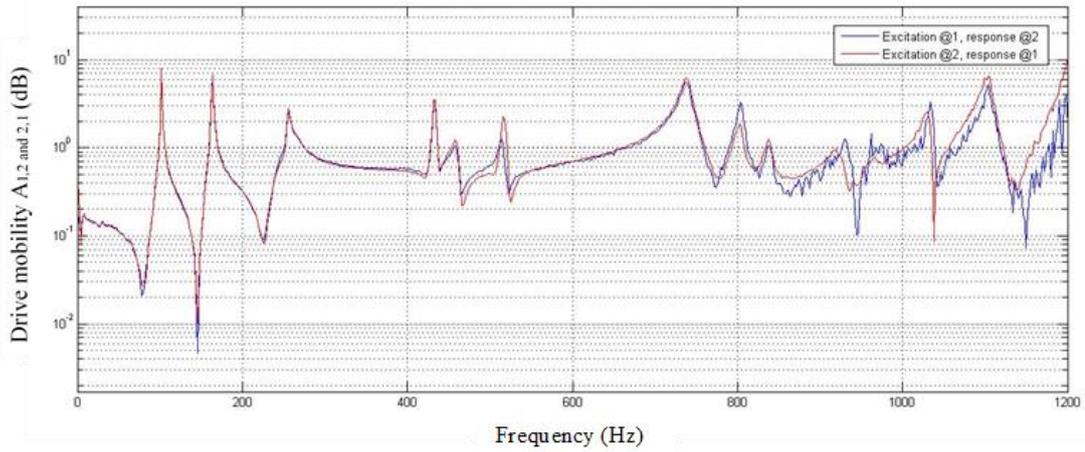
Figure 4.20: Reciprocity check for transfer mobility, A1,2.
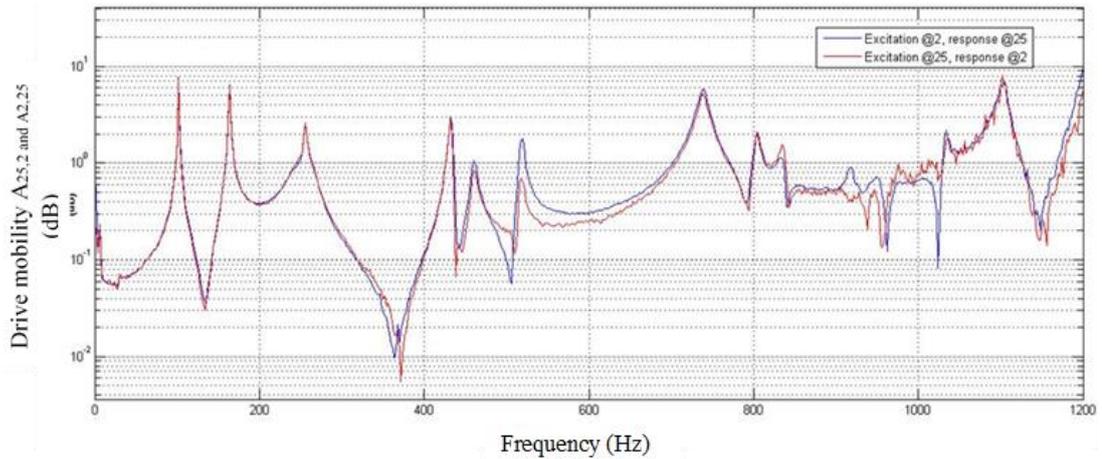
Figure 4.21: Reciprocity check for transfer mobility, A2,25.

Finally, coherence check was performed when the excitation at point 1 and the response at point 2. It can be seen from the Figure 4.22 the coherence values are shown as peaks for the most of the frequency range and their values tend to the unity. The coherences were studied with the Frequency Response Function (FRF) spectrum to check the linearity of the specimens in order to check the reliability of the results.
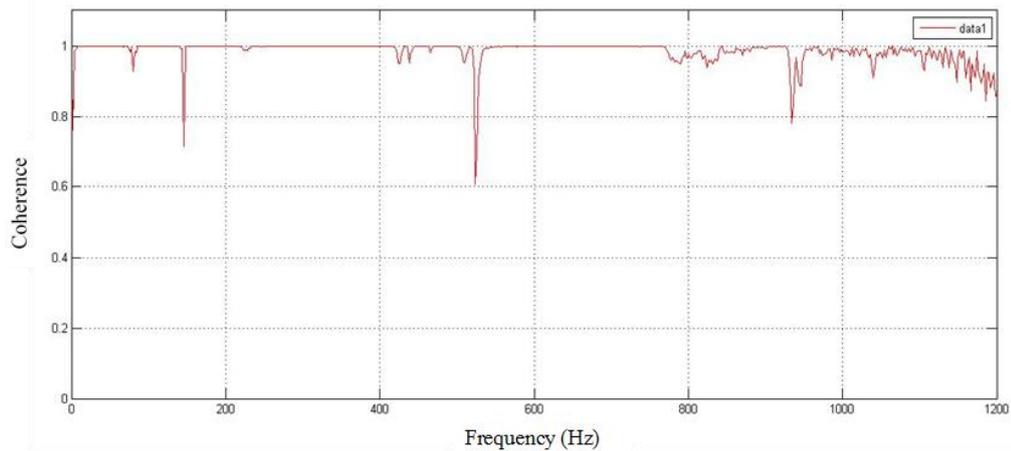
Figure 4.22: Coherence function check, A1,2.

It can be seen from the above figures that the excitation, the response signals, immediate repeatability check, homogeneity check, reciprocity check as well as coherence check look like what was expected without observing any strange behaviour. Quality assurance checks agree with the theoretical description. It is clear from the measured frequency response function checks that there is a good agreement for the excitation and its corresponding response. As a result, the used impact hammer and accelerometers and other necessity equipment are compatible to be used to identify the dynamic behaviour of RC slabs. Through following testing procedures with the necessary checks, one can ensure that the vibration measurements (whether in the time or frequency domain) represent a realistic experimental model of the dynamics of the reinforced concrete slab.

4.4   Laboratory Scaled Reinforced Concrete Slabs Groups

Once the quality assurance checks were assured for initially tested slabs, the laboratory reinforced concrete slab specimens were classified into four main groups. Four laboratory groups of scaled-RC slabs were constructed and modelled with various parameters. The parameters were dimensions, aspect ratio, incremental loads, and artificial void. Each group consisted of two RC slabs, where they had almost similar concrete strength and steel reinforcement type and spacing. Some basic knowledge of the material properties of both concrete and reinforced steel which were used for making specimens are briefly introduced in section 4.4.1. It is important to mention that all RC slabs were tested under free-free boundary conditions.

These four pairs of RC slabs were tested chronologically in the following order:

1. Group A: Tow 1200 x 1200 x 60mm^3 RC slabs were tested dynamically using EMA.

2. Group B: Tow 600 x 600 x 40mm^3 RC slabs were tested dynamically using EMA.

3. Group C: Tow 1200 x 1200 x 40mm^3 RC slabs were tested under five different state conditions, namely: intact, 5kN load, 10kN load, 12kN load and repaired conditions. It is important to note that both static and dynamic were used for testing the specimens of this group. The former test was used in order to damage the RC slabs. While the latter test was performed in order to identify the effects of damages on modal parameters (natural frequencies, modal damping and mode shapes) of the slabs.

4. Group D: Tow 1200 x 1200 x 60mm^3 RC slabs were tested with a purpose-made single void at distance 300 mm in both x and y directions from one its corner. The dynamic test under free-free boundary condition was performed in order to find the location of damage.

It is worth pointing out that the four groups of RC slabs were cast, cured for not less than 28 days as shown in Appendix A; and then tested in the concrete laboratory at Nottingham Trent University, School of Architecture, Design and the Built Environment. Each state condition was represented a practical case from the field of SHM in civil engineering structures. Bigger size RC slabs have been better to be tested to represent a real-life case studies. However, the availability of the place, resources and convenience of the devices dictated the scaled size of tested slabs strictly.

4.5   Description of RC Slabs

The structural state conditions conducted on the eight tested RC slabs can be divided into four main groups. The first group (Group A) was the baseline state condition and referred to as control one. The second group (Group B) was concerned with Group B; this was interested with studying the effect of dimensions (length, width and thickness) on the dynamic characteristics of the slabs. The third group (Group C) was represented by different levels of flexural cracking resulting from successive central point bending loadings. In addition, the third group was interested with studying the

effect of repair work conducting on the similar series slabs. Finally, the fourth group (Group D) included defective RC slabs where artificial void was induced at distance 300 mm in x and y directions with respect to one corner.

4.5.1   Testing Group A Slabs

As soon as the tested RC slabs of group A and equipment related to experimental modal analysis had been prepared, for the first EMA measurements, a full set of data Quality Assurance (QA) checks were performed as it is stated by the UK DTA procedure. However, the experimental results of Quality Assurance (QA) checks of the RC slabs was described in previous section. Moreover, the slabs of this group were used to extract the dynamic properties of intact slab under vibrational excitation, as shown in Figure 4.23. After measuring and analysing the experimental data, the dynamic response of the free-free supported slabs through modal parameters were identified. All the four corners of the RC slab are hanged using two flat webbing slings. The results of this series were also used as the reference to compare with the behaviour of the slabs of groups B, C, and D in order to study the effect of dimensions, aspect ratio, and artificial void on modal parameters respectively.
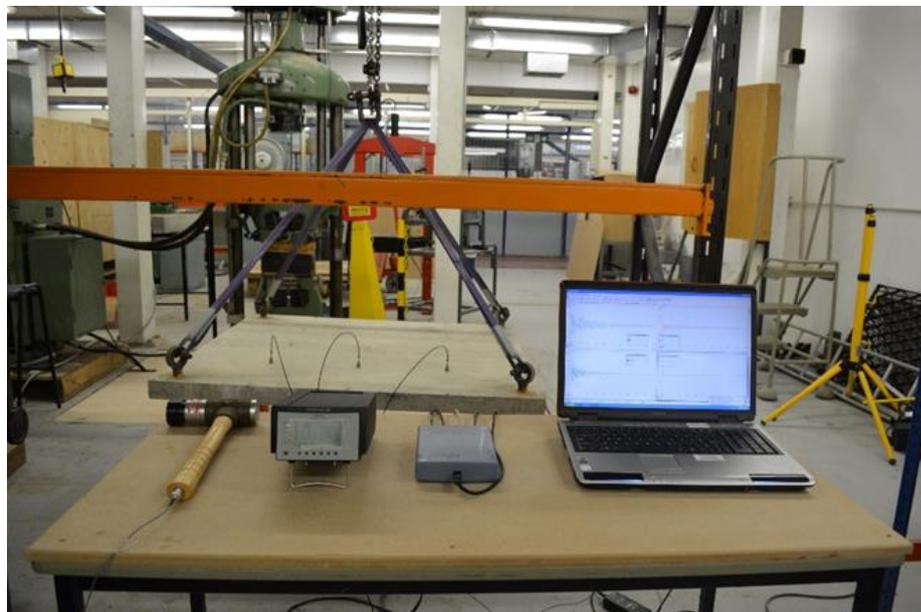
Figure 4.23: Test slab (1200x1200x60mm) under free-free boundary condition.

4.5.2   Testing Group B Slabs

The two slabs of this series were smaller in dimensions than the group A. Since this series slabs had lighter weight than group A, they were safe and possible to be suspended by using flexible elastic ropes (bungee cords) as shown in Figure 4.24.

However, the health and safety rules in NTU dictated to suspend the heavier slabs (all groups except group B) with using two flat webbing slings. It is worthwhile to mention that bungee cords has good elasticity compared with flat webbing slings. When bungee cords were even used to suspend the small slab (group B), it was stretched, but within elastic range as they were not yielded during this process.

By decreasing the length and width of the slabs, the natural frequencies will be increased because of direct relationships of natural frequencies with stiffness. If smaller dimensions mean stiffer element; is direct relationship with mass (smaller dimensions mean smaller mass). In such cases, the device might merely convenient to extract a couples of natural frequencies readings due to limited capability of both the impact hammer and accelerometers. The device was not sufficient to extract more than three natural frequencies in such cases. For this reason, slabs of dimensions 1200mm x 1200mm length and width were relied so as to extract at least six natural frequencies and their corresponding mode shapes and modal damping.

Figure 4.24: Test slab (600x600x40mm) under free-free boundary condition.

4.5.3   Testing Group C Slabs

Group C slabs were set up for both static and then dynamic tests. Both static and dynamic tests were performed on this series of slabs in order to damage the RC slabs and to identify the effects of damages on modal parameters (natural frequencies, modal damping and mode shapes) of the slabs respectively.

The slab was simply supported at all four sides. Figure 4.25 shows rubber pipe and High Impact polystyrene (HIPs) were set on the top of the metal support around all edges, which were the contact lines between the slab and the support in order to fill probable gaps between them. To apply the partially concentrated monotonic load, a metal square of dimensions 120x120x20mm was placed at the top face of the slab's centre where the concentrated load was going to be applied. The purpose of applying partially concentrated load condition was to make large enough interval allowing modal analysis at well-separated levels of cracking without occurrence any punching shear failure mechanism. Partially concentrated monotonic load test with a constant rate of loading was employed during the test. The left side of the Figure 4.26 illustrates static testing setup. The partially concentrated load was gradually applied at the centre of the slab using a hydraulic jack. Both the hydraulic jack and Linear Variable Displacement Transducer (LVDT) were monitored to a data logger to display the load and deflection. At each prescribed loading step (5, 10, 12kN), the deflection was measured using LVDT. Then, the slab was unloaded and gently put on its side; after that its bottom surface was cleaned in order to inspect progressive crack pattern visually.

Figure 4.25: Rubber pipe and HIPs been placed onto the support contact line.

After each unloading and inspecting steps, the slab was suspended by flat webbing slings to simulate a free-free boundary condition In order to avoid influences of supports on responses of specimen. The right side of the Figure 4.26 exhibits the properly suspended slab; it was subjected to an experimental modal analysis, which is the dynamic test portion. It is worth noting that an experimental modal analysis was firstly performed on the undamaged (intact) state of the slab. EMA of intact slabs is important because the results of intact slabs serve as a reference specimen of same series for later comparison of dynamic characteristics at the different damage states, 5kN, 10kN, 12kN and repaired. In addition, the intact case results would be compared with group A in order to know the effect of increasing thickness from 40 mm to 60mm on modal parameters of the slabs.

Figure 4.26: Static and dynamic tests of group C.

It is noteworthy to mention that at the final loading step corresponding to 12kN load, when the slab became too frail, and just before the yield line formation, the slab was not subjected for further loads beyond 12kN. The cracking pattern of the slab was then repaired. In order to repair the damage, the faulty zone (underneath of the slab) was externally strengthened by bonding a single layer of Carbon Fibre Reinforced Polymer (CFRP). Strengthening using CFRP has become one of the increasingly notable materials used in various fields of engineering including civil engineering applications over the past decade in the modern world. CFRP sheets having width

100 mm was then cut to length of 1200 mm as same of slab's length and width. CFRP type TR30S was used to cover the centre of the slab along both directions. 300mm central strip of the slab was covered by using three parts of a single layer of CFRP strip. The tensile modulus of elasticity and tensile strength of this type of sheets is 135GPa and 2.55GPa respectively. Whereas applying CFRP as a post-strengthening material in the repair of concrete increases the strength, it does not have the significant effect on the stiffness. Therefore, the particular use of CFRP sheets is based on the bending moment, where the maximum bending moment zone was strengthened with this material (Al-Ghalib, 2013).

The bonding of an external CFRP laminate on to the tensile stress zone of the slab specimen subject to dynamic tests was carried out with a system approved epoxy resin (West System Epoxy). This is made out of mixing two materials, resin and hardener, was used to stick the CFRP sheets to the slabs. The mixing ratio (1/5) of 1.0g of hardener for every 5.0g of resin was used to assure a good cure. The mixture should normally be mixed for around two minutes, and there is only less than 20min before it turns into solid. A great attention should be given to the behaviour of bond between concrete and CFRP membrane which depends on the epoxy adhesive. Full bond is necessary for transferring stresses between the concrete and CFRP, hence developing composite action. It is important to mention that epoxy used is proved to be durable material and provides excellent bond to concrete. Figure 4.27 shows the slabs when the location of CFRP sheet was marked and the CFRP sheets placed in position.

Figure 4.27: Strengthening RC slab with CFRP sheet.

4.5.4   Testing Group D Slabs

In this series of slab, the configuration of damage induced into the physical system was similar to that modelled numerically. Group D slabs had induced artificial damage. This was achieved by replacing a concrete area with a polystyrene. Small square blocks of polystyrene, 150 x 150 mm in plan and 30 mm deep, was concealed in the slab at distance 300 in x and y directions from one corner during the casting process of slab. The slab with the void arrangement in the lab is shown in Figure 4.28.

Figure 4.28: Artificial void induced on the surface of the slab during the casting process.

The polystyrene block stiffness is expected to be very low compared with the concrete stiffness and, thus, can be assumed to be zero. The artificial void produced a certain level of reduction of the slab and the moment of inertia (second moment of area). Dynamic test (EMA) was performed in order to identify the presence of damage and its location using modal parameters (natural frequencies, modal damping and mode shapes) of the slabs.

The imperfection induced in slab served as models for familiar practical problems in civil engineering structures manifested as voids, unfilled volume with concrete due to any obstruction or any non-homogeneity in concrete elements. It should be noted that this case describes low level of damage for the slab, corresponding to a local reduction in flexural rigidity.

The experimental procedure consisted of measuring the dynamic properties of the system. Furthermore, the testing results of this group were compared with those of group A (intact slabs) in order to determine the effect of artificial void on modal parameter, whereby the location of damage will be identified.

4.6   Summary

This Chapter introduces the main aspects of the methodology of this research. The vibration testing procedure including the essential excitation source, response source, data acquisition system are summed up. This chapter also presents the details and proper dynamic testing set-up for the equipment commissioned for experiment work. In addition, general facts on the signal processing analysis concept and the quality of the measurements are reviewed. Eventually, the paradigm for the procedure of EMA technique is explained comprehensively along with the quality assurance checks involved in the procedure. In term of quality assurance checks, reciprocity, homogeneity, reapitablity and coherences checks, their general checks agree with the theoretical description. It is clear from the measured frequency response function checks that there is a good agreement for the excitation and its corresponding response. Through the accurate testing procedures with the whole necessary checks, it can be ensured that the vibration measurements represent a realistic experimental model of the dynamics of the reinforced concrete slab.

Once the quality assurance checks were assured for initially tested slabs, the laboratory reinforced concrete slab specimens were classified into four main groups. The specifications of each group of RC test slab were described. Each group consisted of two RC slabs, which were had almost similar concrete strength and steel reinforcement type and spacing. The description of the slabs extended to provide illustrated explanation to the scenarios assigned to each state condition. All slabs were tested under free-free boundary conditions. The casting process of the slabs are described; and the set-up of the partially concentrated bending test is presented.

5. Modal Parameter Estimation

5.1   Introduction

After lab measurements were obtained, and their quality was assured as described in chapter four, the post-test analysis phase is required to be achieved. It is worth to mention that FRF measurements are started to be analysed in this phase to estimate modal parameters of the structure and presenting them in the meaningful manner.

Modal parameter estimation, which is also called curve fitting, is a key step in EMA. It is worthwhile to mention that this step has received more attention during the past thirty years. Hundreds of papers documenting many different approaches were published and can be seen in the technical literature (Richardson and Schwarz, 2003). Modal parameter estimation is a step how to extract or calculate the frequency, damping and mode shapes from the measured data. The measured data is relatively raw form in terms of force (excitation) and response data in the time or frequency domain, or in a processed form for instance frequency response or impulse response functions. It is important to mention that most modal parameter estimation is based upon the measured data being the equivalent impulse response function; or frequency response function (Allemang and Brown, 1987). Equivalent impulse response function typically found by inverse Fourier transforming the frequency response function.

Taking an effort in this chapter on the modal parameter estimation is to explain and simplify the understanding of frequencies, damping ratios and mode shapes extraction of a slab.

The first stage in modelling the dynamic behaviour of a structure is to determine the modal parameters as introduced above:

1- The resonance, or modal, frequency
2- The damping for the resonance – the modal damping
3- The mode shape

The two modal parameters (i.e. modal frequencies and damping ratios) are termed "Global Parameters" as can be estimated from all frequency response measurements on the structure (except those located in a nodal position where the displacement is

zero). However, in order to precisely model the associated mode shape, frequency response measurements must be made over some DOF, to ensure a sufficiently detailed covering of the structure under dynamic test.

Experimental results often require to be compared and correlated to find out unavoidable inaccuracies caused by the user intervention, instrument or any other effects. Therefore, to ascertain validity and reliability of the experimental results, they are required to be compared with results of theoretical counterpart. With regard to the terminology used, the comparison and correlation of theoretical and experimental structural dynamic properties are recognised by Ewins (1995) and DTA (1993c) as two significantly different activities. Comparison is a qualitative process of merely observing both similarities and differences between two sets of data, however, the correlation is shown as more complex activity. This is because the correlation comprises of combining the two sets of data endeavoured at quantifying the differences between them and also the sources that causing these differences (Pavic, 1999).

For this reasons, analytical frequencies of the slab (plate) using closed form equation and numerical frequencies and mode shapes using ANSYS software are also explained how to be extracted. Then, the comparison is made to observe the difference between experimental and theoretical results in chapter 6. Whereas, the correlation is made to observe the location of difference between two condition of experimental results in chapter 7.

5.2   Post-test Analysis and Estimation of Modal Parameters

5.2.1   Overview   Modal Parameters Estimation

The post-test analysis phase is achieved after field measurements are obtained, and their quality is assured. Determining the modal parameters of a structural system from field measurements requires a knowledge of structural dynamics as well as signal processing theory. Modal parameter estimation is known as a complex curve-fitting technique which is a key step in Experimental Modal Analysis (EMA). In general, Modal parameters are evaluated from measured data and specifically Frequency Response Functions (FRFs) or Impulse Response Functions (IRFs). It is

important to mention that IRFs are determined using the inverse Fourier transform of the FRF. In this study, FRF measurements are used and analysed to determine the modal parameters of the tested structure. The obtained modal parameters describe the dynamic behaviour of the structure. Numerous modal parameter estimation techniques are available to perform a convenient analysis and obtain the mathematical model based on modal parameter estimation (Avitabile, 2006). The modal post-test analysis method so-called peak-picking or peak amplitude is commonly used in conjunction with Single Degree of Freedom (SDOF) systems to determine the modal parameters. The peak pick methods are widely used owing to its simplicity. SDOF method accomplishes sufficiently with structures whose FRFs show well-defined and adequately separated modes at resonance frequencies. Then, the FRF data at the vicinity of a resonance frequency is treated as SDOF (Ewins, 2000; He and Fu, 2001). SDOF modal parameter estimation methods calculate the parameters of a system in either a local or global sense. Local techniques determine the modal parameters such as a natural frequency and modal damping from a single FRF measurement. While global SDOF methods determine the modal parameters, for instance, natural frequency, modal damping and mode shapes of a system using a complete row or column of the FRF matrix. Figure 5.1 present the flowchart of modal parameters estimation adopted in this research
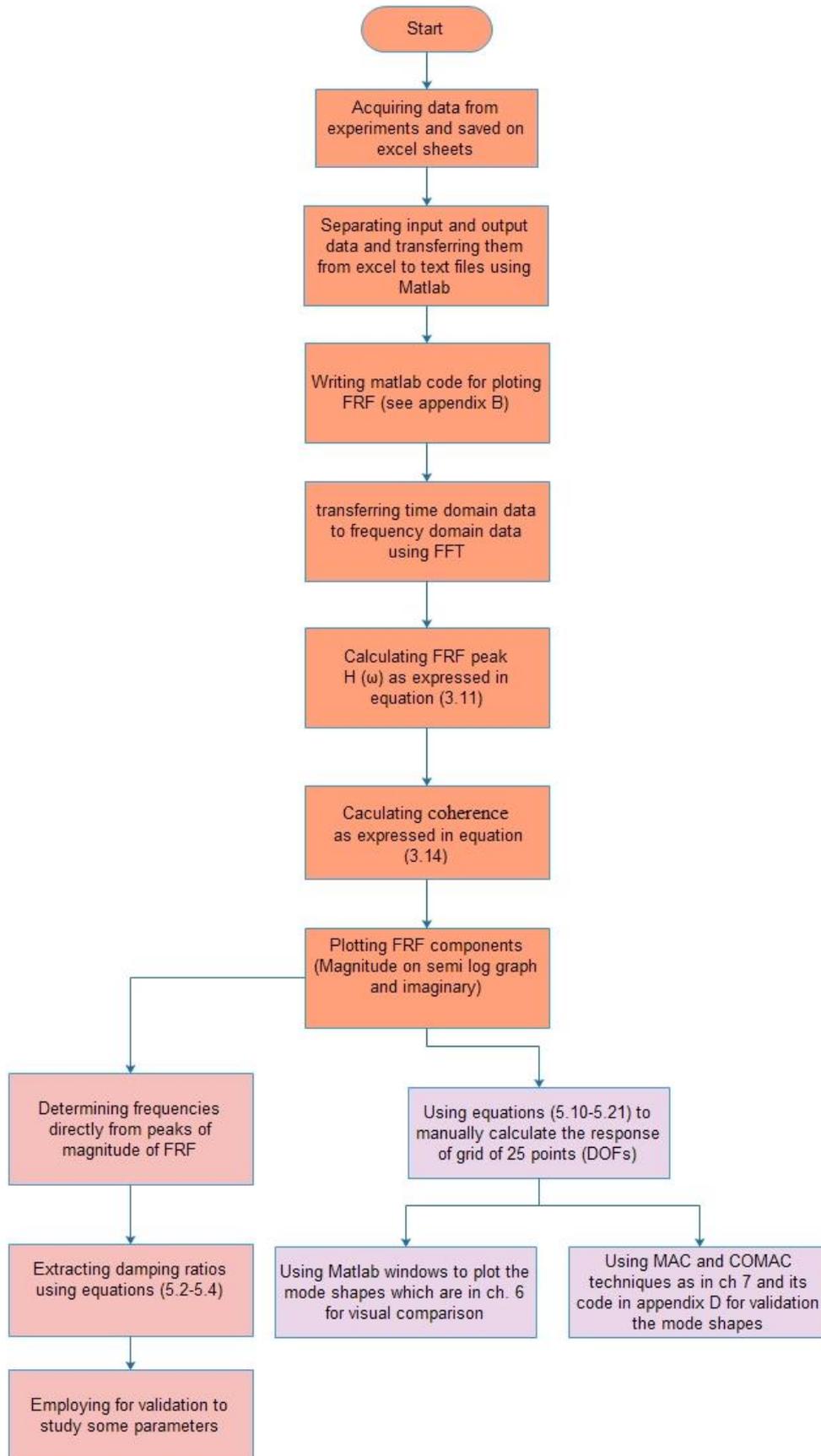
Figure 5.1: Flowchart of modal parameter extraction adopted in this research .

106

5.2.1.1   Resonance Frequency Extraction

FRF is expressed in the following equation which is the ratio of the response to the excitation signals in the frequency domain (McConnell and Varoto, 2008).

$$H(\omega) = \frac{X(\omega)}{F(\omega)} \tag{5.1}$$

Resonance frequency is the easiest modal parameter to be reliably obtained. A resonance frequency is identified as the highest amplitude in the magnitude of the FRF, and the frequency corresponding to the specific peak represents the resonance frequency (ω) of that mode of vibration. The FRF of the slabs were extracted using the program subroutine coded with Matlab. The developed code is presented in Appendix B. From the FRF, the natural frequencies of RC slabs related to each parameters are extracted as shown in Figure 5.2. It is worthy to mention six natural frequencies of the six mode shapes were extracted for groups A, C and D. Whereas, three natural frequencies of group B were extracted.
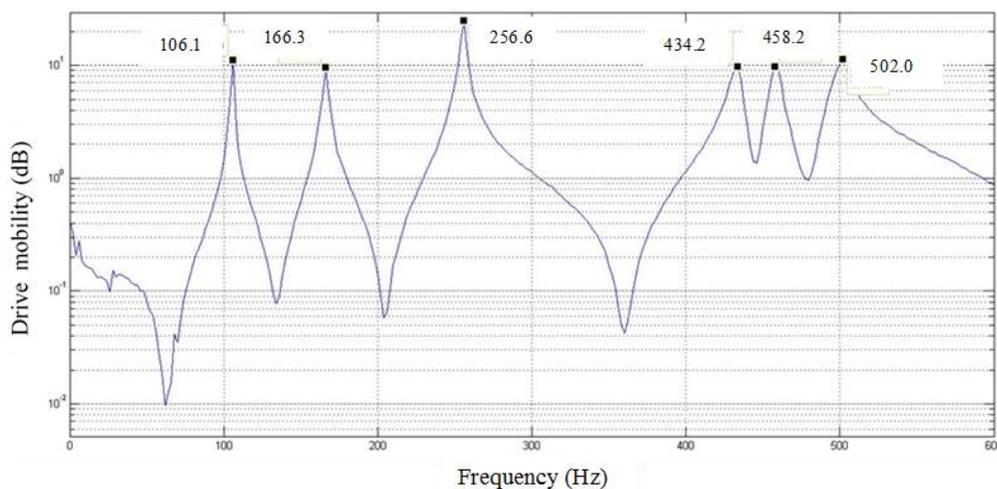
Figure 5.2: Extracting natural frequencies of RC slab.

5.2.1.2   Damping Estimation

It is worth noting that natural frequency and damping of the structure can be extracted from any FRF measurement where the resonance is clearly presented. To

extract the damping of the system, the magnitude of averaged FRF was drawn as shown in Figure 5.3. In the same FRF chart, one of most used method which is called the half power (–3 dB) points of the magnitude of FRF was employed to obtain damping ratio of the slabs. Extraction of the modal damping was relatively simple. From the sharp point of natural frequency, one can easily identify the maximum amplitude and size of half-power. At the value of (–3 dB) and on both sides of the peak, a parallel lines were dropped off on the abscissa axis which is the natural frequency axis.
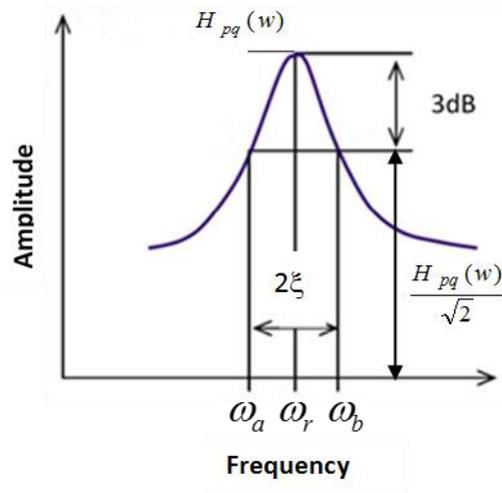
Figure 5.3: FRF log scale plot for extracting damping ratio.

By determining ω_r, ω_a, and ω_b, the modal damping was calculated. Viscous modal damping (ξ) is experimentally identified through the half-power points of a resonance magnitude for FRF and can be written as Equation (5.2) (He and Fu, 2001). Hereby, it is manifested that the width of the response amplitude of SDOF system is proportional to the damping ratio of the system.

$$\xi = \frac{\omega_b - \omega_a}{2 \cdot \omega_r} \tag{5.2}$$

$$\eta = \frac{\omega_b - \omega_a}{\omega_r} \tag{5.3}$$

$$\eta = 2 \cdot \xi \tag{5.4}$$

where:

ξ is the modal damping of the system

ω_r is the resonance frequency

$\omega_b - \omega_a$ is the width of the resonance curve at one over the square root of two

of the resonance

η is the damping loss factor

The calculated viscous modal damping ratios for the RC slabs from the EMA measurements are displayed in Chapter six.

5.2.1.3   Mode Shape Estimation

Mode shapes extraction are more complicated. It is not possible to easily extract the mode shapes from the chart or from only some FRF measurements. Therefore, the mode shapes are usually extracted from sufficient response points. The commonly used single degree of freedom method involves the information at a single frequency as an estimate of the mode shapes of a structure is referred to as Quadrature Picking. This technique is applicable for structure that its modes of vibration are lightly coupled, sufficiently separated; otherwise it is not valid (Agilent Technologies, 2000). Therefore, other SDOF method such as Circle Fit can be used instead when modes of a structure are heavy coupled modes (Ewins, 2000). In practice, RC structures are lightly damped systems where their damping is less than ten percent. As a consequence, the modes of vibration of RC structures will be lightly coupled (Ewins, 2000; Wallack, 1988). Figure 5.4 is a typical example of using the information at the peak frequency location. Negative or positive peak in the imaginary part of the Response (X) Excitation (F) frequency response functions as an estimate of the modal vectors of a simple beam, which are measured from eight equally spaced response points. The imaginary part of the FRF is a more informative plot since amplitude and most importantly the direction of the response are shown (Avitable, 2012). Its amplitude has direct relation with residue, and residue has direct relation with mode shape. Without any scale factor, the drawn mode shapes can be visually observed. It is worthwhile to mention that beam is one dimensional case and it requires a line of response points. However, in two dimensional case, the mode shapes are usually measured from grid response points. Therefore, in this study, the

mode shapes were measured from 25 equally spaced response points on slab's surface.
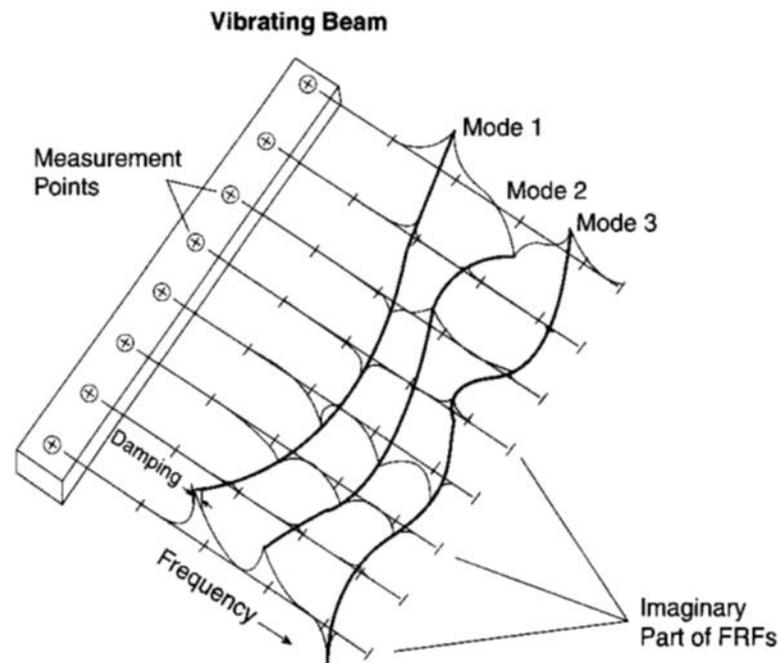
Figure 5.4: Curve fitting FRF measurements (Richardson, 1997).

However, for advanced analysis techniques such as structural dynamic modification, prediction, correlation and simulation, the scaled mode shapes is needed to preserve the correct properties of the structure. The estimation of mode shapes of a system generally follows a two-stage procedure: Firstly, the modal vectors are estimated, which are previously described. Secondly, the modal vectors and modal scaling are determined here. Modal scaling means that mode shapes of a system can more sensibly be derived by including the excitation force by using advanced peak-picking method. In such case, the residues (Ar) of a damped system for a particular mode are estimated at the peaks of an FRF, which are represented as (Ewins, 2000).

$$\mathrm{H}_{pq}(\omega) = \frac{A_r}{\omega_r{}^2 - \omega^2 + 2\xi\omega\omega_r} \qquad (5.5)$$

for under damped system

$$\omega_r = \omega\sqrt{1 - \xi^2} \qquad (5.6)$$

Even, for a 20% of damping ratio, $\omega_r = 0.98 \, \omega$

$$\omega_r \approx \omega \qquad (5.7)$$

$$H_{pq}(\omega) = \frac{A_r}{2\xi\omega\omega_r} \qquad (5.8)$$

Substituted Equation (5.7) into (5.8) and given (5.9):

$$H_{pq}(\omega) = \frac{A_r}{\eta_r \, {\omega_r}^2} \qquad (5.9)$$

$$\left|H_{pq}(\omega)\right| = \frac{A_r}{\eta_r \, {\omega_r}^2} \qquad (5.10)$$

$$A_r = \left|H_{pq}(\omega)\right|\eta_r \, {\omega_r}^2 \qquad (5.11)$$

$$\psi_i = \sqrt{A_r} \qquad (5.12)$$

It is important to mention that the sign of each response point will take from the imaginary part.

where:

η_r is the structural damping loss factor of rth mode of vibration

ω_r is the resonance frequency of rth mode of vibration

A_r is the modal constant/residue of rth mode of vibration

$|H|$ is the maximum amplitude of a receptance FRF

Ψ is the simplified scaled mode shape

The mode shape is scaled at unitary mass. Firstly, the residues Ar are determined from the FRFs of the system, they are scaled according to the driving point information at DOF 1 (DØssing, 1988; Maia and Silva, 1997). Secondly, the damping factor $\sigma r = \xi\omega$ is derived from the width of the pole at the half power points.

111

Finally, the natural frequency of the rth mode is identified from the peak value of the FRF. The damping ratio is estimated from the half –power points which is located at peak with amplitude. The value of the residue A will be calculated afterwards as follows:

$$H_{pq}(\omega) = \frac{A_r}{\sigma_r} \tag{5.13}$$

$$A_r = H_{pq}(\omega) \cdot \sigma_r \tag{5.14}$$

where:

σ_r is damping factor

To mathematically present this method, the residue matrix, which extracted from one measured column of a receptance FRF matrix, is symbolically clarified as:

$$[A]^r = Q_r\{\psi\}_r\{\psi\}_r^T \tag{5.15}$$

where:

$[A]^r$ is driving point residue matrix

Q_r is the scaling factor in relation to r[th] mode of vibration

$\{\psi\}^r$ is the rth mode shape (Eigenvector)

After that, this matrix is disassembled into its equivalent actual mode shape coefficients, and can be expanded to take the form:

$$\begin{bmatrix} A_{11}^1 & A_{11}^2 & \cdots & A_{11}^r \\ A_{21}^1 & A_{21}^2 & \cdots & A_{21}^r \\ \vdots & \vdots & \ddots & \vdots \\ A_{p1}^1 & A_{p1}^2 & \cdots & A_{p1}^r \end{bmatrix} = Q_r \begin{Bmatrix} \psi_{1r} \\ \psi_{2r} \\ \cdots \\ \psi_{pr} \end{Bmatrix} \begin{Bmatrix} \psi_{1r} \\ \psi_{2r} \\ \cdots \\ \psi_{qr} \end{Bmatrix}^T \tag{5.16}$$

Alternatively, for a general residue matrix the corresponding mode shape coefficients can be defined as:

$$\begin{bmatrix} A_{11}^r & A_{12}^r & \cdots & A_{1q}^r \\ A_{21}^r & A_{22}^r & \cdots & A_{2q}^r \\ \vdots & \vdots & \ddots & \vdots \\ A_{p1}^r & A_{p2}^r & \cdots & A_{pq}^r \end{bmatrix} = Q_r \begin{bmatrix} \psi_{1r}\psi_{1r} & \psi_{1r}\psi_{2r} & \cdots & \psi_{1r}\psi_{qr} \\ \psi_{21}\psi_{11} & \psi_{22}\psi_{22} & \cdots & \psi_{2r}\psi_{qr} \\ \vdots & \vdots & \ddots & \vdots \\ \psi_{pr}\psi_{1r} & \psi_{pr}\psi_{2r} & \cdots & \psi_{pr}\psi_{qr} \end{bmatrix} \qquad (5.17)$$

The residue is equal to the expression shown in Equation (5.18) at the driving point location.

$$A_{pq\,r} = Q_r \psi_{pr} \psi_{qr} \qquad (5.18)$$

where:

p is the response DOF

q is the force excitation DOF

The scaling factor Q_r has a relationship between the modal mass of the system, M_r has been shown that the modal mass is equivalent to the expression shown in Equation (5.19) (Dossing, 1988).

$$M_r = \frac{1}{2\omega_r Q_r} \qquad (5.19)$$

where:

M_r is modal mass for r^{th} mode

Q_r is scaling factor for r^{th} mode

ω_r is damped natural frequency for r^{th} mode

When the mode shape is scaled at unitary mass, the modal mass for each mode is assumed equal to one. Equation (5.20) shows the calculation of the scaling factor.

$$Q_r = \frac{1}{2\omega_r} \qquad (5.20)$$

113

Once the driving point residue and scaling factor are calculated, the scaled driving point modal coefficient can be calculated using Equation (5.21). It should start from the point where the excitation force and response are exist simultaneously. For instance, when both excitation and response are at the DOF 1 $\psi_{pr}= \psi qr$, the scaled driving point modal coefficient can be simply calculated using the following equation.

$$\psi_{pr}{}^2 = \frac{A_{pq\,r}}{Q_r} \qquad (5.21)$$

Once this modal coefficient is determined, the rest of the scaled modal coefficients can be calculated using Equation (5.18).

The scaling process is essential to preserve the relative motion between various response points along the model. Furthermore, it is important for utilising mode shape for further analyses such as modelling, correlation, identification and prediction rather than for only visual representation (Avitabile, 2007).

In the two following sections, analytical frequencies of the slab (plate) using closed form equation and numerical frequencies and mode shapes using ANSYS software are also explained how to be extracted. They are required to be compared with results to ascertain validity and reliability of the experimental results,

5.3   Analytical Vibration of Thin Plates

The governing differential equation for the vibration of thin elastic plate assuming small deflection theory and no shear effect is (Blevins, 2001; Lee, 2009):

$$D\left(\frac{\partial^4 w}{\partial_x{}^4} + 2\frac{\partial^4 w}{\partial_x{}^2\partial_y{}^2} + \frac{\partial^4 w}{\partial_y{}^4}\right) + \rho h \frac{\partial^2 w}{\partial t^2} = q \qquad (5.22)$$

Equation (5.23) can also be written in a short form

$$D\,\nabla^2\nabla^2 w - \rho h \frac{\partial^2 w}{\partial t^2} = q \qquad (5.23)$$

Or

$$D\nabla^4 w - \rho h \frac{\partial^2 w}{\partial t^2} = q \qquad (5.24)$$

where:

      w is transverse displacement

      q is applied load on the slab

      ρ is density of the plate material

      D   is bending rigidity of the plate, which is depended as:

$$D = \frac{Eh^3}{12(1 - v^2)} \qquad (5.25)$$

      E is modulus of elasticity of the plate material

      v is the Poisson's ratio of the plate material

      ∇^2 is Laplace operator

$$\nabla^2 = \frac{\partial^2}{\partial_x{}^2} + \frac{\partial^2}{\partial_y{}^2} \qquad (5.26)$$

      ∇^4 is biharmonic operator

$$\nabla^2 = \left(\frac{\partial^4}{\partial_x{}^4} + 2\frac{\partial^4}{\partial_x{}^2\partial_y{}^2} + \frac{\partial^4}{\partial_y{}^4} \right) \qquad (5.27)$$

For free undamped vibration, the external applied load will be zero, hence equation (4.3) will be:

$$D\, \nabla^4 w - \rho h \frac{\partial^2 w}{\partial t^2} = 0 \qquad (5.28)$$

The dynamic response for free undamped vibration of plate can be expressed in the spectral form as (Lee, 2009):

$$w(x, y, t) = \frac{1}{N} \sum_{n=0}^{N-1} W_n(x, y, \omega_n) e^{i\omega_n t} \qquad (5.29)$$

where:

$W_n(x, y)$ is the spectral components of $w(x, y, t)$

N is the sampling number

Substitution of equation (4.8) into equation (4.7) gives:

$$D \, \nabla^4 W_n - \omega_n{}^2 \rho h W_n = 0 \tag{5.30}$$

Solving equation (4.9) for natural circular frequency yields:

$$\omega_n = \frac{\lambda^2}{l \cdot b} \sqrt{\frac{D}{\mu}} \tag{5.31}$$

Or

$$f = \frac{\lambda^2}{2\pi \cdot l \cdot b} \sqrt{\frac{D}{\mu}} \tag{5.32}$$

where:

ω_n is natural circular frequency for n mode, measured in rad/sec

f is natural frequency, measured in Hz

l is dimension of the longer side of the plate

b is dimension of the shorter side of the plate

h is plate thickness

μ is mass density per unit area of plate (ρh)

λ is a dimensionless natural frequency factor

Equation (5.32) offers useful information for finding out approximate natural frequencies of the laboratory slab before any preparation of the experimental work. By knowing the preliminary natural frequencies, appropriate equipment such as impact hammer and accelerometers can be chosen for exciting the specimens as well

as acquiring the responses of such specimens. On this basis, the suitable dimensions of the specimens will be selected otherwise the selected equipment is not capable to clearly acquire the signals which are related to the behaviour of the specimens.

The dynamic modulus of elasticity E_d and Poisson's ratio υ are two important indices for weighing the physical property of concrete material under dynamic loads. Dynamic modulus of elasticity (E), also called dynamic Young's modulus, can be determined from static modulus of elasticity using some specific formula. It represents the elastic property of concrete and is being employed in determining the rigidity of the concrete under dynamic. Lee et al. (1987) and Memory et al. (1995) aimed theoretical analysis to determine dynamic characteristics of reinforced concrete as well as composite constructions, all maintained that is crucial to take into account is dynamic modulus of elasticity of concrete E_d. The dynamic modulus of elasticity is a module which is estimated by means of vibrations of concrete specimens test, only a negligible stress being applied (Neville, 2011). As a matter of fact, the stresses in the structural members under impact vibration condition are extremely small. Owing to a low stress level in concrete, there are no developed micro-cracks and there is no creep. As a result, the dynamic modulus of elasticity is considerably much higher than the secant (static) modulus that is determined by applying the static load onto concrete specimens (Berczynski and Wróblewski, 2010).

Khalil and Gilles, (2002) found that the difference between static and dynamic module of elasticity of concrete is due to heterogeneity of concrete, which affects these two module.

The static modulus of elasticity for normal weight concrete as recommended by ACI 318-11, can be expressed as

$$E_c = 4730 \sqrt{f'_c} \qquad\qquad (5.33)$$

where:

$\quad E_c \qquad$ is modulus of elasticity of concrete expressed in MPa

f'_c is concrete compressive strength based on cylinder test at 28-days, expressed in MPa

While, BS 8110 suggests the following equation for estimating elastic modulus of concretes for normal compressive strength:

$$E_c = 5500 \sqrt{\frac{f_{cu}}{\gamma_m}}$$
                                                                      (5.34)

where:

E_c is static (secant) modulus of elasticity of concrete expressed in MPa

f_{cu} is concrete compressive strength based on cube test at 28-days, expressed in MPa

γ_m is partial safety factor, which is 1.5

Although various empirical relations between static and dynamic modulus of elasticity are valid, the simplest one is proposed by Lydon and Balendran (1986) as quoted by Neville (2011):

$$E_c = 0.83E_d$$
                                                                      (5.35)
where:

E_d is the dynamic (tangent) elastic modulus expressed in MPa

However, the following expression is recommended by British testing standard BS 8110 Part 2, which is utilised to measure the dynamic modulus of elasticity of normal weight concrete. It important to mention that both moduli are expressed in GPa.

$$E_c = 1.25E_d - 19$$
                                                                      (5.36)

Since the compressive strength of cube specimens was taken, equations (3.34) and (3.36) are adopted to work out the static and dynamic modulus of elasticity of

reinforced concrete slab specimens in this study. This is due to the fact that the concrete compressive strength based on cube specimens.

The value of the dynamic Poisson's ratio of concrete is higher than which obtained from the static tests. The average value of the dynamic Poisson's ratio is about 0.24, whereas the static Poisson's ratio is 0.2 (Mather, 1965).

The average concrete compressive strength of three cubes of each slab at 28-days was 29.15MPa. The static modulus of elasticity was calculated after substituting the compressive strength value into equation (3.34). While, the dynamic modulus of elasticity was determined after substituting static modulus of elasticity value into equation (3.36) as presented in Table 5.1. After substitute the dynamic material properties of RC slabs, the natural frequencies of freely supported RC slabs was obtained.

Table 5.1: Static and dynamic material properties of RC slab.

Item	Static	Dynamic
Modulus of elasticity (MPa)	24246	34597
Poisson's ratio	0.2	0.24

5.4   Finite Element Modelling

Finite element modelling is a popular technique employed to analyse complex systems in different engineering disciplines. Its basic idea is that the model is split into a mesh of finite sized elements whose behaviour is generally assumed to be given by applying mathematical expressions. The purpose of finite element (FE) models in many civil engineering applications is to predict the behaviour of structures when subjected to various loading and displacements that would otherwise be difficult to determine. The use of dynamic characteristics in the verification of FE models has become common owing to the global nature of the vibration properties. The dynamic properties are obtained from a FE model through solving an Eigenvalue problem of the system. This involves the extraction of the natural frequencies (eigenvalues) and mode shapes (eigenvectors) in terms of mass and stiffness matrices. The material properties such as Poisson's ratio and dynamic modulus of

elasticity of the FE model of the RC slab are identical to that use in the analytical section.

Several software are available for modelling various structural engineering members to obtain an accurate finite element solution for specific problems. In this study, the linear elastic modal and dynamic response analyses are necessary to be performed by a suitable commercial finite element package. One always has to decide which commercially available package reliable to be opted. Due to its powerful linear dynamic analysis capabilities, it is widely applied to a large number of applications in engineering disciplines such structural, mechanical and aeronautical engineering (Moaveni, 1999). In addition, extensive graphical and pre and post processing capabilities of ANSYS can also be a valid reason to fame this software. As a consequence, ANSYS can also be considered appropriate package to be employed in this work for estimating the dynamic behaviour of reinforced concrete slabs specimens in terms of natural frequencies and their corresponding mode shapes. The following types of ANSYS finite elements are used for FE modelling, both the reinforced concrete slabs; and the cable for hanging the slabs to produce a free-free boundary condition.

• SHELL63

There are three different type of elements namely shell element 63, 181 and 281 provided within ANSYS software which can be used to extract natural frequencies and associated mode shapes for RC slabs. However, after several trials, the author comes to a conclusion that SHELL63” which is shown in Figure 5.5 is the best one to choose for modelling the undamped free vibration analysis of RC slabs. This is because such element is suitable for thin to moderately thick shell structures and commonly used for concrete slabs. Moreover, SHEELL63 is a four-nodded linear elastic element with allowing both bending and membrane action capabilities and six degrees of freedom at each node. More importantly, after several trials, it was found that the natural frequencies of this element is considerably close to the analytical results. In addition, the graphical representation of mode shape of this element is quite obvious to understand.
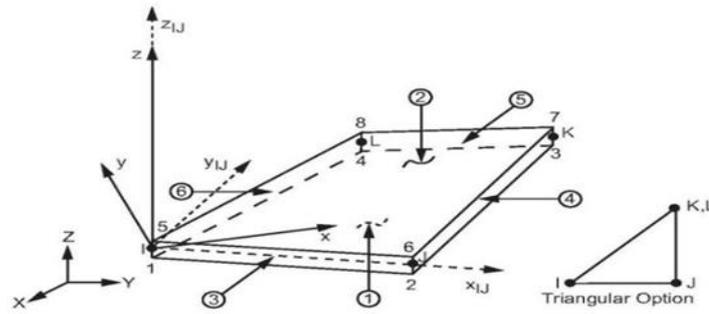
Figure 5.5: Geometry of SIIELL63 element (ANSYS, 2013A).

• COMBIN14 (Spring-Damper)

The Spring-Dampers are chosen as an additional element to model hanging cables for supporting RC slab in order to simulate free-free boundary condition. COMBIN14 is a 2 node element which may have stiffness corresponding to either three translations (linear spring) in the nodal x, y and z directions or three rotations (rotational spring) about the nodal x, y and z axes at each node, depending on which option is desired to be selected.

Figure 5.6 shows the geometry, node location and the coordinate system of COMBIN14 (Spring-Damper). This element is defined by two nodes, a spring constant (k) and damping coefficient (CV).

More detailed description of the mentioned elements can be found in the ANSYS User's Manual (ANSYS, 1995c). After some trail to model free-free boundary condition with or without this element, insignificant difference was found in natural frequencies estimation.
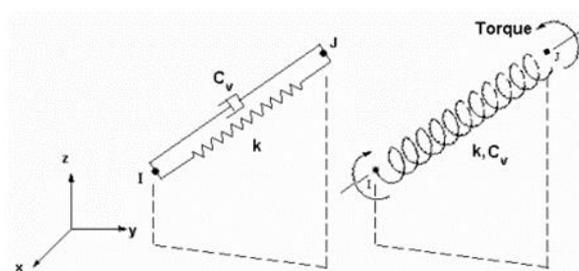
Figure 5.6: COMBIN14 Geometry (ANSYS, 2013B).

A. Boundary conditions

It is widely acknowledged that boundary conditions of the structure are the main source of error between field experiments and laboratory or even computer simulation (McConnell and Varoto, 2008). This mean that the boundary conditions influence the accuracy of the vibration testing results. To minimise such discrepancy error, the structure is required to be tested in a free-free state. Such modelling has already been presented by several researchers including Al-Ghali (2013) and Ndambi et al. (2002).

Freely supported slab implies freely suspended in a space where all its points are not attached to any other member or ground. The reason behind this is that the dynamic measurements have the capability to precisely reflect the properties of the slab when the influence of poorly defined supports are interrupted.

In numerical analyses of free-free conditions, six rigid body modes are exhibited and each of these has a very low natural frequency, close to zero. The frequency will be negligible when the value is lower than those of the bending mode. This context means that the highest natural frequency of rigid body modes is less than 10-20% of the value of the lowest deformation natural frequency (Ewins, 2000). For example, if the first bending mode of a tested structure is 100 Hz, all of the rigid body modes should be less than 10-20 Hz. As a result, such support is considered to be satisfied when the flexural modes of the tested structure are not influenced by suspension approach.

5.5 Experimental and theoretical results of group A slabs

Group A slabs were used to extract the dynamic response of intact slab under vibrational excitation. This group was used as control one. The dynamic response of the free-free supported slabs through natural frequencies were identified after measuring and analysing the experimental data. It is important to mention that some modes shapes from the experiments were disappeared. In experimental modal analysis, it is always possible that some modes are not excited if the force is applied close to the nodal point (Cupial and Artoos, 2001). For symmetric structures, some modes are missing from the model and, therefore, the dynamic properties of the structure for those modes cannot be predicted (Chen, 2001). From experimental work

of this study, the natural frequencies of six mode shapes (1, 2, 4, 6, 8 and 10) were extracted for slabs A. This means that mode shapes corresponding to natural frequencies 3, 5, 7 and 9 were missed in experimental work. This phenomenon is quite normal in the experimental work because it is difficult to identify the natural frequencies of all modes from experimental measurements. This is due to the fact that third and ninth modes may have nodes located at the nodal point. Whereas fifth and seventh mode shapes were missed because of the symmetry of the reinforced concrete slabs which had square dimensions. The natural frequencies of a pair of double modes are almost the same in the symmetric structure. Thus, mode shape 5 and 7 had natural frequency equal to the natural frequencies of mode shapes 4 and 6 respectively. It is able to read or extract only one value of natural frequency of a pair of double modes from the magnitude of the frequency response function.

The experimental and theoretical (analytical and numerical) natural frequencies of six (1, 2, 4, 6, 8 and 10) modes as well as their percentage difference are tabulated in Table 5.2 and they are graphically shown in Figure 5.7. This comparison is to verify the accuracy of the experimental results. The two sets of frequencies are compared on a percentage difference basis as follows:

$$\text{Percentage difference} \ = \ \frac{\left|\omega_{\text{theo}} - \omega_{\text{exp}}\right|}{\omega_{\text{theo}}} \tag{5.37}$$

where:

$\omega_{\text{exp.}}$ is the natural frequency obtained experimentally

$\omega_{\text{theo.}}$ is the natural frequency obtained by analytical and numerical

Table 5.2: Experimental and theoretical natural frequencies of RC slab, group A.

Mode No.	Experimental (Hz)			Analytical (Hz)	Numerical (Hz)	Relative difference %	
	Slab 1	Slab 2	Avg.			Anal. Vs Exp.	Num. Vs Exp.
1	102.3	106.1	104.2	101.1	104.8	3.1	0.6
2	150.7	166.3	158.5	146.8	151.6	8.0	4.6
3	NA	NA	NA	181.8	179.5		
4	250.0	256.6	253.3	260.7	268.0	2.8	5.5
5	NA	NA	NA	260.7	268.0		
6	419.7	434.2	427.0	457.6	459.5	6.7	7.1
7	NA	NA	NA	457.6	459.5		
8	477.2	458.2	467.7	477.1	489.5	2.0	4.5
9	NA	NA	NA	520.6	534.2		
10	502.9	502.0	502.5	581.2	579.9	13.54	13.3

As can be seen in Table 5.2, the relative difference between theoretical (analytical and numerical) and experimental natural frequencies for the second, sixth tenth mode is significant compared to the first, fourth and eighth modes. The lowest error was obtained in the first mode which is only 0.6% when comparing the numerical and experimental, whereas the error 2.0% is found in the comparison between the analytical and experimental in the eighth mode. However, a notable observation of relative difference is found between the experimental and theoretical and numerical natural frequency respectively as about 13.5 and 13.3 % in the tenth mode. This suggests that the higher mode of vibration is more influenced by the flexibility of the hanging cable than the lower modes. The variation of natural frequencies is one of the most common measures used in dynamic testing for condition assessments to monitor the structures. The six experimental natural frequencies of intact RC slabs are recorded and ready to be compared with other groups in order to study the effect of parameters of that group.

When the same process was repeated with group A slabs to extract the natural frequencies, finding any variation to the frequencies in the second trial it means that there is something unusual happening to the specimens. Such trend implies that the natural frequency change is correlated with the imperfection due to any reasons, which will provide the basis for a structural health monitoring of the tested slabs.
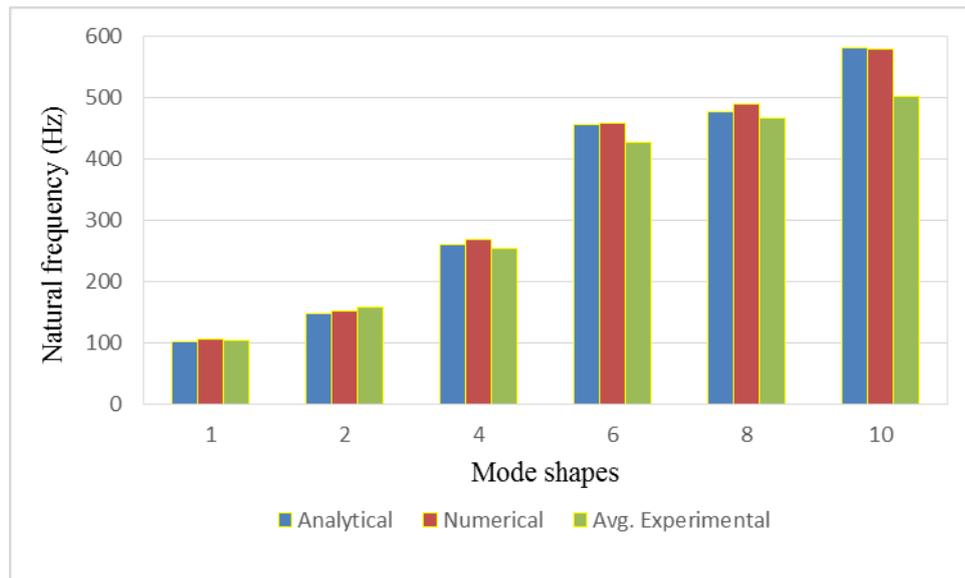
Figure 5.7: Comparison of natural frequencies of RC slab, group A.

The six measured damping ratio of slab A are given in   Table 5.3. Since modal damping is very difficult or unavailable to evaluate analytically, it was evaluated experimentally. As a result, the comparison is made between experimental damping ratios of other groups of slab in Chapter six.

Table 5.3: Damping ratio for test RC slab, group A.

Mode No.	Slab1	Slab2	Average
1	0.85	0.98	0.92
2	0.85	1.1	0.98
4	0.59	1.01	0.80
6	0.89	0.77	0.83
8	0.76	0.76	0.76
10	1.16	0.88	1.02

From previous studies, it is found that the mode shape can also reveal information regarding the state of the structure. It would be expected that the mode shape becomes distorted from the initial shape due to the presence of cracking, change the support or occurrence any other defects.

In experimental modal analysis, it is always possible that some modes are not excited if the force is applied close to the nodal point (Cupial and Artoos, 2001). For symmetric structures, some modes are missing from the model and therefore the dynamic properties of the structure for those modes cannot be predicted (Chen, 2001). From experimental work, the six mode shapes (1, 2, 4, 6, 8 and 10) were extracted for slabs A. These six mode shapes under free-free boundary condition were compared with their counterparts of theoretical analysis. This is to verify that the shapes look to be the same at the corresponding natural frequencies. It is important to note that mode shapes corresponding to natural frequencies 3, 5, 7 and 9 were missed in experimental work. This phenomenon is quite normal in the experimental work because it is difficult to identify the natural frequencies of all modes from experimental measurements. This is due to the fact that modes 3 and 9 may have response points located at the nodal point. Since these mode shapes had a node at the nodal point position, these standing wave patterns for such modes were not be excited. However, mode shapes 5 and 7 were missed because of the symmetry of the reinforced concrete square slabs. The natural frequencies of a pair of double modes are almost the same in the symmetric structure. Therefore, mode shape 5 and 7 had natural frequency equal to the natural frequencies of mode shapes 4 and 6 respectively. Usually, one mode of a pair of double modes can be identified while the other is likely to be missing from the experiment. Avitable (1999) described that the peak amplitude of the imaginary part of the FRF is directly related to the residue (which is directly related to the mode shape). In experimental work, the peak amplitude has only one value to be read. Therefore, mode shape 4 and 6 were identified while their pair mode 5 and 7 missed from the experiment. Thus, missing the information of one mode in a pair of double modes will not affect model updating (Chen, 2001).

The intact mode shapes of groups A are visually compared with numerical mode shapes which are display in the following Figures 5. 8 - 5.10. It is important to note that the experimental mode shapes of slab 1 and 2 of group A as displayed in Figure 5.8 and 5.9 respectively can be directly compared to the numerical mode shapes in Figure 5.10 (e.g. 1st mode in the upper left of each figure should show the same pattern). The colours (from both experimental and numerical) graphs correspond to the areas where the response is highest (red) and lowest (blue).
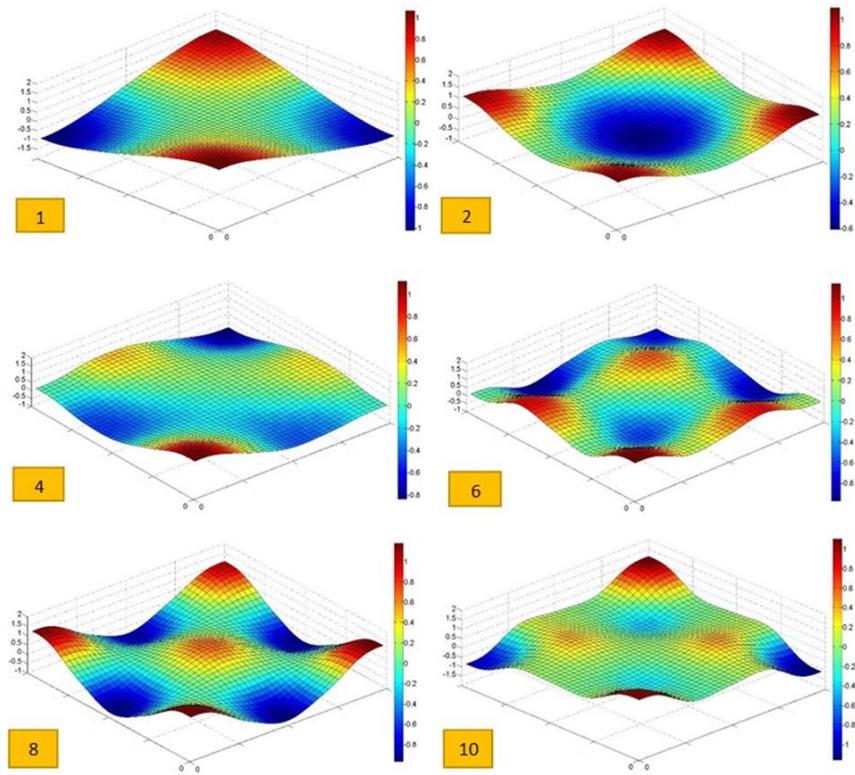
Figure 5.8: Experimental mode shapes of RC slab 1, group A.
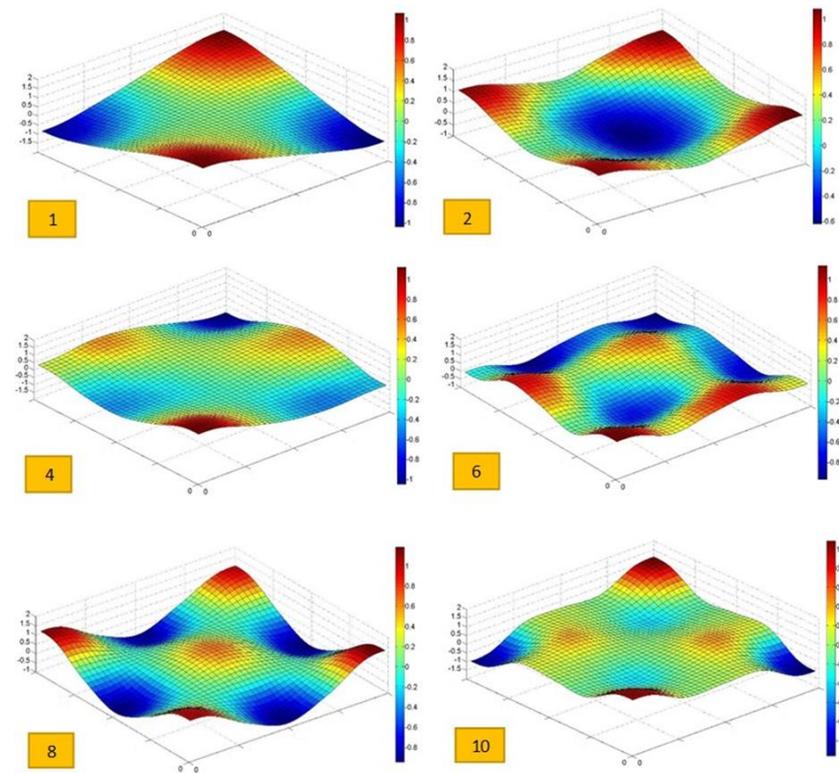
Figure 5.9: Experimental mode shapes of RC slab 2, group A.
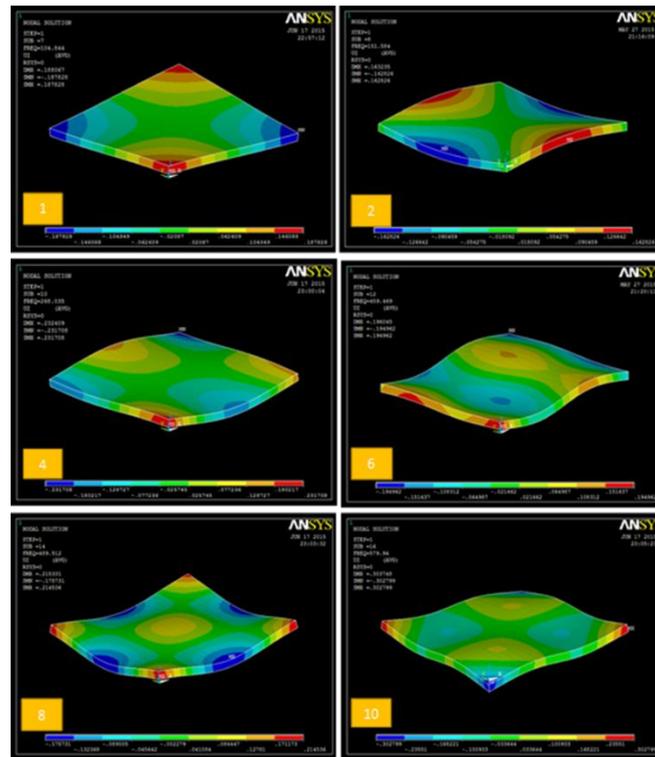
Figure 5.10: Numerical mode shapes of RC slab, group A.

In general, the slab structure was tested while hanging by cables, which closely approximates a free-free boundary condition. The modes of the numerical model were also calculated using free-free boundaries. The main objective of this comparison is to verify the experimental mode shapes with numerical results.

It can be said that close agreement was found between the experimental and numerical mode shapes of the groups A slabs. The first, fourth, sixth and eighth modes as shown in Figure 5.8 and 5. 9 show very clear mode shapes that closely follow the numerical patterns in Figure 5.10. The tenth mode (lower right of Figures 5.8 and 5. 9), resemble the expected patterns, however it has very slight difference (two corners moved up and the other two were moved down) which is contrary to the numerical mode shape. Such slight difference is attributed to the symmetrical condition of the slab. The exception to this case is the second mode which is somewhat different from numerical one. It is expected that the way of hanging of the slab was the source of the difference of this mode. Since the slab was hanged at four corners, the four corners were not fully free as modelled in numerical analysis.

Overall, good agreement was obtained between experimental and numerical mode shapes of reinforced concrete square slabs.

5.6   Summary

It is worth to mention that, this chapter starts how to estimate modal parameters from FRF measurements in the post test analysis and presenting them in the meaningful manner. In this context, modal parameters which is included as resonant frequencies, damping ratios, and mode shapes. The theoretical estimation (analytical natural frequencies using closed form expression and numerical natural frequencies and mode shape using ANSYS software) is also explained. It is also important to mention that dynamic modulus of elasticity and Poisson's ratio are clarified and used for estimating the theoretical results.

In the final section of this chapter, experimental results of control group (A) are compared with theoretical results to ascertain the validity and reliability of the results.

6. Parametric Studies Using Modal Parameter

6.1   Introduction

After lab measurements were obtained, and their quality was assured as described in chapter four, the post-test analysis phase was achieved in chapter five in order to estimate modal parameters. It is worth to mention that modal parameters are started to be analysed in this chapter to study the effect of parametric studies on modal parameters of the reinforced concrete slabs. Therefore, the primary aim of this chapter is to appraise the effect of some important parametric studies on the behaviour of reinforced concrete slabs through modal parameters using experimental modal analysis. Important parametric studies such as dimensions, degree of damage and damage location were studied and tried to examine their effect on modal parameters. Moreover, the effect of parametric studies will be explained. As previously mentioned that experimental results often require comparison to know the degree of possible inaccuracies that might cause during the experiments. Therefore, to ascertain validity and reliability of the experimental results, they are required to be compared with theoretical results.

To study the effect of dimension through changing the flexural rigidity, two slabs of group B were cast and tested and then compared their result with control slabs, group A.

To study the effect of thickness (flexural rigidity), two slabs of group C were cast and tested and then compared its result with control group A. Static and dynamic test were employed for this group. The former test was utilised in order to introduce degree of damage in the slab. Whereas, the latter test was utilised to extract the properties of slab though modal parameters. This case describes gradual increase of damage (in three incremental loading) in reinforced concrete slab corresponding to a gradual reduction in flexural rigidity, which is described as a practical problems in civil engineering structures. To study the effect of degree of damage, the results of slabs under each incremental loading compared with intact case of same group, group C.

To study the effect of artificial damage (void), two slabs of group D were cast and tested and then compared with the results of group A slabs. A polystyrene block was

put in a concrete mix at the particular location of a slab to create artificial damage. The polystyrene block stiffness is expected to be very low compared with the concrete stiffness, and it can be assumed to be zero. As a result, the artificial damage produced an approximate drop in the cross-sectional area as well as drop in the moment of inertia (second moment of area). The imperfection induced in slab served as models for familiar practical problems in structures manifested as voids, unfilled volume with concrete due to any obstruction or any non-homogeneity in concrete elements. It should be noted that this case describes low level of damage for the slab, corresponding to a local reduction in flexural rigidity. Therefore, Dynamic test (EMA) was performed in order to identify the presence of damage and its location using modal parameters (natural frequencies, modal damping and mode shapes) of the slabs.

6.2   Studied Parameters

Important parameters such as dimensions (side length and thickness of the slab), severity and damage location have been studied and tried to examine their effect on modal parameters. In this context, modal properties will be defined as resonant frequencies, damping ratios, and mode shapes. Moreover, the effect of studied parameter on the modal properties will be explained in the following subsections.

6.2.1   Effect on Natural Frequencies

It is known that the stiffness of a structure has direct relation with its natural frequencies. Therefore, any change happens to the stiffness; the effect will be manifested in the natural frequencies. For example, decreasing the thickness of the slab or presence of cracks in it will reduce the stiffness; as a consequence, the reduction in stiffness is revealed as a decrease in the natural frequencies. In this section, it is attempted to evaluate the reliability of natural frequency measurements as a necessary tool. Different parametric studies for instance dimensions of slab; damage severity; the effect of repair works and artificial void of the prescribed slabs were considered using aforementioned technique.

6.2.1.1   Natural Frequencies of Group B slabs

Series slabs of group B were employed to extract the dynamic response of slab under vibrational excitation. The dynamic response of the free-free supported slabs through natural frequencies were identified after measuring and analysing the experimental data. Before studying the effect of parameters of this group of slabs, the comparison between experimental and theoretical natural frequencies of such group is obtained.

Series slab of group B slabs had smaller dimensions and more flexible cable was used for hanging so as to investigate the effects of scaling of the slab modal parameters including natural frequencies. Because of decreasing the dimensions of the specimens (length and width with respect to group A slabs), the natural frequencies is increased, see Equation (5.32). This result is extracting three natural frequencies of the slab instead of six. The average natural frequencies of the two slabs which were taken experimentally are compared with its counterparts, as presented in Table 6.1 and Figure 6.1.

Table 6.1: Experimental and theoretical natural frequencies of RC slab, group B.

Mode No.	Experimental (Hz)			Analytical (Hz)	Numerical (Hz)	Relative difference %	
	Slab 1	Slab 2	Avg.			Anal. Vs Exp.	Num. Vs Exp.
1	237.7	237.7	237.7	269.5	279.5	11.8	14.9
2	369.5	365.6	367.6	395.3	404.0	6.1	9.9
3	NA	NA	NA	484.8	478.5	-	-
4	589.3	571.3	580.3	695.1	714.4	16.5	18.8
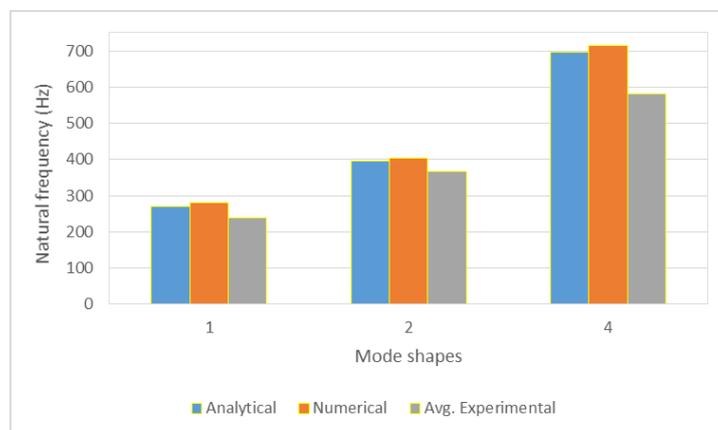
Figure 6.1: Comparison of natural frequencies of RC slab, group B.

It is observed that the first and third modes have the max relative error between experimental and numerical frequencies as thereabouts 14.9%, while it is 18.8% in the fourth mode.

Decreasing the length and width of the slab into half scaled and thickness to two third compared to group A slabs dimensions, the natural frequencies increased significantly. The natural frequencies of group A slabs were 104.2, 158.5 and 256.6 respectively for modes 1, 2, and 4. Whereas, the natural frequencies of group B slabs increased to 237.7, 367.6 and 580.3 respectively for modes 1, 2, and 4.

In addition, the comparison between experimental and numerical natural frequencies of groups A and B is considerably important to be found. Then, it can be decided which dimensions of slab (groups A or B) is better to be tested for further testing. Although the elastic cables was used which is more close to free-free boundary condition than webbing sling, the relative difference of free-free of group B slabs is increased significantly with compared with group A slabs for all three modes. This may due to the fact that small reinforced concrete square slabs with 600 mm edge sides does not precisely reflect the properties of the composite material like reinforced concrete. This means that small defect in the small specimens will cause higher error compared to the big specimens. Moreover, thickness 40mm is not quite enough because any movement of the reinforced mesh during casting will leaves some imperfections (non-uniform cover) that has adverse effect on the dynamic results.

This comparison is quite important to know the accuracy of the tested slabs. The difference between experimental and numerical of all three modes of group A is less than the difference of three modes of the half-size specimens, group B as displayed in Figure 6.2. It is shown that the bigger the size of the specimen, the small the difference between experimental and numerical results. Furthermore, the difference is gradually increased for group A slabs, while it is decreased and then increased for group B slabs.
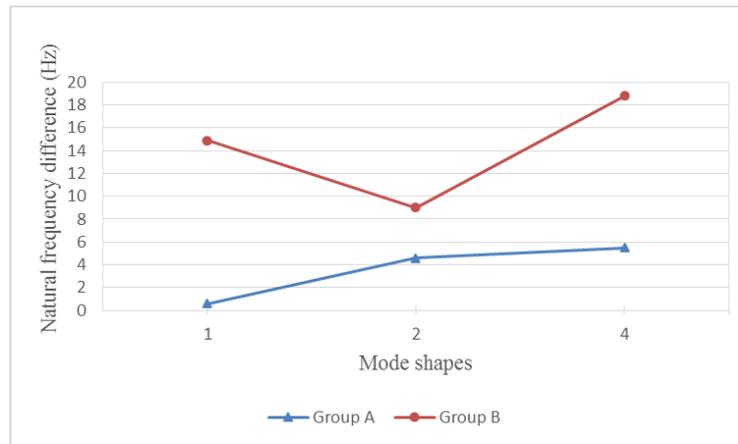
Figure 6.2: Percentage error between numerical and experimental natural frequencies of RC slabs of group A and B.

Even though there is noticeable difference between theoretical and experimental natural frequencies especially of some modes, such difference is quite acceptable for reinforced concrete members. This might be attributed to the fact that the theoretical model assumes concrete slab to be linear, elastic, homogenous and isotropic. Whereas in reality, concrete is heterogeneous and anisotropic material and the specimens are inevitably contain imperfections in forms of crack, defects and steel bars misalignment. Furthermore, such a difference is mainly attributed to the whole process of preparing, making, curing of concrete specimens in lab. For instance, no two batches of concrete mix can be guaranteed of having exactly same ingredients, receiving same degree of compaction or having exactly same dimensions during casting.

Using elastic cable will more closely represent the free-free boundary condition when it is compared with webbing sling cable although there is noticeable discrepancy between the theoretical and experimental natural frequencies of half-size specimen. It is guaranteed that the elastic rope cable which has low stiffness is not the source of the difference, but the difference is due to size of the specimens which is not capable to precisely reflect the behaviour of reinforced concrete slabs.

It was planned to test the RC slabs having small dimensions due to the availability of concrete compression machine to apply static load on such slab dimension. However, after comparison between experimental and theoretical results of the two groups (groups A and B) slabs. As a result, the bigger size slabs were cast and test to study the effect of degree of damage and localised damage on modal parameters for the

rest groups, C and D. Therefore, this conclusion compel to setup new concrete compression machine having capability to apply the concentrated load on bigger size slabs. For this reasons, the installation of new machine to statically test the slab took some months to be prepared and make it ready for testing as shown in Figure 4.26.

6.2.1.2   Natural Frequencies of Group C Slabs

As outlined chapter four, two reinforced concrete slabs were cast in the laboratory, both of which were used to conduct the same tests. There were these purposes of making group C slabs. Firstly, the tests were carried out to validate the experimental results, against theoretical ones. Secondly, it was intended to find out the effect of slab thickness (i.e. slab stiffness) on modal parameters through comparing the results of the group C slabs with those of group A. Thirdly, the reinforced concrete slab specimen was subjected to partially concentrated load at the centre to introduce different degree of damages. Then, the effect of different degree of damages of the reinforced concrete slab on the modal parameters were also determined.

Firstly, six experimental and theoretical (analytical and numerical) natural frequencies of the slab with their relative difference are tabulated in Table 5.3 and they are graphically shown in Figure 5.13.

Table 6.2: Experimental and theoretical natural frequencies of RC slab, group C.

Mode	Experimental (Hz)			Analytical	Numerical	Relative difference %	
No.	Slab 1	Slab 2	Avg.	(Hz)	(Hz)	Anal. Vs Exp.	Num. Vs Exp.
1	72.2	78.5	75.4	67.4	69.9	11.87	7.9
2	108.1	116.4	112.3	97.9	101.0	14.74	11.2
3	NA	NA	NA	121.2	119.7		
4	163.9	178.0	171.0	173.8	178.7	1.61	4.3
5	NA	NA	NA	173.8	178.7		
6	270.5	294.3	282.4	305.1	306.3	7.44	7.8
7	NA	NA	NA	305.1	306.3		
8	291.6	310.8	301.2	318.0	326.3	5.2	7.7
9	NA	NA	NA	347.1	356.1		
10	312.0	326.7	319.4	387.4	386.6	17.6	17.4
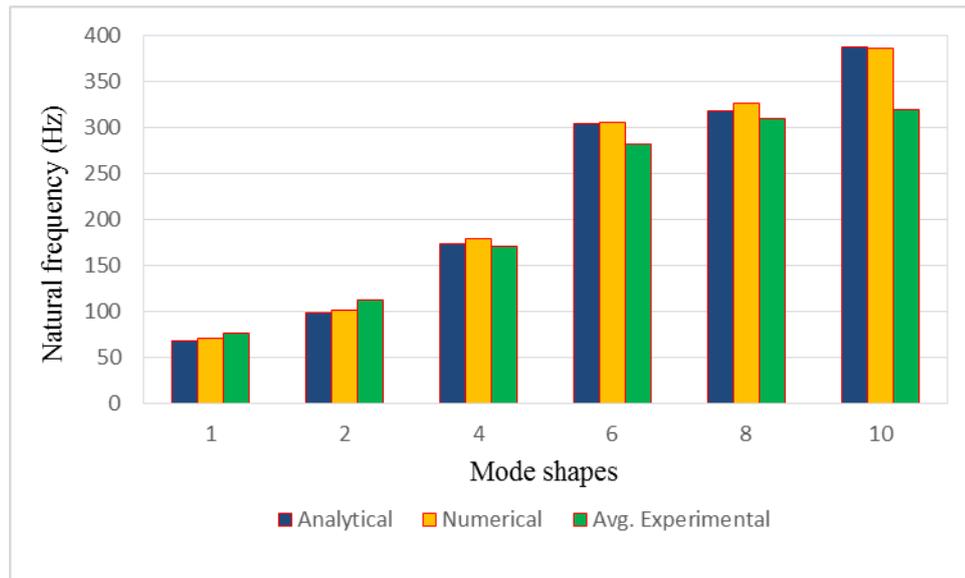
Figure 6.3: Comparison of natural frequencies of RC slab, group C.

The relative difference between theoretical (analytical and numerical) and average experimental natural frequencies for all modes except tenth mode is less than 15%. The lowest difference was obtained in the fourth mode which is only 1.6% and 4.3% when compared experimental frequencies with analytical and numerical frequencies respectively. However, a notable observation of relative difference is determined between the experimental and theoretical natural frequency respectively as approximately 17.6% and 17.4% at tenth mode was obtained.

This means that thickness 40mm may not quite enough because any movement of the reinforced mesh during casting may leave some imperfections (non-uniform cover) that cause such difference between theoretical and experimental results. However, it was intended to make the thickness of this group slab 40mm in order to be more flexible and introduce different degree of damages under low range of loading.

Secondly, in considering the effect of thickness, there are two different thickness by which the effect of natural frequency can be described. For group A, the slab thickness is 60mm, which given span to thickness ratio (L/h = 20). Whereas, group C, the slab thickness is 40mm, which given span to thickness ratio (L/h = 30). The six experimental natural frequencies of both groups (A and C) were determined and plotted as shown in Figure 6.4.
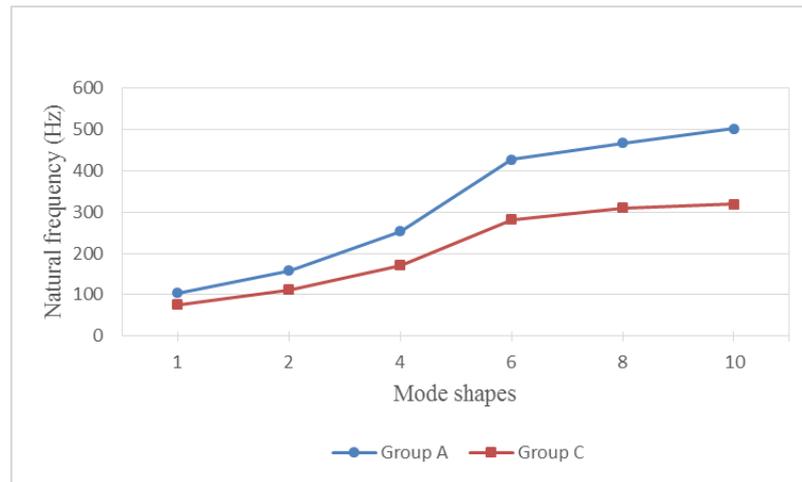
Figure 6.4: Six natural frequencies of groups A and C.

It is concluded that the natural frequencies of all six modes were decreased as the span to thickness ratio was increased. This is due to the fact that decreasing the thickness meant increase span to thickness ratio when slab had constant span. Decreasing the thickness of group C slabs meant decrease the stiffness of the slab which had proportional relation to decrease the natural frequencies of group C slabs compared with natural frequencies of group A slabs.

Furthermore, Figure 6.5 reveals that the higher the mode shape, the higher deviation in natural frequencies might be observed. This is because the lower modes were not be affected as high as the higher modes when the thickness decreased from 60 to 40mm.
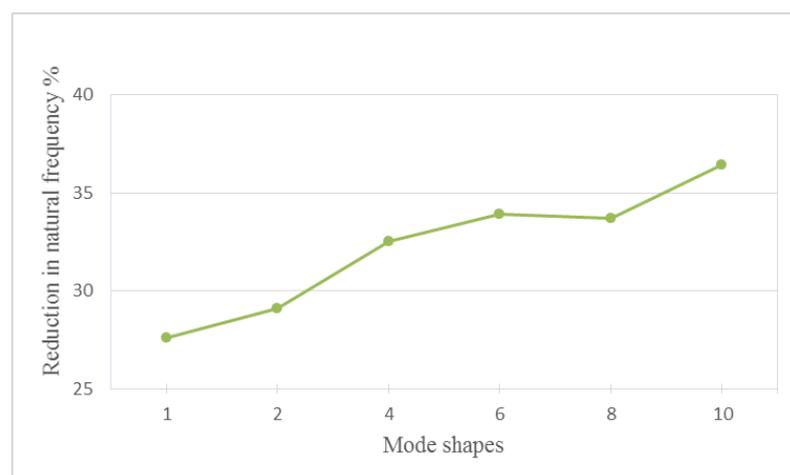
Figure 6.5: Deviation of frequency between groups A and C.

The third objective testing of group C is to extract the natural frequency at various level of damage conditions of the slab. For the intact condition, natural frequencies were determined before applying the partially concentrated load. Then, natural frequencies of the partially damaged slab were determined after applying the partially concentrate load and inflicting the perfection to the slab. For each incremental load, the intact and corresponding defective natural frequencies were compared against each other to identify the degree of defect inflicted to the model under such condition.

The change in natural frequency is correlated with the load level applied to the slab to provide the basis for a structural health monitoring of the tested slabs. By increasing the applied load, gradually and progressively started to experience corresponding level of damage. Before inflicting the damage and after each loading step different modal tests were carried out. For the damage scenario, the slabs were loaded by means of partially concentrated load. The loading was applied in three loading/unloading cycles with peak forces of 5, 10 and 12kN respectively. At the end of each static load step, the slab was unloaded and gently put on its side; after that its bottom surface was cleaned in order to inspect progressive crack pattern visually. The first visually small crack occurred at a load of 5kN, see Figure 6.6.
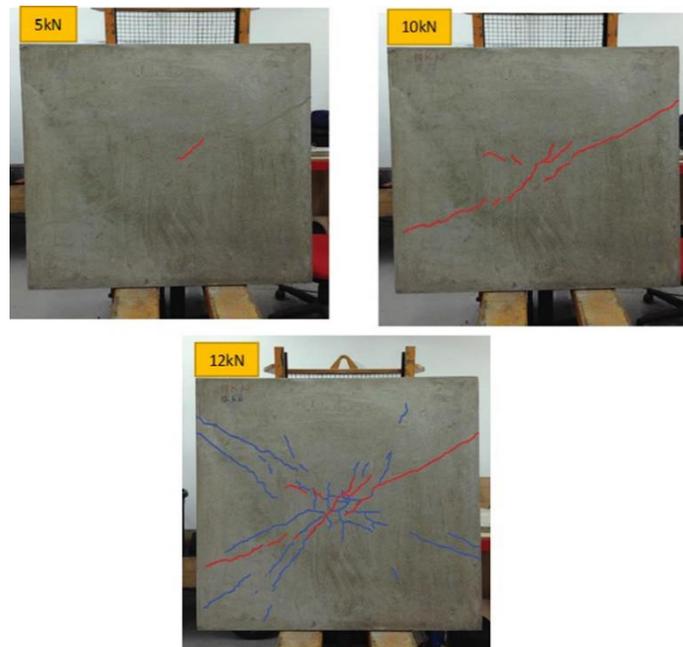
Figure 6.6: Crack patterns under different loadings.

During the penultimate incremental loading, the cracks were observed to increase in length and width. Due to the significant flexural cracks emerged in the slab's underneath in all direction; the loading process was stopped, at 12kN, before the ultimate load is reached. It is worth pointing out that the maximum load of the last loading cycle was decided to be corresponding to about 70% of analytical ultimate load with respect to flexural resistance of Pu=16.72kN. This average load capacity was found according to various codes of practices which are EC2, BS 8110 and ACI318-11. The detailed calculation can be found in appendix C.

After the final static load 12kN and doing the dynamic test, the slab was repaired as the defective zone strengthened by bonding external CFRP sheets. The slab was removed and its tension face was cleaned of dust and debris to ensure proper and effective bond between CFRP and concrete. Once the slab was cleaned, three zones each of which was 100mm wide and 1200mm long were defined on the tension face in both directions in the middle of the slab. These marked areas were the positions where the CFRP sheets were placed, as shown in Figure 6.7.
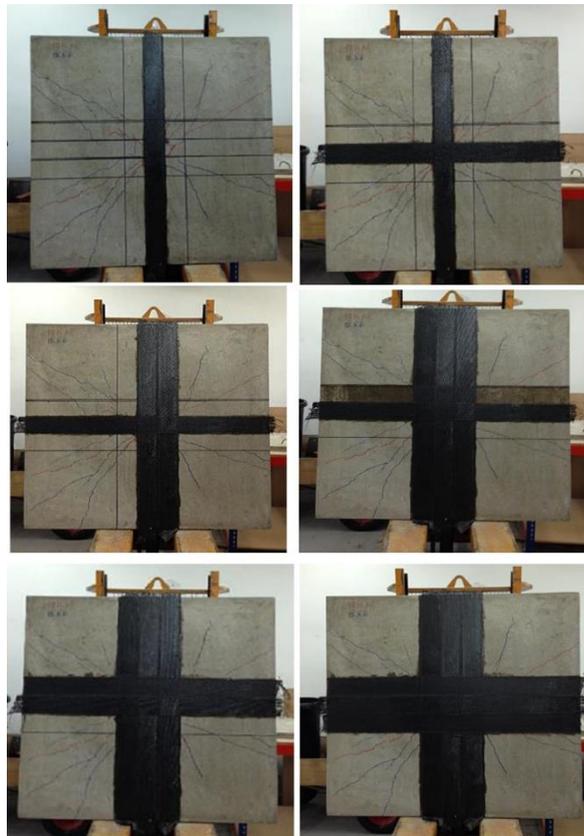
Figure 6.7: Steps for bonding CFRP on the slab.

The 105 epoxy resin and 205 hardener mixture was prepared in required amount. The mixture had a ratio of 5:1 (resin: hardener). After the mixture was well stirred for few minute, it was then applied to the marked positions on slabs underneath. The CFRP fabrics was then applied to the marked position as soon as the resin was applied. CFRP sheets were placed on position in vertical and horizontal direction, over lapping one another, to make an interlock interlace one to the other. Slabs was then left to dry for at least 24 hours to harden completely. After it was checked that the bonding agent was dried, it was then tested dynamically to extract the modal parameters.

Table 6.3 shows the results of natural frequencies of six modes of slabs 1 and 2 and their average under different damage scenarios. After averaging the natural frequencies of both slabs, the shift in natural frequencies is presented in Table 6.4 . The percentage of reduction in natural frequency for each stage is defined as the percentage of difference between natural frequencies of the intact and defective slabs. The frequencies of the defective slabs decrease after damage occurs due to first, penultimate and final load level. Figure 6.8 illustrates the drops in the six natural frequencies for each loading condition from the reference intact case for slab.

Table 6.3: Natural frequencies of RC slabs, group C, under different load levels.

Frequencies of series C (1200x1200x40)					
Slab 1					
Load step Mode No.	Intact	5kN	10kN	12kN	Repaired
1	72.2	69.9	52.1	50.0	58.0
2	108.1	100.1	76.0	75.8	89.1
4	163.9	139.4	102.5	88.62	116.0
6	270.5	268.0	210.0	189.9	238.9
8	291.6	280.4	236.5	220.2	249.7
10	312.0	304.0	272.1	252.3	275.9
Slab 2					
1	78.5	75.9	63.67	60.0	66.6
2	116.4	105.7	98.92	81.53	96.4
5	178.0	168.5	126.1	106.8	138.0
6	294.3	290.2	253.8	229.7	236.7
8	310.6	304.8	276.9	242.5	256.2
10	326.7	324.0	295.7	278.2	286.2
Average of slabs 1 and 2					
1	75.4	72.9	57.9	55.0	62.3
2	112.3	102.9	87.5	78.7	92.8
4,5	171.0	154.0	114.3	97.71	127.0
6	282.4	279.1	231.9	209.8	237.8
8	301.1	292.6	256.7	231.4	253.0
10	319.4	314.0	283.9	265.3	281.1

After the samples were initially loaded to 5kN and then unloaded, hair crack initiation can be seen in the bottom of the slab, see Figure 6.6. Then the dynamic test was performed and the data was analysed and then the natural frequencies for each defective stage compared with the intact case. As can be seen in Figure 6.8, drop in natural frequencies under 5kN for all modes is low when compared to penultimate and final load levels.

Table 6.4: Deviation in natural frequencies of RC slabs, under different loading levels.

Reduction in frequencies due to incremental loads					
Average of Slab 1 and 2					
Load step Mode No.	Intact	5kN	10kN	12kN	Repaired
1	0.0	3.3	23.2	27.1	13.3
2	0.0	8.4	22.1	29.9	17.9
4	0.0	9.9	33.2	42.9	29.9
6	0.0	1.2	17.9	25.7	13.4
8	0.0	2.8	14.8	23.2	9.3
10	0.0	1.7	11.1	16.9	5.9
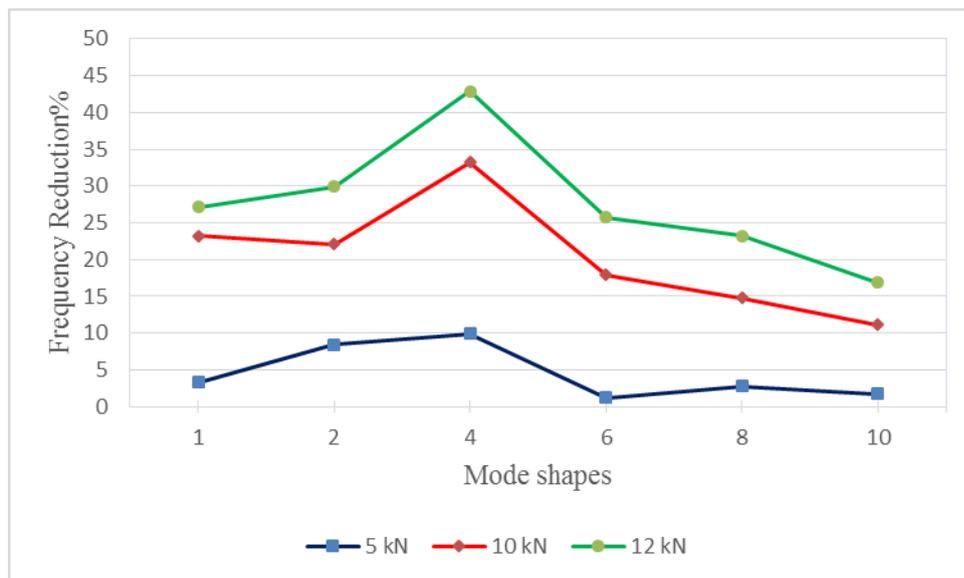
Figure 6.8: Reduction in natural frequencies of RC slabs under different loading levels.

Drops of 3.3%, 8.4%, 9.9%, 1.2%, 2.8% and 1.7% were respectively observed for the six frequencies (corresponding to 5kN load). These percentages of difference is not significant. This trend is due to the fact that the effect of crack on natural frequencies is in its early stage and therefore the slab's sections were visually in a flawless condition.

It is evident that applying a load on the specimens gives energy for the crack initiation and propagation process. Crack initiation and subsequent growth happened quite readily due to increasing the load to 10kN, see Figure 6.6. This means that the one hair crack was diagonally launched at first load level, 5kN. Such crack started to open and developed diagonally to toward the edge of the slab with formation some other cracks at load level 10kN. As can be seen in Figure 6.6., at penultimate load level which is 10kN, the drop in natural frequencies for the first, second and fourth modes is quite significant 23.2%, 22.1% and 33.2% compared to the drop in early stage load level, 5kN. The reduction can be seen in modes sixth, eighth and tenth are about 17.9%, 14.8% and 11.1% respectively. This trend is suggested that the first, second and fourth modes of vibration of the slab is more influenced by the crack pattern than higher modes. Furthermore, the drop in natural frequencies for all modes of penultimate load level is higher when compared to the 5kN load levels.

Near to the ultimate load stage (P=12kN), drops of 27.1%, 29.9%, 42.9%, 25.7%, 23.2% and 16.9% were observed for the frequencies of first, second, fourth, sixth, eighth and tenth mode respectively. The reduction in natural frequency of the slabs under this condition can be divided into typically two regions, that is, increased the reduction from mode 1, 2 and 4, while it is decreased from 4, 6, 8 and 10 respectively. This means that a notable observation is drawn as 42.9% drop in the fourth frequency (corresponding to 12kN load) was obtained. As is seen in natural frequency trends, the frequency reduction of the fourth mode increased significantly responding to the increasing damage. From the crack patterns shown in Figure 6.6 in general, it is obvious that the situation was closed to the ultimate load that is why the loading was stopped to be apply on the slab in order to avoid the formation of the yield line.

Although the slabs sections were visually in an imperfection condition, a percent of 13.3%, 17.9%, 29.9%, 13.4%, 9.3% and 5.9% of frequency deviation was recovered for the six frequencies when the slab was repaired by using CFRP. It is notable that, the rate of recovery was higher for the fourth mode since the modification likewise the deterioration affected heavily the fourth modes as shown in Figure 6.9. This means the rate of recovery of CFRP sheets in the natural frequencies is higher as the damage increases. The same trend was also concluded for the beam specimens tested by Al-Ghalib, 2013.
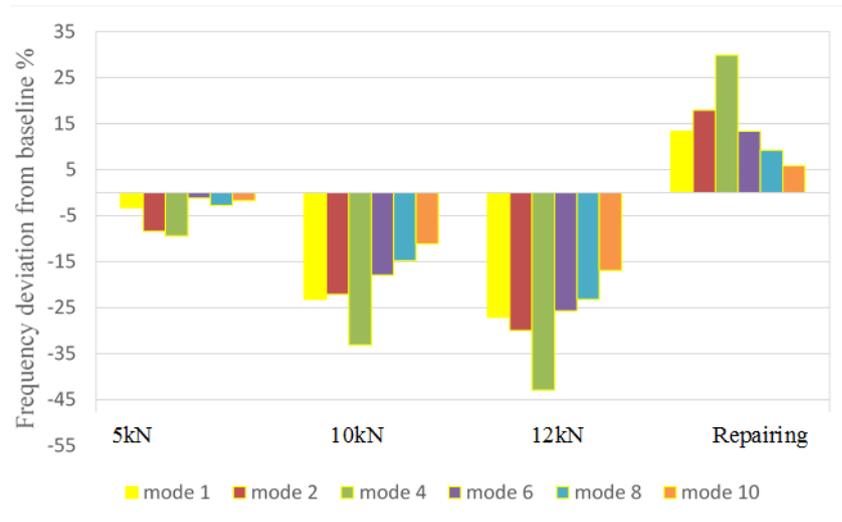
Figure 6.9: Natural frequencies deviations of RC slabs under different conditions.

Although there is clear evidence that the amount of reduction in the natural frequencies appears to increase as the damage increases, different modes have different sensitivities to the damage introduced due to the applied load. For instance, it is observed that the percentage of drop in frequency for all modes non-linearly changes as the applied concentrated load is doubled (5kN to 10kN). For example, in the first incremental load, the percentage of reduction of natural frequencies of the first, second and fourth modes is 3.3%, 8.4% and 9.9% respectively, while it is 23.2%, 22.1%, 33.2% for the same modes under the penultimate load level. The overall trend of frequency decrease after occurring damage that would be expected for all modes. However, it is not guaranteed all modes have same sensitivity to the applied load that inflicts severe cracks.

On the whole, the variation in natural frequencies corresponds to the severity of inflicted damage due to unusual reasons. The variation in natural frequencies can be used as one useful indicator to identify the presence of damage but not for assessing the extent of damage in reinforced concrete slabs precisely.

6.2.1.3   Natural Frequencies of Group D Slabs

For group D slab, the imperfection induced in slab served as models for familiar practical problems in civil engineering structures manifested as void. The configuration of induced void into the physical system of the slab was investigated in an effort to simulate practical defect. At distance 300x300 mm in both directions

with respect to one corner of the slab, a concealed cavity hole of 150x150 mm in plan and 30 mm deep dimension was created, as previously shown in Figure 4.28. Dynamic test (EMA) was performed in order to identify the effect of void presence. A comparison between numerical and the average of the experimental natural frequencies for the six modes of this group was made in order to identify the accuracy of the experimental natural frequencies of this case. Then the six average experimental natural frequencies was compared with the group A which is the intact case in order to find out the effect of the artificial void on natural frequencies. The six natural frequencies resulting from the numerical analysis are listed in Table 5.6 and then compared with the average natural frequencies of two slabs of group D, as shown in Figure 6.10.

Table 6.5: Experimental and numerical natural frequencies of RC slab, group D.

| Mode | Experimental (Hz) | | | Numerical | Relative difference % |
No.	Slab 1	Slab 2	Avg.	(Hz)	Num. Vs Exp.
1	104.0	94.8	99.4	104.3	4.7
2	162.2	150.7	156.5	151.1	3.6
3	NA	NA	NA	178.9	
4	248.6	230.1	239.4	265.3	9.8
5	NA	NA	NA	267.8	
6	406.5	377.2	391.9	456.7	14.2
7	NA	NA	NA	456.9	
8	444.0	429.5	436.8	487.4	10.4
9	NA	NA	NA	532.5	
10	486.8	462.1	474.5	577.5	17.8

The two sets of frequencies were compared against each other. Good agreement was found for modes 1, 2 and 4, which is less than 10%. However, the difference is greater than 10% for modes 6, 8 and 10.
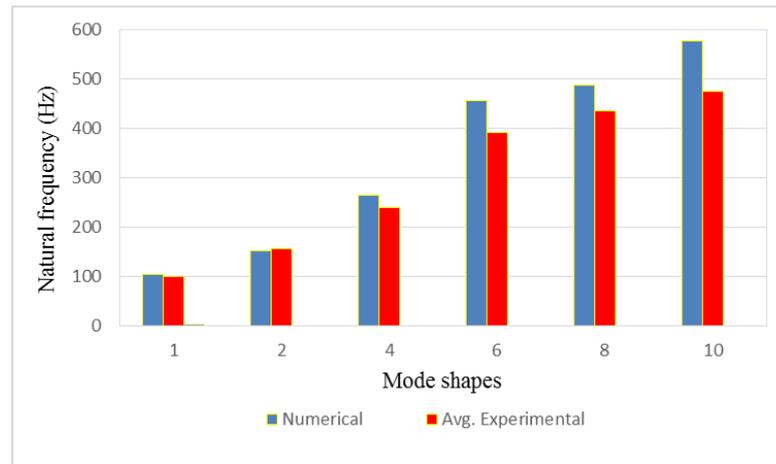
Figure 6.10: Comparison of natural frequencies of RC slab, group D.

Regarding the comparison between group A and D slabs, the natural frequencies of the intact condition of each particular mode were moderately higher than the frequencies of artificial voided sample as presented in Figure 6.11. Figure 6.12 shows the decreases were 4.6%, 5.5%, 6.6% and 5.7% for the first, fourth, eighth and tenth mode, respectively. However, the natural frequency of the second mode for both conditions was considerably close, with the deviation of 1.3%. Conversely, the maximum decrease happened for the sixth mode that was 8.2%. In this case study, the second mode can be accounted to the fact that the reduction of this mode was less likely influenced by damage. Apparently, the effect of the drop in mass for the defective slab on the natural frequencies was compensated by an almost similar reduction in stiffness. These results indicate that when a structure is inflicted with global damage such as voids, deviations in natural frequencies can be considered as modest parameters for structural condition assessment.
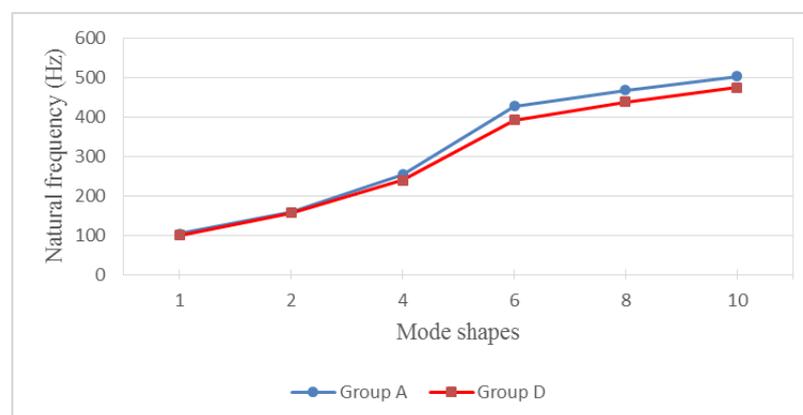
Figure 6.11: Comparison between natural frequencies of groups A and D slabs.
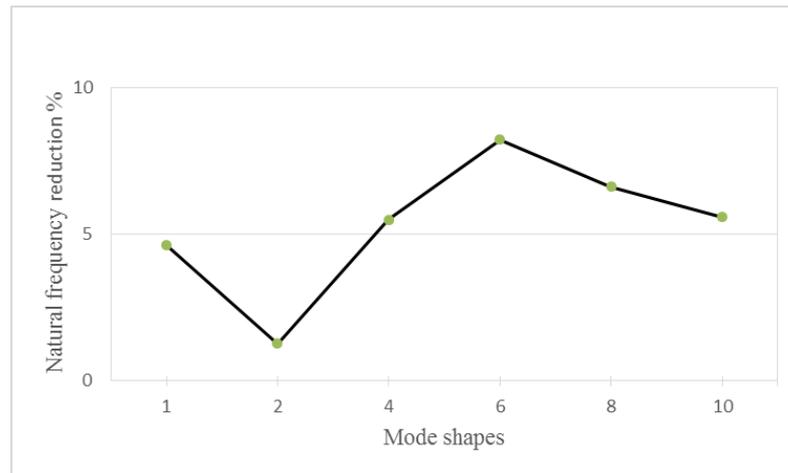
Figure 6.12: Percentage reduction in natural frequencies between groups A and D slabs.

On average, the aforementioned outcomes indicate that when damage such as void is induced into the physical system, such as engineering structure, deviations in natural frequencies can be considered as modest parameters for damage condition assessment.

6.2.2   Effect on Damping Ratios

Damped waveform can die out as it loses energy. The loss of mass and stiffness manifested as high damping ratio as expressed in Equation (6.1). Principally, the stiffness of a structure has an inverse relationship with damping ratios. The presence of damages in structural elements often decrease the stiffness. Thus, the amount of the energy dissipation will increase. This will be manifested through peak height and peak width of the FRF measurements. Since damping is sensitive to changes in stiffness of structural elements, it is utilised as damage detection parameter by researchers. It is imperative to take into consideration the quality factors for instance quality of FRF measurements and resolution of spectral lines when calculating damping ratio value. These factors provide credibility to the estimated results of damping ratio (Gade and Herlufsen, 1994). Owing to the closing of open cracks, damping estimation in unloaded free-free structure under dynamic testing could provide less damping than in the loaded simply supported one. This is due to the fact that the energy dissipation of the open cracks is higher than the close cracks.

The damping ratio is an important parameter in vibration engineering and it is very difficult to evaluate analytically (Mathuria and Kulkarni, 2000). The damping ratio is a measure of energy dissipation and it must be evaluated experimentally. Therefore,

147

the experimental damping ratio of the slabs will be compared in the following sections.

$$\zeta = \frac{c}{2.\sqrt{mk}}$$ (6.1)

Where:

ζ   is the damping ratio

c   is the damping constant

m   is the mass

k   is the spring constant

6.2.2.1   Damping Ratios of Groups B Slabs

The three measured damping ratios of group b slabs are given in Table 6.6. Although the damping is a measure of energy dissipation because of the presence of widely spread cracks, some others factors are also capable to affect it such as stiffness and mass.

Table 6.6: Damping ratio for test RC slab, group B.

Mode No.	Slab1	Slab2	Average
1	0.93	1.2	1.07
2	1.5	1.41	1.46
4	0.56	1.09	0.83

The value of damping ratio of the first mode is lower than of the second mode while it is higher than the fourth mode. The sensitivity of second mode is greater than first mode, whereas the lowest sensitivity can be seen in the fourth mode.

Since damping ratio is very difficult or unavailable to be evaluated analytically, it was evaluated experimentally. As a result, the comparison is made between experimental damping ratio of two groups A and B slabs as shown in Figure 6.13.
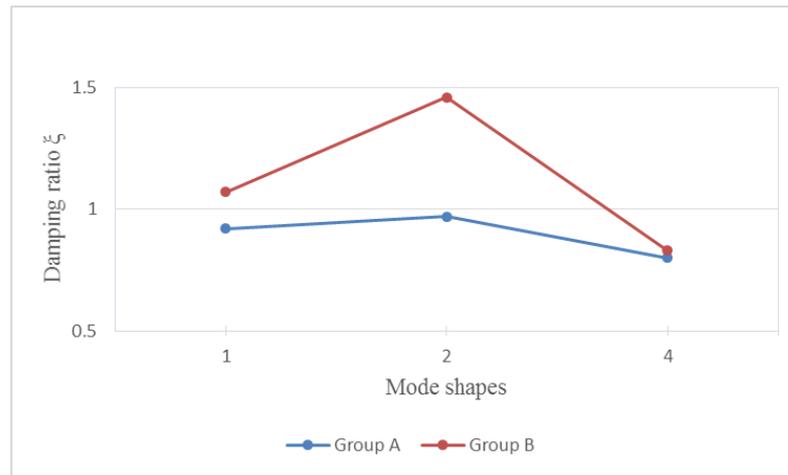
Figure 6.13: Identified damping ratio for tested RC slab, group A and B.

In general, there are six modes of vibration for group A and three for group B that show an apparent change in the modal damping ratio. Owing to changing the dimension or any other factor, the effect of the parametric study on modal damping ratio must differ in both sources, group A and B. It is showed that the measurements of damping ratios of the scaled slab in group A is less than damping of half-scaled slab for all identified three modes. The results revealed that there is a clear direct relationship between decreasing slab's dimensions and increasing in damping, however, it is nonlinear relationship. This means that the damping for all different modes of the slabs did not consistently increase as the dimensions increased.

6.2.2.2   Damping Ratios of Group C Slabs

Testing group C slabs was carried out in order to investigate the effect of thickness on modal damping. In addition, the effect of degree of damage induced in slab due to the incremental loading on damping ratios was investigated. Although there were some successful attempts by some researchers to use damping ratios as an indicator of damage detection (Gomaa et al., 2014; Curadelli et al., 2008), damping is still a controversial factor in the field of damage detection (Navarro et al., 2014; Williams and Salawu, 1997). Despite the fact that inconsistency in changes of damping values have been noted earlier and many researchers believe that damping is an unreliable indicator for damage detection, Abdul-Razak and Choi (2001) draw a different conclusion. They cast and tested three reinforced concrete beams for their research. First beam indicated the undamaged beam, while the other two were subjected to different states of reinforcement corrosion, and were therefore noted as damaged

beams. A conclusion was made that modal damping of the second and third modes reflected a pattern consistent with the severity of the corrosion damage.

For this reason, one pair of reinforced concrete slab (1 and 2) were constructed to introduce the degree of damage by applying the partially concentrated load. The experimental procedure consisted of measuring the initial (undamaged) dynamic properties of the slab, damping ratios, and then incrementally inducing a new state of damage and measuring the damping ratios associated with each state. As previously mentioned that the loading-unloading procedure was applied in three cycles with peak forces of 5, 10and 12kN, respectively. At the end of each static load step, the dynamic test was performed in order to extract modal parameters including damping ratios. After the final load dynamic test, the slab was repaired as the defective zone strengthened by bonding external CFRP sheets, and retested the strengthened slab in order to find the effect of strengthening on damping ratios. The measured damping ratios for both slabs separately and averagely for the six modes of five different conditions are given in Table 6.7.

Table 6.7: Damping ratios for the six modes of the slabs of five different conditions.

Slab 1					
Mode No.	Intact	5kN	10kN	12kN	Repaired
1	1.41	1.60	5.75	5.45	4.15
2	2.68	2.60	3.56	4.20	3.62
4	3.04	3.10	4.58	4.89	3.91
6	2.01	1.25	3.56	4.55	2.70
8	1.87	1.73	2.98	3.54	2.32
10	1.09	1.15	2.45	2.52	1.95
Slab 1					
1	1.26	1.39	4.10	4.25	2.65
2	1.94	1.98	3.23	3.97	3.46
4	1.52	3.24	4.36	4.64	3.59
6	1.46	1.40	2.95	4.10	3.60
8	1.22	1.56	2.67	2.61	2.94
10	1.01	1.1	2.11	2.30	1.70
Average					
1	1.34	1.5	4.93	4.85	3.40
2	2.31	2.29	3.40	4.09	3.54
4	2.28	3.17	4.47	4.77	3.75
6	1.74	1.33	3.26	4.33	3.15
8	1.55	1.65	2.83	3.08	2.63
10	1.05	1.13	2.28	2.41	1.83

The average modal damping ratios for this group C are compared to the damping ratio of the control slab, group A, as shown in Figure 6.14. It can be seen that the average damping ratios for six modes of this group are greater than those of the control slab, group A.
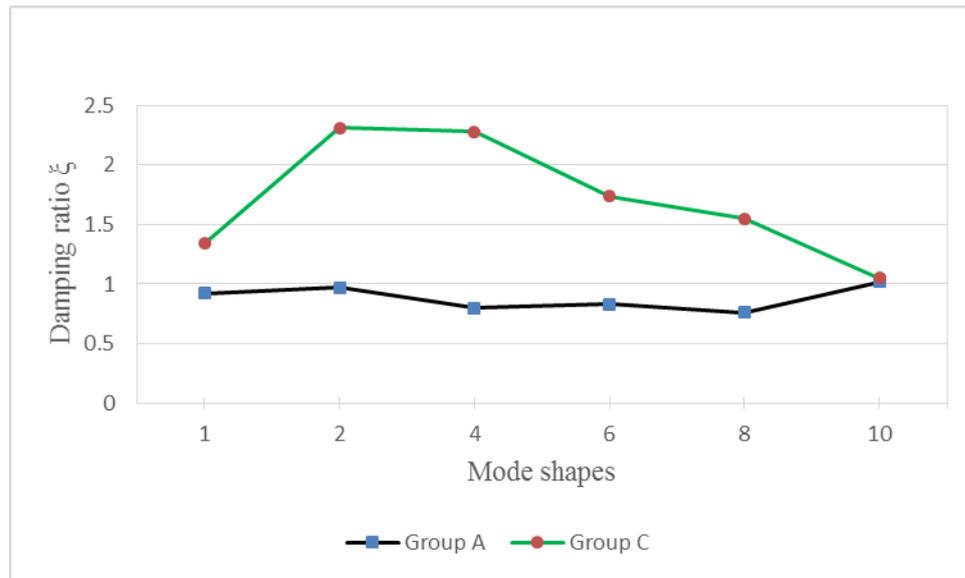
Figure 6.14: Identified damping ratio for test RC slab, group A and C.

Decreasing the thickness of the slab from 60mm (in group A) to 40mm (in group C) caused increasing the damping. The damping ratios increased by 45.65%, 138.14%, 185.0%, 109.64%, 103.95% and 2.94% for the six modes of group C respectively compared to the damping of control slab specimen. Such results revealed that there is a clear nonlinear relationship between two groups. In addition, the percentage difference between two groups means that the damping for the six modes of the slabs did not consistently increase as thickness decreased.

The damping ratio under different (intact, three loadings and repairing) conditions is graphically shown in Figure 6.15. Since the damping is a measure of energy dissipation, it is used to find the difference between degrees of damages. Therefore, the load increments were applied on slab over three load steps in order to introduce different degrees of damages into the slab. The percentage of increase in damping ratio of the slab under different conditions due to presence of widely spread crack are listed in Table 6.8.
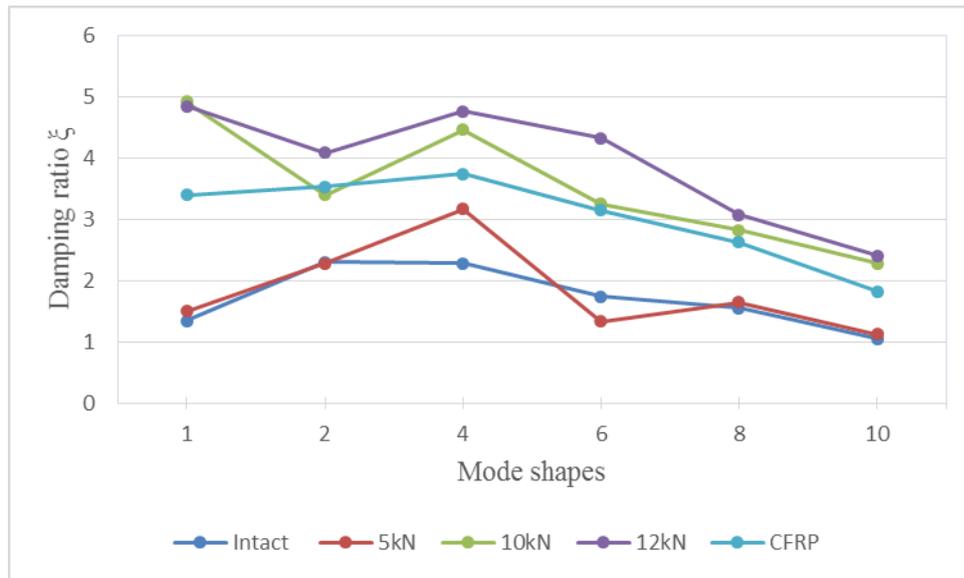
Figure 6.15: Damping ratios of RC slab of group C for different conditions.

Table 6.8: Damping ratios change of the slab under different conditions.

Damping ratios change %					
Mode No.	Intact	5kN	10kN	12kN	Repaired
1	0	11.94	267.91	261.94	29.89
2	0	0.87	47.20	77.06	13.45
4	0	39.04	96.05	109.21	21.38
6	0	23.56	87.36	148.85	27.25
8	0	6.45	82.58	98.71	14.61
10	0	7.62	117.14	129.52	24.07

At the first load damaged stage (P=5kN), the modal damping of the slab increased by 11.94%, 39.04%, 6.45%, 7.62% for the first, fourth, eighth and tenth modes respectively. However, it is decrease by 0.87% and 23.56 for the second and sixth mode compared to the intact slab damping. When the slab was loaded with the second incremental load, 10kN, there are further increase in the damping ratio namely 267.91%, 47.2%, 96.05%, 87.36%, 82.58% and 117.14% for the modes (1, 2, 4, 6, 8 and 10) respectively compared to the damping ratio of the intact case of the same slab. Moreover, the results showed that damping ratio of this condition, 10kN, is considerably higher than damping of defective slab under 5kN for all identified six

modes. This indicates realistic situation of damage for slab at the end of 10kN load step, where the slab went through extensive cracked pattern. This trend is due to the fact that the effect of crack on damping ratios is in its early stage and therefore the slab's sections were visually in a flawless condition under 5kN load level. The applying extra load on the specimens gives energy for the crack initiation and propagation process. Crack initiation and subsequent growth happened quite readily due to increasing the load to 10kN, see Figure 6.15. Therefore, considerably high change in damping ratio of RC slab can be observed under 10kN compared to 5kN for all identified six modes. This trend was similarly obtained for natural frequencies change, as discussed in section 6.2.1.2.

In general, the observation of all modes at 10kN loading are satisfactory with the theory seeing that the damping as expressed in Equation (6.1) is the loss of mass and stiffness manifested as high damping ratio(ζ).

When the slab was loaded with the final incremental load, 12kN, further increase in damping ratio was obtained for all six modes, 261.94%, 77.06%, 109.21%, 148.85%, 98.71% and 129.52% compared to the intact slab damping. In order to know the effects of increasing load from 10kN to 12kN, the damping ratio of slab subjected into two different incremental loads were compared. It can be seen that the modal damping of slab under 12kN for five modes are greater than the damping of the slab under 10kN, while it is lower in the first mode which is unanticipated finding. It is found that the damping ratio of the 10kN load step were oddly higher than the successive 12kN load step by 2.22% for the first mode of vibration. This is not uncommon phenomenon as it was as well experienced by other researcher (Bayissa, 2007 and Al-Ghalib, 2013). This observation may be accounted to the model used to extract the damping ratios or the way of hanging the specimen during testing. Additionally, the variation in position, magnitude and direction of successive excitations also affected the consistency of FRF measurements (Ashory, 1999).

The damping ratios conversely changed after the repair works, in the following manner: the highest decrease can be found 29.89% in the first mode; lowest change 13.45% in the second mode; 21.38% in the fourth mode; 27.25% in the sixth mode; no significant change 14.61% in the eighth mode and 24.07% decrease can be seen in the last mode. This manifests that there was identifiable pattern of the changes in

damping values caused by the repairs. As was seen in natural frequency trends for the 12kN load step, the frequency reduction of the fourth mode increased significantly responding to the increasing damage, while the percentage is increased in the first mode in term of modal damping ratio. For the repaired slab, damping ratios markedly decreased by 29.89% from the severely damaged (12kN) load stage for the first mode. This finding can be accounted to the fact that the reduction of this mode was more likely influenced by damage.

In general, the results indicate that the modal damping is influenced by the cracking introduced by overloading. However, they were unsuitable as a damage indicator. In some modes, it has been noted that tracing the modal damping ratios through the loading history is difficult due to fluctuating values of modal damping ratio produced in some mode shapes. For example, the damping ratios initially decreased in two modes under 5kN load step. Then, damping ratios were stable for all identified modes for 10kN load step because damping was increased for all modes with increasing damage. After that damping ratio is oddly decreased in the first mode for 12kN load step compared to 10kN. Similar trends was observed by Farrer and Jauregui (1998). They found that the damping of a steel plate girder bridge did not consistently increase or decrease as damage increased.

Two-lane reinforced concrete highway bridge of 104m, was tested by Salawu and Williams (1995). The tests were conducted before and after structural repairs to Reinforced Concrete Bridge to examine the correlation between the repair works and changes in the dynamic characteristics of the bridge. The main finding of their experiment was that there had no clear trend in damping value that could be detected.

6.2.2.3   Damping Ratios of Group D slabs

As previously mentioned that a pair of slab had a region with one void (150 x 150 mm in plan and 30 mm deep) located at distance 300x300 in both direction with respect to one corner of the slab. Artificial void was simulated by means of formwork dispositions during concrete pouring. The damping ratios of the artificial voided state for group D are given in Table 6.9. A comparison was made between groups A as an intact slab with group D as artificially voided slab as shown in Figure 6.16. The measurements of modal tests showed that damping ratios of the

intact slab were lower than damping of artificially voided slab for all identified six modes. It would seem clear that the highest and lowest differences were pronounced in the first and second modes between group A and D slabs respectively.

Table 6.9: Damping ratio for test RC slab, group D.

Mode No.	Slab1	Slab2	Average
1	1.63	2.075	1.85
2	1.08	1.1	1.09
4	1.05	1.24	1.15
6	1.55	1.5	1.53
8	1.06	1.08	1.07
10	1.135	1.65	1.39
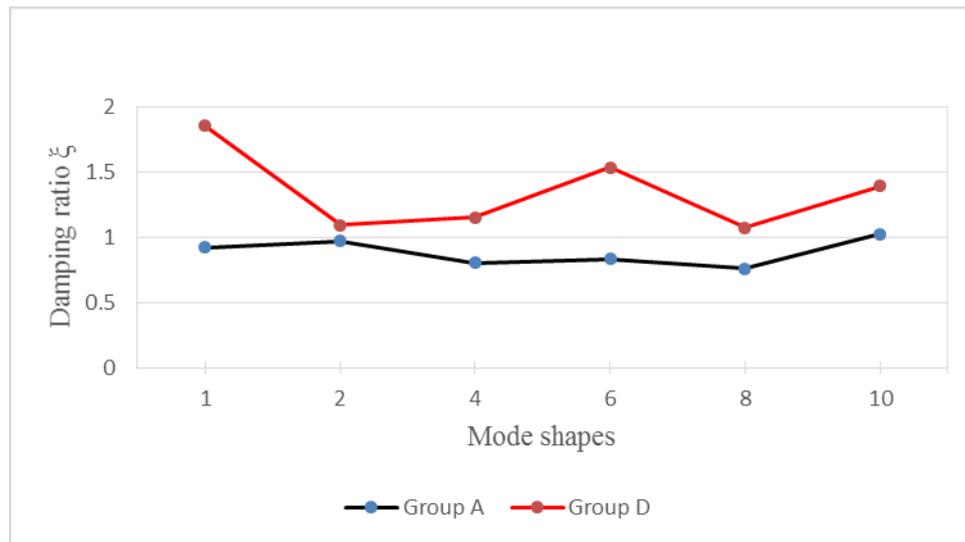
Figure 6.16: Comparison between damping ratios of groups A and D slabs.

In this case, the results of the test revealed clear relationship between intact and artificial void and increase in damping ratio for all identified modes, which holds satisfactorily with the theory seeing that the damping of each mode which is defined by Equation (6.1). According to this equation, the loss of mass and stiffness manifested as high damping ratio (ξ). This means the damping ratio of the system is inversely related to the stiffness and mass of the system.

6.2.3   Effect on Mode Shape

An overwhelming majority of researches suggest that modal shapes are a far more satisfactory damage detection indicator than natural frequencies and damping (Wang, 2010). It has been found from the earlier studies that the mode shape can also reveal useful information regarding the state of the structural behaviour. It is being studied for health monitoring as an indicator of damage detection, which is to be used on different structural members that have known "suspect" areas. It would be presumed that the mode shape displays distorted from the initial shaped owing to the present of defects, giving less stiff areas. Although the mode shapes for all studied state conditions will be displayed, much more attention has been paid to the incremental concentrated load and induced void slabs (groups C and D). Parametric studies in these two groups can be described as the popular problem cases in civil and other field of engineering.

6.2.3.1   Mode Shape of Groups B Slabs

It would be expected that the mode shape becomes distorted from the initial shape due to the presence of cracking. It is worthwhile to mention that slabs of groups A and B had been tested in an intact condition with varying the dimensions. Visual comparison between numerical and experimental mode shapes was made in order to satisfy the experimental results. Two slabs for each group were separately explained. It is difficult to interpret the average mode shape because the response of mode of each slab may have different amplitude, especially in case of damage localisation.

Since the capacity of the modal analysis equipment was limited, three mode shapes for group B slabs were extracted. It can be highlighted that the third mode shape for this group was also missed due to the same aforementioned reason in group A slabs. Mode shapes 1, 2 and 4 under free-free boundary condition were compared with the corresponding modes obtained numerically.

It is important to note that the experimental mode shapes of slab 1 and 2 of group B as displayed in Figure 6.17 and Figure 6.18 respectively can be directly compared to the numerical mode shapes in Figure 6.19 (e.g. 1st mode in the upper left of each figure should show the same pattern). The colours (from both experimental and numerical) graphs correspond to the areas where the response is highest (red) and lowest (blue).

157
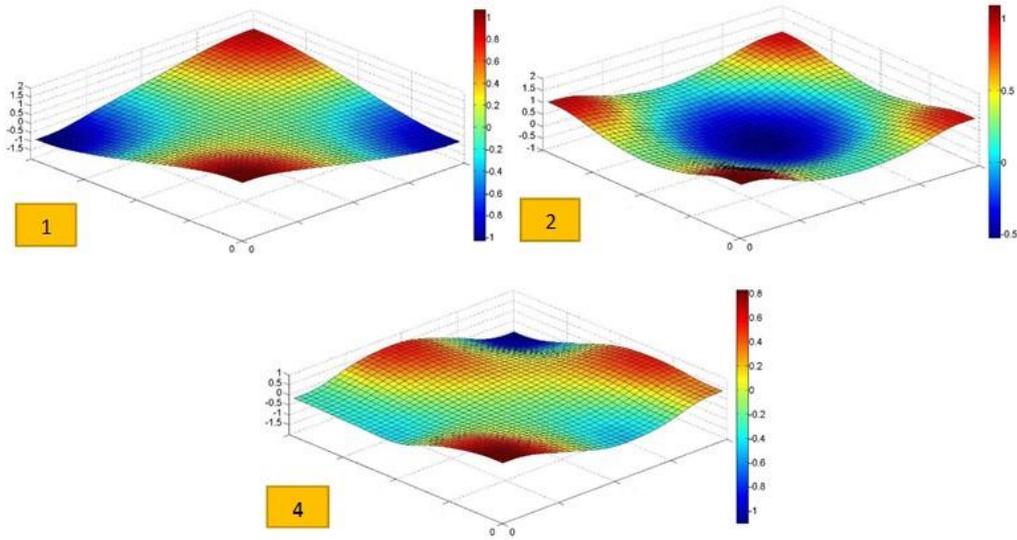
Figure 6.17: Experimental mode shapes of RC slab 1, group B.
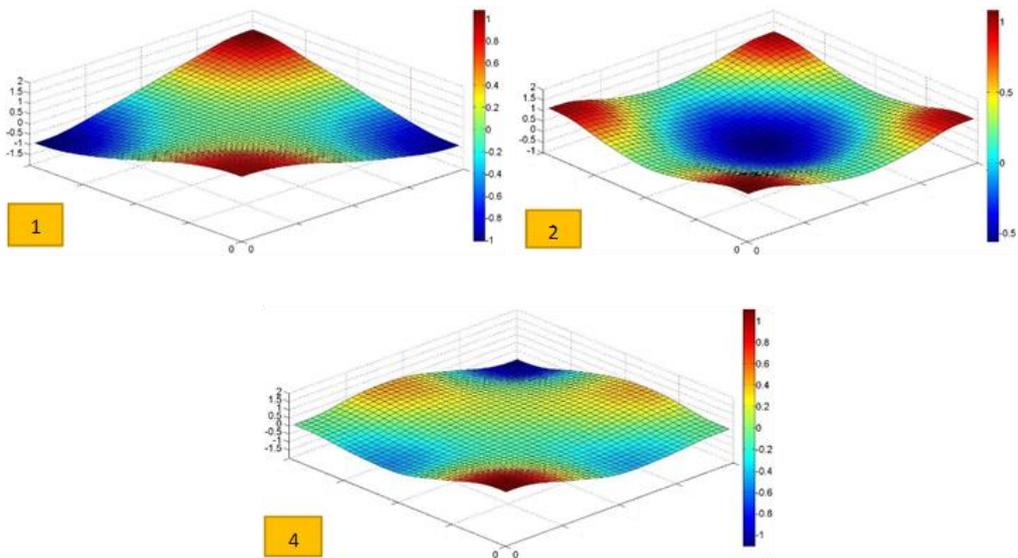
Figure 6.18: Experimental mode shapes of RC slab 2, group B.
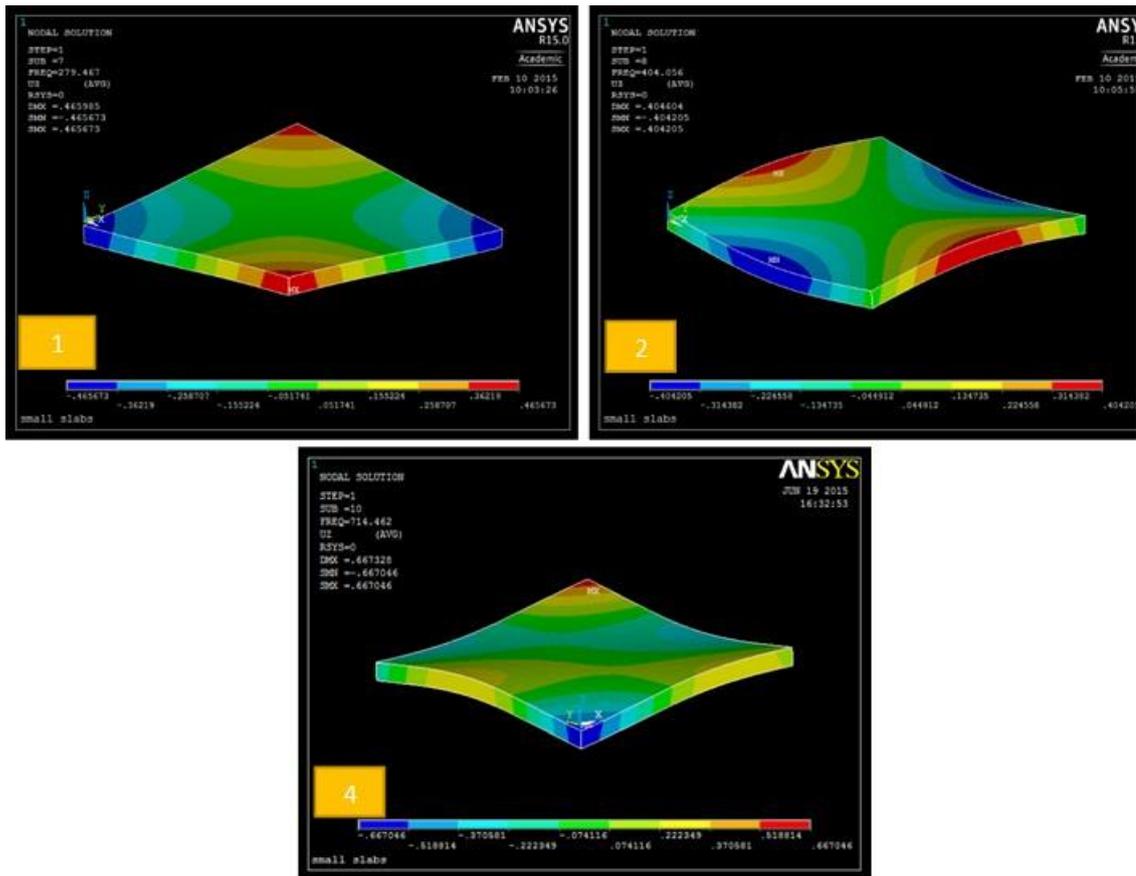
Figure 6.19: Numerical mode shapes of RC slab, group B.

The main objective of this comparison is to verify the experimental mode shapes with numerical results.

The first and fourth modes as shown in Figure 6.17 and 6.18 show very clear mode shapes that closely follow the numerical patterns in Figure 6.19. The second mode (upper right of Figures 6.17 and 6.18 is somewhat different from numerical one as in figure 6.19. As previously mentioned that it is expected that the way of hanging of the slab was the source of the difference of this mode. Overall, good agreement was obtained between experimental and numerical mode shapes of reinforced concrete square slabs of group B.

When compared the mode shapes of group A slabs (1, 2 and 4) in Figures 5.8 and 5.9 with same mode shapes of group B slabs in Figures 6.17 and 6.18, a good agreement was obtained between groups A and B slabs mode shapes. It is concluded that changing the thickness of the slab and both its length and width with preserving the

square shape will not highly affect the general shapes of the modes when they are tested under same boundary condition.

6.2.3.2   Effect of Mode Shape for Group C

After gathering, analysing, and extracting modal parameters of the slab including the mode shapes, the six mode shapes for group C (slab 1 and 2) are extracted. Firstly, the intact mode shapes of this group are visually compared with numerical mode shapes through Figures 6.20 – 6.22. As previously mentioned the comparison way is that the experimental mode shapes of slab 1 and 2 of group C as displayed in Figure 6.20 and Figure 6.21 respectively can be directly compared to the numerical mode shapes in Figure 6.22. The colours (from both experimental and numerical) graphs correspond to the areas where the response is highest (red) and lowest (blue).

Then, the visual and quantitative comparison is made between different states of each slab (1 and 2) separately in order to identify the effect of the degree of damages on mode shapes. Since the slabs were subjected to three incremental load levels (5kN, 10kN and 12kN), they were strengthened with carbon reinforced polymer sheet (CFRP). The experimental mode shapes under each condition was compared with intact condition of the same slab at all DOFs.
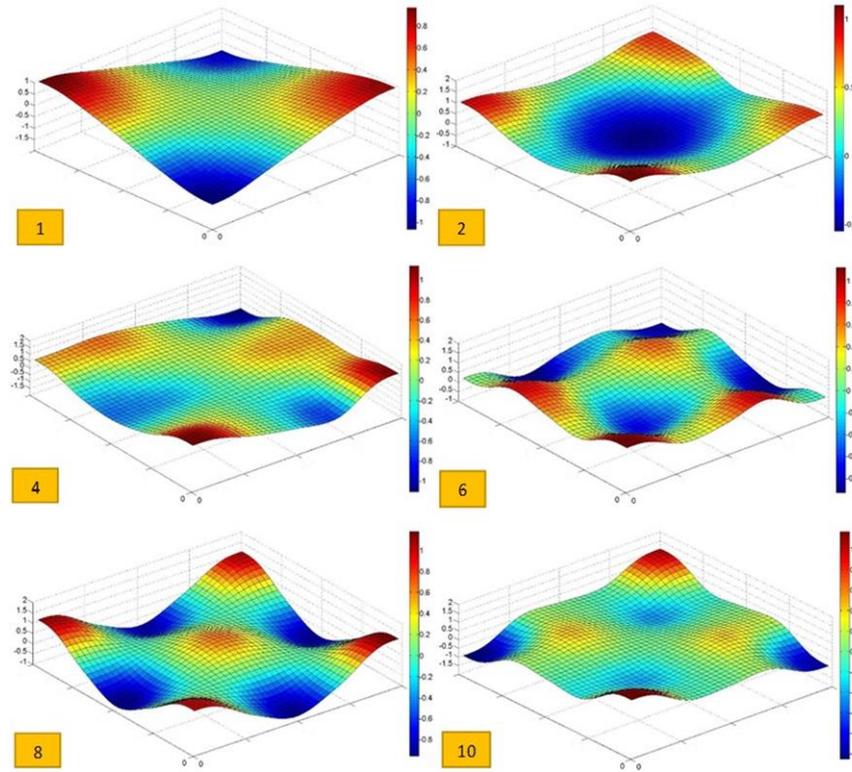
Figure 6.20: Experimental mode shapes of RC slab 1, group C.
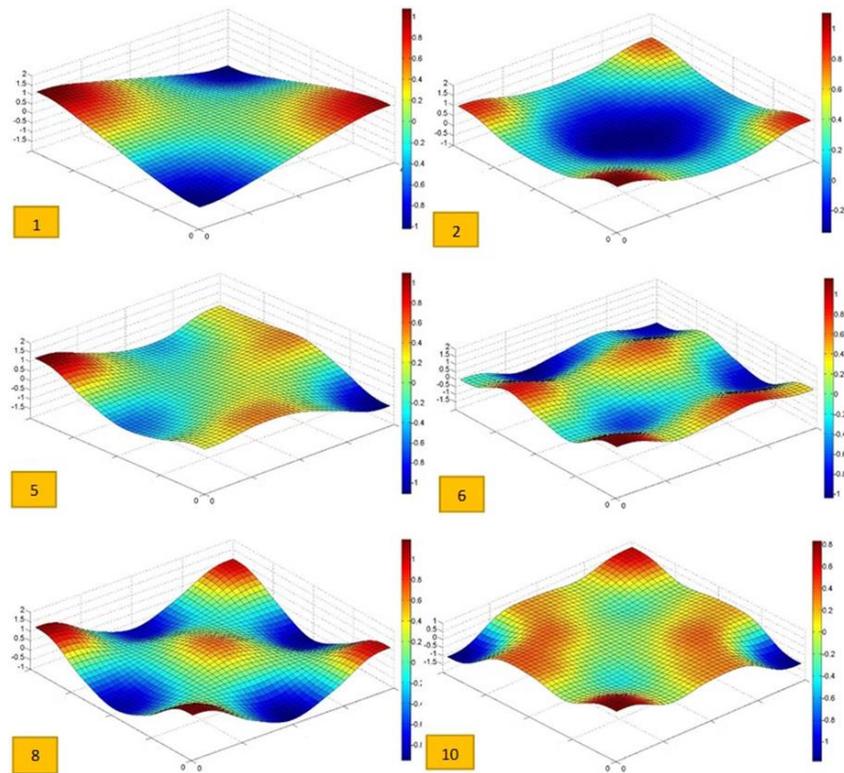
Figure 6.21: Experimental mode shapes of RC slab 2, group C.
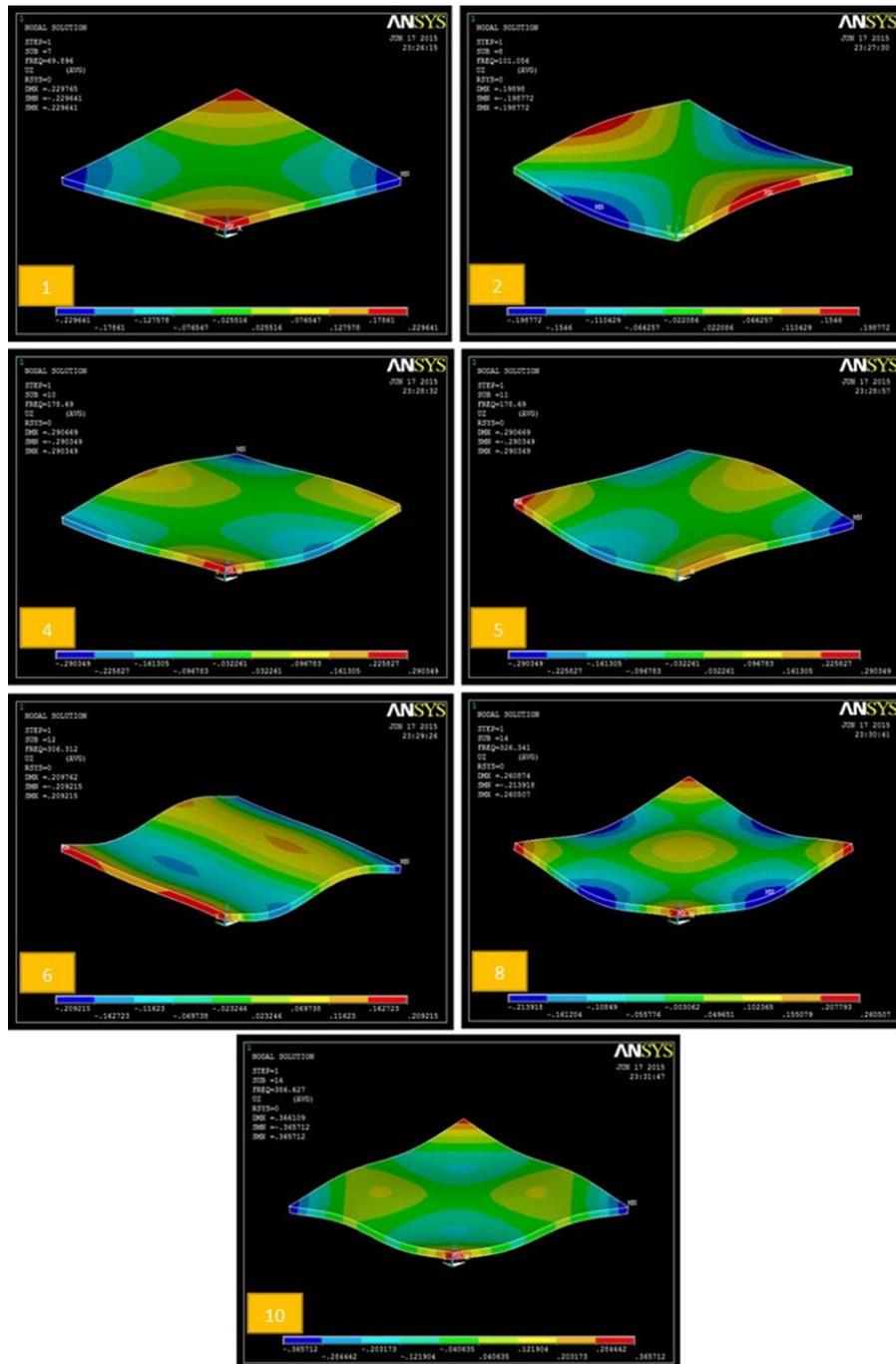
Figure 6.22: Numerical mode shapes of RC slab, group C.

Firstly, two mode shapes are disappeared in this case because the excitation force might be placed on a nodal pattern line which is unavoidable situation. Since mesh of 25 measurement points (DOFs) was evenly distributed on the slab surface, exciting the slab at any response point may cause missing some mode shapes. The excitation was fixed at response point seven for this group while it was fixed at first response point at all other cases. This is because at the beginning this group of slabs were

planned to be tested under two different boundary conditions, free-free and simply supported slab. The slab was not excited at first response point because the first response point was located on the support line. However, the slabs were not tested under simply supported boundary condition owing to unavailability of big stiff supported frame. In both slabs of the group, there were somewhat different between experimental and numerical one for the second and tenth modes due to hanging and symmetrical condition respectively as explained in group A slabs.

The natural frequencies of a pair of double modes are almost the same in the symmetric structure. Therefore, mode shape 4 has natural frequency 178.7 equal to the natural frequencies of mode shapes 5. Usually, one mode of a pair of double modes can be identified while the other is likely to be missing from the experiment. This situation happened to the slabs of this group. Mode shape 4 were identified while its pair mode 5 were missed from the experiment of slab 1. Conversely, mode shape 5 were identified while its pair mode 4 were missed from the experiment of slab 2. Having somewhat different between experimental and numerical mode shapes did not affect the results because the experimental mode shapes under each condition is compared with experimental intact condition of the same slab at all DOFs. Since the somewhat different exists under all conditions (5kN, 10kN, 12kN and repaired), the discrepancy was omitted when each of these condition compared with the intact one. Intact case of each slab was compared with itself under different conditions (loading and repairing). Therefore, if there was any discrepancy between numerical and experimental mode shapes, the experimental results were not be affected.

Overall, most of the experimental modes of both slabs (as shown in Figures 6.20 - 6.22) very clear mode shapes that quite similar to their numerical counterpart, which were the expected patterns. Good agreement was obtained between the numerical experimental and numerical mode shapes of reinforced concrete square slabs of group C.

Throughout this section, the observed mode shapes of the two slabs of group C and for all loading steps (5kN, 10kN and 12kN) as well as the repaired case were thoroughly generated and verified with the initial healthy case of each slab separately. The six mode shapes for the specified state condition of each slabs are displayed through Figures 6.23 – 6.30.
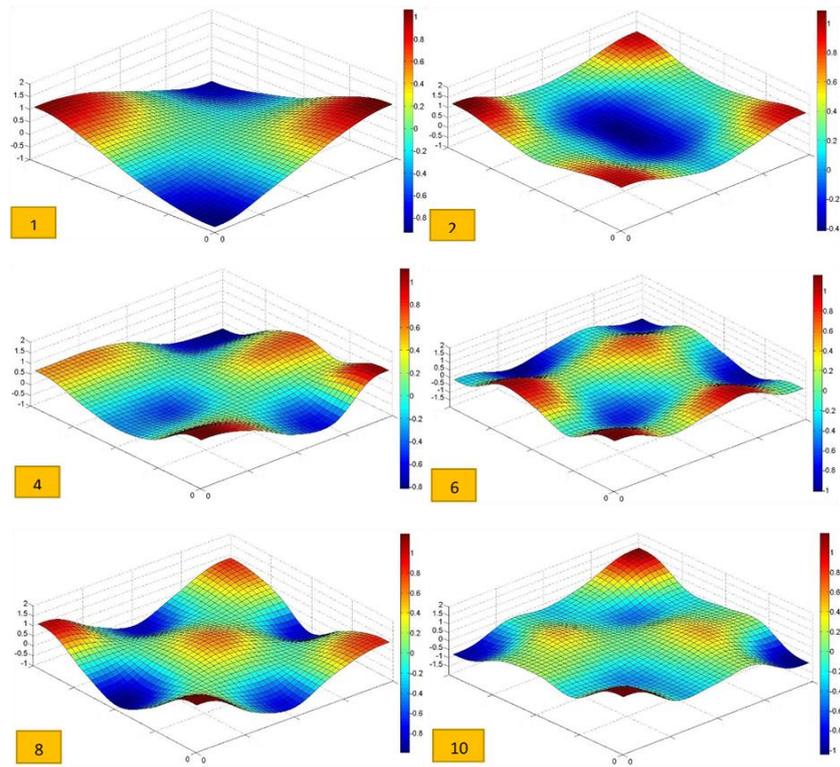
Figure 6.23: Experimental mode shapes for slab 1 under 5kN.
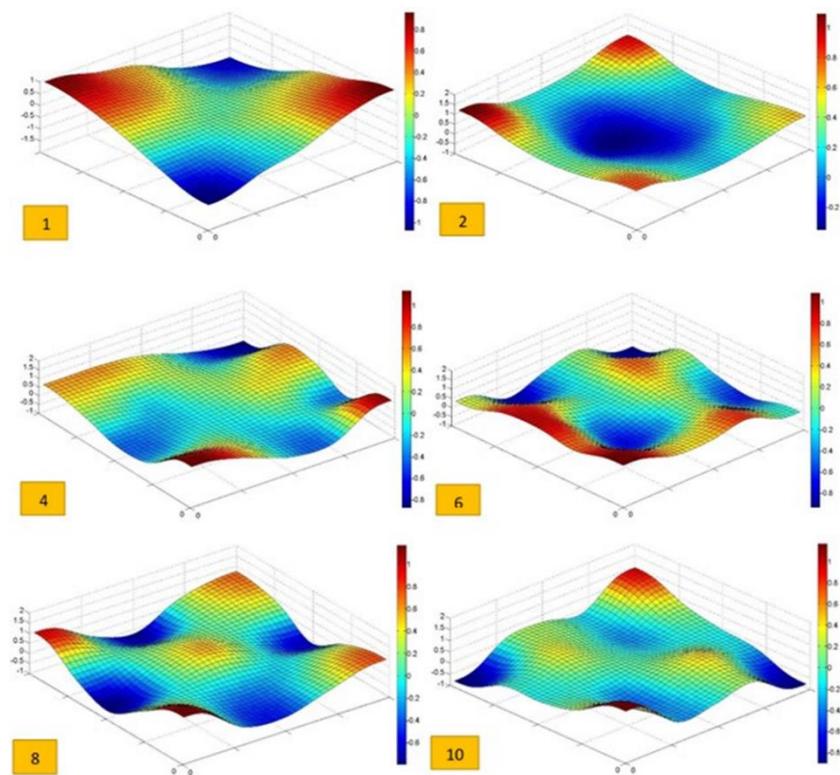
Figure 6.24: Experimental mode shapes for slab 1 under 10kN.
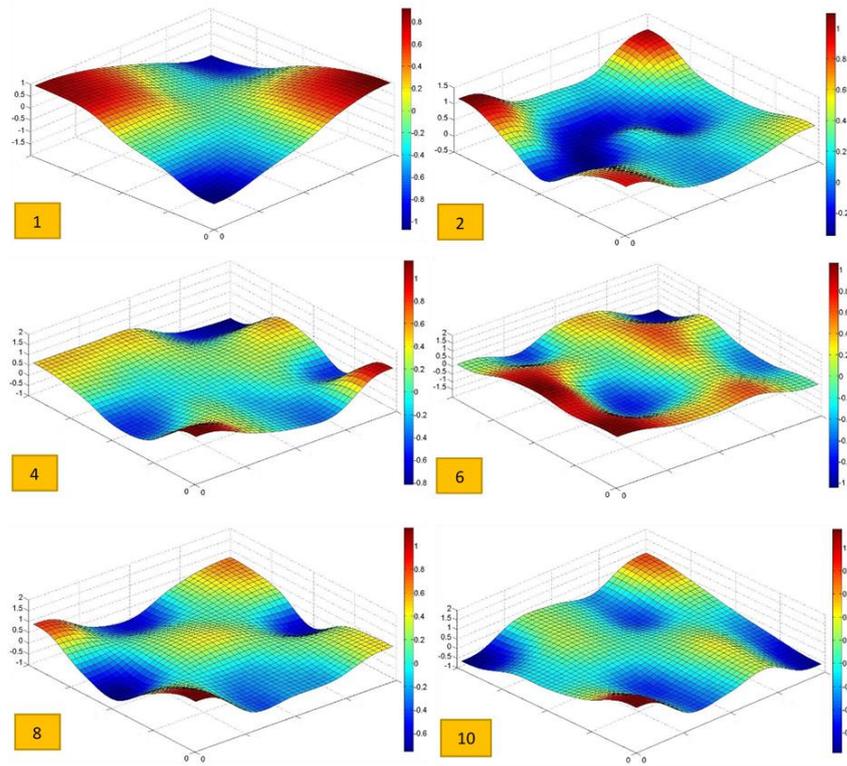
Figure 6.25: Experimental mode shapes for slab 1 under 12kN.
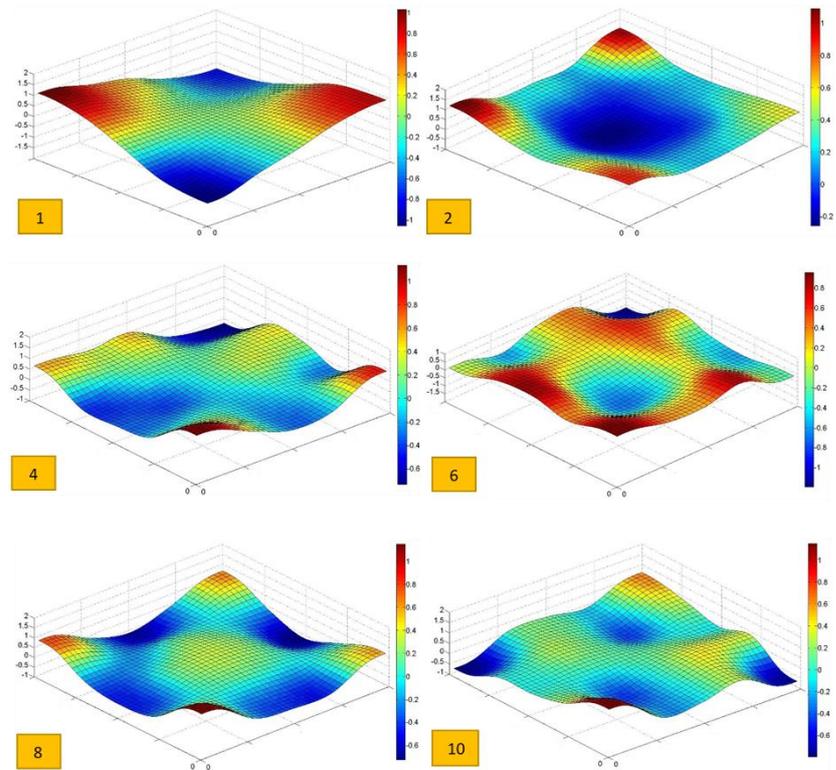
Figure 6.26: Experimental mode shapes for slab 1 under repaired condition.
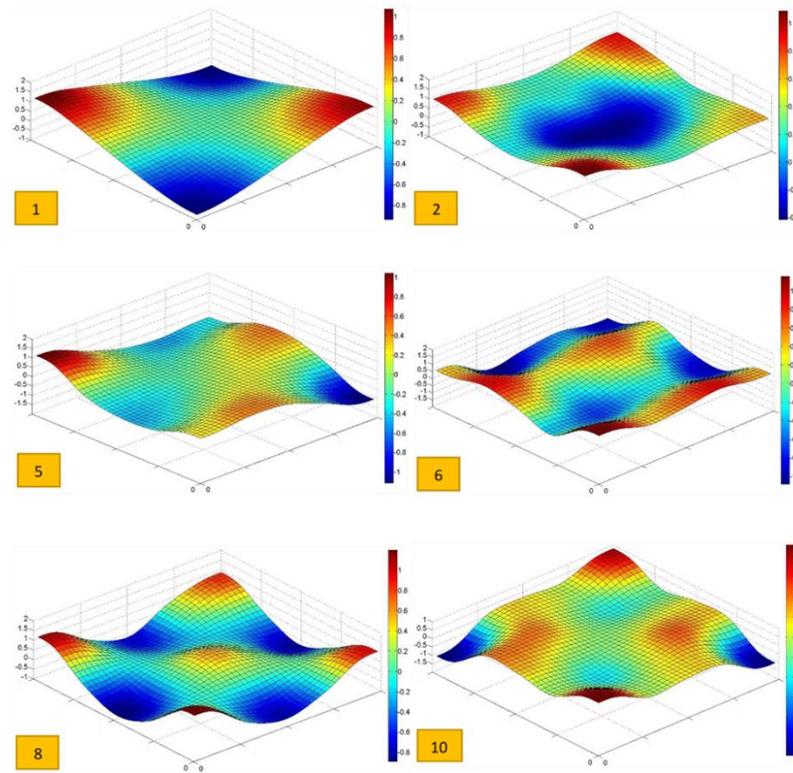
Figure 6.27: Experimental mode shapes for slab 2 under 5kN.
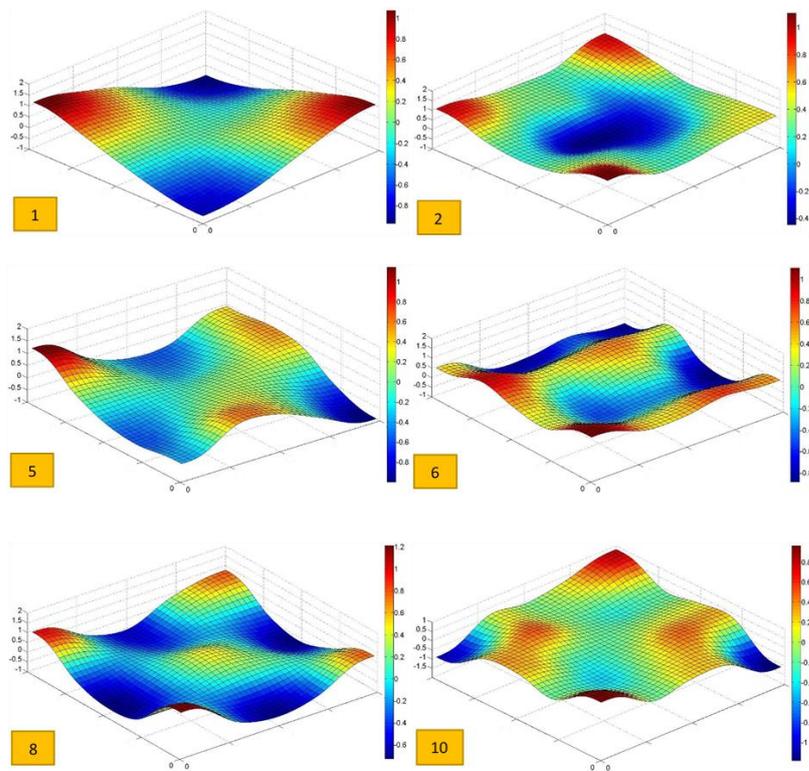
Figure 6.28: Experimental mode shapes for slab 2under 10kN.
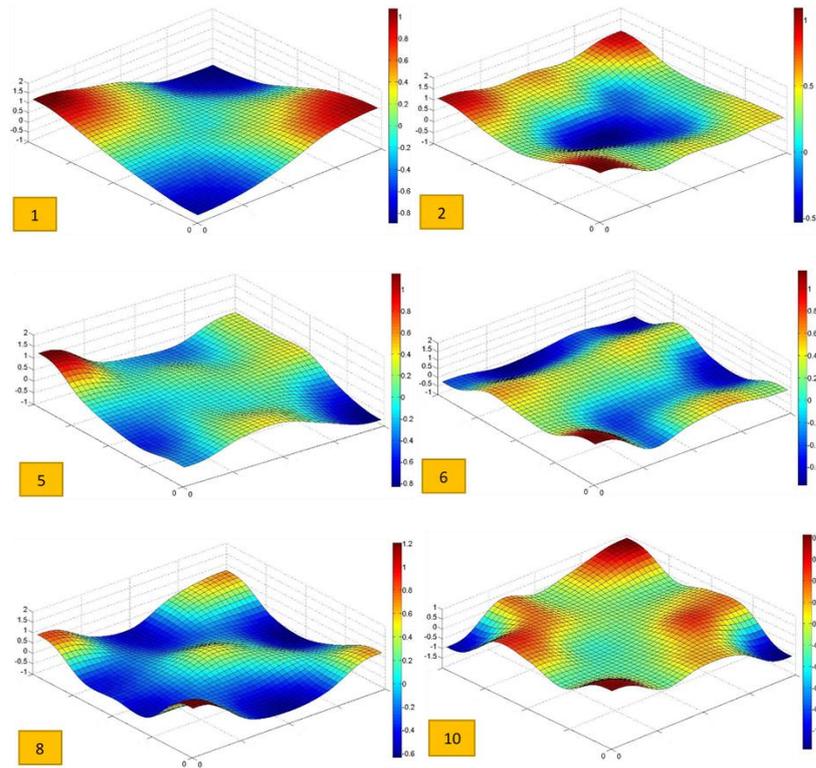
Figure 6.29: Experimental mode shapes for slab 2under 12kN.
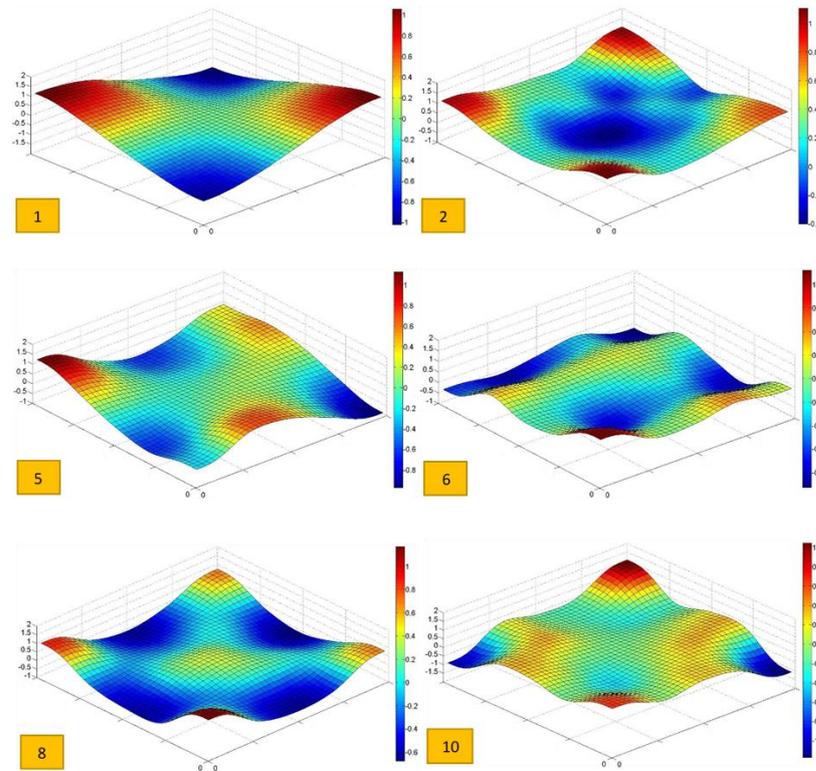
Figure 6.30: Experimental mode shapes for slab 2 under repaired condition.

From visual inspection of the mode shapes of both slabs, it does not appear that the cracking introduced has a significant influence on the shapes of the modes found. In the early loading stages (5kN), hair cracks were just launched under first load level and that is why the visual inspection was capable to reveal only one small and short crack in this stage, see Figure 6.6. The cracks were started to distribute in the penultimate load level and they were more obvious than the first load step. The changes of mode shape were not restricted at the damaged area of the slab, but were distributed over the entire area. The distribution of the stiffness change in the structure affects the mode shape, such that evenly distributed damage does not cause a significant change in the general shape of the modes of vibration. Similar findings to this research were also found for the case of reinforced concrete beams investigated by Al-Ghalib (2013) and pre-stressed concrete bridge girder carried out by Huth et al. (2005). Nevertheless, such observation contradicts suggestions of other researchers (Owen et al., 2004; Yeung and Smith 2005) that mode shapes of different damage conditions may change a little, if the induced damage is widespread cracking in concrete beams.

The presence of imperfection was quite obvious at the 12kN load level compared to first and penultimate load levels. It was well pronounced in some mode shapes than the others. Distinguished observation through the visual evaluation of the different damage is quite difficult for mode shape. This is due to the fact that each mode shape had a mesh of 25 measurement points (DOFs) that evenly distributed on the slab surface. As a result, all these response points had effects on the correlation and the effect of all points were not be taken into account through the visual evaluation.

In general, the changes in mode shapes tend to increase with increasing damage level. This implies that the more cracks and flaws a slab is inflicted with, the more a mode shape magnitude will respond to escalating damage. Even small damage induced poised changes to the mode shapes, but it may not be visually obvious. Therefore, two different statistical methods were explained and employed in this work for quantitatively comparing mode shapes. Such methods were utilised (in the next chapter) as a measure of the deterioration of the mode shapes. In addition, they attempt to account measurement and weight contribution of each degree of freedom. Hence, which degrees of freedom contribute negatively can be identified.

6.2.3.3   Mode Shape of Group D Slabs

Two reinforced concrete slabs with the same scenario were also used for this group. The scenario of this group is the flaw was induced by having void on the top surface of the slab during casting process. Evenly spaced response points along slab's surface were employed to obtain the mode shapes. The spacing between response points was held constant at 29 cm. It should be recalled that the artificially created void was located at response point number 7, see vibration grid measurement points in Figure 4.11. The average of 5 measurement configurations were also used to gather the desired data from all 25 response points to plot the mode shapes. After obtaining the experimental data, the data were analysed to extract six modes.

Thus, the six experimental mode shapes of slab 1 and 2 of group D as displayed in Figures 6.31 and 6.32 respectively can be directly compared to the numerical mode shapes in Figure 6.33. For instance, first mode shape at the upper left of Figures 6.31 and 6.32 can be directly compared to the modal patterns in Figure 6.33. The colours on (from both the numerical and the experimental) graphs correspond to the areas where the response is highest as red and lowest as blue.
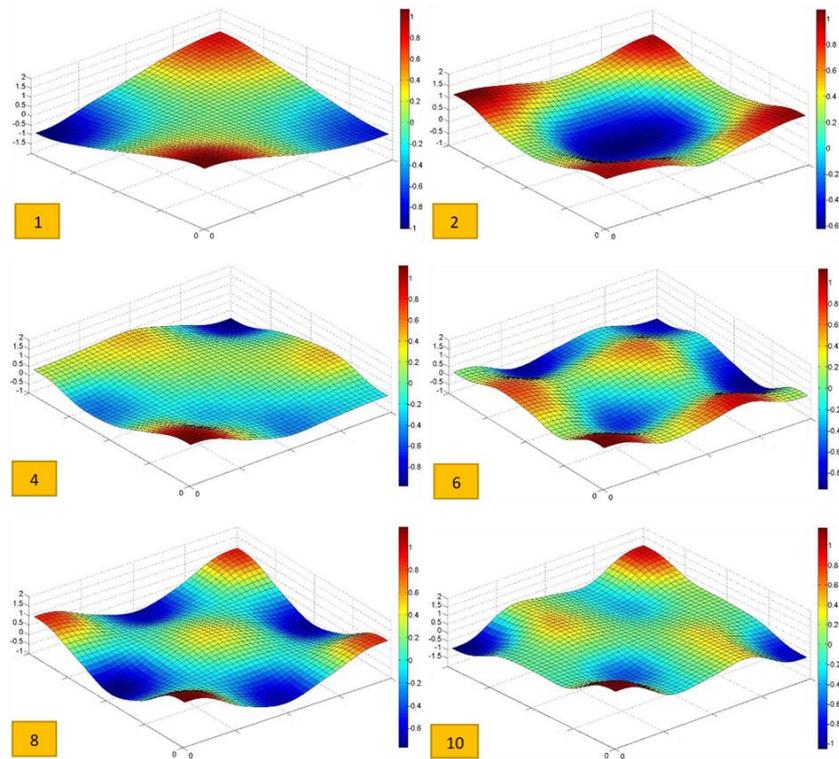
Figure 6.31: Experimental mode shapes of RC slab 1, group D.
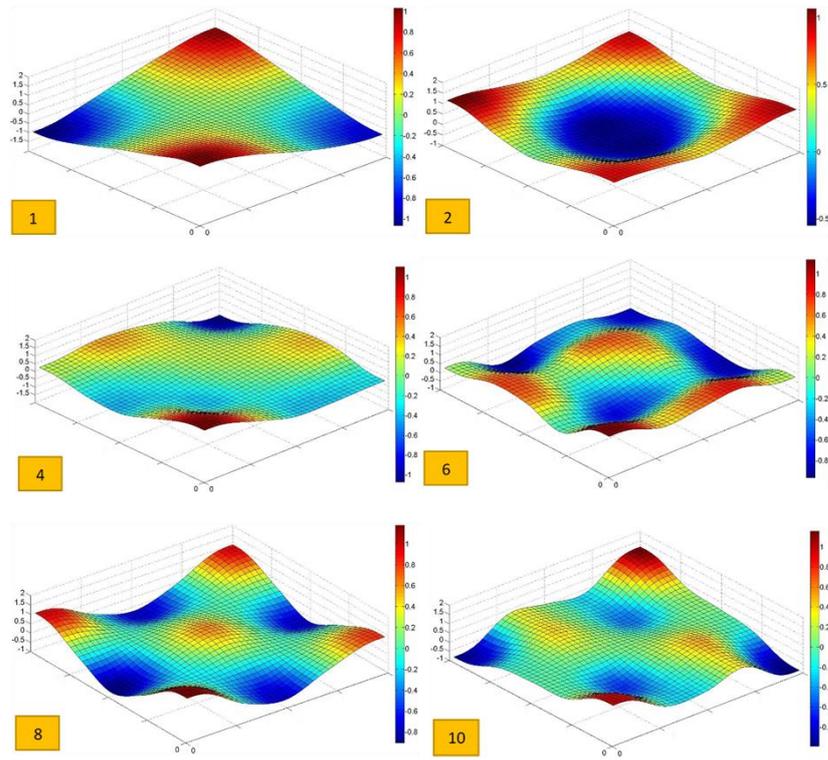
Figure 6.32: Experimental mode shapes of RC slab 2, group D.
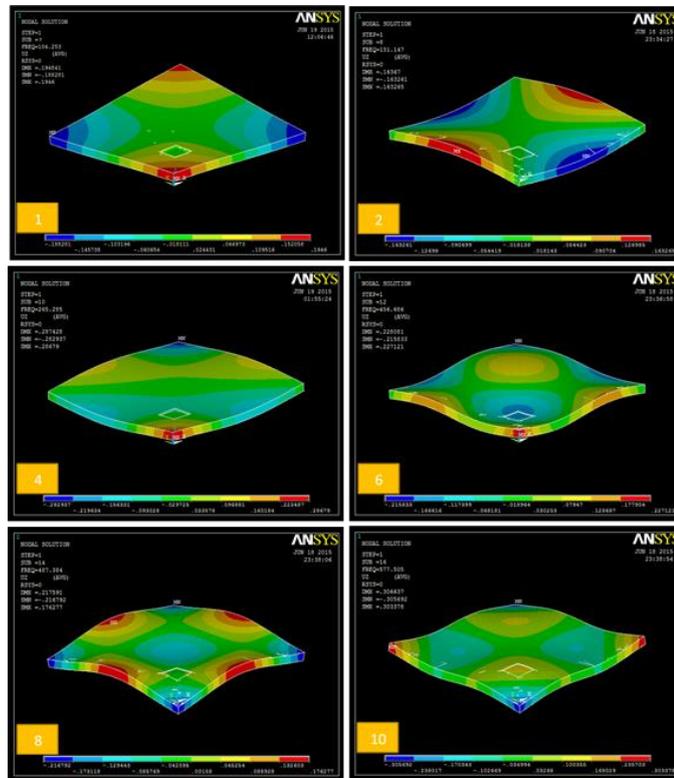
Figure 6.33: Numerical mode shapes of RC slab, group D.

Based on visual inspection of Figures 6.31 - 6.33, one clear observation is found in mode shape eight. There is a difference between experimental and numerical mode shape number eight. This variance is potentially due to the fact that the induced void slab is exactly on the top surface of the slab. However, in the experimental work, the induced void is simulated by putting a polystyrene hexahedron on the surface of reinforced concreted slab during the casting process. When the slab was vibrated, the polystyrene hexahedron become slightly submerged and therefore polystyrene was covered with thin layer of concrete. Although the cover of the cement mortar on the polystyrene hexahedron was less than 0.5 cm, this may change the behaviour from open to close void that caused the dissimilarity between experimental and numerical of the eighth mode shape. It is important to mention that groups A and D had the same discrepancy in second and tenth experimental mode shapes. As a results, such difference did not affect the experimental results when comparing groups A and D slabs against each other.

For the case of localised damage, visual inspection of the mode shapes alone cannot be relied on to identify the location of damage. Therefore, more suitable and robust statistical techniques should be required. These methods are explained thoroughly and applied systematically in the next chapter to locate the defect in the slab.

6.3   Summary

The Modal parameters (natural frequencies, damping ratio and mode shapes) were evaluated from measured data and specifically frequency response functions. The obtained modal parameters describe the dynamic behaviour of the reinforced concrete slab.

The experimental natural frequencies, damping ratio and mode shapes of each state condition of slab were obtained and graphically illustrated. The experimental results were compared with those obtained theoretically (analytically using closed form expression and numerically using ANSYS software). The results showed that the natural frequencies of the slab decrease and the damping ratio shifts upward as the load increases, damage increases.

The overall trend of frequency decrease after occurring damage, but it was not guaranteed all modes had same sensitivity to the applied load that inflicts severe

cracks. However, the variation in natural frequencies can be used as one useful indicator to precisely identify the presence of damage in reinforced concrete slabs. The results indicate that the damping ratios were influenced by the cracking introduced by overloading. However, they were unstable as a damage indicator, in some modes. It was noted that tracing the damping ratios through the loading history is difficult due to fluctuating values of damping ratio produced in some mode shapes.

Visual comparison between numerical and experimental mode shapes was made in order to satisfy the experimental results. A good agreements was obtained between experimental and numerical mode shapes. More sophisticated statically analysis is also be used in the next chapter in order to identify the location of void in the slab, which is not possible to rely on visual comparison alone.

7. Statistical Analysis of Damage Identification

7.1   Introduction

It is sometimes difficult one distinguishes the observation of mode shapes changes due to damage through the visual evaluation. Visual inspection of the mode shapes alone cannot be enough to be relied on to identify the location or the degree of damage. This is due to the fact that the distribution of the stiffness change in the structure influences the mode shape, but it does not cause a significant change in the general shape of the modes of vibration. In order to overcome this discrepancy, two different statistical methods were employed in this study for quantitatively comparing mode shapes.

Different indices have been developed to quantify the consistency between two modal vectors from numerical model and test observation. In other words, comparison between two series of mode shapes, which are obtained from two different dynamic investigations performed on a same structure, is calculated by using specific indices. There are a number of methods in the field of experimental and theoretical modal analysis that can be utilised for correlation. The available methods for comparing vibration data are applicable to any sets of mode shapes, such as analytical versus analytical, analytical versus experimental or even experimental versus experimental. In experimental work, the change of degree of freedom of mode shapes under different conditions have to be compared due to occurrence of any defect in the RC slab.

7.2   Correlation Analysis

The correlation method includes a set of techniques to compare the initial healthy case slab with the defected slab conditions. The outcome of the correlations study helps to find which mode shapes were found to be in large error. Furthermore, it will also help to find which response point adversely affects the caused discrepancy. The natural mode shapes of healthy case for each slab were compared with those for different damage conditions.

The two most commonly methods are employed to compare two sets of dynamic mode shapes. These two criteria are called the modal assurance criterion (MAC) and

the coordinate modal assurance criterion (COMAC), which are performed for revealing the change between two mode shapes. The definition, principle and theory of these robust statistical techniques for damage identification in RC slab are explained thoroughly and their application are applied systematically in the following sections of this chapter.

7.2.1   Modal Assurance Criterion

The Modal Assurance Criterion (MAC) method among many methods is the most widely utilised to provide a measure of consistency between pair mode shapes, which was first proposed by Allemang and Brown (1982). The MAC is defined as a scalar constant relating the degree of consistency between two modal vectors. This value can be obtained for example between two mode shapes, for instance analytical versus analytical, analytical versus experimental or even experimental versus experimental. In general, it can be employed to compare mode shapes with respect to mode shape in a different condition. The following expression is used to determine MAC:

$$\text{MAC(ANA, EXP)} = \frac{|\{\emptyset_{\text{EXP}}\}^{\text{T}}\{\emptyset_{\text{ANA}}\}|^2}{\{\emptyset_{\text{EXP}}\}^{\text{T}}\{\emptyset_{\text{EXP}}\} \cdot \{\emptyset_{\text{ANA}}\}^{\text{T}}\{\emptyset_{\text{ANA}}\}} \tag{7.1}$$

where:

$$\{\emptyset_{\text{EXP}}\} = \sum_{i=1}^{n}(\emptyset_{\text{EXP}}) \tag{7.2}$$

$$\{\emptyset_{\text{ANA}}\} = \sum_{i=1}^{n}(\emptyset_{\text{ANA}}) \tag{7.3}$$

$\emptyset_{\text{EXP}}$ is mode shape expressed in matrix form (Eigen mode matrices) of $(n \times m_{\text{EXP}})$

$\emptyset_{\text{ANA}}$ is mode shape expressed in matrix form (Eigen mode matrices) of $(n \times m_{\text{ANA}})$

N   is total number of measurement points on the structure

174

(i)   is i^{th} coordinate degree of freedom

m_{EXP} is number of experimental investigation modes

m_{ANA} is number of analytical investigation modes

For a fixed mode shape, MAC index measures the correlation (similarity) of two corresponding series of modal amplitudes (Foti, 2013). The MAC assumes values always between 0 and 1. This value indicates degree of consistency between two mode shapes. This means that good correlation, consistent correspondence, is obtained when MAC value is close to unity while no correlation, poor resemblance, of the two mode shapes are obtained when this value is close to zero. However, Ewins (2000) mentioned that when using this value to estimate the correlations of two modal vectors in practical cases, some cautions should be carefully used in attaching quantitative significance to the absolute values of MAC. Besides the obvious reasons, MAC value could be attributed to some facts that cause its value less than expected results. The value of MAC less than the expected value of unity or other elements being remarkably greater than the expected zero can be caused due to some reasons, such as nonlinearities in the tested structures; inappropriate choice of DOFs included in the correlation; poor modal analysis of measured data and noise on the measured data (Ewins, 2000; Allemang, 2003). It is therefore recommended that, in practice applications, it is questionable when the correlation, MAC value, between two mode shapes is less than 0.6 (Pan, 2007). It is worth nothing that only consistency between a pair of mode shapes can be indicated by using MAC value, but this cannot indicate any validity. For instance, if the same error or random exists in all modal vectors, this discrepancy cannot be delineated by the modal assurance criterion.

7.2.2   Coordinate Modal Assurance Criterion

The coordinate modal assurance criterion (COMAC) is another common method to compare pair of vibration mode shapes which is the extension of MAC. As previously mentioned that MAC indicates correlation (similarities) between two sets of mode shapes whereas its extension COMAC indicates the correlation between the mode shapes at a selected measurement point, individual locations, on the structure (Lieven and Ewins, 1988; Allemang, 2003). As a consequence, the COMAC

attempts to indicate which measurement degrees of freedom (DOFs) contribute negatively and cause the discrepancies to the value of MAC (Allemang, 2003). The coordinate modal assurance criterion (COMAC) index is generally calculated using the following expression:

$$\text{COMAC(ANA, EXP)} = \frac{\sum_{l=1}^{L}|\{\emptyset_{\text{EXP}}\}\{\emptyset_{\text{ANA}}\}|^2}{\sum_{l=1}^{L}\{\emptyset_{\text{EXP}}\}^2 \cdot \sum_{l=1}^{L}\{\emptyset_{\text{AN}}\}^2} \tag{7.4}$$

where:

L   is total number of paired modal vectors included in comparison.

A COMAC value close to unity indicates good correlation, at the selected measurement location, between the two data sets. Ewins (2000) mentions that COMAC can be displayed in different way, the most obvious way is drawn a diagram and shown its value versus the number of degree of freedom.

7.3   MAC and COMAC Values and Calculations

As aforementioned that obvious observation through the visual evaluation of the different damage groups is quite difficult for mode shape. This is due to the fact that each mode shape has mesh of some response points (DOFs) that distributed on the member surface. As a result, all these response points have effects on the correlation and the effect of all points will not be taken into account through the visual evaluation. They mentioned that a large number of methods for interpretation of mode shape data were suggested, and amongst all these methods, most work on mode shapes has concentrated on looking at the MAC. The importance of the MAC is to compare the damaged mode shape of mode (r) against the undamaged reference mode shape of mode (ℓ). For all the mode shapes, ℓ and r measured and then a correlation value developed between each damaged mode shape and each reference mode shape. For undamaged structures it would be expected that MAC is 1 when r equals ℓ (there is perfect correlation between r and ℓ) and MAC is 0 when r does not equal ℓ (there is not a good correlation between r and ℓ). MAC values can

successfully use to find the presence of damage in a structure. However, it cannot be relied on for determining the location of the damage introduced to the structures.

An extension to Modal Assurance Criterion (MAC) is Coordinate Modal Assurance Criterion (COMAC). A COMAC value is determined for each (measurement) degree-of-freedom (Lieven and Ewins 1988). The COMAC value attempts to identify which measurement degrees-of-freedom contribute negatively to a low value of MAC. This means that the location of the damage will be known (Alampalli et al., 1997). A COMAC value close to unity indicates good correlation, at the selected measurement location, between the two data sets. Whereas, a value close to zero indicates poor correlation.

The characterisation of defect especially in RC elements using vibration data is reported challenging task in the identified literature. Accordingly, this chapter endeavours to shine light on dynamic methods when applied to RC slabs simulated with various scenarios of defect. For this purpose, two groups (C and D) of RC slabs were used in this chapter. As aforementioned that group C was loaded statically before reaching the failure in three successive load cycles and then rehabilitated. Group D slabs were devised with cavity produced at specific distance to model localised the defect. The slabs were tested under a free-free support condition to remove the intervention of support rigidity dilemma using EMA.

The theory and procedure for calculating MAC and COMAC values are well explained. A purpose built computer program was developed in this work utilising MATLAB code facilities to calculate MAC and COMAC values. The flowchart of the program is shown in Figure 7.1, while the algorithm code is presented in Appendix D.
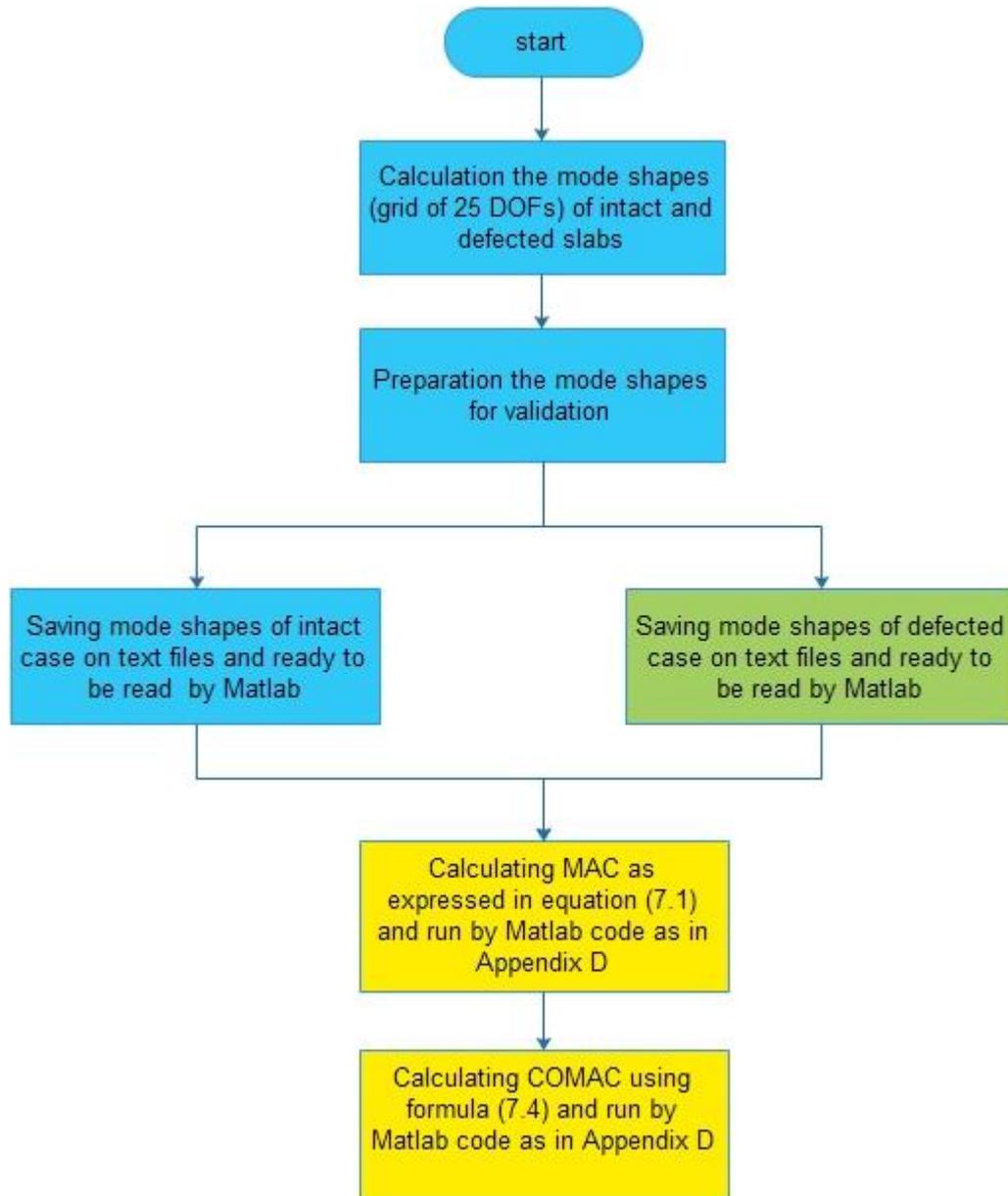
Figure 7.1: Flowchart for MAC and COMAC calculation.

7.3.1   MAC and COMAC for Group C Slabs

The MAC matrix of the six correlated mode pairs between the modal data from the intact case and three loading steps as well as repaired case calculate using developed MATLAB code. The MAC method was employed to compare two sets of dynamic mode shapes. MAC was performed for revealing the change between six mode shapes of all five conditions with respect to intact case in order to identify the effect of each condition on MAC values, see Figure 7.2 and Figure 7.3. Elements of the main diagonal of the MAC matrix as presented in these Figures for the specified state conditions can be listed in Table 7.1. As it is mentioned that a good correlation will

be obtained if the MAC value is (1). This implies that there is no discrepancy between the mode shapes. However, there is discrepancy between the mode shapes when MAC value less than one.
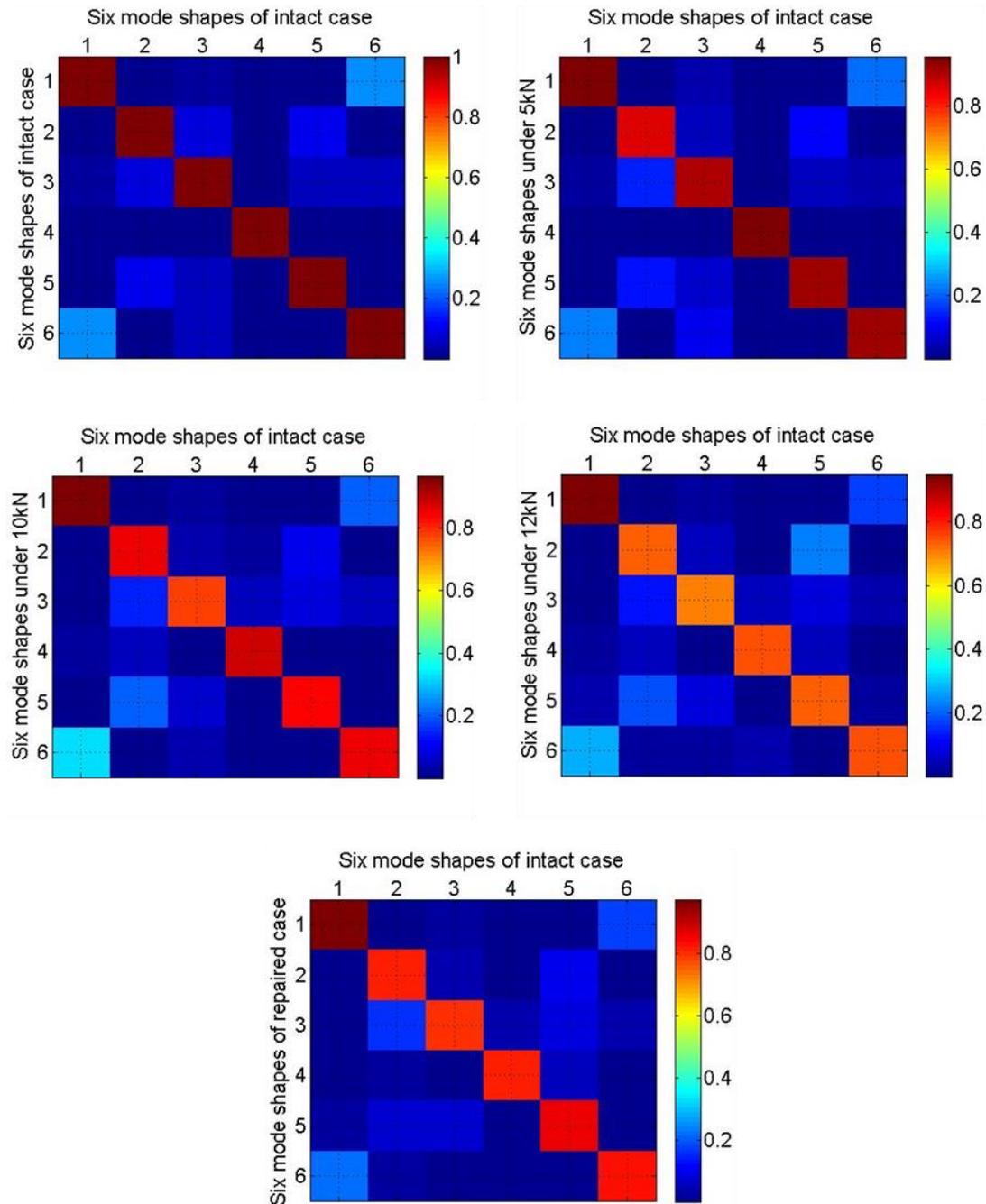
Figure 7.2: Degree of damage influence on MAC values for RC slab 1, group C.
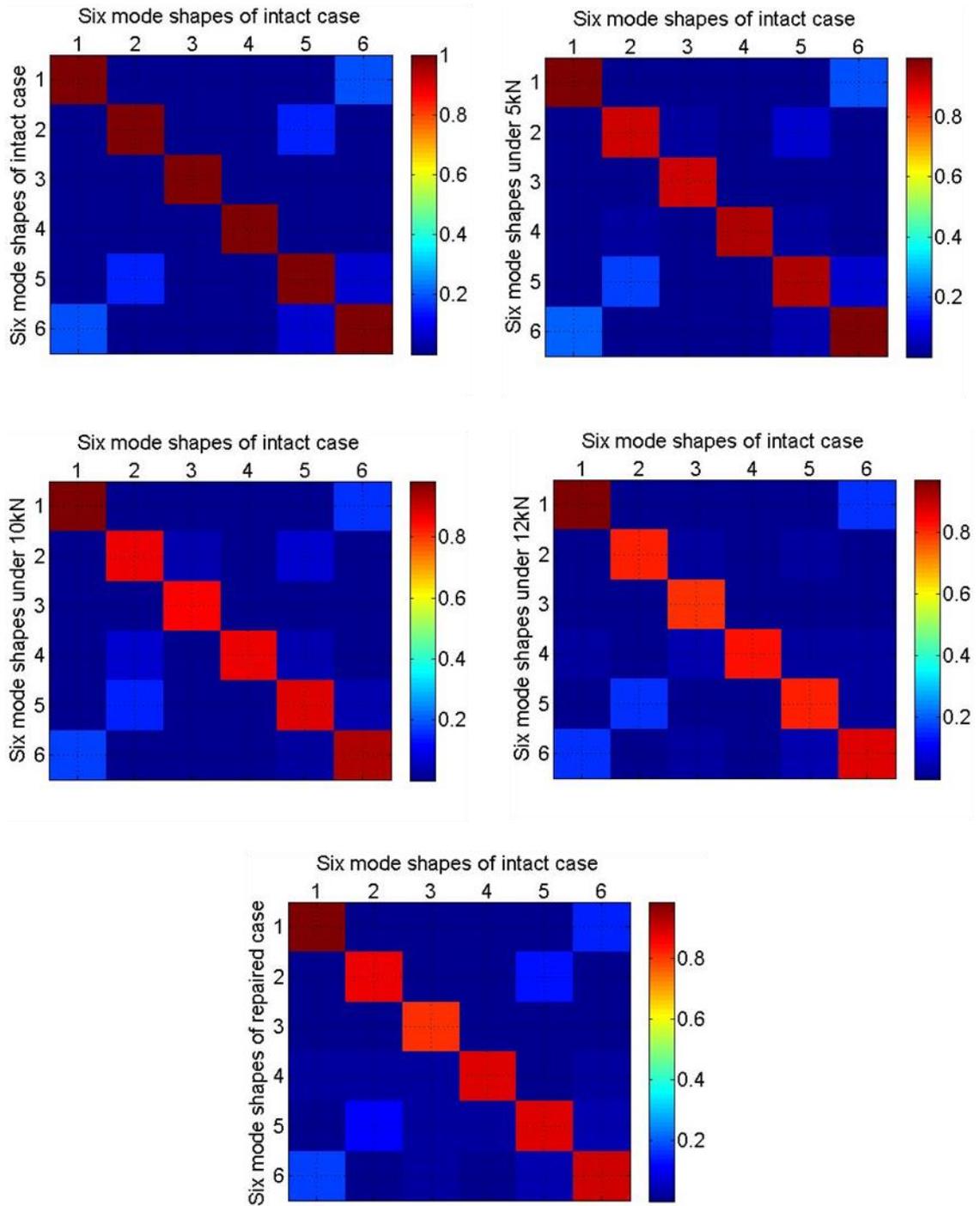
Figure 7.3: Degree of damage influence on MAC values for RC slab 2, group C.

Table 7.1: Damage influence on MAC values for the RC slabs 1 and 2 of group C.

MAC values for slab 1 with respect to intact reference case					
Mode No.	Intact	5kN	10kN	12kN	Repaired
1	1	0.9534	0.9674	0.9493	0.9756
2	1	0.8566	0.8484	0.7285	0.8131
4	1	0.9023	0.7777	0.7107	0.8058
6	1	0.9578	0.8870	0.7562	0.8148
8	1	0.9276	0.8460	0.7306	0.8666
10	1	0.9182	0.8530	0.7460	0.8283
MAC values of slab 2 with respect to intact reference case					
1	1	0.9976	0.9838	0.9724	0.9872
2	1	0.9174	0.8731	0.8198	0.8699
5	1	0.9085	0.8488	0.7937	0.8167
6	1	0.9501	0.8671	0.8298	0.8936
8	1	0.9475	0.8842	0.8120	0.8872
10	1	0.9823	0.9373	0.8768	0.9077

A MAC values of 1 in the second column of Table 7.1 for both slabs implies there is no damage is present for the two cases. This is because the intact case was compared with itself. For first incremental load 5kN for both slabs, MAC values for all mode shapes were greater than 0.9023, except the second mod shape of slab 1 which is less than this value. Value 0.9023 is used as a reference to be compared with other values. The value of MAC ensures that the two different states are well correlated in this step of loading.

When the load increased from 5kN to 10kN, the MAC values of almost all mode shapes were gradually decreased. Unexpectedly, the MAC value for the first mode shape of slab 1 tended to slightly increase when the load changed from 5kN to 10kN. The change is small and unrealistic which may be potentially due to bending the support of the slab as a result of the static load increase from 5kN to 10kN.

The most significant changes were obtained at last load step (12kN) as the changes of natural frequencies were significant. The most significant changes were obtained for the fourth and fifth modes shape of slab 1 and 2 respectively, while lower

decrease in MAC values is exhibited for the first mode shape. As previously mentioned that modes 4 and 5 are pair has same theoretical natural frequency. Usually, one mode of a pair of double modes can be identified while the other is likely to be missing from the experiment. As a consequence, mode four was identified for slab 1, while mode 5 was appeared in slab 2. Using MAC values is proved to be successful in determining changes as can be seen in Figures 7.4 and 7.5 for slab 1 and 2 respectively. The effect of repair work using carbon fibre reinforced polymer was observed through an increase in the values of MAC compared with MAC values of the last load step, 12kN.
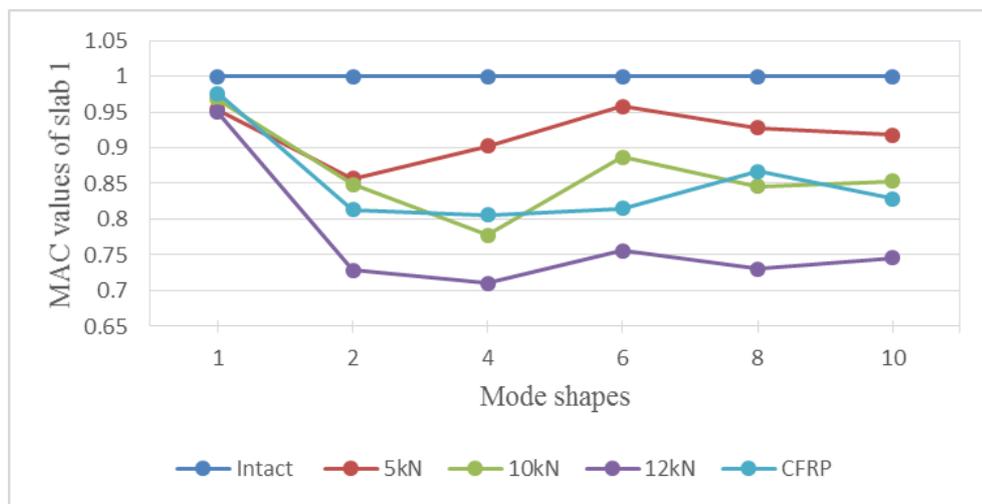
Figure 7.4: MAC values of RC slab 1, under different status.
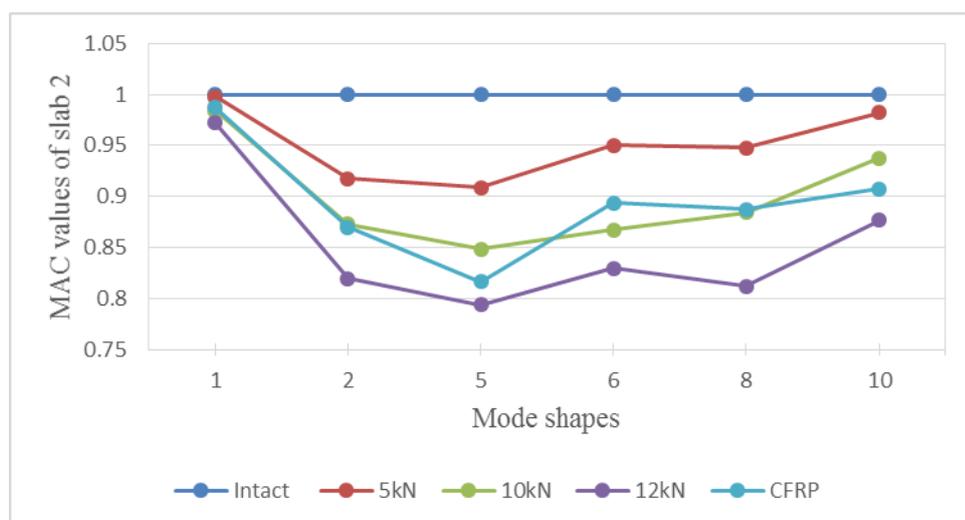
Figure 7.5: MAC values of RC slab 2, under different status.

Comparison was made between the effect of repairing RC slabs 1 and 2 of group C on MAC values. The effect of repair work for slabs 1 exhibits the higher percentage of increase in MAC values for all mode shapes compared to slab 2 as shown in Figure 7.6.
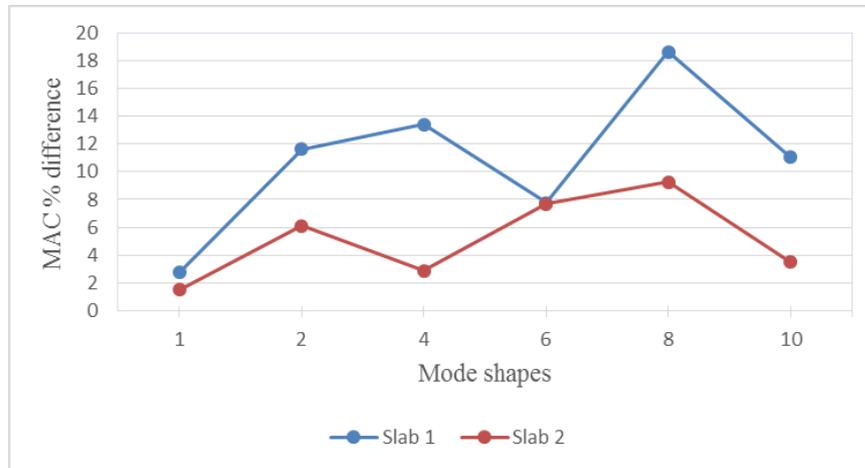
Figure 7.6: Effect of repairing RC slabs 1 and 2 on MAC values.

The effect of repair work in the MAC values of slab 1 is well obvious in all mode shapes, except the sixth mode shape which was slightly increased. Accordingly, higher percentage differences in MAC values of the repair work of slab 1 is owing to the fact that slab 1 is exhibits more damaged than slab 2 and therefore CFRP is more effective for enhancing intensive damaged slab. Generally, it has been noted that there is a change in the mode shapes as the slab become increasingly more damaged. As the load level increases on the slab, the number of modes that can successfully be correlated with those from the previous load step becomes less. In other words, when the load increase from 5kN to 10kN and then to 12kN, the number of mode shapes has MAC value (moves away from 1) was increase. It is concluded that the sensitivity of mode shapes, as measured by the MAC values, depends very much on the nature of damage. The distribution of the stiffness change in the structure affects the mode shape, such that evenly distributed damage in RC element does not cause a significant change in the general shape of the modes of vibration especially in the early load level.

As mentioned previously, as the load level increases on the slab, the number of modes that can successfully be correlated with those from the previous load step becomes less. Although, this trend is based on the results of applying a MAC

algorithm, it does not appear to be possible to localise the defect in mode shapes. Therefore, COMAC values for the tested slabs 1 and 2 were calculated and presented in Table 7.2 and Table 7.3 to identify which response point adversely caused the MAC values decrease. This would help to identify which response point has adverse effect on MAC values.

Table 7.2: COMAC values of RC slab 1 under different conditions with respect to intact reference case.

Point No. (j)	Intact	5kN	10kN	12kN	Repaired
1	1	0.9926	0.9845	0.9920	0.990
2	1	0.9282	0.7969	0.6541	0.9722
3	1	0.8848	0.8396	0.8242	0.7021
4	1	0.8560	0.9058	0.9168	0.9177
5	1	0.9753	0.9758	0.9580	0.9515
6	1	0.7490	0.7840	0.7783	0.8610
7	1	0.9648	0.9442	0.9310	0.9426
8	1	0.6267	0.8780	0.6994	0.8830
9	1	0.9244	0.7823	0.7520	0.6989
10	1	0.9657	0.9804	0.9298	0.9162
11	1	0.9168	0.9003	0.6310	0.8863
12	1	0.8519	0.8467	0.6602	0.721
13	1	0.9615	0.8599	0.6876	0.6947
14	1	0.8072	0.7466	0.6832	0.6979
15	1	0.8866	0.8978	0.8243	0.7729
16	1	0.9722	0.9449	0.8580	0.7891
17	1	0.9395	0.9097	0.9367	0.9318
18	1	0.6300	0.6622	0.8321	0.7045
19	1	0.9662	0.9324	0.9590	0.9652
20	1	0.9151	0.9559	0.8600	0.8883
21	1	0.9650	0.9693	0.9062	0.9297
22	1	0.9806	0.9643	0.8544	0.8642
23	1	0.9044	0.9482	0.9292	0.9249
24	1	0.9127	0.7543	0.7829	0.8020
25	1	0.9703	0.9746	0.9465	0.9031

Table 7.3: COMAC values of RC slab 2 under different conditions with respect to intact
reference case.

Point No. (j)	Intact	5kN	10kN	12kN	Repaired
1	1	0.9971	0.9865	0.9895	0.9943
2	1	0.9394	0.9166	0.8802	0.909
3	1	0.9674	0.9135	0.7926	0.9379
4	1	0.9966	0.9772	0.8569	0.8078
5	1	0.9885	0.9769	0.9677	0.9671
6	1	0.9494	0.9336	0.8669	0.9441
7	1	0.9855	0.8632	0.7975	0.958
8	1	0.9838	0.8778	0.7502	0.7114
9	1	0.9041	0.9363	0.8291	0.8825
10	1	0.9916	0.8661	0.8427	0.827
11	1	0.9721	0.962	0.8283	0.8691
12	1	0.9906	0.9106	0.7974	0.9179
13	1	0.9788	0.9141	0.8685	0.8958
14	1	0.9663	0.9577	0.8442	0.9736
15	1	0.9863	0.8932	0.7468	0.821
16	1	0.9731	0.9539	0.8586	0.8535
17	1	0.9729	0.9134	0.9367	0.9212
18	1	0.9249	0.8633	0.8508	0.8329
19	1	0.9887	0.9432	0.8742	0.7055
20	1	0.9657	0.9417	0.9162	0.9046
21	1	0.9857	0.9648	0.9524	0.9745
22	1	0.9817	0.9236	0.8629	0.8799
23	1	0.9723	0.9092	0.9328	0.9467
24	1	0.8769	0.9286	0.9002	0.9455
25	1	0.9849	0.9699	0.9449	0.9171

As aforementioned that, the MAC determines the relationship between two modes
shapes. If the two mode shapes are exactly parallel vectors (linearly dependent) the
MAC value is equal to one, but if they are completely dissimilar (orthogonal) the
MAC value is equal to zero. If the mode shapes are equal at coordinate j, the
COMAC value between two sets of mode shapes is equal to one. While its value will

be zero if no correlation exists between the mode shapes. This means that a low COMAC value would indicate discordance at a point.

Searching for the lowest values of COMAC helps finding the points have adverse effect on MAC values. For first incremental load, the minimum MAC values for six mode shapes of slab 2 is 0.9085 at load step 5kN, while it is 0.8566 for mode shapes of slab 1 as presented in Table 7.1. The value 0.9085 ensures that the two different states (healthy and step 5kN) of slab 2 are well correlated in this step of loading, whereas the 0.8566 value is not well correlated as in slab 2. This is due to the fact that there is only one coordinate (which is DOFs 24) of slab 2 has COMAC value less than 0.9 which has adverse effect on the MAC value. Whereas, there are about eight coordinates of slab 1 have COMAC value less than 0.9 which is selected as a reference; and the lowest COMAC value (0.6267) can be found at coordinate 8. The decrease in MAC values for the 10kN and 12kN load steps was gradual. Therefore, at the two load steps (10kN and 12kN), the number of coordinate which has COMAC value less than 0.9 become higher. For almost all DOFs, steeper reduction in COMAC values were obtained for both slabs when the incremental load increased from 10kN to 12kN. This implies that when the damage became severe, smaller COMAC values response points were obtained.

It is concluded that MAC values was successfully used to find the presence and degree of damage in RC slabs. Whereas, COMAC values was successfully employed to identify which degrees of freedom (among 25 DOFs) on slab surface contribute negatively to a low value of MAC. It is also concluded that as the load level increased from 5kN to 10kN and then to 12kN, the fewer number of modes that can successfully be correlated with those from the previous load step is found. In other words, when the load increase, the number of mode shapes has MAC value (moves away from 0.9) was increase. Similarly, when the load increased from 5kN to 10kN and then to 12kN, the number of coordinates has COMAC value (moves away from 0.9) was increase. However, the number of mode shapes has MAC value and the number of coordinate has COMAC were decreased under repairing with CFRP.

7.3.2   MAC and COMAC for Group D Slabs

In order to know the location of defect, the baseline healthy case mode shapes were required to be compared with defected case mode shapes. Therefore, a comparison between results of mode shapes of the baseline healthy group A slabs with identical modes from imperfect case group D slabs were provided. Slab 1 of group A with slab 1 of group D and slab 2 of group A with slab 2 of group D were compared to localise the defect location. This is due to the fact that the most of natural frequencies of slab 1 were less than slab 2 in group A, whereas all six natural frequencies of slab 1 are greater than slab 2 in group D. Since the location of damage was required, MAC and COMAC numerical methods were employed for quantitatively comparing mode shapes at all DOFs. These two robust techniques were required to obtain the approximate correlation between the mode shapes. This is because there is not obvious changes that can be observed of the experimentally obtained mode shapes for artificially created defect slabs. This may be owing to the fact that the changes were not only confined to the flaws area, but the change were spread across the entire area. As a consequence, the correlation between mode shapes using visual inspection becomes undependable. The MAC determines the relationship between two mode shape measurements on a reinforced concrete slab, which can be interpreted as an indication of damage. In particular, the natural mode shapes of intact case were compared with those for artificially induced damage, using MAC, as displayed in Figure 7.7. Table 7.4 lists the elements of the main diagonal of the MAC matrix for the two group A and D slabs.
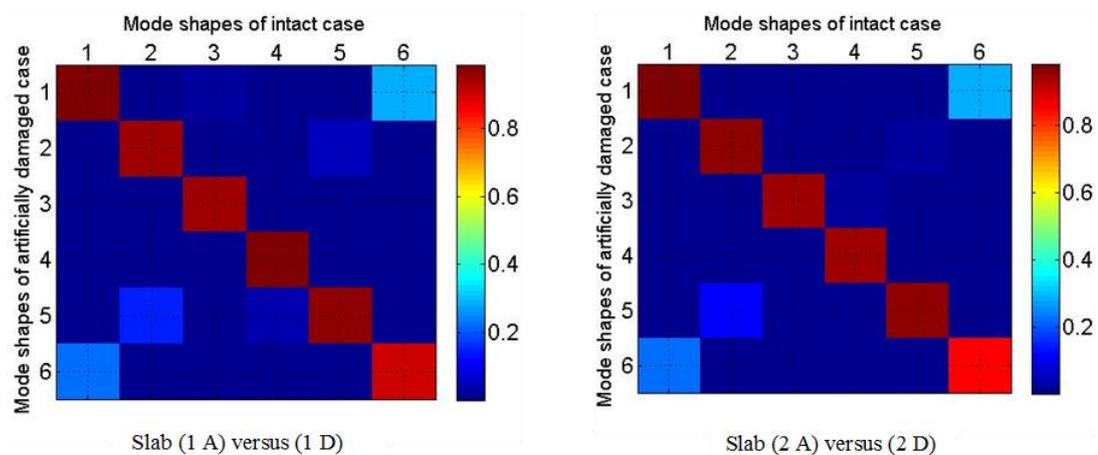
Figure 7.7: Degree of damage influence on MAC values for groups A and D slabs.

Table 7.4: Artificial damage influence on MAC values for the slab, groups A and D.

MAC values for slab 1 and 2 of groups A and D		
Mode No.	Slab (1 A) and (1 D)	Slab (2 A) and (2 D)
1	0.9868	0.9819
2	0.9550	0.9524
4	0.9539	0.9372
6	0.9795	0.9486
8	0.9692	0.9563
10	0.9088	0.8541

It is obvious that the artificial induced void on the top surface of the slab caused reductions in MAC values. The difference of MAC value from unity is observed in all mode shapes. However, the most substantial differences of a MAC value from unity is appeared in the higher (tenth) mode. This implies that the nature of reduced stiffness and mass of induced void on the top slab's surface at coordinate 7 as shown in Figure 4.11 strongly affected the higher mode compared with the rest mode shapes. As a consequence, MAC values in RC slab could be used as a measure to identify the damage at its advanced stage, whereby relative changes up to 9.12% and 14.59 % can be observed between the correlated modes of slab (1 A) and (1 D) and slab (2 A) and (2 D) respectively.

As mentioned that MAC could provide information about overall stiffness change of the structure because of damage, but it could not determine the stiffness change at each DOFs. For such task, the COMAC measurement should be used as an indicator to locate damage by identifying the maximum deviation of the mode shape from the undamaged value at coordinates, DOFs. Table 7.5 displays the COMAC values for the tested slabs which are used to locate artificially induced void. Searching for the lowest values of COMAC helps finding the location of artificially induced void on slab surface.

Table 7.5: Artificial damage influence on COMAC values for RC slab.

COMAC values of group D slab with respect to intact reference case group A slabs		
Point No. (j)	Slab (1 A) and (1 D)	Slab (2 A) and (2 D)
1	0.9977	0.9957
2	0.9761	0.9053
3	0.9791	0.9951
4	0.9593	0.9678
5	0.9719	0.9827
6	0.9067	0.9551
7	0.8929	0.8939
8	0.9120	0.8834
9	0.9836	0.9675
10	0.9263	0.9465
11	0.9362	0.8951
12	0.9632	0.9681
13	0.9623	0.9884
14	0.9584	0.9769
15	0.9241	0.9052
16	0.9215	0.9124
17	0.9626	0.9867
18	0.9883	0.9059
19	0.9938	0.9816
20	0.9094	0.9011
21	0.9798	0.9913
22	0.9684	0.9486
23	0.9263	0.9272
24	0.9299	0.8963
25	0.9858	0.9931

Previously explained the different sensor positions which were the response point locations. COMAC measurements for every response point is listed in Table 7.5 and displayed in the bar diagram as shown in Figures 7.8 and 7.9. This Figure shows the COMAC of the intact state A and the artificially voided state D with respect to the

measurement points. Variations can be detected, and a location of the damage becomes possible by comparison of the actual COMAC values with their maximal value 1. In the case of a safe locations, response points will have a COMAC value near to one. However, in the case of damages, the indicators in damage location and in the neighbourhood of the damage will be smaller than all others.
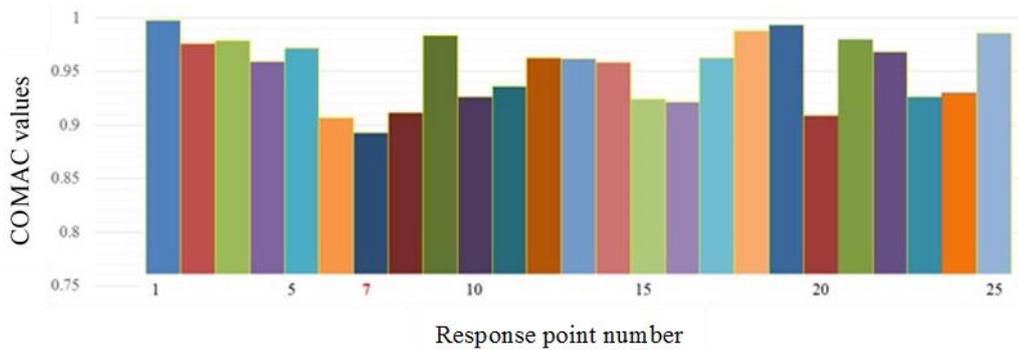
Figure 7.8: COMAC values at 25 coordinates, Slab (1 A) and (1 D).
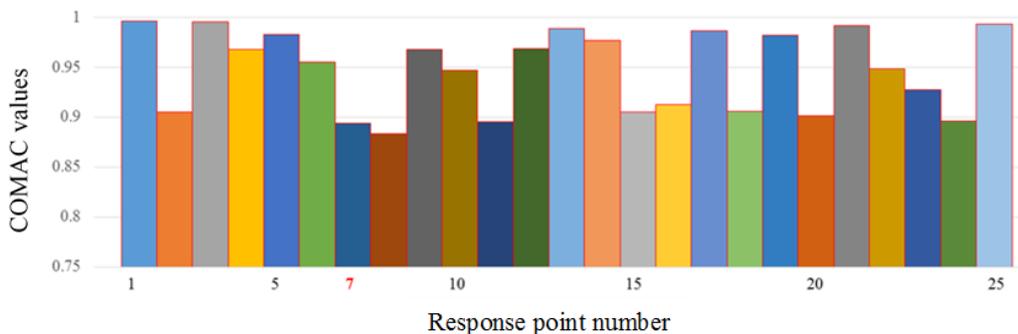
Figure 7.9: COMAC values at 25 coordinates, Slab (2 A) and (2 D).

For slab 1A and 1D, COMAC values were greater than 0.92 for all DOFs on the slab's surface except DOFs 6, 7, 8 and 20. The differences in the neighbourhood of the position of the response point 6 and 7 are greater than all others response points so that a trend could be identified. Even more precise results were gained by the COMAC values. The remarkable reductions are observed for this case of a stiffness variation for the position 7. The higher difference of a COMAC value from unity, the more the possibility of the corresponding point being a damage site. This implies that the artificially damage was placed at DOF 7.

For slab 2A and 2D, COMAC values of 17 DOFs were greater than 0.91. The positions 7, 8, 11 and 24 are less than 0.90. As shown, COMAC values at the two neighbour points 7 and 8 are small, indicating the damage present in these positions. The COMAC value of response point 8 is slightly less than response point 7. Although the COMAC value of response point 8 slightly less than 7, the response point 2 also has low COMAC value 0.9053 which is closer to response point 7 than 8. Therefore, it is indicated that the artificial void is located at response points 7 rather than response points 8.

It is recalled that COMAC values at some other locations are also small where damage is not present. The low values of COMAC are seen for outer response points such as response points 2, 15 and 20. The COMAC values of response points 2, 15 and 20 are 0.9053, 0.9052 and 0.9011 respectively. The low values of COMAC for the outer response points may be due to small perturbation during the dynamic test (for example, noise measurement). The small perturbation caused the slight decrease of COMAC value for the outer response points. However, such small perturbation was not affecting damage localisation.

In brief, from the vibration data (mode shapes), damage locations can be identified via MAC and COMAC techniques when both intact and damaged data were compared. It is demonstrated in this study that MAC can indicate a clear change in the mode shape, while the COMAC provide the change in specific location whereby the location of damage can be identified. The drop in COMAC corresponds to the location of the severity of inflicted damage. It can be used as one good indicator to identify at which DOFs the imperfection was occurred in reinforced concrete slab. This finding is supported by Al-Galib (2013), who found that COMAC values are more sensitive to the localised flaws compared with subtle gradual damage of a RC beams. Moreover, Nolambi et al. (2002) similarly used COMAC to successfully locate damage in a reinforced concrete beam.

7.4 Summary

In this chapter, two pairs of reinforced concrete slabs (group C and D) were investigated with the calculation of two techniques (MAC and COMAC) to make the comparison between the healthy and non-healthy states. The two methods were used to assess the sensitivity of vibration characteristics to damage in term of group C slabs. Whereas such techniques were employed to identify the location of the defect, in group D slabs.

The slabs (of group C) were cracked by applying a partially concentrated load in increments. Three loading regimes were employed to produce damage and cracking under loading, and then the slabs were repaired using CFRP. After each incremental loading, the slabs were tested to determine the natural frequency, mode shape and damping ratios. The mode shapes of the healthy state and each damaged and repaired state were compared using MAC and COMAC values to investigate the effect of different degrees of cracking as well as repairing using CFRP. In group D, the cavity was created on the surface of the slab. The influenced of the void was not obvious through visual comparison. Therefore, the mode shapes of the healthy state (group A) and damaged state (group D) were compared using MAC and COMAC values to identify the location of artificially induced void.

The details of the MAC and COMA values obtained from the static loading and repairing were presented by tables and figures and discussed. There was clear evidence that the amount of reduction in the MAC value appears to increase as the damage increases, but each mode had different sensitivities to the introduced damage. The results indicate that the COMAC values is affected by the cracking introduced by overloading and repairing.

Defect location characterisation, based upon mode shapes calculation, holds fairly well for the defected area after using MAC and COMAC. The COMAC values worked better than the MAC for damage localisation because COMAC value is dealing with coordinates rather than the whole mode shape, as in MAC value. Therefore, the COMAC value can successfully indicate which degrees of freedom measurement contribute negatively to a low value of MAC, whereby the location of was identified.

8. Artificial Neural Network Application for Void Detection

8.1   Introduction

Artificial Neural Network (ANN) is defined as a computational model inspired by the structure and the information process capabilities of the human brain. It is a parallel information processing paradigm based on models of biological neurons. It is an assembly of a considerable number of a highly interconnected simple processing unit (neurons). The ANN stores knowledge in the form of connection strengths. Such strengths are represented by numerical values that are called weights. Weights can be determined through a series of the training process. ANN is typically referring to a powerful mathematical model that have been employed to a wide variety of problems. (Arbib, 2003). Although ANN field was established before the advent of the computer era, its simulation has been recently developed (Bandara, 2013). ANN has been introduced to many field of sciences including in structural engineering. The concept of the neural network technique imitates the behaviour of biological neural network in the human brain. ANN can learn from trial and error, or experience and examples, and then to adapt by changing situation in most cases. The ANN applies to different tasks such as classification the fault in deficient members, regression and clustering (Rafiq et al., 2001). The structure of the ANN contains a set of parameters that can be adjusted to achieve a certain task. Recently, several types of neural networks have been designed and used in different areas of engineering and science. The types of neural networks can be categorised into two main forms which are Feed-forward networks and Recurrent-feedback networks. These two types are subdivided into several classification forms as shown in Figure 8.1.
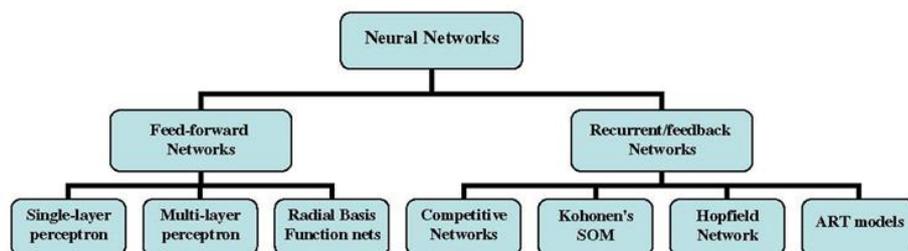
Figure 8.1: Type of neural networks (Jabbari and Talebi, 2001).

SOM =Self Organized Map
ART= Adaptive Resonance Theory

The Multilayer Perceptron (MLP) network among all other types of network architectures is the most frequently used and much more considerably mentioned in the literature on ANN (Meruane and Mahu, 2004). The learning problem for this type of network has been formulated in terms of the minimisation of an error function of the free parameters, in order to fit the neural network outputs to an input-target data set (Bandara, 2013).

8.1.1   Artificial Neuron Model

Artificial neuron is known as a basic building block of every ANN. Its functionalities and design is originated from the conception of a biological neuron which builds a biological neural networks. Therefore, the information processing of the neurons in the neural networks behave like a brain in human beings (Haykin, 1999). The similarities in design of both artificial and biological neurons are depicted in Figure 8.2. The right figure illustrates the artificial neuron which includes inputs, weights, bias, transfer function and outputs, while the left figure represents the biological neuron which consist of dendrite, soma and axon.
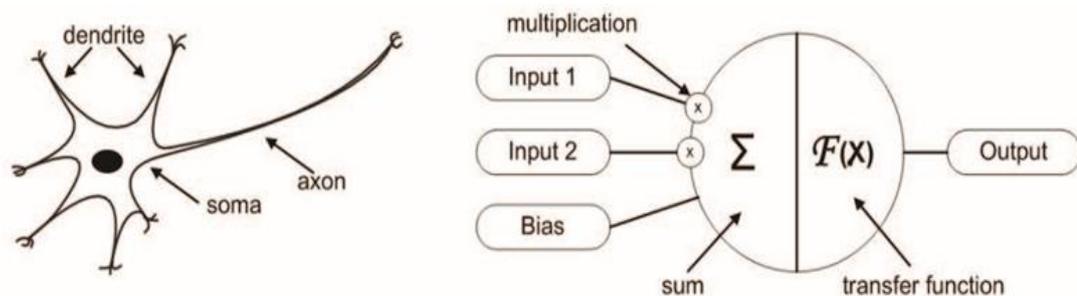
Figure 8.2: Biological and typical artificial neuron (Krenker et al., 2011).

The artificial neuron functionalities launch when the information, $x_i(k)$, are entered via inputs and then they are transmitted into the body of an artificial neurons through the connections that multiplied the strength of each input individually with a scalar weight $w_i(k)$ to form the product $w_i(k) \cdot x_i(k)$. All the weighted inputs $w_i(k) \cdot x_i(k)$ are added to obtain the sum $\sum w_i(k) \cdot x_i(k)$ and the scalar bias b is added to the sums in the body of an artificial neuron. Then, the sums of the weighted inputs and bias are processed and the result is the argument of the transfer function. At the final stage, an artificial neuron produces the treated information via output. The bias is

much like a weight, except that it has a constant input of 1. The benefit of a typical artificial neuron model is simply shown in the following mathematical description (Krenker et al., 2011).

$$y(k) = F\left[\sum_{1=0}^{n} w_i(k) \cdot x_i(k) + b\right]$$

(8.1)

Where:

$x_i(k)$ is the input value in discrete time k where i rages from 0 to n,

$w_i(k)$ is the height value in discrete time k where i ranges from 0 to n,

b   is the bias,

F   is a transfer function.

$y(k)$ is the output value in discrete time k.

8.1.2   ANNs Classification

ANNs can be generally classified into two general types (Bandara, 2013). Firstly, the most common structure of connecting artificial neuron into network is based on the number of layers such as single and multilayer networks. Secondly, it can be categorised according to the possible topologies. Topology is the way that individual artificial neurons are interconnected to each other (Krenker et al., 2011). The interconnection of the neurons can be done in considerable ways results in considerable possible topologies that are separated into two common classes such as feed-forward and recurrent topologies.

The simplest form of layered network is single layer which is depicted in the Figure 8.3. As illustrated in the figure, each neuron in the input layer is directly connected to every artificial neuron in the output layer. Accordingly, there are no hidden layers in single layer networks. Therefore, the neurons in the input layers are connected to the neurons in the output layers through the connection weight.
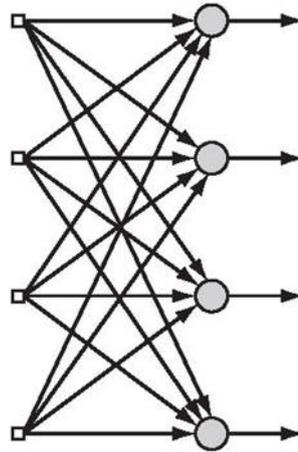
Figure 8.3: Single layer feed – forward network (Hykin, 2009).

A Multilayer network is frequently used by researchers in different fields of science and engineering. In this types of network, there is an input layer of units through this layer the rest of the network is gradually fed. Next, input layer is connected to one or more hidden or intermediate layers of neurons, which evaluate the same sort of function of the weighted sum of inputs. Then, the information is sent to the units in the following connected layer which are neurons in the output layer. Figure 8.4 shows a typical multilayer network, and illustrates that each neuron in the layer is completely connected to all neurons in the following layer. The same figure also shows that an input layer consists of ten neurons, one hidden layer with four nodes and an out layer comprise of two neurons. The output of the neurons in any layer is becoming the input of the neurons in the next layer (Jabbari and Talebi, 2011). This process is continuing until the output target is acquired.
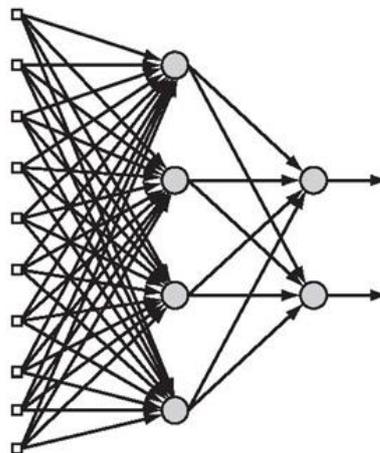
Figure 8.4: Multi-layer feed-forward network (Hykin, 2009).

In addition to classification of ANNs in term of number of layers, Figure 8.5 shows the two basic topologies that analyse the data in two different flows. The left side of the figure exhibits feed-forward topology where neurons in each layer are connected to the neurons in the following layer and information flows from input side of the network to the output part in only one direction. While, the right side of the figure exhibits recurrent topology where neurons in a layer are connected to each other and some of the data flows not only in forward direction, input to output, but also in backward direction, which is opposite of forward direction. Thus, artificial neural network with the feed-forward topology and with the recurrent topology are called Feed-Forward artificial neural network and recurrent artificial neural network respectively.

Feed-forward FNN   Recurrent RNN
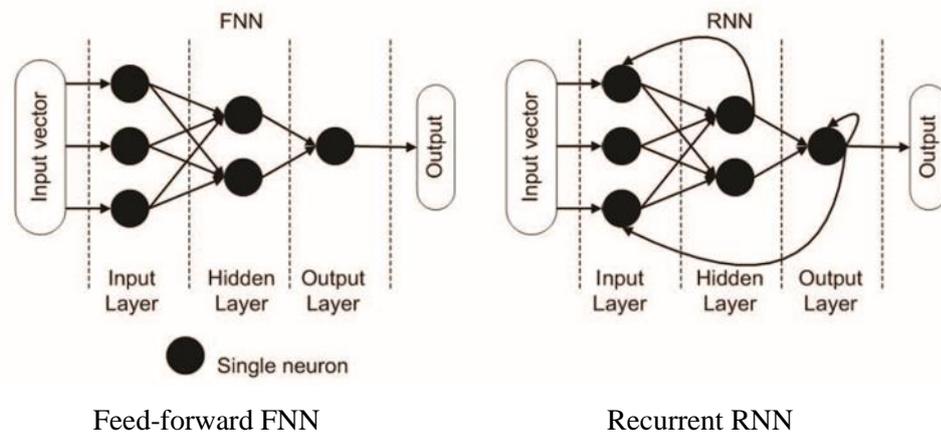
Figure 8.5: Feed-forward FNN and recurrent RNN topology of an artificial neural network (Krenker et al., 2011).

8.1.3   Architecture of Artificial Neural Network

The best architecture of ANN can be obtained when considerable attention has been paid for modelling. This is justified where the typical method is followed. Since there is no theoretical background as to how the typical architecture, structure, will be gained or what it should resemble, the best method to achieve the purpose is repetitive trial and error (Bandara, 2013). During which, numerous type of architectures are examined and compared to one another. This is distinctly time consuming process and is not mainly based on person's past experience but also on his intuition.

An ANN is generally formed by interconnected group of artificial neurons to build a complex network in order to imitate the human nervous system. The behaviour of neurons is influenced by each other through a weight. Each neuron, node, calculates a nonlinear weighted sum of its inputs and then simply transfers the output over its outgoing connections to other neurons. Therefore, the behaviour of the network depends predominately on the way of interaction between these neurons. Besides the way of neurons' interaction, there are five main elements, which build the ANN's architecture, and has direct impacted on the behaviour of the network (Bandara, 2013). These five components of ANN architecture are: the number of layers; the number of neurons in each layer; the transfer functions of each layer; the weights and biases; and the training algorithm.

8.1.3.1   Number of Layers

The Multilayer Perceptron (MLP) network among different types of network architectures is the most frequently used (Meruane and Mahu, 2004). A MLP network usually comprises of array of input neurons known as the first layer or input layer, a number of intermediate layers or hidden layers, which are not constantly involved due to its less significant use in some conditions, and an array of output neurons known as the last layer or output layer. It is important to mention that neurons are usually organised into groups called layers for easier handling and mathematical describing of an ANN (Krenker et al., 2011). An optimum number of layers is generally dependent on the number of training cases, amount of noise in the target and on the complexity of the problem. It is true a network with numerous hidden units tends to memorise the training cases and leads to a low training error owing to over fitting and high variance. Although two hidden layers are recommended for most structural cases (Masri et al., 1996), Hecht-Nilsen (1987) proved that a network with one hidden layer with sufficient number of neurons could simply compute any arbitrary function of its inputs. In most practical problems, neural networks with three (input, hidden and output) layers or occasionally four (input, two hidden and output) layers are excessively used, but five or more layers are rarely used (Jha, 2007).

8.1.3.2   Number of Neurons

Increasing attention is needed to be paid in order to predict the number of neurons in a neural network layers. Although there is no magic formula for calculating the

optimum number of neurons in each layer, some thumb rules are available to predict the appropriate number of neurons in each layer (Bandara, 2013; Jha, 2007). The geometric pyramid rule is employed to obtain the rough approximation which proposed by Master (1993). This rule states that the right number of neurons can be predicted when following a pyramid shape. A pyramid shape means that the numbers of neurons are reduced from input layer to the output layer. As a result, each layer can possess different number of neurons. Each neuron behaves as an independent element, and it receives information, or fed a weighted sum, from the neuron in the preceding layer. Then, neuron provides an input to every neuron of the following layer for further processing.

Different trials of number of neuron in ANN layer are required to be emplyed in order to determine the best possible number of neurons in hidden layer. It was revealed that the neural network may not be able to represent the system adequately if the number of neurons in the layer in the neural network is too small. Conversely, it becomes over-trained if the network is too big (Yun and Bahng, 2000). Over training is the most typical problem in neural network. Tetko et al. (1995) explained that the over fitting problem refers to exceeding some optimal network layers and neurons, ANN size. While overtraining also refers to the time of the ANN training process that may subsequently make the network with worse predictive ability.

8.1.3.3   Transfer Function

The activation of each neuron is governed by the mathematical formula that predict the output which is known by the transfer function (Meruane and Mahu, 2004). This function is another component of ANN architecture that also needs to be specified. Each neuron takes its net information input and provides an activation function to it. Neural network architecture employ the activation function to prohibit the output from reaching very large range so as not to incapacitate the network and thereby inhibit training (Jha, 2007). Many forms of activation functions have been used to meet certain requirements according to the specific problem. Figure 8.6 shows the typical examples of the transfer function, such as hyperbolic tangent sigmoid, logarithm sigmoid, linear, saturating linear and symmetric saturating linear. In practice, transfer function such as hyperbolic tangent sigmoid function, which is also known as sigmoid function, is mostly utilised by the researchers. This is because

sigmoid function is continuously differentiable and nonlinear and therefore it is desirable for network learning. The hyperbolic tangent sigmoid function is described in Figure 8.6, which generates the outputs between -1 and +1.
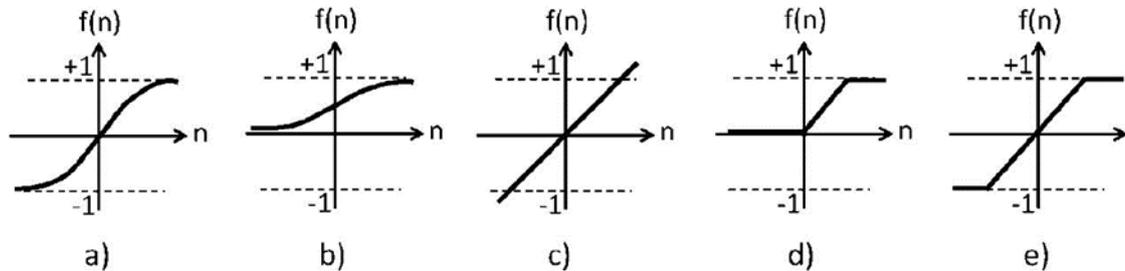
Figure 8.6: a- hyperbolic tangent sigmoid, b- logarithm sigmoid, c- linear, d- saturating linear and e- symmetric saturating linear (Meruane and Mahu, 2004).

8.1.3.4   Weights and Biases

The weights and biases are also other components of ANN architecture. The former is employed to scale the inputs which received from input neurons to the network or from neurons of layer to neurons of the following layer. The latter is much like a former, except that it has a constant input of 1. Although the ANN can be created with or even without the biases, the network with biases is more powerful than those without biases (Bandara, 2013). When ANN is trained according to a specified learning algorithm, it adjusts both the weight matrix and bias vector. In other words, a bias is only connected to neurons in the hidden and output layers with modifiable weighted connections (Caglar et al. 2008).

8.1.3.5   Neural Network Learning

There are two major learning methods are employed for neural networks such as supervised learning and unsupervised learning. They can be used by any given type of neural network architectures (Krenker et al., 2011). The decision of utilising them is dependent on the data obtained for training the network. Each of the learning method has many training algorithms. However, Back Propagation Neural Network (BPNN) and Learning Vector Quantisation are the most popular algorithm of supervised and unsupervised learning respectively (Abbas, 2013).

Supervised learning is probably the considerably utilised technique in the neural network realm. The network is capable to learn when training examples, set of input and output patterns, and is provided by a user. The learning rule is provided with the train set (set of examples) of proper network behaviour.

$$\{x_1, d_1\}, \{x_2, d_2\}, \ldots \ldots \ldots \ldots \ldots .. \{x_n, d_n\}$$

where:

(x_n) is input to the network,

(d_n) is corresponding target output.

Where the inputs are provided to the network, the network actual outputs are compared with the targets. The learning rule is then used to adjust the weights and the biases of the network to obtain the outputs which is closer to the target.

However, other type of learning method of neural network is unsupervised learning. This learning approach is implemented when there are no target outputs available for the input data. In other words, this training can be employed when there is a lack of knowledge of target output for the training data.

Among different algorithms, for instance Hebbian learning algorithm, the perceptron learning algorithm and Widrow-Hoff learning algorithm, the back propagation learning algorithm is the most frequently used in the field of neural network (Bandara, 2013). It is capable of solving non-linearity separable pattern classification. Multilayer feed forward neural network is most commonly employed with the back propagation learning algorithm (Fausett, 1994). The number of neurons in successive layers is non-linearly arranged depending on the problem (Caglar, 2008; Jha, 2007). Each neuron has an associated transfer function, which describes how the weighted sum of its inputs is converted to the results into an output value.

The back propagation algorithm involves two basic phases. Firstly, the forward phase where the activations are propagated from the input to the output layer. Secondly, the backward phase where the error between the observed actual value and the desired nominal value in the output layer is propagated backwards, from the left to right in order to modify the weights and bias values (Murthyguru, 2005; Caglar et al., 2008).

The fundamental property of back propagation neural network is learning by examples and working by algorithms in small iterative steps and it changes the network's weights. This means that examples are required to be given to train the network. The training of the network is actually achieved by adjusting the weights and is carried out through extensive number of training cycles. The main goal of the training procedure is to obtain the optimal set of weights, which would produce the right output for any input in the ideal case. Training the weights of the network is iteratively adjusted to capture the ideal relationship between the input and output patterns.

In forward phase, the weighted sum of input components is computed by the following expression (Caglar, 2008).

$$\text{net}_j = \sum_{i=1}^{n} w_{ij} \cdot x_i + \text{bias}_j \qquad (8.2)$$

where:

    net_j is weighted sum of the jth neuron for the received input from the preceding layer with n neurons

    w_{ij} the weight between the jth neuron and the ith neuron in the proceeding layer.

    x_i is the output of the ith neuron in the proceeding layer.

Then, the input value is passed through the sigmoid transfer function to compute the out of the jth neuron out_j as follows (Caglar, 2008). It is guaranteed that the generated output, which is expresses in equation (8.3), is bounded between 0 and 1.

$$out_j = f(net_j) \frac{1}{1 + e^{-(net_j)}} \qquad (8.3)$$

When training is finished, the calculated output, for a particular input, is then compared with the target output to calculate the sum square errors (SSE) and mean square errors (MSE). It is required to highlight that the error value is propagated backwards through the network, and small changes are made to the weights in each layer. The process of feed forward and back propagation repeats until the desired value of square errors is captured, error value drops below the predetermined threshold. The SSE is defined as follows (Caglar, 2008).

$$SSE = \sum_{i=1}^{m}\left(T_i - out_j\right)^2 \tag{8.4}$$

where:

T_i is target output of the neural network value for i^{th} output

out_j is actual output of the neural network value for i^{th} output

m is number of neurons in the output layer

Mean squared error (MSE) is used as the error function, which is defined by equation (8.5).

$$MSE = \frac{1}{n}\sum_{j=1}^{n}\left(O_t - O_p\right)^2 \tag{8.5}$$

where:

O_t is the target outputs

O_p is the predicted outputs

n   is the number of data

MSE   indicates the difference between the ANN output value and the desired value

Multilayer feed forward neural network is most commonly employed with the back propagation learning algorithm. In general, Multi-layer perceptron (MLP) or multilayer feed forward neural network learned by back propagation algorithm which is based on supervised technique is more desirable neural network and is used more than other due to its capability to solve variety tasks (Jha, 2007).

In this study, the modal parameters such as natural frequencies are extracted to estimate the presence of damages. The author proposed an approach based on Artificial Neural Networks (ANN) that are able to successfully train natural frequencies from the undamaged and the damaged structure. As a consequence, natural frequencies were utilised as input variables, while the void severity was utilised as the output. It is worth to mention that, one of the distinct characteristic of the ANNs versus other detection methods is that modelling the considered structure in a detailed physical model is not required by the neural network because it possess

the ability to implicitly treat mechanisms of damage through given natural frequencies (Pearson, 2003; Zapico and Molisani, 2009).

8.2   Artificial Neural Network Model

Neural network consists of a multitude of highly interconnected artificial neurons, which are also called cells, units, nodes, or processing elements. Neural network consists of several layers of neurons, such as input layer, one or more hidden layers and an output layer. It is important to mention that the number of neurons in input and output layer depends on the length of input and output vectors. However, there are no standard rules available for determining the appropriate number of hidden layers and hidden neurons per layer. Every neuron in a layer receives its input from the output of the neuron in the previous layer or from the network's input layer. The connections between neurons are associated to synaptic weights (w, z). They are adjusted iteratively during the training process. In the hidden and output layers, an additional node with a constant output (usually 1) is often added. Such nodes are known as bias neurons (Choubey et al., 2006).

The multilayer perceptron (MLP) is the most common neural network model which is adopted for its successful applications (Hu and Hwang, 2002). Such type of network requires a desired output to learn, therefore it is known as a supervised network. The goal of MLP is to create a model that rightly maps the input to the output using historical data. Then, the model can be used to produce the output when the desired output is unknown. Figure 8.7 shows a graphical representation of MLP network.
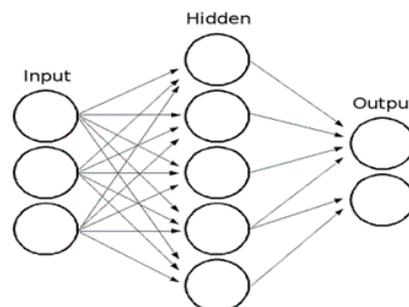
Figure 8.7: Graphical representation of MLP network.

With the back propagation algorithm, the input data is repeatedly represented to the neural network. With each presentation, the output of the neural network is compared to the desired (predicted) output and the difference is computed. The differences between desired output and the predicted output are combined and denoted by an error function. Then, this error is fed back, back-propagated, to the neural network and utilized to adjust the weights in such a way that the error decreases with each iteration. The neural model gets closer and closer to producing the desired output that will produce the minimal error. This process is known as "training".

8.3   Damage Detection Using ANNs

There has recently been growing interest in applying artificial neural networks to estimate and predict damage behaviour in complex structures. Neural networks are powerful data analysis tools in modelling, identification, diagnosis, and classification. The function of the neural networks is similar to the human brain, and its merit is to map the relationship between the input and output. Its function is similar to the human brain because of two main reasons (Tawfik et al., 2014). Firstly, a neural network acquires knowledge through learning. Secondly, a neural network's knowledge is stored within interneuron connection strengths known as synapses. It is important to recognise that, in damage detection, ANN is employed for mapping relationships between measured features and structural damage/physical parameters. ANN has to be trained for known damage features and their corresponding physical parameters when employing it for damage detection. The most common neural network in use is the multi-layer perceptron (MLP) trained by back propagation (BP) (Haykin, 1999). The BP learning algorithm is a way of adjusting weights and biases by minimising the error between predicted and measured outputs of the network. The most commonly applied ANN among many different types is the feed forward, multi-layered, supervised neural network with error back propagation algorithm, which is used in this work.

8.3.1   RC Simulations and Data Preparation.

The first step of RC simulation is building a geometrical model. According to the provided specifications from experimental reinforced concrete slabs, a geometrical model was created used finite element software ANSYS. Introducing a defect alters

the modal parameters (natural frequencies and mode shapes) of the structure. The changes in these two parameters can be utilized to detect defect occurrence. In this work, Artificial Neural Networks (ANNs) were applied to detect void sizes in a reinforced concrete slabs. The ANSYS software was used to extract the frequencies of RC slab of dimensions (1200mm x 1200mm x 60mm). Then, the extracted natural frequencies were used as the input to the ANN for void size classification because it can be measured easily and accurately. The geometric models were built for RC slab to calculate the first ten natural frequencies in the structural field. To ensure that the model acts in same way as tested in the laboratory, a free-free boundary conditions were applied for the model.

The input parameters of the neural network are the first ten natural frequencies, while the output parameter is the void size (length and width). Many actual sets of input-output data are required to train the neural networks successfully. It is labour intensive and time-consuming, thus very expensive to produce large enough training data sets from the experiments (Tawfiq et al., 2014). Therefore, using numerical method can overcome these obstacles.

Regarding the data preparation, the geometrical dimensions of the RC slab specimen, the mechanical and physical properties for the specimen are required to be initially defined and kept constant throughout the whole process. The slab was made of concrete properties with the modulus of elasticity (E) is $2x10^4$ MPa, Poisson's ratio (v) is 0.24 and density (ρ) is 2400 kg/m^3. Induced void in the slab can be characterised by two parameters, void location and the void size. The location of the void was varied as shown in Figure 8.8. Taking advantage of the symmetry, all the voids were located in one-quarter of the slab. Ten locations were chosen in this domain as indicated in Table 8.1. Four different induced void sizes, specifically for light (50 x 50mm^2), medium (100 x 100mm^2), severe (150 x 150mm^2) and extra severe (200 x 200mm^2) were considered in each location. In total, 40 simulations were carried out (4 void sizes times 10 locations) as presented in Table 8.1.

Forty simulations with voids were performed plus one extra without any defect. Therefore, forty one data sets for the analysis were generated. Each set had first ten natural frequencies, this means 410 natural frequencies were used for training the network. Three-dimensional FEM models with a single void were analysed using

ANSYS software to generate the data sets of natural frequencies (ωn). Even though neural networks have been applied on various civil and structural engineering problems, there still no attempt have been made regarding the different levels of fault severity in reinforced concrete slabs.
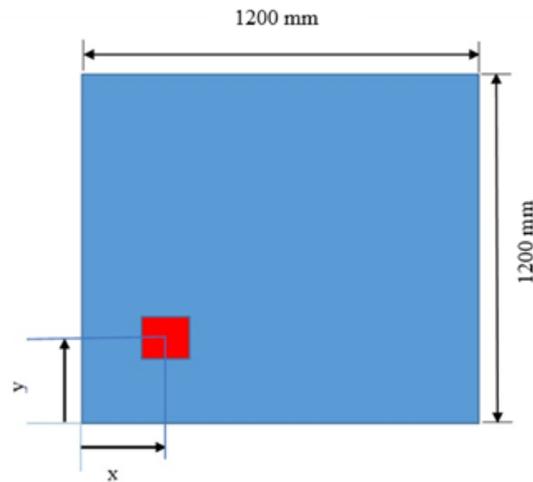
Figure 8.8: Location of void from the corner of the slab.

Table 8.1: Voids sizes and their locations

Void sizes (mm)							
50x50		100x100		150x150		200x200	
x	y	x	y	x	y	x	y
25	25	50	50	75	75	100	100
25	300	50	300	75	300	100	300
25	500	50	500	75	500	100	500
25	600	50	600	75	600	100	600
300	300	300	300	300	300	300	300
300	300	300	300	300	300	300	300
300	300	300	300	300	300	300	300
500	500	500	500	500	500	500	500
500	500	500	500	500	500	500	500
600	600	600	600	600	600	600	600

8.3.2   MATLAB Code Demonstration

Feed-forward multi-layer neural networks training were used to learn the input-output relationship. Natural frequencies as input and the void size (length and width) as output were introduced as shown in Figure 8.9. Utilising the subroutines and toolbox facilities of MATLAB, the managed to successfully establish a code for conducting the simulation of a multilayer perceptron model. The code has the capability for testing and retesting new untrained data. The general flowchart of the code is illustrated in Figure 8.10.
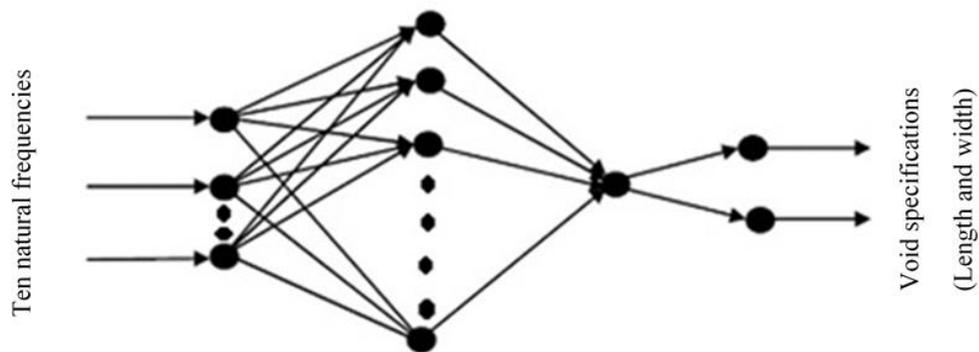
Figure 8.9: Schematic representation of the proposed ANN.
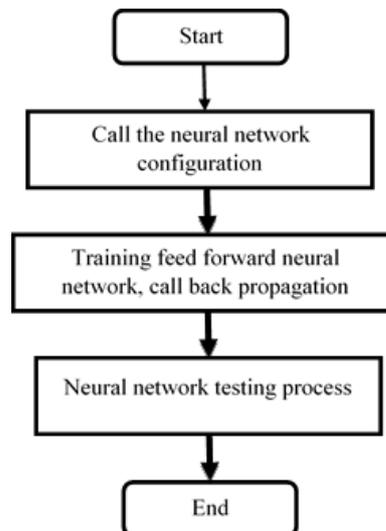
Figure 8.10: General flow chart for the ANN Code.

The two back propagation training algorithms which are Conjugate gradient and Levenberg-Marquardt are substantially more efficient for many problems. A comparison study between these two training algorithm was carried out by Hagan

and Menhaj (1994). The authors found that Levenberg-Marquardt outperformed Conjugate gradient algorithm in terms of their rapid convergence speed in training and performances in testing. As a consequence, this study adopted Levenberg Marquardt algorithm to train the feed-back propagation network. This algorithm is a variation of Newton's method that was designed for minimising functions that are sums of squares of other nonlinear functions. A detailed derivation of Levenberg Marquardt algorithm can be found in Bishop (1995) and Hagan et al. (1995). Mean squared error (MSE) was used as the error function, which is defined by equation (8.5). The relationship between input and output variables can be deemed to be established when the MSE value approaches zero.

The first step of the learning process of the ANN is loading three data sets, namely, training, validation, and testing. Training data sets are presented to the network, and the network is adjusted according to its error. Validation data sets are used to measure network generalisation, and to halt training when generalisation stops improving. While, testing data sets have no effect on training and so provide an independent measure of network performance during and after training. These data sets have been divided to the specific percent for training, validation and testing. The training, testing, and validation data sets consist of a number of input variables (i.e. natural frequencies data is represented in 41 sets and 10 natural frequencies in each set measurement) and a number of output variables (i.e. crack size). Each batch (training, testing and validation) has a particular function in the neural network. The training set is used to adjust the weights and teach the neural network. The second batch of the data (validation set) is used to minimise over fitting. The final batch of the data (testing set) is used to provide a completely independent measure of network accuracy to confirm the actual predictive power (input-output relationship) of the network. Generally, training, validation and testing data are used for learning, tuning the parameters and assessing the performance of the network respectively.

Another component in an ANN model that needs to be specified is the transfer function. Since the transfer function is chosen by the designer to meet certain requirements of the problem, the effects of different transfer functions on the performance of an ANN were proposed. This transfer function may be a linear or a nonlinear function of n, where n is the input as indicated in Figure 8.11. There are different transfer functions, such as hyperbolic tangent sigmoid, logarithmic-sigmoid

and pure linear neuron. A hyperbolic tangent sigmoid function (tansig) and pure linear transfer function were used in this study. The hyperbolic tangent sigmoid function, is also known as sigmoid function.
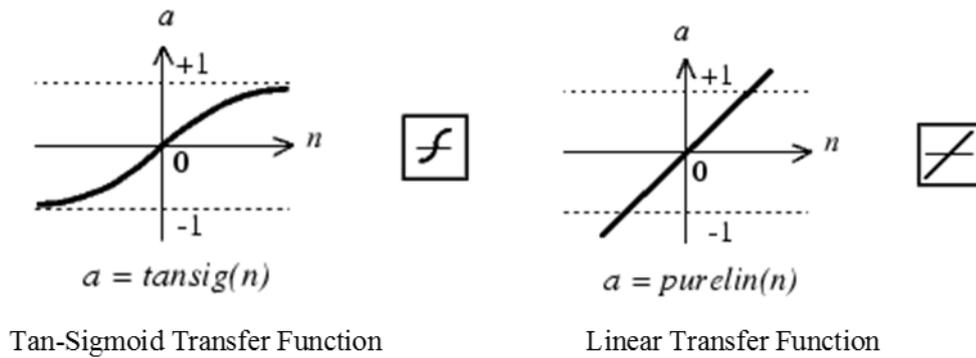
Figure 8.11: Types of transfer function.

These transfer functions take the input and squashes the output into the range of -1 to 1, according to the expression defined in Table 8.2 : where a is the output and n is the input.

Table 8.2: Transfer Functions in hidden and output layer (Hykin, 2009).

Name	Input/Output Relation	Icon	MATLAB Function
Hyperbolic Tangent Sigmoid	$a = \dfrac{e^n - e^{-n}}{e^n + e^{-n}}$		Tansig
Linear	$a = n$		Purelin

In this study, a proper built computer program was developed to simulate ANN model through utilising the subroutine and neural network toolbox embedded within MATLAB. The general properties of selected network during generation are shown in Table 8.3.

Table 8.3: Applied Feed-forward neural networks properties.

Input Layer	Loading natural frequencies
The number of Neurons in Hidden Layer	10
Output Layer	Void size (length and width)
Net Architecture	10-10-2
Network Type	Feed-Forward
Net Algorithm	Back-Propagation
Training Function	Levenberg-Marquardt (trainlm)
Hidden Transfer Function	Tansig
Output Transfer Function	PURELIN
Performance Function	MSE

8.3.3   Proposed ANN Based

Finite element analysis of square slabs of dimensions (1200 x 1200 x 60mm^3) was used to generate many sets of input-output data for damage detection algorithm. The actual input-output data are obtained from the numerical model of the different cases. Some cases of slabs' dimensions and damage size and location were created. The four different sizes of induced void 50 x 50mm^2, 100 x 100 mm^2, 150 x 150 mm^2 and 200 x 200 mm^2 were created. Induced void is created as square openings at various location with the slab. These different void severities correspond to a loss of moment of inertia (the second moment of area) that cause to decrease flexural rigidity of the slab.

A three (input, hidden, and output layer) back propagation neural network was trained with the natural frequencies of slabs having four different void sizes at ten different locations as identified in Table 8.1. Using developed program, the neural networks were then trained by means of feed forward back propagation method.

Since there are no available specific rules to find the best number of neurons in neural network layers, some trials were done to select the required number of neurons in the input layer, which were frequencies in this work. Three proposed technique were used until reaching the suitable number of natural frequencies (neurons) in the input layer of the ANN. In the first proposed technique, first three natural frequencies were employed as the input of the ANN. After training the

network, inaccurate results was obtained because the first three natural frequencies of all cases are considerably close to each other. Therefore, the network was unable to distinguish between the cases of the different severity of damage. As a consequence, the number of natural frequencies in the input layer of the ANN was increase to first five frequencies, which is the second proposed technique.

The results were improved as compared to the first proposed technique's results, but was not good enough as desired. Therefore, the third proposed technique was used. In the third proposed technique, the number of natural frequencies was increased to first ten frequencies. After training the network, the error was decreased as compared to the results of the second proposed technique. This means that increasing the number of neurons in the input layer into ten frequencies makes the identification of void size (length and width) more accurate than those obtained from the first and second proposed techniques. Once the results were improved in the third technique, the number of natural frequencies was fixed with 10. On the other side, it was demonstrated that high numbers of input data might give unstable performance of ANN (Zang and Imregun, 2001a). In conclusion, the first 10 natural frequencies was taken into consideration for all ANN problems considered in this work.

The training of the network was done through Levenberg-Marquardt back propagation. The neural network information moves in one direction, forward, from the input neurons, through the hidden neurons and to the output neurons. This system implies that there are no cycles or loops in the network. The model created in this study was a MLP neural network with three layer network as in Figure 8.12 where the inputs of 10 neurons and hidden layers of 10 neurons and output of 2 categories. The hyperbolic tangent function was employed as the activation function for hidden layer neurons while the linear transfer function was employed for output layer neurons.
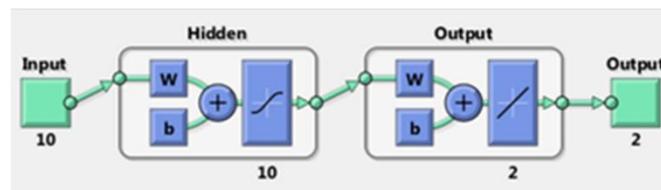
Figure 8.12: The proposed classification neural network for void size detection.

The application randomly divides input vectors and target vectors into three sets, as follows. Eighty percent of the input-output data was used for training the network. Ten percent was used to validate that the network was generalising and to stop training before over-fitting. The last 10% was used as a completely independent test of network generalisation.

It is important to mention that over-fitting is one of the problems of the neural network that occurs during the training process. The network is over-fitted when the error of the training set is driven to an extremely small value (approaching to zero). When unseen data is presented to such trained network, the error is become large. Such problem happens because the network has memorized the training examples, but it has not learned to generalise well to new situations (Hu and Hwang, 2002).

8.3.3.1   Input-output data

As aforementioned that the first ten natural frequencies of four void size cases at ten different locations for each void size were computed. The simulation of the first ten natural frequencies for 41 simulations of the reinforced concrete slab are shown in Figure 8.13. For all considered simulations of void sizes, the natural frequencies undergo a noticeable change, especially for the extra severe voids compared to the baseline case. These 41 sets of data have been used as the input of the network.
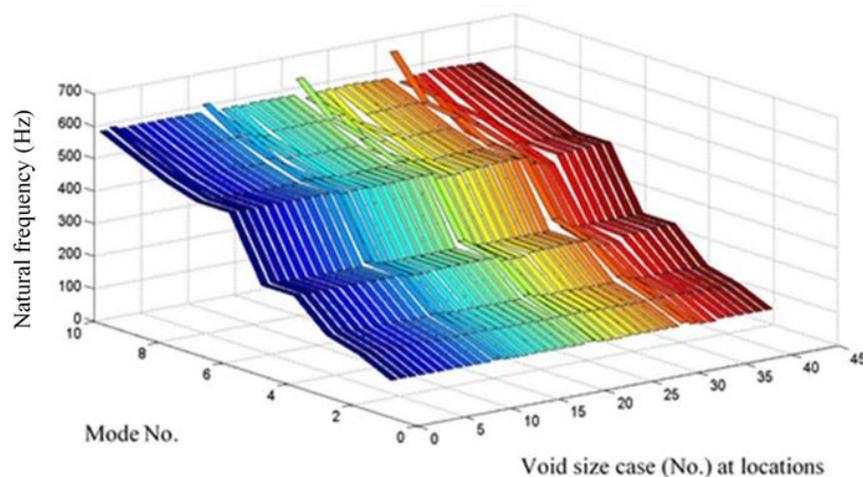
Figure 8.13: First ten modes of the slab for different sizes and locations.

As evident from Figure 8.13 the change in natural frequencies is slightly different for every void location for the same void size. Void size cases of the slabs can be

distinguished from changes of the computed natural frequencies, light void which is blue colour to the extra sever void which is red colour. It is important to mention that the natural frequencies of the slab decreases as the void grows in size.

Figure 8.14 shows the output of the network in terms of length and width of the void for the 41 cases of void size and location (see Table 8.1). It is worthwhile to mention that void size can be classified as light, medium, severe and extra severe voids depending on the size of the void.

Natural frequencies data sets were used as input for training the adopted Feed Forward Artificial Neural Network (FFANN) classifier; the void size (void length and width) represent the output of the network. The complete data sets are divided into three subsets. As mentioned that the first subset of the data sets was randomly selected to be used for training, whereas the remaining 10% were used for validation and the other remaining 10% for testing. Then, the all data was retested and the output is shown in Figure 8.14.
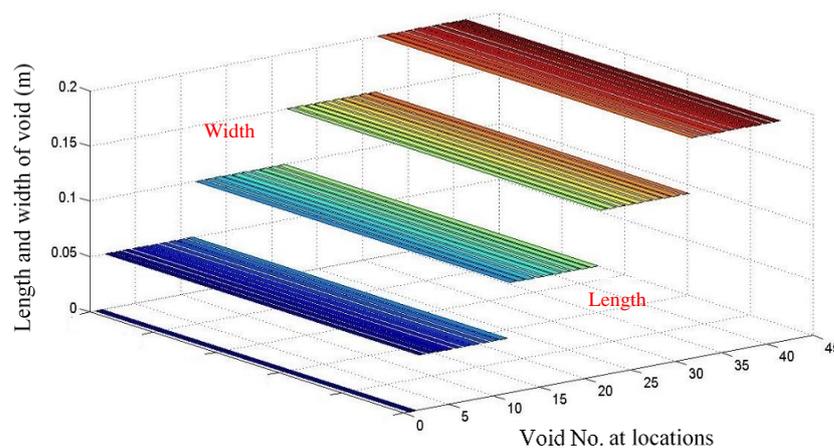
Figure 8.14: ANN output of void length and width for 41 cases of void size and location.

8.3.3.2   Early stopping network

There are some criteria specified by MATLAB that can be used to early stopping training the neural network as listed in Table 8.4. During the training process, the progress is constantly updated in the training window. The training process is

terminated when the mean square error (MSE) for training samples falls below a specified limit, or when there is no error improvement for a limited number of cycles, or when it reaches the maximum number of iterations. Besides, the number of validation checks represents the number of successive iterations that the validation performance fails to decrease, the training then will stop (Beale et al., 2012).

Table 8.4: The criteria of early stopping training.

Parameter	Stop criteria
Min. grad.	Minimum gradient magnitude
goal	Minimum performance value
epochs	Maximum number of training epochs (iterations)
Max. fail	Maximum number of validation increases
time	Maximum training time

In addition to the criteria for early stopping training network, the training process can be also stopped if ones click the stop training button in the training window, as shown in Figure 8.15. This can be done if the performance function fails to decrease significantly over many iterations, or after a long time of training. Then, it is always possible to continue the training the network by reissuing the train command. As a consequence, it will continue to train the network from the completion of the previous run.

In this work, the training network automatically stops when generalisation stops improving, as indicated by an increase in the mean square error (MSE) of the validation samples.
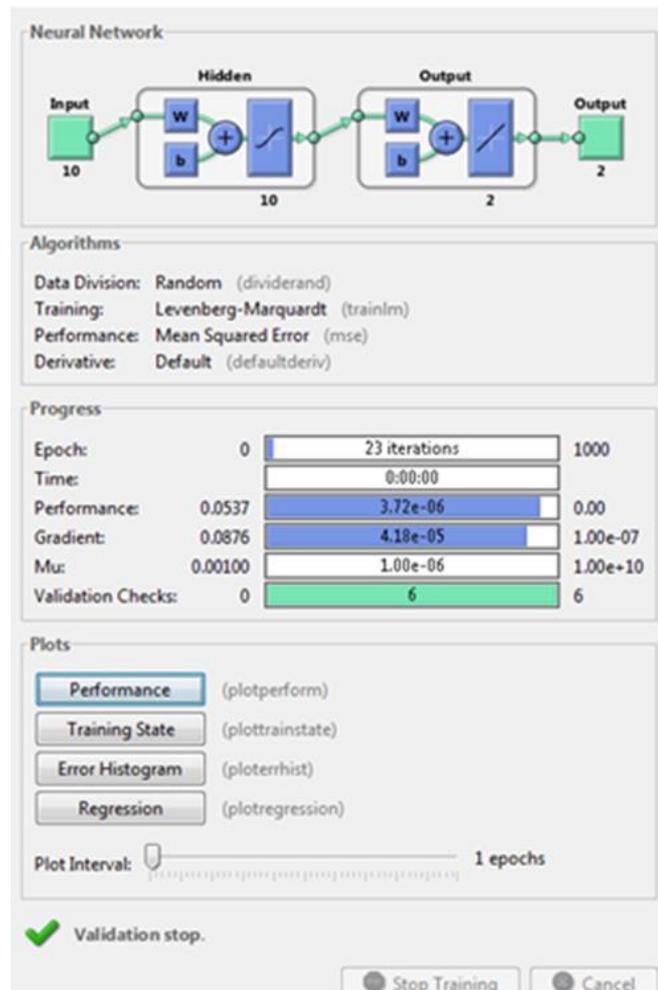
Figure 8.15: MLP network training window.

8.3.3.3   Performance of the network

The Best Validation Performance of feed-forward back propagation (FFBP) is presented in Figure 8.16. The figure shows that the process of the network's performance has improved during the training process. The performance of the network is measured in terms of mean square error (MSE) and it is displayed in log scale. It is apparent that the MSE has declined rapidly along epochs while the neural network is trained. It is clear from the results are reasonable considering in this study. The final mean-square error is lowest at about 17 epochs. The test set error of the network (the training, testing and validation error) get stabilised at epochs 17. The MSE at epoch 17 is 8.4899×10^{-5}.
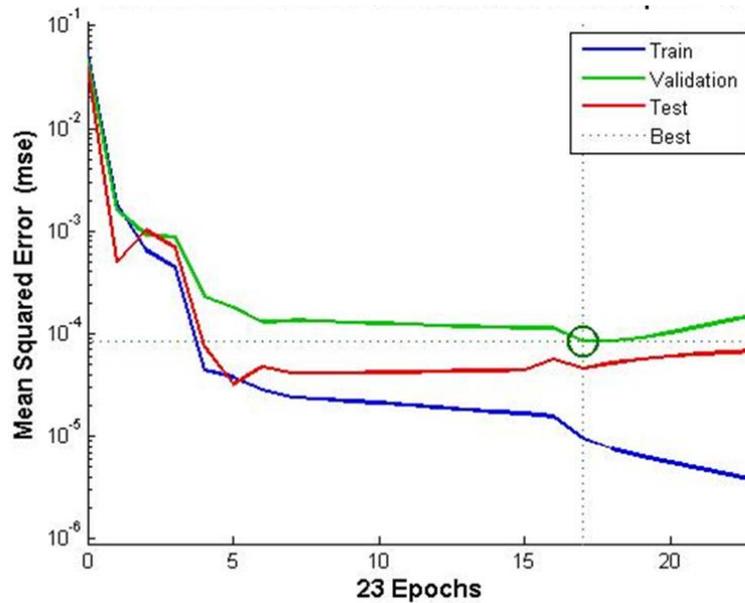
Figure 8.16: Validation Performance (MSE) of FFBP.

In this case, the final MSE which is the test set error of the network is very small at epoch 17 whereby the performance of the network can be identified and judged. Furthermore, the regression set has similar characteristics. The regression analysis capacity of the neural network can be checked after the training phase. Figure 8.17 shows the regression plots for the network outputs with respect to targets for training, validation, and test sets. In the same figure, the validation and test results also show that the overall values is greater than 0.99. In the plot fitness, the training, testing and validation data indicate very good degree of correlation between the target and output. It is noteworthy that the proposed neural networks were able to learn the relationship between natural frequencies with the corresponding void state. Therefore, it was found that the network well learned to improve the overall estimation error.

For an impeccable plot, the data should fall along a 45° line, where the network outputs and targets are equal. In this study, the fit was very good degree of correlation for all data sets, with regression values R in each case of 0.98 or higher. If even more accurate neural network results were required for the intended purpose, re-train the network by clicking re-train in nftool can be performed. Re-train the network will change the initial weights and biases of the network, and, therefore, may produce an enhanced performance network after retraining. Typically, when most errors are close to zero, it has been obtained a better-trained network model.

217
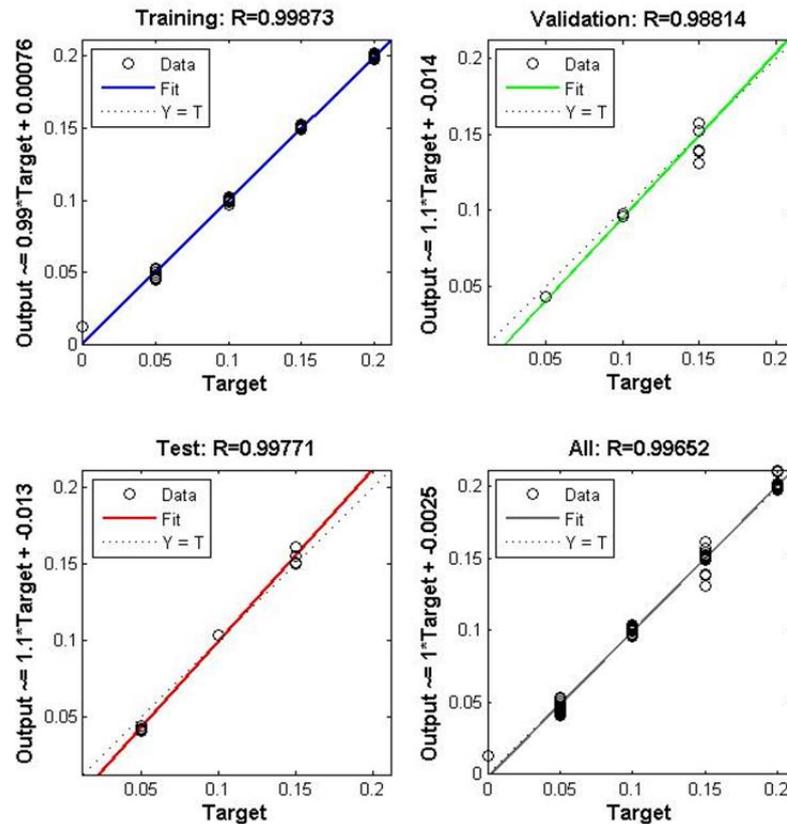
Figure 8.17: The Regression values between the actual and target values (FFBP).

In addition to aforementioned metrics, the typical metrics utilised for neural network performance evaluation is the regression of the tested data. It is used to measure the learning performance of the neural network model. Test data regression method is prediction/confidence intervals defined to measure the reliability of the network output. The neural network is then expected to promptly respond to, adapt to, and accommodate environmental changes.

8.3.3.4   Proposed ANN classifier results

The natural frequencies data sets (each consists of 10 natural frequencies) were used as the input for training ANN models; and the void size represents the output of the network. As can be observed from the Figures (8.18 - 8.20), feed-forward back propagation neural network (FFBPNN) structure performs very good results because the validation performance value MSE is lowest as indicated in Figure 8.16. Furthermore, the regression graph for testing data as presented in Figure 8.17 gives very good relationship between the output and the target of the network. The

regression value R = 0.997, which means that the output network is matching to the target data set. After training FFBPNN, the output of the network was obtained as shown in Figure 8.18.
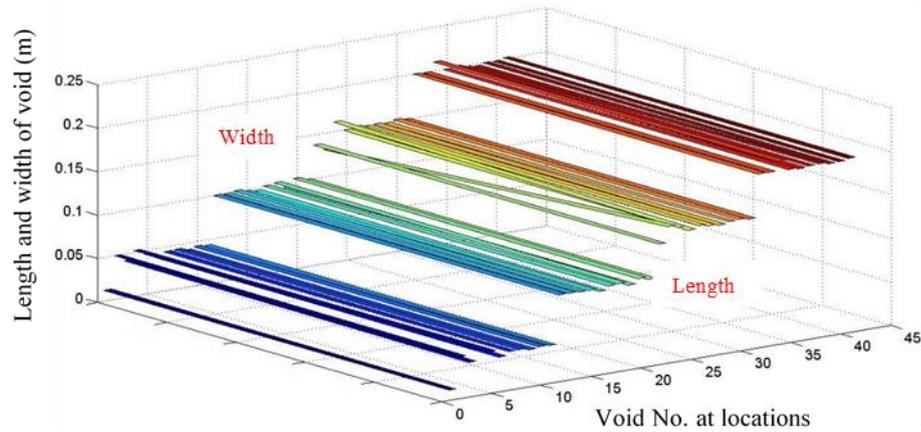
Figure 8.18: The output (void length and width) of the network.

The output layer gives the network response, and the error can be assessed by the variation between the target and the output value of the trained network. The error value between target and output values for the identification results of the void size were determined, and the results are shown in Figures 8.19 and 8.20. It is shown from the figures that the maximum error is less than 0.02m of length and width of the void. The small error value indicates the accuracy of the results. In other words, the classification of the void size in four categories is very accurate and precise.
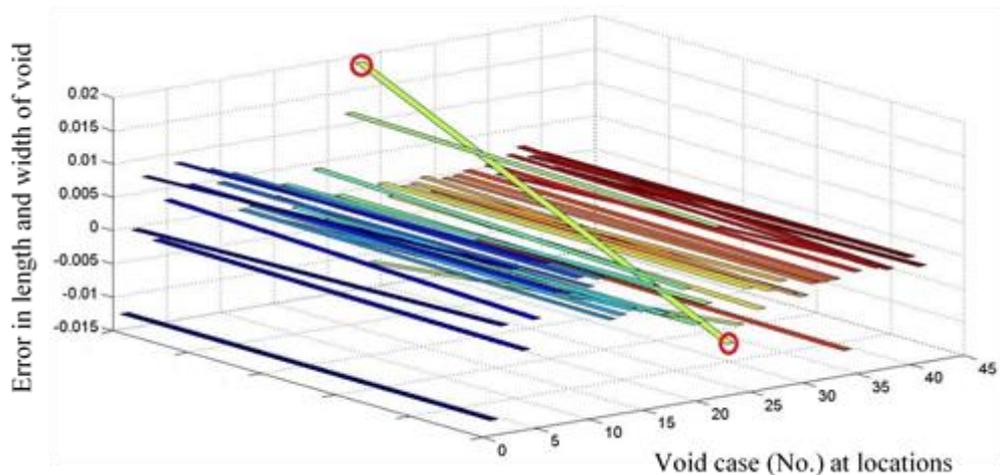
Figure 8.19: The error between target and output of the network.
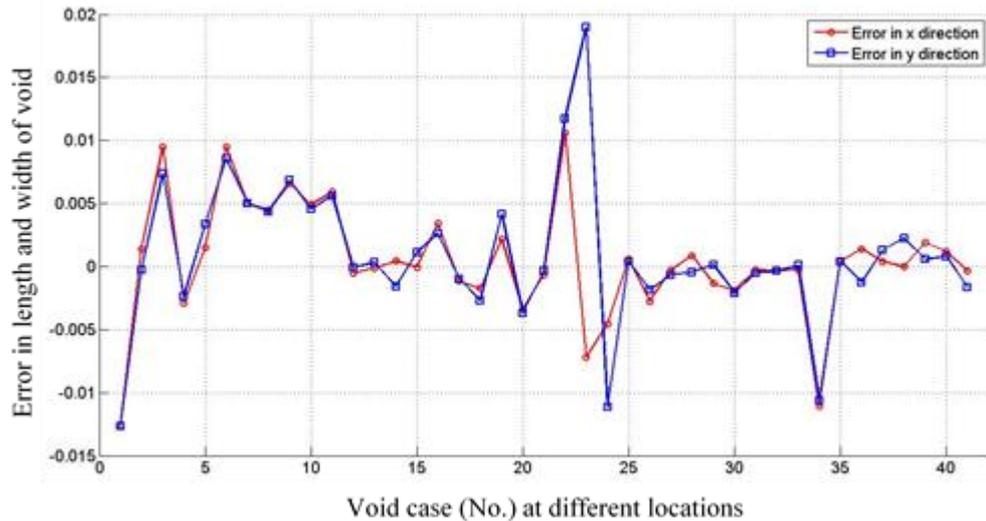
Figure 8.20: The error between target and output size (error in x direction=length and error
in y direction=width) of the void.

As demonstrated in the above figures, it clearly shows that the errors are small value
for all the cases. The corresponding small error to estimate the void length and width
are acceptable to get best identifications of the crack specification. Here the plot
clearly indicates that the classification of the void size in four categories is very
precise. Thus, it can be concluded that one hidden layer of the network with 10
neurons is sufficient to identify the void length and width since the errors are quite
small. Accordingly, the proposed networks can be deemed to accurately predict the
void specification (length and width).

8.4   Void Size Detection Using ANNs

The accuracy of the prediction by using FFBPNN depends on the training process. A
well trained ANN gives good predictions when an untrained, or unseen, data set is
given as input of the network for testing. After considerable number of trainings, the
network was correctly understand the task and it made the good relationship between
input and output of the network. Once the network is well-trained using training data,
it is ready for predicting void size. Thus, the network was saved with no more
training.

Once the code generated, sim function was used to test the data with the trained
network in order to test the performance of the accuracy of the trained network. For

testing data, ten natural frequencies of some different cases were chosen to identify the void size. The testing data was used to test the trained networks with before seen and unseen data as displayed in Figure 8.21. The natural frequencies of the twelve selected cases were fed to ANN as inputs. The outputs parameters of ANN are void's length and width. Nine sets were already given to the network and then tested to identify the size of induced void in the slab. Set of natural frequencies of 2 unseen cases were also given to the network to determine the size of the void. Finally, experimentally induced void as described in previous chapter was also tested to identify the void size. Since the first ten experimental natural frequencies were not be able to be extracted from the experiment, both numerical and experimental natural frequencies were used for testing this case in the network. Therefore, six experimental natural frequencies with four numerical one, which were experimentally disappeared, were given to the network in order to identify the void specifications. Table 8.5 lists the comparison between the actual and predicted void size for different 12 cases using ANN.
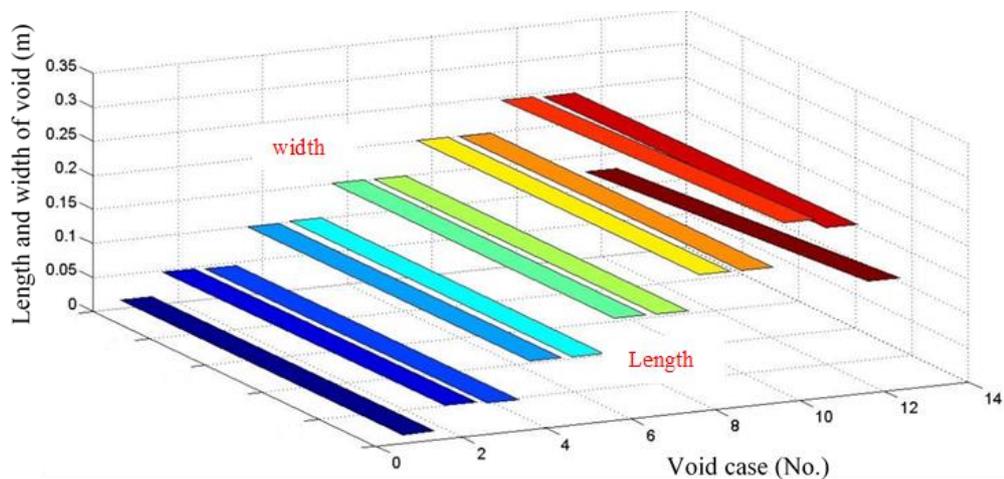
Figure 8.21: ANN prediction size of voids (length and width).

Table 8.5: Comparison of actual and prediction void sizes (length and width).

Cases	Actual size (mm)		ANN prediction size (mm)		Difference	Error %	Avg.
	Length	width	Length	width	Area (mm^2)	area	Error
1	0	0	12.6	12.7	160.0	-	-
2	50	50	48.5	46.7	235.1	9.4	13.0
3	50	50	45.6	45.7	416.1	16.6	
4	100	100	100.1	99.7	20.0	0.2	0.7
5	100	100	99.6	101.6	119.4	1.2	
6	150	150	150.3	150.6	135.2	0.6	0.45
7	150	150	149.1	150.4	75.4	0.3	
8	200	200	200.3	200.4	140.1	0.4	0.4
9	200	200	199.6	199.6	159.8	0.4	
10	250	250	263.4	246.2	2349.1	3.8	3.2
11	250	250	248.8	244.6	1643.5	2.6	
12 *	150	150	163.9	126.8	1717.5	7.6	7.6

* Experimentally induced void

8.5   Result Analysis and Discussion

One focus of this study was to investigate the ability to train ANNs using measurements based on the intact state and a limited number of void size cases. Input-Output data was used to test whether the trained network can accurately estimate the void size (length and width) from measurements that were used and not used to train the ANNs.

The error percentages associated with the actual and predicted area of the void are presented in Table 8.5. These results are to be seen as outcomes of the proposed ANN classifier for void size identification. It can be observed from the table that the interpolated void size do not lie perfectly with the actual void size. By comparing the obtained results, the trained model using only data from the intact case has not accurately captured the relationship between the natural frequencies set and the actual void size. However, it does give a reasonable estimate with maximum difference area is 160 mm^2.

For the 50 x 50 mm^2 void size configurations, the ANN model estimated the void size as opposed to the actual void size for cases 2 and 3, resulting in a 13.0% difference. As for the 4th and 5th cases with the 100 x 100m^2 void size configuration, the void length and width estimation for these two cases using ANN are represented in Table 8.5. The average percentage area difference of these two cases is 0.7%. While as for the 6th and 7th cases with the 150 x 150m^2 void size, the average percentage area difference of these two cases is 0.45%. Similarly for void size 200 x 200m^2 case, the variation between actual and predicted area of such void size is only 0.4%, which is very small value.

It is observed from the results that with the increased void dimensions used to train the ANN model, the generalisation ability of the ANNs has been improved. The error of the predicted void size for big size cases is closer to the actual value than the small void size, suggesting that the networks are able to interpolate the void size between the trained cases. Therefore, ANN can accurately predict the void size, especially for the bigger size. In other words, the test results of the network showed that the precision of the models is reduced when dealing with small size void, particularly, when the void size sides are smaller than 10mm. while, the large size void can be detected more accurately than small size void. This can be attributed to the fact that the natural frequencies alone are not considerably good enough to make good identifications for small size void.

In addition to seen data cases, there are 3 unseen cases were tested to determine the void size. The natural frequencies set of 10th and 11th cases were given to the proposed network in order to predict the void size. Thus, the predicted void size area appears to have 3.2% difference compared to the actual value. It is evident that the difference of the predicted void size for cases which were not used to train the ANN model is closer to the actual void size than the small void size (50 x 50mm^2) even though they were given to the network for training. For example, the average area difference of the two cases of small void size which were given to the network for training is 13.0%, while it is just 3.2% for bigger void size which were not given to the network. For the small void size (50 x 50mm^2), natural frequencies set may not be well recognised by the network after training. This is due to the fact that change in a particular frequencies could be attributed to the different void size at different location of the slab. Furthermore, same size void but at different locations may cause

too small change in natural frequencies, which are too close to be differentiated. Thus, ANN can predict even small void size, but with error about 13% which is acceptable in composite structure.

Experimental case is also unseen data were used to test the ability of the network for identifying the void size. After giving the first ten natural frequencies, which taken from both numerical and experimental, the proposed network predicted the void size with error of 7.6%. This discrepancy may be due to two important factors. Firstly, the tested natural frequencies were taken from both numerical and experimental. Secondly, there was some variation when the numerical and experimental natural frequencies were compared. As noted that the input of the neural network were taken from the numerical data. Hence, it is concluded from the results that the ANNs are a valid tool to make an early detection of damage in a structure.

8.6   Summary

This chapter is devoted to Artificial Neural Network (ANN). The information on artificial neural networks is presented. The first section opens with an introduction of neural network models. Afterwards, an overview of neural network model and classification as well as neural network architectures are discussed.

Furthermore, this chapter presents the background of Artificial Neural Network (ANN) which is used for damage identification techniques. This chapter presents a non-model based method to detect the severity of damage in reinforced concrete slab. Besides, the ability to train ANNs using measurements based on the intact state and a four number of void size cases was investigated. FFBPNN was tested with numerical measured first ten natural frequencies as an input data to test its performance. Input-Output data was used to train the ANN whereby the void size (length and width) which were used and not previously used to train the ANN can be accurately estimated.

The regressions of the test results show that the proposed ANN are capable of predicting the void sizes specifically for light (50 x 50mm^2), medium (100 x 100mm^2), severe (150 x 150mm^2) and extra severe (200 x 200mm^2) with network high accuracy. The large size void can be detected more accurately than small size void, particularly, when the void size sides are greater than 50 x 50mm^2. The

obtained results show that the proposed network can predict the void specifications even for unseen data with high accuracy.

Clearly, as evidenced by the testing results, the FFBPNN is clearly capable of identifying the relationship between the natural frequencies and damage severity for novel cases that were included and not included in the training cases. The technique would be more useful in identifying and tracking defects and damage in reinforced concrete slabs.

9. Conclusions and Recommendations

9.1   Conclusions

From the present work, the following conclusions have been drawn.

1- To the best of the author's knowledge which is based on extensive literature review, the methodology followed in this work for damage detection in reinforced concrete slabs is novel when compared to the breadth and depth of all other previous works carried out in this field. Accordingly, some distinguished and outstanding results have been achieved as presented throughout the thesis and summarised in the points mentioned below.

2- Two reinforced concrete slabs were initially prepared for quality assurance checks. Firstly, impact hammer was used as excitation source in order to excite the slabs. Secondly, accelerometers were employed to acquire the response of the excited slabs. Then, Pico Scope software was employed for acquiring experimental data. Regarding data processing, MATLAB as practical software implementation was used to run a developed code for signal processing. Quality assurance checks, namely, reciprocity, homogeneity, reapitablity and coherences agree with the theoretical description. It is clear from the measured frequency response function checks that there was a good agreement for the excitation and its corresponding response. On this basis, the aforementioned equipment was fixed to be implemented during conducting all the tests.

3- A number of systematic test of Experimental Modal Analysis (EMA) was implemented on four pairs of laboratory-scale Reinforced Concrete (RC) slabs under freely supported condition. The testing programme started with two pairs of RC slabs, namely, groups A and B. Groups A and B slabs were modelled with dimensions 1200 x 1200 x 60mm^3, 600 x 600 x 40mm^3 respectively. Modal parameters were successfully presented that were well-correlated with the theoretical results. Theoretical analysis deals of analytical using the closed term solution and numerical modelling (finite element analysis) using ANSYS software. There was very good agreement between theoretical and experimental results in term of natural frequencies, except few modes where the difference

was between 9.9%-18.8%. However, such difference is acceptable which might be attributed to the fact that the theoretical model assumes concrete slab to be linear, elastic, homogenous and isotropic. Whereas in reality, concrete is heterogeneous and anisotropic material and the specimens are inevitably contain imperfections in forms of crack, defects and steel bars misalignment. Furthermore, such a difference is mainly attributed to the whole process of preparing, making, curing of concrete specimens in laboratory. For instance, no two batches of concrete mix can be guaranteed of having exactly same ingredients, receiving same degree of compaction or having exactly same dimensions during casting. Between group A and B slabs, the former slabs had better results. As a consequence, group A slab used as control one; and group C and D slabs were cast with similar dimensions (length and width) of group A.

4- Using freely supported condition, the specimens will have rigid body frequencies. This phenomenon occurred in numerical analysis when ANSYS software was used. Rigid body frequencies are required to be taken into account if they fall into range 10-20% of the lowest bending mode frequency of the specimens. It is important to mention that rigid body frequencies in numerical analysis were beyond this range and therefore they were neglected. However, such phenomenon did not appear in experimental frequency response function.

5- Another two pairs of group C and D slabs of dimensions 1200 x 1200 x 40mm^3 and 1200 x 1200 x 60mm^3 respectively were constructed. Group C slabs was used in order to study the effect of degrees of cracks on modal parameters. Whereas, group D slabs was utilised to find out the effect of concealed void on modal parameters. It is concluded that four modes shapes from first ten were disappeared in the experimental modal analysis. In experimental work, it is always possible that some modes are not excited if the force is applied close to the nodal point. For symmetric structures, some modes are missing from the model and, therefore, the dynamic properties of the structure for those modes cannot be predicted. The mode shapes corresponding to natural frequencies 3, 5, 7 and 9 were missed in experimental work. This phenomenon is quite normal in the experimental work because it is difficult to identify the natural frequencies of all modes from experimental measurements. This is due to the fact that third and

ninth modes may have nodes located at the nodal point. Whereas fifth and seventh mode shapes were missed because of the symmetry of the reinforced concrete slabs which had square dimensions.

6- Group C slabs were cracked by incrementally applying a partial concentrated load at slabs centre. Three loading regimes were employed to produce damage under loading, and then the slabs were repaired using CFRP. After each incremental loading, the slabs were tested to determine the natural frequency, mode shape and damping ratios. There is clear evidence that the amount of reduction in the natural frequencies appears to increase as the damage increases. It is observed that the percentage of drop in frequency for all modes non-linearly changes as the applied concentrated load is doubled (5kN-10kN). For example, at 5kN load, the percentage of reduction in natural frequencies of the first, second and fourth modes is 3.3%, 8.4% and 9.9% respectively, while it is 23.2%, 22.1%, 33.2% for the same modes under load 10kN. The overall trend of frequency decreases after occurring damage. However, it is not guaranteed all modes have same sensitivity to the applied load that inflicts severe cracks. Overall, the variation in natural frequencies can be used as one useful indicator to identify the presence of damage in reinforced concrete slabs precisely.

7- The relative difference in term of natural frequencies between all modes of intact (group A slabs) and artificially voided (group D slabs) were determined. The natural frequencies of the intact condition of each particular mode were moderately higher than the frequencies of artificial voided sample. The decreases were 4.6%, 5.5%, 6.6 and 5.7% for the first, fourth, eighth and tenth mode, respectively. However, the natural frequency of the second mode for both conditions was considerably close, with the deviation of 1.3%. Conversely, the maximum decrease happened for the sixth mode that was 8.2%. In this case study, the second mode can be accounted to the fact that the reduction of natural frequency for this mode was less likely influenced by artificially created void. Apparently, the effect of the drop in mass for the defective slab on the natural frequencies was compensated by an almost similar reduction in stiffness. These results indicate that when a structure is inflicted with global damage such as

voids, deviations in natural frequencies can be considered as the modest parameters for structural condition assessment.

8- The measurements of damping ratio of group A slabs is less than damping ratio of half-size slab in group B for all identified three modes. The damping for the all different modes of the slabs did not consistently increase as the dimensions decreased. The value of damping ratio of the first mode is lower than of the second mode while it is higher than the fourth mode. This means that the sensitivity of second mode is greater than first mode, whereas the lowest sensitivity can be seen in the fourth mode.

9- The damping ratio, of group C slabs, under three load steps (5, 10 and 12kN) and repaired condition were obtained. The results indicate that the modal damping is influenced by the cracking introduced by overloading. However, they were unstable as a damage indicator, in the some modes. It has been noted that tracing the damping ratios through the loading history is difficult due to fluctuating values of damping ratio produced in some mode shapes. For example, the damping ratios initially decreased in two modes under 5kN load step. Then, damping ratios were stable for all identified modes for 10kN load step because damping was increased for all modes with increasing damage. After that it is decreased in the first mode for 12kN load step compared to 10kN. However, the damping ratios conversely changed after the repairing the slabs with CFRP.

10- The measurements of modal tests showed that damping ratios of the intact slab as in group A is lower than damping ratios of artificially voided slab as in group D for all identified six modes. The loss of mass and stiffness manifested as high damping ratio. This is because the damping ratio of the system is inversely related to the stiffness and mass of the system. It would seem clear that the highest difference in damping ratio between group A and D slabs was pronounced in the first mode.

11- The changes in mode shapes tended to increase with increasing damage level. This implies that the more cracks and flaws a slab was inflicted with, the more a mode shape magnitude responded to escalating damage. Even small damage

induced poised changes to the mode shapes, but it may not be obvious visually. From visual inspection of the mode shapes of both slabs, it did not appear that the cracking introduced has a significant influence on the shapes of the modes. In the early loading stages (5kN), hair cracks were just launched under first load level and that is why the visual inspection was not capable to reveal any cracks in this stage. The cracks were started to distribute in the penultimate load level (10kN) and they were more obvious in the last load step (12kN). The changes of mode shape were not restricted at the damaged area of the slab, but were distributed over the entire area. Therefore, two robust statistical techniques MAC and COMAC were used to reliability classify the damage.

12- One of the major contribution to the knowledge of this research is the established methods for damage identification, which are vital steps in higher level of damage detection in structures. The proposed MAC and COMAC techniques as advanced statistical classification model. It is concluded that MAC values was successfully used to find the presence and degree of damage in group C slabs. Whereas, COMAC values was successfully employed to identify which degrees of freedom (among 25 DOFs) on slab surface contribute negatively to a low value of MAC. It is also concluded that as the load level increased from 5kN to 10kN and then to 12kN, the fewer number of modes that can successfully be correlated with those from the previous load step is found. In other words, when the load increase, the number of mode shapes has MAC value (moves away from 0.9) was increase. Similarly, when the load increased from 5kN to 10kN and then to 12kN, the number of coordinates has COMAC value (moves away from 0.9) was increase. However, the repair work with CFRP increased the MAC values of the mode shapes and COMAC values of coordinates with respect to that values under load 12kN. The effect of repair work of group C slab 1 on the MAC values is well obvious in all mode shapes compared to slab 2, except the sixth mode shape which was slightly increased. Accordingly, higher percentage differences in MAC values of the repair work of slab 1 is owing to the fact that slab 1 exhibited more damaged than slab 2 and therefore CFRP is more effective for enhancing intensive damaged slab, as for slab 1.

13- In addition to utilising MAC and COMAC for partially concentrated loads as in group C slabs, they were used to successfully identify the location of damage in group D slabs. From the vibration data (mode shapes), damage location can be identified via MAC and COMAC techniques when both intact (group A) and artificially induced void (group D) slabs were compared. It is demonstrated in this study that MAC indicated a clear change in the mode shape, while the COMAC provided the change in specific location whereby the location of damage could be identified. The drop in COMAC corresponds to the location of the severity of inflicted damage. On this basis, it was indicated that the artificial void was located at response points 7. Therefore, COMAC can be used as one good indicator to identify at which DOFs the imperfection was occurred in reinforced concrete structure.

14- Beside the aforementioned contributions in this research, Feed-Forward Back Propagation Neural Network (FFBPNN) was adopted to classify void sizes in reinforced concrete slabs. The FFBPNN was initially trained with first ten natural frequencies of 41 cases employed as an input data. Then, it was tested with first ten natural frequencies of seen and unseen data to test the network performance. The regressions of the test results show that the proposed ANN were capable of predicting the void sizes with considerably high accuracy. In addition to the regression to test the performance and the accuracy of the trained network, the comparison between the results for the void size obtained from ANN with those actual one were obtained. The results demonstrated that the neural network is capable of learning about the behaviour of different void sizes from patterns in the natural frequencies of the structure. Since, the simulation results showed that the proposed FFBPNN can precisely detect the void sizes, it could form an efficient tool to detect the void size in slab specimen. It worthy to note that the increased number of neurones of the input layer of void cases used to train the ANN model, the generalisation ability of the ANNs was developed.

15- The results of the ANN showed that the precision of the models was reduced when dealing with small size void. The large size void can be detected more accurately than small size void, particularly, when the void size sides were greater than $50 \times 50 \text{mm}^2$. This could be due to the fact that the natural frequencies

of small void of different location interfere together. Furthermore, the natural frequencies set of three new untrained void specifications were used as FFBPNN inputs to test the performance of the neural networks. The obtained results show that the proposed network can predict the void specifications with high accuracy even for unseen data.

9.2   Recommendations for Future Work

The recommendations for further work are summarised in the following points to have comprehensive coverage of damage detection in reinforced concrete structures.

1- The technique in this research is found decisive of identifying the structural changes under different conditions. Eight lab-scale RC slabs were modelled with some important practical different parameters. In order to increase confidence and other findings in the drawn conclusions, the programme and expertise of this field of research can be utilised and applied the impact hammer technique to full-scale structures under different boundary conditions to determine the feasibility of implementing such method. The results from full-scale structures, which represent real-life case studies, can be compared to the lab-scale structures in term of accuracy of the obtained outcomes.

2- The damage of the slabs in this study was presented as different flexural cracking levels and concentrated purpose-made voids that represent common defects in reinforced concrete structural members. In addition to these, several practical defects in RC structures, such as corrosion of rebar; freeze-thaw action as well as boundary support changes are required to be studied in order to obtain further investigation. Additionally, using uniformly distributed load such as water or sand to introduced different flexural cracking levels of the lab-scale specimens instead of partially concentrated load. Moreover, the programme can also be extended to learn the influence of different strengthening, retrofitting and bracing works on modal parameters using impact hammer technique.

3- In this study, one honeycomb damage (void) was created by replacing a concrete area with a polystyrene hexahedron block of size 150 mm (square side) × 30 mm (height). The configuration of damage induced in the physical system was

created during the casting process and it was located at a specific distance from the corner of the slab. However, the robustness of the classifier can further be tested on more recurrent defects and in large dimensions. Different numbers of damages with different size are required to be studied in order to identify the effect of gradually increasing the number and the size of the void on modal parameters (natural frequencies, damping ratios and mode shapes).

4- The number and spacing of sensors are critical to the dynamic behaviour of a structure in term of damage detection results. Effect of number and spacing of sensors can be carried out to determine the optimal balance between test time and grid size. It will be important to study the effect of grid mesh on sensitivity of modal parameters especially mode shapes for damage detection.

5- The current work can be further extended to cover other slab geometries such as rectangular slabs having different length to width (aspect) ratios, or slabs with different degree of skewness which is commonly found in bridge decks. Damage detection in prestressed concrete elements is another area need to be explored.

6- ANN performance has a great influence on the accuracy of damage detection results. Therefore, the ANNs performance and predictions to identify the damage location for both single and multiple damage status are recommended. This particular characteristic makes the proposed damage detection system suitable for real applications where multiple damages scenarios are quite common. Furthermore, additional number of measurement points in the input data is required to precisely introduce damage behaviour in the structure in order to improve the interpolation capabilities of the ANN during the training process.

7- It is recommended to use both natural frequencies and amplitudes together as input for training the artificial neural network. Employing two different input together may improve the interpolation capabilities of the ANN for identifying damage. Therefore, utilising the qualified ANN, different sizes and locations of the voids can be successfully identified.

References

Ab Rahman, A. (2009). Theoretical model for damage and vibration response in concrete bridges, final research report. Faculty of civil engineering university teknologi malaysia.

Abbas , J., K. (2013). Investigation into the effects of fixturing systems on the design of condition monitoring for machining operations. A thesis submitted for the degree of doctor of philosophy in engineering, Nottingham Trent University, Uk.

ACI 318-11. (2011). Building code requirements for structural concrete, ACI manual of concrete practice part 3: use of concrete in buildings – design, specifications, and related topics, 443 pp. cited in Neville.

Adams, R., D., Cawley, P., Pye, C., J. and Stone, B., J. (1978). A vibration technique for non-destructively assessing the integrity of structures. Journal of mechanical engineering science, 20 (2), PP. 93–100.

Adeli, H. (2001). Neural networks in civil engineering: 1989-2000. Computer-Aided Civil and Infrastructure Engineering, 16(2), 126-42.

Adeli, H., and Yeh, C. (1989). Perceptron learning in engineering design. Microcomputers in civil engineering, 4 (4), PP. 247-256.

Agilent Technologies. (2000). The fundamentals of modal testing. Application note 243-3, USA.

AL-Ghalib , A. , A. (2013). Damage and repair identification in reinforced concrete beams modelled with various damage scenarios using vibration data. PhD thesis. Nottingham Trent University.

Allemang, R., J. (2003). The modal assurance criterion – twenty years of use and abuse. Sound and vibration, 37 (8), PP. 14–21.

Allemang, R.J. and Brown, D.L. (1987). Experimental Modal Analysis and Dynamic Component Synthesis. Volume 3. USAF technical report, vol 3, Pp. 130.

Allemang, R., J. and Brown, D., L. (1983). 'Correlation coefficient for modal vector analysis', proceedings of 1st international modal analysis conference, society for experimental mechanics, inc., pp. 690-695.

Allemang, R., J., Brown, D., L. (1982). A correlation coefficientfor modal vector analysis, proceedings, international modal analysis conference, pp.110-116,

Alsayed, S., H., Al-Salloum, Y., A. and Almusallam, T., H. (2000). Fibre-reinforced polymer repair materials-some facts. Proceedings of the institution of civil engineers, civil engineering, 138 (3), PP. 131-4.

ANSYS. (2013A). ANSYS Mechanical APDL Feature Archive. [Accessed 15/11/2014]; Available from: http://148.204.81.206/Ansys/150/ANSYS%20Mechanical%20APDL%20Feature%20Archive.pdf.

ANSYS. (2013B). ANSYS Mechanical APDL Element Reference. [Accessed 15/11/2014]; Available from: http://148.204.81.206/Ansys/150/ANSYS%20Mechanical%20APDL%20Element%20Reference.pdf

Arbib, M., A. (2003). The handbook of brain theory and neural networks. 2nd edition. Bradford book.

Ashory, M.R. (1999). High quality modal testing methods. A thesis submitted imperial college of science, technology and medicine for the degree of Doctor of Philosophy.

Avitabile, P. (2012). Modal space in our own little world. Society for experimental mechanics. University of Massachusetts Lowell.

Bakhary, N. (2008). Structural condition monitoring and damage identification with artificial neural network. PhD thesis, the university of Western Australia.

Bandara, R., R. (2013). Damage identification and condition assessment of building structures using frequency response functions and neural networks. A thesis submitted for the degree of doctor of philosophy, Queensland university of technology, school of civil engineering and built environment faculty of science and engineering, Australia.

Berczynski, S. and Wroblewski, T. (2010). Experimental verification of natural vibration models of steel-concrete composite beams, journal of vibration and control, vol. 16, pp. 2057-2081.

Bisby, L.A. (2006) ISIS Canada Educational Module No. 5: An Introduction to Structural Health Monitoring, ISIS Canada.

Bishop, C., M. (1995). neural networks for pattern recognition. Oxford university press, Oxford, UK.

Bishop, C., M. (2006). Pattern recognition and machine learning. Springer science business media, spring street, New York, USA.

Bledzki, A., K., Kessler, A., Rikards, R., B. and Chate, A. (1999). Determination of elastic constants of glass/epoxy unidirectional laminates by the vibration testing of plates. Composites science and technology, 59 , PP. 2015-2024.

Blevins, R., D.(2001). *Formulas for natural frequency and mode shape*, krieger pub.

British Standards, (1997). Structural use of concrete: code of practice for design and construction, BS 8110, part 1, BSI, London.

British Standards Institution (2004). Eurocode 2: Design of Concrete Structures: Part 1-1: General Rules and Rules for Buildings. British Standards Institution.

Brüel & Kjær. (2012) Product data - Heavy Duty Impact Hammer - Type 8208. [Accessed 21/10/2015]; Available from: http://www.bkhome.com/doc/bp2079.pdf

Büyüköztürk, O., and Yu, T. Y. (2003). Structural health monitoring and seismic impact assessment.

Caglar N., Elmas M., Yaman Z., D., Saribiyik M. (2008). Neural networks in 3-dimensional dynamic analysis of reinforced concrete buildings. Construction and building materials, 22, PP. 788–800.

Carrera, E., Giunta, G., and Petrolo, M. (2011). *Beam structures: classical and advanced theories*. John Wiley and Sons.

Cawley, P. and Adams, R., D. (1979). 'The location of defects in structures from measurements of natural frequencies', journal of strain analysis, vol. 14, no. 2, pp. 49-57.

Chen, H., Kurt, M., Lee, Y. S., McFarland, D. M., Bergman, L. A., & Vakakis, A. F. (2014). Experimental system identification of the dynamics of a vibro-impact beam with a view towards structural health monitoring and damage detection. Mechanical Systems and Signal Processing, 46(1), 91-113.

Chen, H., Spyrakos, C., Venkatesh, G. (1995). Evaluating structural deterioration by dynamic response, ASCE, journal of structural engineering, vol.121, no.8.

Choubey, A., Sehgal, D.K., Tandon, N. (2006). Finite Element Analysis of Vessels toStudy Changes in Natural Frequencies Due to Cracks", International Journal of Pressure Vessels and Piping 83(3): 181-187.

Cornwell, P., Doebling, S., W., and Farrar., R. (1999). Application of the strainenergy damage detection method to plate-likestructures, journal of sound and vibration 224 , PP.2359–374.

Curadelli, R. O., Riera J. D., Ambrosini D., and Amani M., G. (2008). Damagedetection by means of structural damping identification. Engineering structures 30 (12): 3497.

Dackermann, U., Li, J., and Samal, B. (2011). Damage identification on numerical two story frame structure using ambient vibration response and artificial neural network in references. Asia pacific vibration conference. Faculty of engineering and information technology conference. Astrulia.

Dackermann, U. (2010). Vibration-based damage identification methods for civil engineering structures using artificial neural networks. PhD thesis. Faculty of Engineering and Information Technology University of Technology Sydney.

Dawari, V. B., & Vesmawala, G. R. (2013). Modal Curvature and Modal Flexibility Methods for Honeycomb Damage Identification in Reinforced Concrete Beams. Procedia Engineering, 51, 119-124.

Deobald, L., R. and Gibson, R., F. (1988). Determination of elastic constants of orthotropic plates by modal analysis/rayleigh-ritz technique, journal of sound and vibration, vol. 124, pp. 269- 283.

Dhakal, D. R., Neupane, K., Thapa, C., and Ramanjaneyulu, G. V. (2013). Different techniques of structural health monitoring. research and development (IJCSEIERD), 3(2), 55-66.

Dimarogonas, A., D. (1996). Vibration of cracked structures: a state of the art review. Engineering fracture mechanics 55 (5), PP. 831-857.

Doebling, S., W., Farrar, C., E., and Prime, M., B. (1998). A summary review of vibration-based damage identification methods. The shock and vibration digest, 30 (2), PP. 91-105.

Dong, Y., Song, R., & Liu, H. (2010). Bridges Structural Health Monitoring and Deterioration Detection-Synthesis of Knowledge and Technology. University of Alaska Fairbanks.

Dora Foti (2013). Dynamic identification techniques to numerically detect the structural damage. The open construction and building technology journal, 7, PP. 43-50.

DØSSING O (1988). *Structural Testing, Part II: Modal Analysis and Simulation*. Brüeland Kjær, Denmark.

Emmons, R. H. (1993). Concrete repair and maintenance illustrated. problem analysis. repair strategy. techniques.

EN 1992-1-1:2004 Eurocode 2: Design of concrete structures, Part 1-1: General rules and rules for buildings.

Ewins, D., J. (2000). *Modal testing: theory, practice and application,* second edition, research studies press ltd., Baldock, Hertfordshire, England.

Fang, X., Luo, H., and Tang, J. (2005). Structural damage detection using neural network with learning rate improvement. Computers and structures, 83 (25-26), PP. 2150-2161.

Farrar, C. R and Cone, K. M. (1995). vibration testing of the I-40 bridge before and after the introduction of damage. Proc. 13th int. modal analysis conference (IMAC-XIII).

Farrar, C. R., and Doebling, S. W. (1999). Damage detection and evaluation II. In Modal analysis and testing (pp. 345-378). Springer Netherlands.

Farrar, C., Doebling, S., and Nix, D. (2001). Vibration-based structural damage identification. Philosophy transactions royal society, vol. 359, pp. 131-149.

Farrar, C., R. and Doebling, S., W. (1997). An overview of modal-based damage identification methods. Los Alamos national laboratory, Los Alamos, New Mexico 87545.

Farrar, C., R. and James III, G., H. (1997). "System identification from ambient vibration measurements on a bridge", journal of sound and vibration, 205 (1), PP. 1-18.

Fausett, L. (1994). Fundamentals of neural networks: architectures, algorithms, and applications. Englewood cliffs, nj: prentice-hall;

Friswell, M. I. (2007). Damage Identification using Inverse Methods. Philosophy.Transactions of Royal Society, Vol.365, pp. 393-410.

Gadelrab, R., M. (1996). The effect of delamination on the natural frequencies of a laminated composite beam. J sound vib, 197 (3), PP. 283–292.

Gao, Y. and Spencer Jr, B.F. (2008). Structural health monitoring strategies for smart sensor networks. Newmark Structural Engineering Laboratory. University of Illinois at Urbana-Champaign.

Garesci, F., Catalano, L. and Petrone, F. 2006, 'Experimental Results of a Damage Detection Methodology using Variations in Modal Parameters', Experimental Mechanics, Vol. 46, pp 441-451.

Gassman, S., and Tawhed, W. (2004). Non-destructive Assessment of Damage in Concrete Bridge Decks. Journal of Performance of Constructed Facilities, ASCE, Vol.18, No.4, pp. 220-231.

Golinval, J. C. (2009) Product data ‐ Model Updating of Linear Mechanical Systems. [Accessed 21/12/2015]; Available from: http://www.ltasvis.ulg.ac.be/cmsms/uploads/File/Mvibr_part%202_2009.pdf

Gomaa, F. R., Nasser, A. A., and Ahmed, S. O. (2014). Sensitivity of Modal Parameters to Detect Damage through Theoretical and Experimental Correlation.

Gunes, B., and Gunes, O. (2012). Structural health monitoring and damage assessment Part I: A critical review of approaches and methods. Int. J. Phys. Sci.(IJPS). İn press.

Hagan, M. T., and Menhaj, M. (1994). Training feedforward networks with the Maquardt algorithm. IEEE Transaction on Neural Networks, 5(6), 989-993.

Hagan, M., T., Demuth, H., B., and Beale, M., H. (1995). *Neural Network Design, 1st edn*, PWS publications, Boston.

Havaldar, S., & Chate, U. N. (2015). Estimation of Modal Damping Ratio from Specific Shear Modulus for Monolithic Materials and Hybrid Cored Multilayer Composites. Procedia Materials Science, 10, 124-138.

Haykin, Simon O. (2009). *Neural Networks and Learning Machines.* (3rd Edition). Pearson, New York.

Haykin. S. (1999) Neural Networks: A comprehensive foundation, Second edition, Pearson Prentice Hall publications.

He, J. and Fu, Z., F. (2001). Modal analysis. Butterworth-heinemann, Oxford, England.

Hearn, G. and Testa, R., B. (1991). Modal analysis for damage detection in structures. Journal of structural engineering, vol. 117, no. 10, pp. 3042–3063.

Hebb, D., O. (1949). The organization of behaviour: a neuropsychological theory, wiley,New York.

Hecht-Nielsen, R. (1987). Proceedings of first international joint conference, neural networks, San Diego, CA.

Hopfield, J. J. (1982). Neural network and physical system with emergent collective computational capabilities. In proceeding of the national academy of science (USA) 79, pp 2554-2558.

Hu, Y., Hwang, J.N. (2002); "Handbook of Neural Network Signal Processing", Washington, USA, CRC Press.

Huang, L., Agrawal, H., and Borowski, V. (1997). Durability analysis of a vehicle body structure using modal transient methods. In Proceedings of SPIE, the International Society for Optical Engineering (Vol. 3089, pp. 407-414). Society of Photo-Optical Instrumentation Engineers.

Huang, Q., Gardoniand, P., Hurlebaus, S. (2012). A probabilistic damage detection approach using vibration-based nondestructive testing. Structural safety 38, PP. 11-21.

Hudson, M., Hagan, M., and Demuth, H. (2012). Neural Network Toolbox User's Guide. Mathworks Inc., Natick, Massachusetts.

Hwang, H., Kim, C. (2004). Damage detection in structures using a few frequency response measurements, journal of sound and vibration, vol. 270.

Iliopoulos, A., Shirzadeh, R., Weijtjens, W., Guillaume, P., Van Hemelrijck, D. and Devriendt, C. (2015). A modal decomposition and expansion approach for prediction of dynamic responses on a monopile offshore wind turbine using a limited number of vibration sensors. Mechanical Systems and Signal Processing.

Iraqi planning minister. (2009). [Online] Available at:http://www.mop.gov.iq/mop/index.jsp?sid=1&id=579&pid=115 [Accessed on 12 October 2015].

Ismail ,F., lbrahim, A. and Martin H., R. (1990). Identification of fracture cracks from vibration testing, journal of sound and vibration, vol.l40 (2), PP. 305-317.

Jabbari, E. and Talebi, O. (2011). Using artificial neural networks for estimation of scour at the head of verticalwall breakwater. Journal of coastal research, si 64 (proceedings of the 11th international coastal symposium), Szczecin, Poland, issn 0749-0208, pp 521-526.

Jassim, Z., A., Ali, N., N., B., Mustaphac, F., and Abdul Jalil, N., A. (2013). A review on the vibration analysis for a damage occurrence of a cantilever beam. Engineering failure analysis, 31 , 442–461.

Jha, G. K. (2007). Artificial Neural Networks. Indian Agricultural Research Institute, PUSA, New Delhi 110012.

Kaewunruen, S., Remennikov, A. (2005). Application of experimental modal testing for estimated dynamic properties of structural components, ASEC.

Khalil, A., Greimann, L., Wipf, T. J., and Wood, D. (1998). Modal testing for non-destructive–evaluation of bridges issues. In Transportation conference proceeding (pp. 109-12).

Khalil, H., and Gilles, P. (2002). Influence of porosity on fracture characteristics in mortar structures, 15th asce engineering mechanics, Columbia University.

Kijewski-Correa, T., Kilpatrick, J., Kareem, A., Kwon, D. K., Bashor, R., Kochly, M., and Baker, W. F. (2006). Validating wind-induced response of tall buildings: Synopsis of the Chicago full-scale monitoring program. Journal of Structural Engineering, 132(10), 1509-1523.

Kim, H.,Y. and Hwang, W. (2002). Effect of debonding on natural frequencies and frequency response of honeycomb sandwich beams. Composite structures, 55, 51-62.

Kiremidjian, A., S., Straser, E., G., Meng, T., Law, K. and Sohn, H. (1997). Structural damage monitoring for civil structures. Proc. Of the first international workshop on structural health monitoring. Current status and perspectives, stanford, CA, USA, PP. 371-382.

Ko, J., M., Chak, K., K., Wang, J., Y., Ni, Y., Q. and Chan, T., H., T. (2003). Formulation of an uncertainty model relating modal parameters and environmental factors by using long-term monitoring data", smart systems and nondestructive evaluation for civil infrastructures, S.-C. Liu (ed.), spie vol. 505.

Kondru, L., and Rao, M., R., N. (2013). Damage detection in cantilever beams using artificial neural networks. International journal of mechanical and production engineering research and development (ijmperd). 3 (1), 259-268.

Kostic, B., and Gül, M. (2015). Damage Detection under Varying Temperature Influence using Artificial Neural Networks and Time Series Analysis Methods. proceeding of third conference on smart monitoring assessment and rehabilitation of civil structures, Antalya, Turkey.

Krenker, A., Bešter, J., and Kos, J. (2011). Introduction to the artificial neural networks. INTECH Open Access Publisher.

Kudva, J., Munir, N., and Tan, P., (1991). Damage detection in smart structures using neural networks and finite element analysis. proceedings of ADPA/AIAA/ASME/SPIE conference on active materials and adaptive structures, PP. 559-562.

Kumar, A. (2014) . Artificial neural networks. Indian agricultural statistics research institute, New Delhi-11012.

Kwon,D. K., and Kijewski-Correa, T., Kareem, A., and Abdelrazaq, A (2011). Smart Sync Framework in Structural Health Monitoring. Proceedings of the 35th International Symposium on Bridge and Structural Engineering, jointly organised by IABSE-IASS, London, UK.

Labonnote, N. (2012). Damping in timber structures. PhD thesis. Norwegian university of science and technology faculty of engineering science and technology department of structural engineering.

Lee, L. S., Karbhari, V. M. and Sikorsky, C. (2004). Investigation of integrity and effectiveness of RC bridge deck rehabilitation with CFRP composites. Report no. SSRP-2004/08, department of structural engineering, university of California, San Diego, 2004.

Lee, P., K., K., Ho, D., and Chung, H., W. (1987). Static and dynamic tests of concrete bridge, journal of structural engineering 113 (1), PP. 61–73.

Lee, U. (2009). Spectral element method in structural dynamics. John Wiley and Sons (Asia) Pte Ltd. 2 Clementi Loop, Singapore.

Levin, R. and Lieven, I. (1998). Dynamic finite element model updating using neural networks. Journal of sound and vibration, vol. 210, no. 5, pp. 593-607.

Li, H., Fang, H., & Hu, S. L. J. (2007). Damage localization and severity estimate for three-dimensional frame structures. *Journal of Sound and Vibration*, *301*(3), 481-494.

Lieven, N., A., J. and Ewins, D., J. (1988). Spatial correlation of modespaces: the corridnate modal assurance criterion (COMAC), 6th international modal analysis conference, kissimmee, Florida, US, pp. 1063-1070.

Lydon, F., D. and Balendran, R., V. (1986). Some observations on elastic properties of plain concrete, cement and concrete research, 16, no. 3, pp. 314-24 . Cited in neville, 2011 .

Maeck, J., and De Roeck, G. (2002). Damage assessment of a gradually damaged RC beam using dynamic system identification. Proceedings of the 20th international modal analysis conference, society for experimental mechanics, Los Angeles, CA,US, 1560-1566.

Maia N., Silva J., He, J., Lieven N., Lin R., M., Skingle G., W., To W-M and Urgueira A. (1997). Theoretical and experimental modal analysis. Editors: maia and silva, UK: research studies press ltd., Taunton, Somerset, England.

Marwala, T. (2010). Finite element model updating using computational intelligence techniques. Springer-verlag, London, UK.

Masri, S., F., Nakamura, M., Chassiakos, A., G., and Caughey, T., K. (1996). Neural network approach to detection of changes in structural parameters. Journal of engineering mechanics, 122 (4), 350-360.

Masri, S., F., Smyth, A., W., Chassiakos, A., G., Caughey, T., K., and Hunter, N., F. (2000). Application of neural networks for detection of changes in nonlinear systems. journal of engineering mechanics, 126 (7), 666-676.

Masters, T. (1993). *Practical neural network recipes in C++*. Academic Press, London, UK.

Mather, K. (1965). Hight strength, hight density concrete, J. Amer. Concr. Inst., 62, no. 8, pp. 951-62. cited in Neville, 2011 .

Mathuria, P. H., and U. P. Kulkarni. (2000). Damping Loss Factor for Damping Materials for Continuous Structures.

McCarthy, J., Minsky, M. L., Rochester, N., & Shannon, C. E. (1955). A proposal for the dartmouth summer research project on artificial intelligence, august 31, 1955.

Mcconnell, K., Varoto, P. (2008). *Vibration Testing: Theory and Practice*, John wiley and Sons, Inc., USA.

Mcculloch, W., S. and Pitts, W. (1943). A logical calculus of the ideas immanent in nervous activity. Bull. Math. Biophy., 5, pp 115-133.

Memory, T., J., Thambiratnam, D., P., and Brameld, G., H. (1995). Free vibration analysis of bridges, engineering structures 17 (10), 705–713.

Meruane, V. and Mahu , J. (2004). Real-time structural damage assessment using artificial neural networks and anti-resonant frequencies.

Moaveni, S. (1999). Finite element analysis. Theory and application with Ansys. Prentice hall, new jersey.

Modena, C., Sonda, D. and Zonta, D. (1999). Damage localization in reinforced concrete structures by using damping measurements. Key engineering materials, 167:132-141.

Mohan, V., Parivallal, S., Kesavan, K., Arunsundaram, B., Ahmed, A. F., & Ravisankar, K. (2014). Studies on Damage Detection Using Frequency Change Correlation Approach for Health Assessment. Procedia Engineering, 86, 503-510.

Montalvao, D., Ribeiro, A., M., and Duarte-Silva, J. (2008). A method for the localization of damage in a CFRP plate using damping, mechanical systems and signal processing, doi:10.1016/j.ymssp.2008.08.011.

Murthyguru, I. (2005). Novel approach to study compression properties in textile, autex research journal, vol. 5, no 4, pp 176-193.

Nagarajaiah, S., Dyke, S., Lynch, J., Smyth, A., Agrawal, A., Symans, M. and Johnson, E. (2008). September. Current directions of structural health monitoring and control in USA. In Advances in Science and Technology Vol. 56, pp. 277-286.

Nair, K., Krishnan, Prasad, A., Meher, and Menon, D. (2008). Load combination studies for reinforced concrete slabs.

Navarro, M., Vidal, F., Aranda, C., Enomoto, T. and Alguacil, G. (2014). Changes in dynamic characteristics of RC buildings determined from ambient vibration measurements performed pre-and post-the Lorca 2011 earthquake. Proceedings of the 9th International Conference on Structural Dynamics. Porto, Portugal.

Ndambi, J., M., Vantomme, J., and Harri, K. (2002). Damage assessment in reinforced concrete beams using eigenfrequencies and mode shape derivatives. Engineering structures,24 (4), 501-515.

Neville, A., M. (2011). *Properties of concrete.5th ed. Pearson Education Limited*, Essex, England.

Nguyen, V. V., Dackermann, U., Li, J., Alamdari, M. M., Mustapha, S., Runcie, P., & Ye, L. 2015. Damage Identification of a Concrete Arch Beam Based on Frequency Response Functions and Artificial Neural Networks.

Ostachowicz, W., M. and M., Krawczuk. (2001). On modelling of structural stiffnessloss due to damage. Key engineering materials 204-205: 185-200.

Owen, J., Pearson, R. (2004). The use of dynamic data for the structural health monitoring of bridges, Proceedings of 1st FIG international symposium on engineering surveys for construction works and structural engineering, Nottingham, United Kingdom.

Owolabi, G. M., Swamidas A. S. J. and Seshadri, R. (2003). Crack detection in beams using changes in frequencies and amplitudes of frequency response functions. journal of sound and vibration 265 (1), 1-22.

Pan, Q. (2007). System identification of constructed civil engineering structures and uncertainty . A thesis submitted for the degree of doctor of philosophy in engineering, the faculty of Drexel University, United States.

Pandey, A., K., and Biswas, M. (1994). Damage detection in structures using changes in flexibility. Journal of sound and vibration, 169 (1), 3-17.

Pandey, A., K., Biswas, M., and Samman, M., M. (1991). Damage detection from changes in curvature mode shapes. Journal of sound and vibration, 145 (2), 321-332.

Pandey, P., C., and S., V. Barai (1994). Sensitivity-based weighted-average in structural damage assessment. Journal of performance of constructed facilities, 8 (4), 243–263.

Paolozzi, A. and Peroni, I. (1990). Detection of debonding damage in a composite plate through natural frequency variations, journal of reinforced plastics and composites, vol. 9, pp. 369-389.

Pavic, A. (1999). Vibration serviceability of long-span cast in-situ concrete floors. A thesis submitted for the degree of doctor of philosophy in engineering, university of Sheffield, department of civil and structural engineering, Sheffield, UK.

Pearson, S., R. (2003). On using vibration data to detect damage in model-scale reinforced concrete bridges. a thesis submitted for the degree of doctor of philosophy in engineering, university of Nottingham, school of civil engineering, and Nottingham, UK.

Petyt, M. (2010). Introduction to finite element vibration analysis, 2nd ed. Cambridge university press.

Prader, J., B. (2012). Rapid impact modal testing for bridge flexibility: towards objective evaluation of infrastructures. A thesis submitted for the degree of doctor of philosophy, Faculty of Drexel University, Philadelphia, PA, United States.

Radomski, W. (2002). Bridge rehabilitation, imperial college press, 476 pages.

Rafiq, M., Y., Bugmann, G. and Easterbrook, D., J. (2001). Neural network design for engineering applications. Computers and structures 79, 1541-52.

Razak, H., A. and Choi, F., C. (2001). The effect of corrosion on the natural frequency and modal damping of reinforced concrete beams engineering structures 23 1126-33.

Razavitosee, S., & Jumaat, M. Z. (2014). Load-deflection Analysis of CFRP Strengthened RC Slab Using Focused Feed-forward Time Delay Neural Network. Concrete Research Letters, 5(3).

Reynolds, P. (2000). The effects of raised access flooring on the vibrational performance of long-span concrete floors. a thesis submitted for the degree of doctor of philosophy in engineering, university of Sheffield, department of civil and structural engineering, Sheffield, UK.

Reynolds, P. and Pavic, A. (2000). Quality assurance procedure for the modal testing of building floor structures. Structural testing series: part 8, experimental techniques, pp. 36-41.

Richardson, M. H. (1997). Is it a mode shape, or an operating deflection shape?. SV Sound and vibration, 31(1), 54-61.

Richardson, M. and Schwarz, B. (2003). Modal parameter estimation from operating data. Sound and vibration, vibrant technology, Inc., Jamestown, California37 (1), pp.28-39.

Rosenblatt, F. (1958). The perceptron: A probabilistic model for information storage ang organization in the brain. Psychological review, 65, pp 386-408.

Ručevskis, S., Wesolowski, M. and Čate, A. (2009). Vibration-based damage identification in laminated composite beams. Construction science. Vol.10, pp.100-113. ISSN 14077329.

Rumelhart, D., E., Hinton, G., E. and Williams, R., J. (1986). Learning internal representation by error propagation, in parallel distributed processing: exploration in microstructure of cognition, vol. (1) (D.E. Rumelhart, J., L., Mcclelland and the PDP research gropus, edn.) Cambridge, MA: MIT Press, pp 318-362.

Rytter, A. (1993). Vibration based inspection of civil engineering structures, PhD thesis, Aalborg University, Denmark.

Rytter, A. and Kirkegaard, P. (1997). Vibration based inspection using neural networks. Structural damage assessment using advanced signal processing procedures, proceedings of the 2nd international conference on damage assessment of structures, DAMAS'97, university of Sheffield, Sheffield, UK, pp. 97-108.

Salawu, O., S., and Williams, C. (1997). Theoretical and experimental vibration analysis of a reinforced concrete bridge, in: 15th int. Modal analysis conference, Orlando, IMAC, pp. 278–285.

Salawu, O., S. and Williams, C. (1995). Bridge assessment using forced vibration testing. Journal of structural engineering, ASCE , 121 (2): 161–73.

Salawu, O., S. (1995). Non-destructive assessment of structures using the integrity index method applied to a concrete highway bridge. Insight 37 (11): 875-878.

Salawu, O., S. (1997). Detection of structural damage through changes in frequency: a review, journal of engineering structures, vol.19, no. 9.

Salawu, O., S. and Williams, C. (1994). Damage location using vibration mode shapes, in proc. Of 12th international modal analysis conference, pp. 933–939.

Saravanos D. A, Hopkins D. A. (1995) Effects of delaminations on the damped dynamic characteristics of composites. Journal of Sound and Vibration, 192,977-993.

Schwarz, B., J. and Richardson, M., H. (1999). Experimental modal analysis, application note vibrant technology, inc.

Sharma, V., Rai, S. and Dev, A. (2012). A comprehensive study of artificial neural networks. International journal of advanced research in computer science and software engineering, 2, 10, pp 278-284.

Shi, Z., Law, S., and Zhang, L. (2000). Damage localization by directly using incomplete mode shapes., J. Eng. Mech., 126 (6), 656–660.

Shih, H. W., Thambiratnam D. P. and Chan T. H. T. (2009). Vibration based structural damage detection in flexural members using multi-criteria approach. Journal of sound and vibration 323 (3-5): 645-661.

Sinou, J., J. (2009). A review of damage detection and health monitoring of mechanical systems from changes in the measurement of linear and non-linear vibrations, in: robert c. sapri (ed.), mechanical vibrations: measurement, effects and control, 643-702.

Slastan, J., and S., Pietrzko. (1993). Changes of RC beam modal parameters due to cracks, in proc. of the 11th international modal analysis conference, 70–76.

Smart wireless sensor networks 2015, Smart monitoring of historic structures. Available from: <http://www.smoohs.eu/tiki-index.php?page=Smart+Wireless+Sensor+Networks>. [20 June 2015].

Sohn, H., Farrar, C., R., Hemez, F., M., Shunk, D., D., Stinemates, D., W. and Nadler, B., R. (2004). A review of structural health monitoring literature: 1996-2001. Los Alamos national laboratory report no. LA-13976-MS, Los Alamos, New Mexico.

Soltis, L. A., Wang, X., Ross, R. J., & Hunt, M. O. (2002). Vibration testing of timber floor systems. Forest products journal, 52(10), 75-81.

Storck, H., Sumali, H., & Pu, Y. (2001). Experimental modal analysis of automotive exhaust structures (No. 2001-01-0662). SAE Technical Paper.

Sultan, R., Guirguis, S., Younes, M. and El-Soaly, E. (2012). Delamination detection of composite laminates using natural frequency vibration method. International journal of mechanical engineering and robotics research, 1, 2, 286-296.

Sundaram, B. A., Ravisankar, K., Senthil, R., and Parivallal, S. (2013). Wireless sensors for structural health monitoring and damage detection techniques. Current Science(Bangalore), 104 (11), 1496-1505.

Tawfik, M. A., Abu-Tabikh, M. I., and Hamdoon, F. O. (2014). Vibration based-crack detection in simplified wind turbine blades using artificial neural networks. Eng. And Tech. journal, Vol. 32 No.8.

Tetko, I.V., Livingstone, D.J. and Luik, A.I. (1995). Neural network studies. 1. Comparison of overfitting and overtraining. Journal of Chemical Information & Computer Sciences, 35, 826-833.

Wahab, M., A. and Roeck, G. (1997). Effect of temperature on dynamic system parameters of a highway bridge. Structural engineering international 4, 266-270.

Wallack, P., Skoog, P. and Richardson, M. (1988). February. Simultaneous structural dynamics modification(S 2 DM). In International Modal Analysis Conference, 6 th, Kissimmee, FL, Proceedings. (Vol. 2, pp. 1033-1038).

Wang, Y. (2010). A non-destructive damage detection method for reinforced concrete structures based on modal strain energy. PhD diss., university of technology, Sydney.

WENZEL, H. (2009). Health Monitoring of Bridges. John Wiley & Sons Ltd., West Sussex, United Kingdom.

Widrow, B. and Hoff, M., E. (1960). Adapative switching circuit. Irewescon convention record, 4, pp 96-104.

Worden, K., Ball, A. and Tomlinson, G. (1993). Neural networks for fault location, in proc. Of the 11th international modal analysis conference, 47–54.

Wu, X., Ghaboussi, J., and Garrett, J., H. (1992). Use of neural networks in detection of structural damage. Computers and structures, 42 (4), 649-659.

Yeung, W. T., and Smith, J. W. (2005). Damage detection in bridges using neural networks for pattern recognition of vibration signatures. Engineering Structures,27(5), 685-698.

Yoo, S., H., Kwak, H., K., and Kim, B., S. (1999). Detection and location of a crack in a plate using modal analysis, proceedings of international modal analysis conference (Imac-xvii), Orlando, FL, 1902-1908.

Yousaf, E. (2007). Master of Science Thesis, 'Output only modal analysis', Department of Mechanical Engineering, Blekinge Institute of Technology, Karslkrona, Sweden: pp 64.

Yu, C., R, Ventura, G., Ruiz, G. and Carmona, J. (2008). Numerical modeling in reinforced concrete and its validation, in: 8th world congress on computational mechanics (WCCM8) 5th. European congress on computational methods in applied sciences and engineering (ECCOMAS), Venice, Italy.

Yun, C.B., Bahng, E.Y. (2000). Substructural Identification Using Neural Networks, Computers and Structures 77(1): 41-52.

Zang, C., and Imregun, M. (2001a). Structural damage detection using artificial neural network and measured FRF data reduced via principal component projection." journal of sound and vibration, 242 (5), 813-827.

Zang, C., and Imregun, M. (2001b). Combined neural network and reduced FRF techniques for slight damage detection using measured response data". Archive of applied mechanics, 71 (8), 525-536.

Zapico, A. and Molisani, L. (2009). Fault diagnosis on steel structures using artificial neural networks. In mecánica computacional, volume xxviii, pages 181–188.

Zapico, J. L., and Gonzalez, M. P. (2006). Vibration numerical simulation of a method for seismic damage identification in buildings. Engineering Structures, (28), 255-263.

Zhang, Z. and Aktan, A., E. (1995). Damage indices for constructed facilities, paper presented at and published in the proceedings of IMAC 13, pp: 1520-1529.

Zhang, Z., Hartwig, G. (2004). Relation of damping and fatigue damage of unidirectional fibre composites, international journal of fatigue 24 , 713-738.

Zhengsheng, L, Swanson, J., Helmicki, A., Hunt, V. (2005). Modal contribution coefficients in bridge condition evaluation. ASCE, journal of bridge engineering, 10 (2).

Zhou, Z. (2006). Vibration-based damage detecton of simple bridge superstructures (doctoral dissertation, university of saskatchewan saskatoon).

Appendix A: Preparation of Experimental Work

The mould of the slab was firstly placed on platform trolley so as to be lifted with a forklift without difficulty or effort. The casted slab was be able to move from place to place. A release mould agent oil was coated on the mould surface as shown in Figure A.1 to ensure slab bottom and sides to be easily released from the mould after proper hardening. Before casting the slab, slab mould level was checked using a spirit bubble level to ensure the slab surface is flat and levelled after casting. After levelling the mould, the steel reinforcing mesh was placed in position into the slab mould as exhibited In Figure A.2. Then, some batches of concrete were carefully distributed into the mould so as not to cause any movement to the steel reinforcing mesh, see Figure A.3. After adding further concrete batches, a vibrator was subsequently used to compact the concrete in order to reduce the amount of bubbles in the concrete mix which helped to make the concrete mix homogeneous throughout the slab. Afterwards, the slab was flattened using a trowel to ensure levelled and smooth surface as presented. This ensured almost same thickness throughout the slab. The casted slab was left in place, as illustrated in Figure A.4, to be hardened for about 24 hours.

Figure A. 1: Oiling the mould with release mould agent before being ready for use.

Figure A. 2: Placement of steel reinforcing mesh.

Figure A. 3: Placement of some concrete batches into the well-oiled mould.

Figure A. 4: Completion the concrete slab casting process.

Later on, the sides of the mould were carefully removed. One of the crucial steps in the lab work was curing the reinforced concrete slab. Concrete should be cured properly and, therefore, adequate amount of moisture are required for continued hydration and development of concrete strength. Concrete is extremely vulnerable at age of 24 hours. Therefore, it can be easily damaged, so I was very careful and thoughtful in my handling of the mould. The screws were removed using screwdriver and the wooden boards were pried away carefully from the sides and ends (four altogether) of the mould. As it is known that the slab has two large and one small dimensions. Since slab was difficult to be moved and lifted for curing process, a strip of mortar was made around slab's edges to build a pond water as shown in Figure A.5. The pond water was built to keep the surface of the slab watery as presented in Figure A.6. After a proper curing for not less than 28 day, the strip of the mortar was carefully removed as seen in Figure A. 7 and the slab was hosed and brushed immediately beforehand.

Figure A. 5: Create a water pond over the RC slab surface for its curing.

Figure A. 6: A reinforced concrete slab ponded while curing in the laboratory.
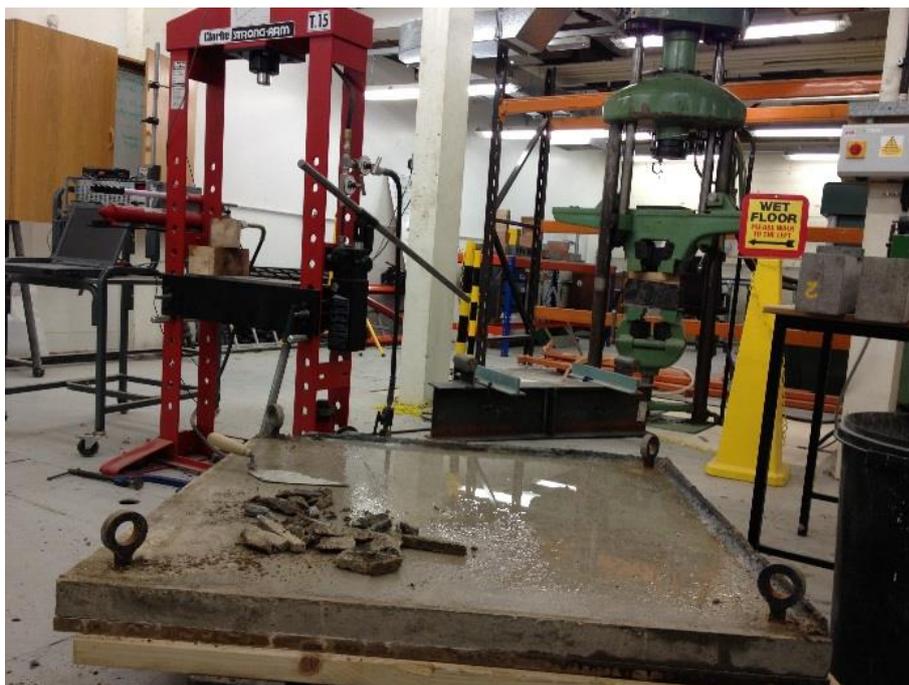
Figure A. 7: Breaking the pond sides and flowing the water out after 28 days of curing.

After 28 days of curing the concrete cubes (100 x 100 x 100 mm^3) and slab, the three concrete cubes as depicted in Figure A.8 were tested and the slabs were prepared for static (regarding to group C slabs) and dynamic tests. Such cubes had mix design 0.6:2.82:4.25 were tested under compression machine, as show in Figure A.9, to determine the concrete compressive strength. Furthermore, during the concrete cubes test, the compression machine was set up to apply the load on the cube, as depicted in Figure A.10, until cubes were failed as seen in Figures A.11-A13. Table A.1 shows the calculated average concrete compressive strength of the tested cubes at 28 days for four pairs of slabs, groups (A, B, C and D) slabs.

Figure A. 8: Removing the concrete cubes from the curing water basin and preparing them for testing

Figure A. 9: Concrete compression testing machine.

Figure A. 10: Confinement of a concrete cube.

Figure A. 11: Concrete cube failure under compression testing machine.

Figure A. 12: Continuous failure to concrete cube.

Figure A. 13: Final shape of failed concrete cube.

Table A. 1: Concrete compressive strength of the tested cubes at 28 days.

Groups	Average compressive strength (N/mm^2)
A	29.15
B	29.83
C	31.4
D	30.2

Before starting the tests, the equipment as shown in Figure A.14 was prepared and make it ready to mark the slab surface with a grid of 25 equally spaced locations. Afterwards, the location of partially concentrated load at slab centre was marked, as seen Figure A.15, in order to apply the static load. While, Figure A.16 shows the partially concentrated load when it was exactly placed at slab centre. The setup of both static and dynamic tests are presented in Figure A.17. It is imperative to mention that the forklift as shown in Figure A.18 was used for loading and unloading the slabs during the tests.

Figure A. 14: Preparation the equipment to mark the slab with a grid of response points.

Figure A. 15: Marking the location of partially concentrated load on slab centre.

Figure A. 16: Placement the partially concentrated load on slab centre.

Figure A. 17: Static and dynamic set-up of test specimen.

Figure A. 18: Loading-unloading and transporting RC slab.

After applied the load 12kN on group C slabs, they were strengthened and then applied experimental modal analysis test to find the effect of the strengthening on modal parameters. The quality of the strengthening is mainly dependent on skill of the operator, the materials used, and the cleanliness of the contact area between defected specimen and repairing material. These important factors ensure the optimum envelope for production of the best repairing. It is important to mention that

a typical repair procedure takes the following steps. Decide on the repair technique and materials to be used is the first step. As a result, it was planned to repair the slabs with CFRP. Therefore, The CFRP fabric roll as presented in Figure 19 was cut into strips as needed, say 1200mm length. Then, a mixture of West system 105 epoxy resin and 205 harder was employed to offer excellent bond strength between CFRP and the concrete surface, see Figure A.20. The ratio 5:1 of the epoxy resin to hardener was utilised. The 205 hardener is usually used to ensure a rapid curing which develops and retentions the physical properties of the structure. Table A.2 shows some of the mechanical properties of the CFRP, which was provided by the manufacturer company. Whereas, Table A.3 presents the property of the pack of 105 epoxy resin and 205 hardener, which was provided by the supplier.

Figure A. 19: CFRP fabric roll.

Figure A. 20: Adhesive agent 105 epoxy resin and 205 hardener.

Table A. 2: Mechanical properties of the CFRP.

Types of CFRP	Tensile strength (GPa)	Modulus (GPa)	Strain (%)
TR30S	2.55	135	1.7

Table A. 3: Mechanical properties of Epoxy resin and Hardener.

Types of Epoxy and hardener	Tensile strength (MPa)	Modulus (GPa)	Density (g/cm^3)	Strain (%)	Cured to solid state (Hours)	Cured to max strength (days)
105/205	54.09	2.81	1.11	3.4	5-7	5-7

There are some certain considerations are important to be taken into account during setting and operating repairing. Protective equipment such as gloves and glasses should always be worn by operators in order to prevent contamination of prepared repair areas and minimise personnel health risks. The epoxy adhesive was firstly applied to the marked locations on the tension surface as shown in Figure A. 21. The strips of CFRP were subsequently applied to the tension faces of the slabs as marked and they were pressed using a small roller as shown in Figures A.22 and A.23. The roller was used to squeeze out the excess epoxy adhesive that was easily removed. This process helped to remove the trapped air bubbles to ensure excellent bond between the CFRP sheets and concrete surfaces. After the entire application process was achieved as shown in Figure 24, the epoxy adhesive was then allowed to be properly cured in the laboratory environment prior to implement the dynamic test.
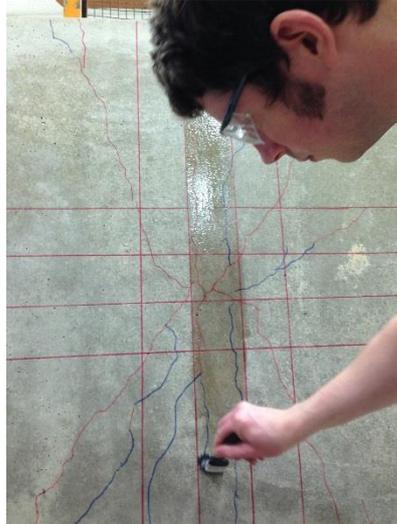
Figure A. 21: Coating the epoxy adhesive to the marked locations on the tension surface.
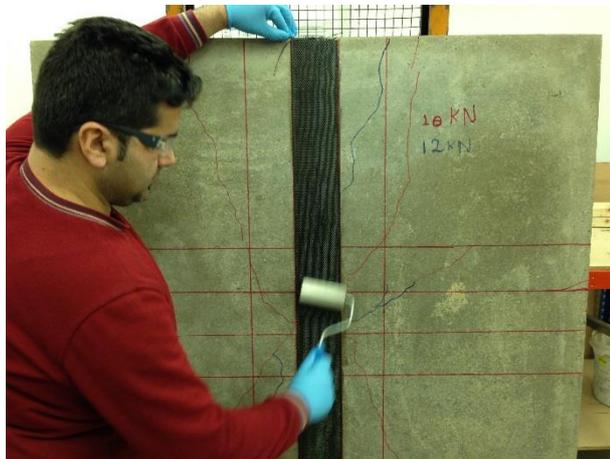
Figure A. 22: Strengthened RC slab specimen with first CFRP sheets.

Figure A. 23: Continuous process of Strengthening RC slab specimen with CFRP sheets.

Figure A. 24: View of RC slab after completion of strengthening with CFRP sheets.

Appendix B: Matlab Code for Drawing FRF.

In this appendix, the Matlab code for the slab element used in this thesis is presented. The Matlab code was used for transforming data, averaging and drawing the FRF and its components. After plotting the FRF, the natural frequencies, damping ratios and mode shapes were then manually extracted.

```matlab
clear all
contents = dir('*.txt');
c=0;
for i = 1:numel(contents)

    filename = contents(i).name;
    % Open the file specified in filename, do your processing...
    %PIP = calcFeatures(imgPath);
    [path name] = fileparts(filename);
    if name(1:3) ~= 'out'                    % see three word in the
name
    Inp(:,i) = load(filename);%I{i} = load(filename);
    else
        c=c+1;
    Out(:,c) = load(filename);%I{i} = load(filename);
    end
    names{i}=name;
end
c=0;
for i=1:9
for j=1:5
c=c+1;
inp{i,j}=Inp(:,c);
X{i,j}=fft(Inp(:,c));
Sxx{i,j}=X{i,j}.*conj(X{i,j});
end
end
c=0;
for i=1:25
for j=1:5
c=c+1;
out{i,j}=Out(:,c);
Y{i,j}=fft(Out(:,c)./1000);
Syy{i,j}=Y{i,j}.*conj(Y{i,j});
end
end
c=0;
for i=1:9
    if i~= 9
    for j=(3*i-2):3*i
        for n=1:5
        Sxy{j,n}=X{i,n}.*conj(Y{j,n});
        Syx{j,n}=Y{j,n}.*conj(X{i,n});
        end
        Averaged_Coherence(j,:) =
abs((Sxy{j,1}.^2+Sxy{j,2}.^2+Sxy{j,3}.^2+Sxy{j,4}.^2+Sxy{j,5}.^2))...
            ./((Sxx{i,1}.*Syy{j,1})+(Sxx{i,2}.*Syy{j,2})+(Sxx{i,3}.*
Syy{j,3})+(Sxx{i,4}.*Syy{j,4})+(Sxx{i,5}.*Syy{j,5}));
        Sum_Sxx(i,:)=Sxx{i,1}+Sxx{i,2}+Sxx{i,3}+Sxx{i,4}+Sxx{i,5};
        Sum_Syx(j,:)=Syx{j,1}+Syx{j,2}+Syx{j,3}+Syx{j,4}+Syx{j,5};
```

```matlab
            FRF(j,:)=Sum_Syx(j,:)./Sum_Sxx(i,:);
    end
    else
        for n=1:5
            Sxy{25,n}=X{i,n}.*conj(Y{25,n});
            Syx{25,n}=Y{25,n}.*conj(X{i,n});
        end
        Averaged_Coherence(25,:) =
abs((Sxy{25,1}.^2+Sxy{25,2}.^2+Sxy{25,3}.^2+Sxy{25,4}.^2+Sxy{25,5}.^
2))...
            ./((Sxx{i,1}.*Syy{25,1})+(Sxx{i,2}.*Syy{25,2})+(Sxx{i,3}
.*Syy{25,3})+(Sxx{i,4}.*Syy{25,4})+(Sxx{i,5}.*Syy{25,5}));
        Sum_Sxx(i,:)=Sxx{i,1}+Sxx{i,2}+Sxx{i,3}+Sxx{i,4}+Sxx{i,5};

Sum_Syx(25,:)=Syx{25,1}+Syx{25,2}+Syx{25,3}+Syx{25,4}+Syx{25,5};
        FRF(25,:)=Sum_Syx(25,:)./Sum_Sxx(i,:);
    end
end


freq_axis=0:2:8190;


for i=1:25
folder=['output',num2str(i)];
mkdir(folder);

h=figure (i);      % Figure (1) magnitude of FRF in Semilogy

semilogy(freq_axis,abs(FRF(i,:)));
ma=max(abs(FRF(i,:)));
mi=min(abs(FRF(i,:)));

title('Magnitude of FRF')
xlabel('Frequency (Hz)')
ylabel('Drive Accelerance (dB)')
axis([0 1200 (mi-0.1*mi) (ma+0.2*ma)])
grid on

saveas(h,['Semilog' num2str(i) '.jpg'])
movefile(['Semilog' num2str(i) '.jpg'], folder);
saveas(h,['Semilog' num2str(i) '.fig'])
movefile(['Semilog' num2str(i) '.fig'], folder);

h=figure (i);       % Figure (2) Magnitude of FRF

plot(freq_axis,abs(FRF(i,:)));
ma=max(abs(FRF(i,:)));
mi=min(abs(FRF(i,:)));
title('Magnitude of FRF')
xlabel('Frequency (Hz)')
ylabel('abs(output frequensy spectrum)')
axis([0 1200 mi (ma+0.05*ma)])

 grid on

saveas(h,['plot' num2str(i) '.jpg'])
movefile(['plot' num2str(i) '.jpg'], folder);
saveas(h,['plot' num2str(i) '.fig'])
movefile(['plot' num2str(i) '.fig'], folder);
```

```matlab
h=figure (i);           % Figure (3) Imaginary of FRF

plot(freq_axis,imag(FRF(i,:)));
ma=max(imag(FRF(i,:)));
mi=min(imag(FRF(i,:)));
 title('Imaginary of FRF')
 xlabel('Frequency (Hz)')
 ylabel('Imag(FRF)')
 axis([0 1200 mi ma]) % Error on the min check please
 grid on

saveas(h,['Imag' num2str(i) '.jpg'])
movefile(['Imag' num2str(i) '.jpg'], folder);
saveas(h,['Imag' num2str(i) '.fig'])
movefile(['Imag' num2str(i) '.fig'], folder);

 h=figure (i);           % Figure (4) Real Part of FRF

plot(freq_axis,real(FRF(i,:)))
ma=max(real(FRF(i,:)));
mi=min(real(FRF(i,:)));
title('Real of FRF')
xlabel('Frequency (Hz)')
ylabel('Real(FRF)')
axis([0 1200 (mi+0.1*mi) (ma+0.1*ma)])
 grid on
saveas(h,['Real' num2str(i) '.jpg'])
movefile(['Real' num2str(i) '.jpg'], folder);

h=figure (i);           % Figure (5)Phase of FRF

plot(freq_axis,angle(FRF(i,:)))
ma=max(angle(FRF(i,:)));
mi=min(angle(FRF(i,:)));
title('Phase of FRF')
xlabel('Frequency (Hz)')
ylabel('Phase (FRF)')
axis([0 1200 (mi+0.1*mi) (ma+0.1*ma)])
 grid on
saveas(h,['Phase' num2str(i) '.jpg'])
movefile(['Phase' num2str(i) '.jpg'], folder);

h=figure (i);           % Figure (6)Averaged_Coherence

plot(freq_axis,Averaged_Coherence(i,:))
ma=max(Averaged_Coherence(i,:));
mi=min(Averaged_Coherence(i,:));
title('Coherence)')
xlabel('Frequency (Hz)')
ylabel('Coherence (FRF)')
axis([0 1200 mi (ma+0.05*ma)])
 grid on
saveas(h,['Coherence' num2str(i) '.jpg'])
movefile(['Coherence' num2str(i) '.jpg'], folder);
saveas(h,['Coherence' num2str(i) '.fig'])
movefile(['Coherence' num2str(i) '.fig'], folder);

end
```

266

Appendix C: Analysis of RC Slab According to EC2, BS 8110 and ACI 318 codes

The moment resistance of a simply supported reinforced concrete square slab subjected to partial concentrated load at the centre of the slab is determined according to three codes of practices: EC 2, BS 8110 and ACI 318 as shown below. This calculation is done to help find the value of the maximum concentrated load to be applied for an intended degree of damage (light, moderate and severely damaged) in the slab when tested statically under various load progression, for more details see chapter 6.

<u>Slab properties</u>

Slab thickness (h) = 40mm

Concrete cover to steel centre = 10mm

Effective depth (d) = 40 − 10 = 30mm

Slab side length = 1.2m

Concrete compressive strength (based of cube test), f_{cu} = 30N/mm^2

Concrete compressive strength (based of cylinder test), f'_c =f_{ck} = 25N/mm^2

Characteristic yield strength of steel = 500N/mm^2

Reinforcing bar diameter = 6mm

Ares of single bar = 28.3mm^2

Reinforcing bar spacing 60mm c/c

Total area of steel per metre run = 28.3 x 1000/60 = 471.7mm^2

Boundary condition: simply supported on four edges

EC 2 Method

Assume the steel has yielded.

Exposure class related to environmental conditions in accordance with EN 206-1 for the slabs is X0. This means that is no risk of corrosion or attack of reinforced concrete, very dry condition.

$F_{cc} = F_{st}$

$0.567 f_{ck} b s = 0.87 f_{yk} A_s$

$0.567 \times 25 \times 1000 \times s = 0.87 \times 500 \times 471.7$

$s = 14.48$mm

$x = s / 0.8$

$= 14.48 / 0.8$

$= 18.09$mm

Check

$0.617 d = 0.617 \times 30 = 18.51$mm

Since 18.51mm > 18.09mm, then the assumption that steel has yielded is correct.

$z = d - s / 2$

$= 30 - 14.48 / 2$

$= 22.76$mm $\leq 0.95 d = 0.95 \times 300 = 285$mm   O.K.

$M = F_{st} z$

$M = 0.87 f_{yk} A_s z$

$= 0.87 \times 500 \times 471.7 \times 22.76$

$= 4.671 \times 10^6$N.mm

$= \underline{4.671\text{kN.m}}$

This means, the resistant design moment of the slab according EC2 is:

$M_{RD} = 4.671$kN.m

In research where slab is tested in a laboratory, the nominal moment is to be taken into account. This is means the resistant moment might be calculated without considering material partial safety factors, i.e. concrete and steel safety factors equal 1. Accordingly, the nominal moment of the slab will be:

$M_n = \underline{5.767\text{kN.m}}$

BS 8110 Method

Assume the steel has yielded

$F_{cc} = F_{st}$

$0.447\ f_{cu}\ b\ s\ = 0.87\ f_{yk}\ A_s$

$0.447 \times 30 \times 1000 \times s = 0.87 \times 500 \times 471.7$

$s = 15.30mm$

$x = s\ /\ 0.9$

$\quad = 15.30\ /\ 0.9$

$\quad = 17.00mm$

Check

$0.636\ d = 0.636 \times 30 = 19.08mm$

Since $19.08mm > 17.00mm$, then the assumption that steel has yielded is correct.

$z = d - s\ /\ 2$

$\quad = 30 - 15.3\ /\ 2$

$\quad = 22.35mm\ \leq 0.95\ d = 0.95 \times 300 = 285mm \qquad O.K.$

$M = F_{st}\ z$

$M = 0.87\ f_{yk}\ A_s\ z$

$\quad = 0.87 \times 500 \times 471.7 \times 22.35$

$\quad = 4.586 \times 10^6 N.mm$

$\quad = \underline{4.586kN.m}$

This means, the resistant design moment of the slab according BS 8110 is:

$M_u = \underline{4.586kN.m}$

In research where slab is tested in a laboratory, the nominal moment is to be taken into account. This is means the resistant moment might be calculated without considering material partial safety factors, i.e. concrete and steel safety factors equal 1. Accordingly, the nominal moment of the slab will be:

$M_n = \underline{5.44kN.m}$

ACI 318-11 Method

Assume the steel has yielded

$F_{cc} = F_{st}$

0.85 f'$_c$ b a = f$_y$ A$_s$

a = f$_y$ A$_s$ / (0.85 f$_{ck}$ b)

0.85 x 25 x 1000 x a = 500 x 471.7

a = 11.10mm

c = a / β_1

β_1 = 0.85   for   f'$_c$ ≤ 028 N/mm^2

c =11.10 / 0.85

  = 13.06mm

ε_s = ε_{cu} (d / c - 1)

  = 0.003 (30 / 13.06 – 1)

  = 0.0039

Since 0.0039 > ε_y = 0.002, then the assumption that steel has yielded is correct.

M$_n$ = f$_y$ A$_s$ (d – a / 2)

    = 500 x 471.7 x (30 – 11.10 / 2)

    = 5.767 x 10^{6}N.mm

    = <u>5.767 kN.m</u>

M$_u$ = 0.9M$_n$

    = 0.9 x 5767

    = <u>5.190kN.m</u>

The summary of the design and nominal moment of resistance according the three codes of practices is shown in Table C.1.

Table C.1: Design and nominal moment of resistance of RC square slab specimen

	EC 2	BS 8110	ACI 318 -11
Design Moment (kN.m)	4.671	4.586	5.190
Nominal Moment (kN.m)	5.767	5.44	5.767

For square slab, the moment due to uniformly distributed load is given in Table 8 of (Timoshinko and Woinowsky-Krieger (1959) which is:

$M_{self\ wt} = 0.0479\ wL^2$

Where

w = Load intensity per square metre

L = side length of the slab

w = 24 x 0.04

= $0.96 kN/m^2$

$M_{self\ wt} = 0.0479 \times 0.96 \times 0.96 \times 1.2^2$

= 0.066 kN.m

For a square plate of size 1200 mm x 1200 mm subjected to partial concentrated load (Pu) over an area of 120 m x 120 m, (i.e. load plate side/slab side 120/1200=0.1), the bending moment is given in Table 20 of Timoshinko and Woinowsky-Krieger (1959) which is:

$M_{partial\ load} = 0.284\ P$

Total maximum moment exerted on the slab due to combined self-weight of the slab and partial concentrated load will be:

$M_{total} = M_{self\ wt} + M_{partial\ load}$

= 0.066 + 0.284 P

At collapse the total moment equals to the nominal moment, i.e.

$M_n = 0.066 + 0.284\ P_n$

Or

$P_n = (M_n - 0.066) / 0.284$

Therefore, considering nominal moment, the nominal load P_n will be:

According EC 2, $P_n = (5.767 - 0.066) / 0.284 = 20.07$ kN

According BS 8110, $P_n = (5.44 - 0.066) / 0.284 = 18.92$ kN

According ACI 318-11, $P_n = (5.767 - 0.066) / 0.284 = 20.07$ kN

The average nominal collapse load $\underline{P_n = 19.69\ kN}$

On the other hand, considering design moment, the ultimate collapse load P_u will be:

$P_u = (M_u - 0.066) / 0.284$

According EC 2, $P_u = (4.671 - 0.066) / 0.284 = 16.21$ kN

According BS 8110, $P_u = (4.586 - 0.066) / 0.284 = 15.92$ kN

According ACI 318-11, $P_u = (5.19 - 0.066) / 0.284 = 18.04$ kN

The average ultimate collapse load $\underline{P_n = 16.72}$ kN

The partially concentrated load stopped at (12/16.72) 71.8% of the average nominal collapse load. Then, the slabs were repaired and retested dynamically to find the effect of the strengthening on modal parameters.

Appendix D: MAC and COMAC Values Code

In appendix D, the Matlab code for calculating MAC and COMAC used in this thesis is obviously given. The Matlab code was employed for calculating these tow values whereby the discrepancy location is identified.

```matlab
clear all
files = dir('*.txt');
for l=1:length(files)
    eval(['load ' files(l).name ' -ascii']);
end

U1=S1_mode_shape_1; %Reference_mode_shape_1
U2=S1_mode_shape_2; %Reference_mode_shape_2
U3=S1_mode_shape_3; %Reference_mode_shape_3
U4=S1_mode_shape_4; %Reference_mode_shape_4
U5=S1_mode_shape_5; %Reference_mode_shape_5
U6=S1_mode_shape_6; %Reference_mode_shape_6

U1(:);       %change matric of undamaged slab from 5x5 to 25x1
U2(:);
U3(:);
U4(:);
U5(:);
U6(:);

D1=S2_mode_shape_1;  %Test_mode_shape_1 ;
D2=S2_mode_shape_2;  %Test_mode_shape_2 ;
D3=S2_mode_shape_3;  %Test_mode_shape_3 ;
D4=S2_mode_shape_4;  %Test_mode_shape_4 ;
D5=S2_mode_shape_5;  %Test_mode_shape_5 ;
D6=S2_mode_shape_6;  %Test_mode_shape_6 ;

D1(:);       %change matric of damaged slab from 5x5 to 25x1
D2(:);
D3(:);
D4(:);
D5(:);
D6(:);

U = zeros(25,6);       %Create the main matric of undamaged slab
U(:,1) = U1(:);
U(:,2) = U2(:);
U(:,3) = U3(:);
U(:,4) = U4(:);
U(:,5) = U5(:);
U(:,6) = U6(:);
U;

D = zeros(25,6);       %Create the main matric of damaged slab
D(:,1) = D1(:);
D(:,2) = D2(:);
D(:,3) = D3(:);
D(:,4) = D4(:);
D(:,5) = D5(:);
D(:,6) = D6(:);
D;
```

273

```matlab
   for u=1:6;
        for k=1:6;
        Qd25=D(:,u);    % row of MAC are damaged mode
        Qh25=U(:,k);    % column of MAC are damaged mode
        MAC(u,k)=
((Qh25)'*Qd25*(Qh25)'*Qd25)/((Qh25)'*Qh25*(Qd25)'*Qd25);
    end
  end
 MAC

 for i=1:25;
    j=1:6;
    M(i,j)=U(i,j).*D(i,j);
 Y=abs (M(i,j));
 sum(Y);
 sum(U(i,j).^2);
 sum(D(i,j).^2);
 COMAC(i)=sum(Y)^2/( sum(U(i,j).^2)*sum(D(i,j).^2));

end
COMAC'

figure (1)
imagesc(MAC)
% title('MAC','FontSize', 16)
xlabel('Six mode shapes of intact case','FontSize', 16)
set(gca, 'XAxisLocation', 'top')
ylabel('Six mode shapes under 5kN','FontSize', 16)
colorbar;                               % set  the colorbar
set(gca,'FontSize', 16);        %  fonts
grid on

figure (2)
bar(COMAC)
xlabel('Response point number','FontSize', 16)
set(gca, 'XAxisLocation', 'bottom')
ylabel('COMAC value at each response point','FontSize', 16)
axis([0 26 0 1])
set(gca,'FontSize', 16);        %  axies number fonts
grid on
```